

Novel Rubber Nanocomposites with Adaptable Mechanical Properties

DISSERTATION

zur Erlangung des akademischen Grades eines
Doktors der Naturwissenschaften (Dr. rer. nat.)
an der Fakultät für Biologie, Chemie und Geowissenschaften
der Universität Bayreuth

vorgelegt von

Chih-Cheng Peng

geboren in Taichung/Taiwan (R.O.C.)

Bayreuth, 2005

Die vorliegende Arbeit wurde in der Zeit von Dezember 2001 bis März 2005 in Bayreuth am Lehrstuhl Makromolekulare Chemie II unter Betreuung von Herrn Prof. Dr. Volker Abetz angefertigt.

Vollständiger Abdruck der von der Fakultät für Biologie, Chemie und Geowissenschaften der Universität Bayreuth zur Erlangung des akademischen Grades eines Doktors der Naturwissenschaften genehmigten Dissertation.

Dissertation eingereicht am:

Zulassung durch die Promotionskommission:

Wissenschaftliches Kolloquium:

Amtierender Dekan: Prof. Dr. O. Meyer

Prüfungsausschuß:

Prof. Dr. Volker Abetz (Erstgutachter)

Prof. Dr. Volker Altstädt (Zweitgutachter)

Prof. Dr. Hans-Werner Schmidt (Vorsitzender)

Prof. Dr. Karlheinz Seifert

To my Family and my Wife

*Imagination is more important than knowledge,
for knowledge is limited to all we now know and understand,
while imagination embraces the entire world,
and all there ever will be to know and understand.*

Albert Einstein

TABLE OF CONTENTS

Chapter 1 Introduction

1-1 Chemical Modification of Rubber	2
1-1-1 The Ene Reaction	3
1-1-2 Epoxidation Reaction	7
1-1-3 Other Reactions	10
1-2 Sol-Gel Process	13
1-2-1 Hydrolysis	17
1-2-2 Condensation	19
1-2-3 Summary	20
1-3 Tire Performance	21
1-3-1 Rolling Resistance	23
1-3-2 Relation Between Rolling Resistance and Dynamic Mechanical Properties	26
1-3-3 Rubber Polymer Influences on Tire Performance	28
1-4 Payne Effect	29
1-5 Polymer-Filler Interaction	33
1-5-1 Filler Geometry (shape, size and porosity)	39
1-5-2 Volume Fraction	40
1-5-3 Filler Surface	42
1-5-4 Wettability	43
1-5-5 Filler Surface Modification	44
1-5-6 Carbon Black versus Silica	48
1-6 Objectives of the Work	51
References	55

Chapter 2 A Simple Pathway toward Quantitative Modification of Polybutadiene - A New Approach to Thermoreversible Crosslinking Rubber Comprising Supramolecular Hydrogen Bonding Networks

2-1 Abstract	62
2-2 Introduction	62
2-3 Experimental	65
2-3-1 Materials	65
2-3-2 Synthesis of PB-E (1) (Epoxidation)	65
2-3-3 Synthesis of Hydrochlorinated PB, PB-OH (2) (Ring-opening)	66
2-3-4 Synthesis of PB-SU (3) (Sulfonyl isocyanate addition)	66
2-3-5 Characterizations	67
2-4 Results and Discussion	68

2-4-1	Chemical Modification of PB	68
2-4-2	FTIR Analysis	69
2-4-3	DSC Analysis	71
2-4-4	Dynamic Mechanical Analysis	72
2-5	Conclusion	75
2-6	Acknowledgement	75
	References	77

Chapter 3 Synthesis and Characterization of Silica Nanoparticles

3-1	Abstract	80
3-2	Introduction	81
3-3	Experimental	84
3-3-1	Materials	84
3-3-2	Synthesis of Modified Silica Nanoparticles via Modified Stöber Method	84
3-3-3	Synthesis of Unmodified Silica Nanoparticles via Stöber Method	85
3-3-4	Synthesis of Modified Silica Nanoparticles via Stöber Method	86
3-3-5	<i>In-situ</i> Dynamic Light Scattering in Monitoring Silica Particle Growth	87
3-3-6	Characterizations	88
3-4	Results and Discussion	89
3-4-1	Modified Silica Nanoparticles via Modified Stöber Method	89
3-4-2	Surface Unmodified and Modified Silica Nanoparticles via Stöber Method	90
3-4-3	<i>In-situ</i> Dynamic Light Scattering	94
3-5	Conclusion	97
3-6	Acknowledgement	98
	References	99

Chapter 4 “Smart” Silica-Rubber Nanocomposites in virtue of Hydrogen Bonding Interaction

4-1	Abstract	102
4-2	Introduction	102
4-3	Experimental	105
4-3-1	Materials	105
4-3-2	Synthesis of Surface Unmodified and Modified Silica Nanoparticles	106
4-3-3	Preparation of Silica-Rubber Nanocomposites	107
4-3-4	Characterizations	108
4-4	Results and Discussion	109
4-4-1	Surface Unmodified (Si-OH) and Modified (Si-Ph) Silica Nanoparticles	109
4-4-2	Dynamic Strain Sweep (Payne Effect Analysis)	111
4-4-3	Dynamic Temperature Sweep	118

4-4-4 Dynamic Frequency Sweep	123
4-4-5 TEM Analysis	123
4-5 Conclusion	125
4-6 Acknowledgement	126
References	127

Supplement Synthesis and Characterization of Polymeric Microgels Filled Elastomer

S-1 Introduction	130
S-2 Experimental	134
S-2-1 Materials	134
S-2-2 Epoxidation of PB	134
S-2-3 Ring-opening of Epoxidized PB (Hydrochlorination)	135
S-2-4 Esterification of Hydrochlorinated PB	135
S-2-5 Sulfenyl Chloride Addition onto PB	136
S-2-6 Reduction of Nitro Compounds	137
S-2-7 Polymeric Microgel	139
S-2-8 Dynamic Mechanical Analysis (RPA and ARES)	141
S-3 Results and Discussion	141
S-3-1 Payne Effect Analysis (RPA Strain-sweep)	141
S-3-2 Frequency-dependent Properties Analysis (ARES Frequency-sweep)	146
S-3-3 Temperature-dependent Properties Analysis (ARES Temperature-sweep)	155
S-4 Conclusion	159
References	160

Summary

Zusammenfassung

Acknowledgement

Erklärung

Appendix Rubber Process Analyzer

Figure Index

Table Index

Chapter 1

Introduction

1-1 Chemical Modification of Rubber

The most efficient route to modification of synthetic rubbers with chemically functional groups is to incorporate a monomer carrying the desired group in the polymerization process although chemical manipulation of the rubbers has also been employed. Since so far one cannot interfere with the biochemical polymerization leading to natural rubber, modification of the latter must be achieved by direct chemical reactions on the rubber itself.

Natural rubber can be viewed as a simple olefin and therefore subject to the myriad of reactions of such species. The all-*cis*, trialkyl substituted double bond is electron rich via inductive and hyper-conjugative effects although somewhat sterically hindered. While almost all the expected reagents react with natural rubber they have usually been employed in solution phase and with very variable degrees of efficiency. Modification of rubber can be achieved by one of the following means:

- (a) Changing the structure, or geometry of the rubber molecule without introducing new material.
- (b) Attaching to the rubber molecule of groups having specific physical characteristics or chemical reactivities.
- (c) Grafting short or long chains of a different polymer type onto the rubber hydrocarbon.

Chlorinated, hydrochlorinated and cyclized natural rubber have all been produced commercially, but oil-based synthetic products dominate these materials today [1-3]. Reaction with carbenes, maleic anhydride, aldehydes and many others have been employed, but no technically or economically significant materials have resulted [4,5]. For technical and economic viability any modification reaction must occur in high efficiency either in latex or during conventional mixing or curing of dry rubber. The heterogeneous nature of latex and the presence of adsorbed films of protein and surfactant on latex particles lead to obvious difficulties while diffusion control of reactions in solid rubber has to be considered. Given also that the non-rubbers present are inhibitors of many catalysts such as metal complexes and of some free radical

reactions, it is not surprising that candidate reagents are few in number.

It is possible to define the level of modification on economic grounds [6]:

- (a) Reagents which can insert pendent functional groups are expensive and, therefore, must be used at the lowest level adequate for providing sites for crosslinking etc. i.e., about 1 mole% giving a spacing of 6800 molecular weight units between tetrafunctional crosslinking groups. Even so, a reagent costing ten times as much as natural rubber and having a molecular weight of 200 will add 30% to the price.
- (b) Only cheap reagents can be used for macro modification at the 10-100 mole% level to give new physical properties to the natural rubber.

1-1-1 The Ene Reaction

Many reagents that react with natural rubber have been investigated with these previous arguments in mind. The conclusion reached is that the thermal ene reaction, as shown in **Figure 1-1**, is possibly unique in meeting these requirements in that it

- (a) does not rely on catalysts that can be poisoned by non-rubbers in natural rubber (although non-rubbers may compete for the reagent in a stoichiometric manner)
- (b) is usually known for high efficiency without side reactions
- (c) is particularly suited to natural rubber as it works best with an electron-rich alkyl substituted double bond
- (d) is versatile – can carry various functional groups

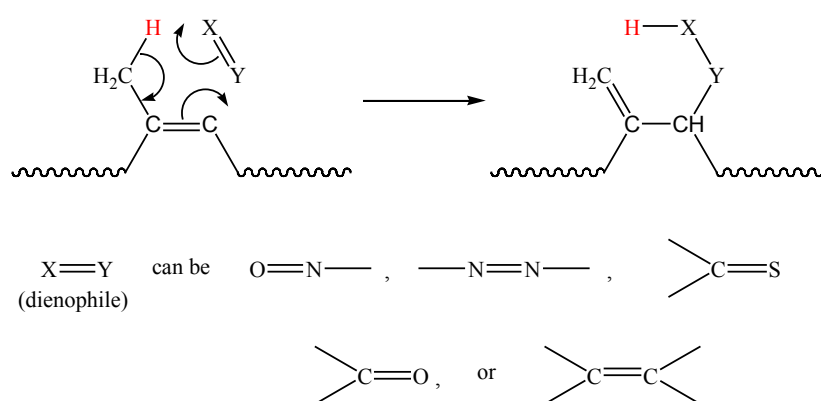


Figure 1-1: General mechanism of ene reaction.

The chemistry of the general ene reaction has been reviewed by Hoffmann [7] and Knight et al. [8].

The high temperature reaction of maleic anhydride is the most typical example of ene reaction used in rubber industry. F. Ferrero et al. reported the first kinetic study of ene reaction at different temperatures, by reacting maleic anhydride with oligomeric butadiene rubber of different molecular weights and microstructures [9], therein they concluded:

- (a) a long reaction time and a high temperature (180 to 220 °C) are needed for satisfactory efficiency.
- (b) the reaction rate increases with increasing temperature, increasing maleic anhydride concentration (first-order) and 1,4-*cis* microstructure content.
- (c) the kinetic data follow a first-order mechanism in spite of different butadiene microstructures.

D. Derouet et al. also studied the ene reaction of maleic anhydride and liquid natural rubber (LNR) [10]. They reported that at high temperatures (200 to 220 °C) with the exception of the partial succinic ring opening that occurs during the maleic anhydride addition process, a theoretical partial modification fixed at 20%, a maximum yield of 70% was achieved under optimum reaction conditions.

K. Chino et al. utilized the ene reaction of maleic anhydride to natural rubber in order to synthesise thermoreversible crosslinking rubber using a hydrogen bonding network [11]. They claimed an efficiency of 59% of grafting maleic anhydride onto polyisoprene rubber, using a mixture of polyisoprene ($M_w = 390,000$ g/mol) with 10 mole% maleic anhydride (relative to isoprene unit), 6PPD (*N*-phenyl-*N'*-1,3-dimethyl-butyl-*p*-phenylenediamine, antioxidation agent) and xylene as solvent. Subsequently 3-amino-1,2,4-triazole (TAT) was added to the modified rubber, opening the succinic ring, in order to have hydrogen bonding accepting and donating groups, as shown in Figure 1-2 and Figure 1-3. They also concluded that the introduction ratio of maleic anhydride into rubber could be changed by controlling the reaction time, reaction temperature and the amount of maleic anhydride, which is exactly in accordance with the conclusion made by F. Ferrero et al..

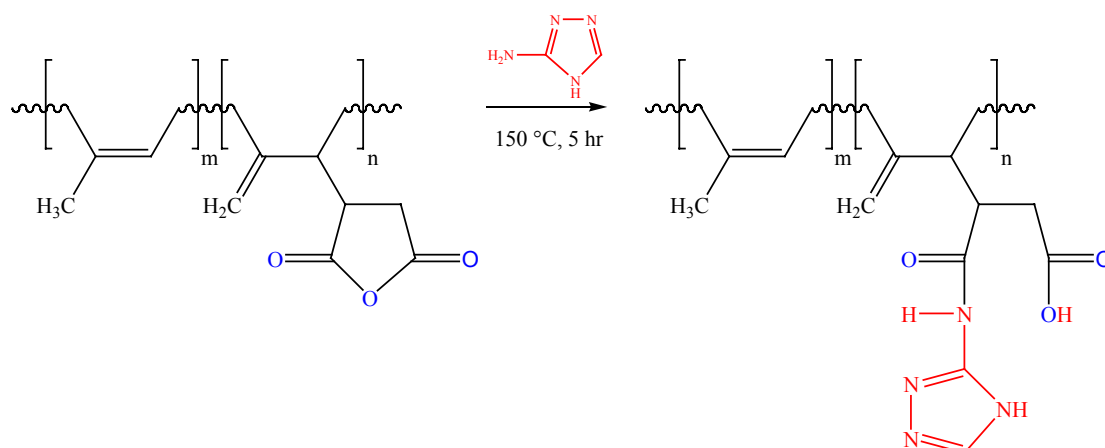


Figure1-2: Synthesis of addition of ATA to maleic polyisoprene.

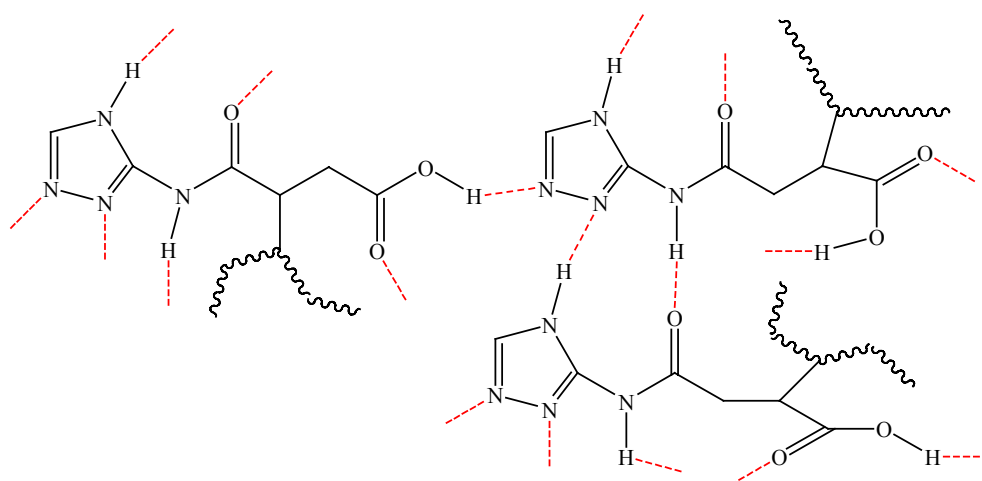


Figure1-3: Speculated model of thermoreversible crosslinking structure. (six-point hydrogen bonding)

Nitroso compounds can undergo ene reaction as well if they are adding to natural rubber. For example, as shown in [Figure 1-4](#), nitrosoarenes give a hydroxylamine as the main product if $X = \text{NH}_2$, NHR or NR_2 (*p*-nitrosoanilines) or OH (*p*-nitrosophenol) [12]. If $X = \text{NH-Ar}$, the pendent group has the structure of an *N,N*-aryl, alkenyl-*p*-phenylenediamine, and the derivative is a rubber-bound antioxidant [13]. Such antioxidants are not leached during washing or solvent treatment and may therefore be useful in the production of rubber thread for garments. If $X = \text{OH}$, the derivative

contains the pendent aminophenol group, which is the basis of the urethane vulcanization system for natural rubber [14].

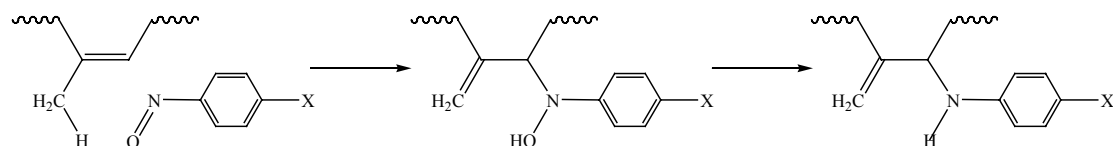
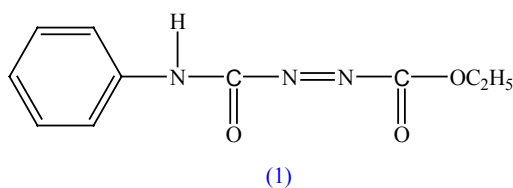


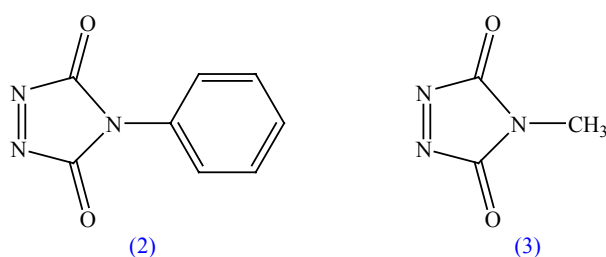
Figure 1-4: Addition of nitrosoarene to natural rubber by ene reaction.

Compounds containing an azo group activated by carbonyl groups add readily to natural rubber, e.g., azodicarboxylates [15]. Bisalkyl azodicarboxylate was used to crosslink natural rubber [16]. The reaction of ethyl *N*-phenylcarbamoylazofornate (ENPCAF), (1), and natural rubber may have practical applications [17], which is completed in 7 minutes in an internal mixer or in a few hours at 33 °C in deammoniated latex, with an efficiency > 90%.



The hydrazo ester groups are polar and readily undergo hydrogen bonding. It is reported that a 1% modification is sufficient to retard the low temperature crystallization of natural rubber [17] and the glass transition temperature is increased to 30 °C at a 16% modification. The ENPCAF modified natural rubber can be vulcanized with organic peroxides, urethane agents, or sulfur, though the crosslinking efficiency of sulfur is reduced [17]. The vulcanizates are hard and highly damped and exhibit lower air permeability and higher resistance to swelling in hydrocarbon oils. Natural rubber derivatives containing a wide range of pendent groups can be prepared with ENPCAF derivatives containing functional groups, however, none of the derivatives has attained commercial significance because of the high cost of the ENPCAF reagents.

4-phenyl-1,2,4-triazoline-3,5-dione, (2), is a “record dienophile and enophile” that can undergo ene reactions under extremely mild conditions [18]. It is reported that it is at least by a factor of 1000 more reactive in the Diels-Alder reaction with 2-chlorobutadiene than tetracyanoethylene, and is 2000 times more reactive than maleic anhydride. 4-methyl-1,2,4-triazoline-3,5-dione, (3), is at least 30,000 times more reactive towards cyclohexene than its open chain analog, ethylazodicarboxylate [19]. The many reactions of these powerful electron-acceptor molecules are generally quite rapid, being complete after a few seconds within the range from 0°C to room temperature.



Reimund Stadler et al. reported a series of results on polybutadiene modified with 4-phenyl-1,2,4-triazoline-3,5-dione and its derivatives, in which they observed that, due to the formation of hydrogen bonds between urazole groups, the rheological and mechanical properties of polybutadiene were altered from rubber material to thermoplastic elastomer [20-30].

1-1-2 Epoxidation Reaction

So far the introduction of epoxy groups along the polymer backbone is one of the most promising methods of modifying polydienes and has been known for a long time. Natural rubber was first epoxidized by Pommer and Burkhard as early as in 1922 [31]. The chemistry of epoxidation of unsaturated compounds and subsequent ring-opening reactions has been studied by Rosowsky [32] and Swern [33]. Swern and Witnauer [34] showed that epoxidation is a stereospecific reaction and the rate of epoxidation is governed by the substituents on the double bond. The ease and positioning of ring-

opening of epoxy groups is again controlled by the neighboring groups. Epoxidation of diene elastomers can be achieved by the action of various peroxides and peracids.

Peroxides and Hydroperoxides

Benzoyl peroxide has been used to epoxidize polyisoprene while BR has been epoxidized with *t*-butylhydroperoxide in the presence of dioxomolybdenum-*bis*-(acetyl acetonate) as catalyst [35]. Although peroxides have been used for epoxidation, peracids appear to be more effective.

Direct Use of Peracids

Peracids are used to epoxidize diene rubbers either in solution or as latex. Thus, BR and NR dissolved in solvents have been epoxidized using peroxybenzoic acid [36,37]. Monoperphthalic acid was used by Roux et al. to epoxidize various diene rubbers, such as *cis* and *trans* polyisoprene, SBR, BR and polychloroprene (CR) [38]. Dreyfuss and Kennedy [39] epoxidized ethylene propylene diene rubber (EPDM) and butyl rubber (IIR) with the same reagent. Among the various peroxycarboxylic acids used for epoxidation of diene polymers, *m*-chloroperbenzoic acid has been found to be the most efficient. Dreyfuss and Kennedy [40] showed that it reacts with the double bonds of diene polymers quantitatively. One of the most widely used peracids is peracetic acid. Gelling and Smith [41] reported the use of this peracid to epoxidize NR in the latex-stage. Nippon Zeon Company Ltd. patented the process of solution epoxidation of BR with peracetic acid at 60 °C, but this reagent possesses problems as a health hazard and loss of available oxygen [42]. Burfield et al. studied the kinetics of epoxidation with peracetic acid [43].

***In-Situ* Generated Peracids**

This process accomplishes the charging of hydrogen peroxide and a carboxylic acid with the epoxidizing substrate in a reaction vessel. Hydrogen peroxide and the carboxylic acid react to generate the peracid *in-situ*, which in turn reacts with the olefinic double bonds to convert them into epoxy groups. A schematic representation of the reaction is given in **Figure 1-5**.

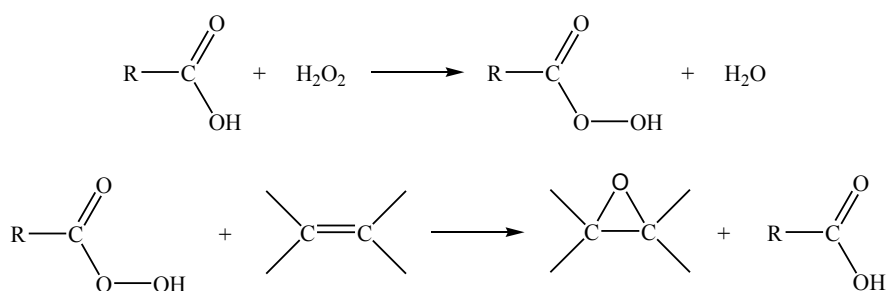


Figure 1-5: *In-situ* epoxidation reaction.

The *in-situ* generated peroxy carboxylic acid has been used for the production of low-molecular weight products and is found to be a better epoxidizing agent for diene polymers, in terms of reaction rate, product purity and yield. Mainly acetic and formic acids have been used to generate *in-situ* peroxy carboxylic acids to epoxidize various diene polymers, in which the effects of temperature [44-46], solvents [47], catalysts [48], acid to hydrogen peroxide ratio [49] and the microstructures of polydienes [50] on the degree of epoxidation were fully investigated.

H₂O₂ in the Presence of an Organic or Organometallic Catalyst

The yield of the product from the *in-situ* formed peracid route was good when the epoxidation level was less than 50%, but above the 50% level formation of the side products becomes a concern. In addition, trace amounts of unreacted acid present in the rubber matrix become detrimental from a stability point of view. Several attempts to epoxidizing polydienes were made in the presence of metal-based catalysts, in which it is successful to produce side-product-free epoxidized NR, BR, SBR, EPDM and IIR rubbers [51-54].

The reactivity of different double bonds toward epoxidation for a particular reagent were found to be: *cis*-1,4-polyisoprene > *trans*-1,4-polyisoprene > 1,2 and 3,4-polyisoprene > *cis*-1,4-polybutadiene > *trans*-1,4-polybutadiene > 1,2-polybutadiene > SBR > polychloroprene [38,50]. The reason for such reactivity is that any group adjacent to the double bond that enriches the electron density of C=C will contribute to a higher rate of epoxidation. Polychloroprene, which has an electron-withdrawing

group, shows the least tendency toward epoxidation.

1-1-3 Other Reactions

The addition of thiols or mercaptans to low molecular-weight compounds has been known since the early part of the last century. This reaction, which tolerates presence of most functional groups (-OH, -NH₂, -COOH, etc.) without disturbing the proceeding of radical grafting, is well-established in synthetic organic chemistry [55], however, due to the low grafting efficiency, the reaction have not received much attention and only limited applications in polymeric systems have been investigated. The thiol addition reaction may occur by a radical mechanism, in which the radical addition appears to be more efficient if the initiator is added in small increments rather than in one dose [56]. Much of the early work involved alkane thiols that add to the double bonds of natural rubber, in which it is found that *cis*, *trans* isomerization also occurs during the addition of the thiol reagent to the double bonds but apart from this complication the reaction is straightforward and no substitution occurs at the methylene groups in the polyisoprene chain. The representative reaction scheme of a thiol compound added to natural rubber is shown in **Figure 1-6**.

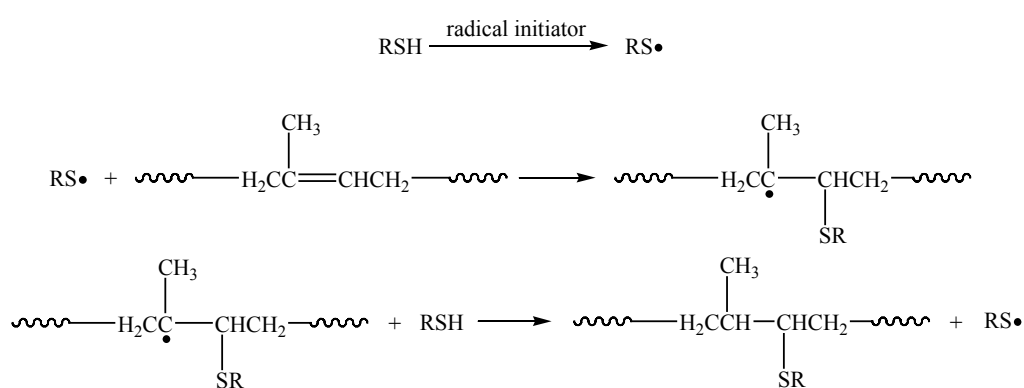
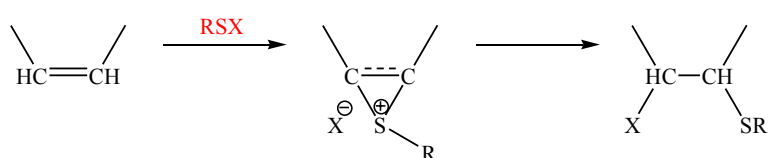


Figure1-6: Thiol addition at the double bonds of natural rubber.

In 1948, Serniuk et al. used the addition of thiol radicals on the 1,2-units of a

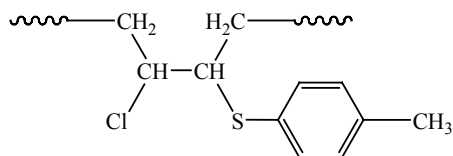
polybutadiene (PB) chain to obtain further information on the structure of butadiene polymers and copolymers [57]. Mercaptans were also used for the modification of natural and synthetic rubbers [58-61]. Boutevin et al. used 2-mercaptoethanol to increase the hydroxyl functionality of PB [62]. The same group also described the synthesis of phosphonated PB by grafting PB with a phosphorus-containing mercaptan, an interesting material for the preparation of fire retardant polyurethane network [63]. However, in neither case did the addition of the mercaptan go to completion. Schapman et al. carried out the modification of PB with (3-mercaptopropyl)-triethoxysilane and studied the influence of the mercaptan and initiator concentration on the progress of the reaction [64]. In the case of the modification of butadiene containing copolymers, the free radical addition of mercaptan has been employed to introduce carboxyl and ester functionalities into styrene/butadiene random copolymers (SBR) [65,66].

There has been periodic interest in the modification of unsaturated rubbers using sulphenyl derivatives. These compounds have the general structure RS-X, where X is an electronegative function such as halogen (sulphenyl halides), -NR'₂ (sulphenamides), -OR' (sulphenyl esters) and -OCOR' (sulphenyl carboxylates). A large number of these compounds have been reviewed by Kharasch [67] and Kühle [68], in which they show that the sulphenyl chlorides have been the most intensively investigated sulphenyl derivatives. As it is, many sulphenyl derivatives add readily, in some case rapidly, to olefinic double bonds. Superficially the addition is similar to that of thiols but in this case the mechanism is a polar one involving the intermediate formation of the episulphonium ion:

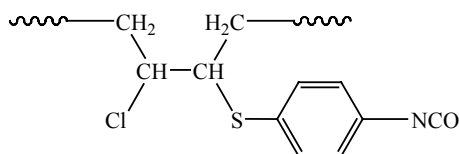


A number of patents describe the addition of aromatic sulphenyl halides to *cis*-polybutadiene, *cis*-polyisoprene and butyl rubber. It is claimed that the modification provides a rubbery material of high resistivity with excellent adhesion to metals and

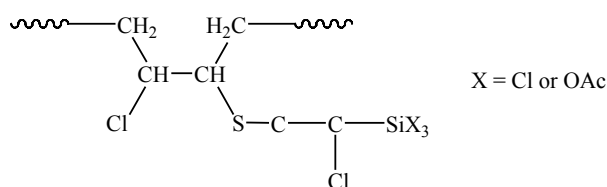
rubbery polymers. Toluene-*p*-sulphenyl chloride adds rapidly at room temperature to *cis*-1,4-polybutadiene in solution [69]. Quantitative conversion of double bonds is easily reached, providing a new polymer with the repeat unit:



As the degree of saturation is increased, the physical properties change from those of an elastomer to a leathery material and ultimately to a hard resin at complete saturation. There is no loss in solubility with increasing degree of reaction, but the glass transition temperature, as expected, increases [69]. The reaction of sulphenyl derivatives promises to be useful for attaching functional groups to unsaturated polymers. Holdschmidt et al. successfully modified *cis*-1,4-polybutadiene with *p*-isocyanatobenzenesulphenyl chloride [70]:



The isocyanate group offers possibilities for further modification by reaction with hydroxyl- and amino-compounds, including polymers terminated by these groups. Organosilicon moieties have been attached to unsaturated polymers by the addition of 2-chloro-2-(trichlorosilyl)- and 2-chloro-2-(triacetoxysilyl)-ethylsulphenyl chlorides [71]. These adducts are capable of further modification since chloro- and acetoxy-silanes are highly reactive.



1-2 Sol-gel Process

Sols are dispersions of colloidal particles in a liquid. *Colloids* are solid particles with diameters of 1-100 nm [72]. A *gel* is an interconnected network with pores of sub-micrometer dimensions and polymeric chains whose average length is greater than a micrometer. The term “gel” embraces a diversity of combinations of substances that can be classified in four categories as discussed by Flory: (1) well-ordered lamellar structures; (2) covalent polymeric networks, completely disordered; (3) polymer networks formed through physical aggregation, predominantly disordered; (4) particular disordered structures [73].

Interest in the sol-gel processing of inorganic ceramic and glass materials began as early as the mid-1900s with Ebelman [74,75], and Graham’s [76] studies on silica gels. In these early investigations it was observed that the hydrolysis of tetraethyl orthosilicate (TEOS), $\text{Si}(\text{OC}_2\text{H}_5)_4$, under acidic conditions yielded SiO_2 in the form of a “glass-like material”. For a period from the late 1800s through the 1920s gels became of considerable interest to chemists stimulated by the phenomenon of Liesegang rings [77,78] formed from gels. Many noted chemists, including Ostwald [79] and Lord Rayleigh [80], investigated the problem of the periodic precipitation phenomena that lead to the formation of Liesegang rings and the growth of crystals from gels. A huge volume of descriptive literature resulted from these studies [81-83] but a relatively sparse understanding of the physical-chemical principles [78]. Roy and co-workers [84-87] recognized the potential for achieving very high levels of chemical homogeneity in colloidal gels and used the sol-gel method in the 1950s and 1960s to synthesize a large number of novel ceramic oxide compositions, involving Al, Si, Ti, Zr, etc., that could not be made using traditional ceramic powder methods. During the same period Iler’s pioneering work in silica chemistry [88] led to the commercial development of colloidal silica powders, Du Pont’s colloidal Ludox spheres. Stöber et al. extended Iler’s findings to show that using ammonia as a catalyst for the TEOS hydrolysis reaction could control both the morphology and size of the powders, yielding the so-called Stöber spherical silica powder [89]. The final size of the spherical silica powder is a function of the initial concentration of water

and ammonia, the type of silicon alkoxide (methyl, ethyl, pentyl, esters, etc.) and alcohol (methyl, ethyl, butyl, pentyl) mixture used [90], and reactant temperature [91].

The motivation for sol-gel processing is primarily the potentially higher purity and homogeneity and the lower processing temperatures associated with sol-gels compared with traditional glass melting or ceramic powder methods. Mackenzie [91] summarized a number of potential advantages and disadvantages and the relative economics of sol-gel methods in general. Hench and colleagues compared quantitatively the merits of sol-gel-derived silica optics over the alternative high-temperature processing methods [92]. The goal of sol-gel processing and ultra-structure processing in general is to control the surfaces and interfaces of materials during the earliest stages of production [93]. Long-term reliability of a material is usually limited by localized variations in the physical chemistry of the surface and interfaces within the material. The emphasis on ultra-structure processing is on limiting and controlling physical chemical variability by the production of uniquely homogeneous structures or producing extremely fine-scale (10-100 nm) second phases. Creating controlled surface compositional gradients and achieving unique physical properties by combining inorganic and organic materials are also goals of ultra-structure processing.

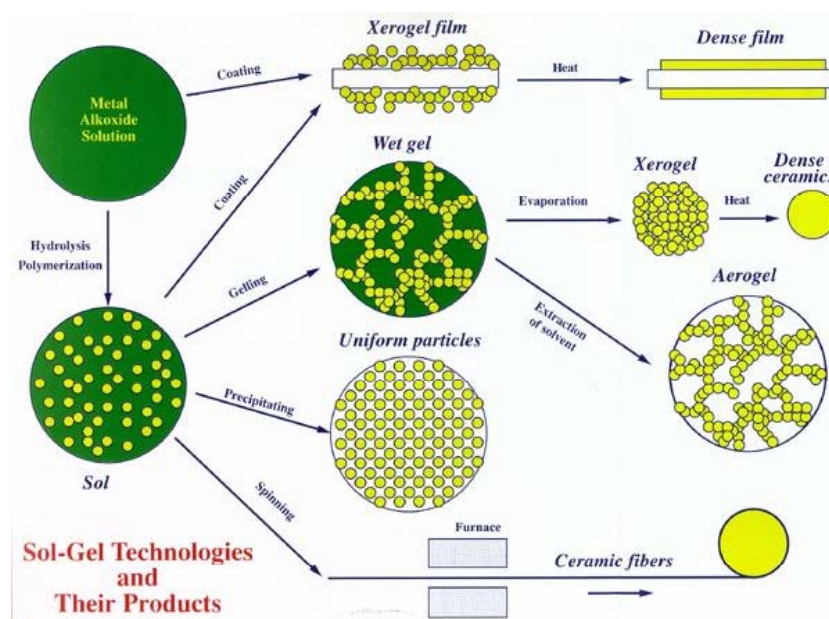


Figure1-7: Sol-gel process in general. [88]

The sol-gel process, as the name implies, involves the evolution of inorganic networks through the formation of a colloidal suspension (sol) and gelation of the sol to form a network in a continuous liquid phase (gel), as shown in [Figure 1-7](#).

The precursors for synthesizing these colloids consist of a metal or metalloid element surrounded by various reactive ligands. Metal alkoxides are most popular because they react readily with water. The most widely used metal alkoxides are the alkoxysilanes, such as tetramethoxysilane (TMOS) and tetraethoxysilane (TEOS). However, other alkoxides such as aluminates, titanates, and borates are also commonly used in the sol-gel process, often mixed with TEOS. At the functional group level, three reactions are generally used to describe the sol-gel process: (a) hydrolysis, (b) water condensation, and (c) alcohol condensation. This general reaction scheme can be seen in [Figure 1-8](#).

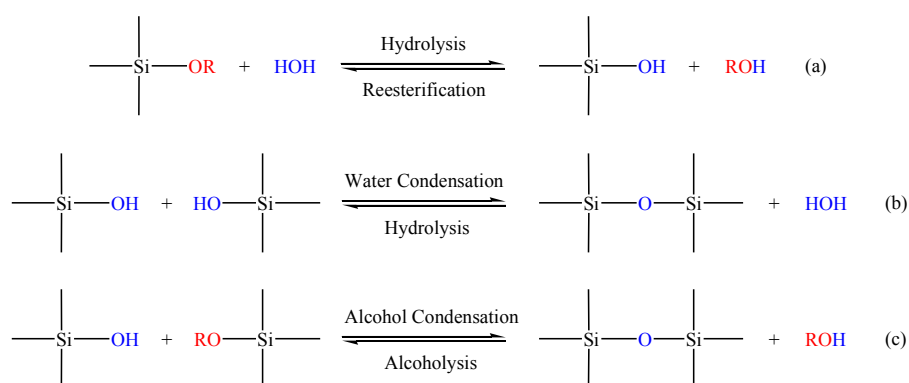


Figure 1-8: Reaction scheme of sol-gel process.

However, the characteristics and properties of a particular sol-gel inorganic network are related to a number of factors that affect the rate of hydrolysis and condensation reactions, such as pH, temperature and time of reaction, reagent concentrations, catalyst nature and concentration, H₂O/Si molar ratio (R), aging temperature and time, and drying [93,94]. Of the factors listed above, pH, nature and concentration of catalyst, H₂O/Si molar ratio (R), and temperature have been identified as most important. Thus, by controlling these factors, it is possible to vary the structure and properties of the sol-gel-derived inorganic network over wide ranges. For example, Sakka et al. observed that the hydrolysis of TEOS utilizing R values of 1 to 2 and 0.01

M HCl as a catalyst yields a viscous, spinnable solution. It was further shown, that these solutions exhibited a strong concentration dependence on the intrinsic viscosity and a power law dependence of the reduced viscosity on the number average molecular weight:

$$[\eta] = k[Mn]^\alpha \quad (1-1)$$

where α value varies from 0.5 to 1.0, which indicates a linear or slightly branched molecule or chain. In contrast, when R values greater than 2 and/or base catalysts were utilized, solutions were produced which were not spinnable at equivalent viscosities [95,96]. Values of α ranged from 0.1 to 0.5, indicating spherical or disk shaped particles. These results are consistent with the structures that emerge under the conditions employed by the Stöber process for preparing SiO₂ powders [89]. It was further shown that with hydrolysis under basic conditions and the R values ranging from 7 to 25, mono-disperse, spherical particles could be produced. Generally speaking, the hydrolysis reaction (a), through the addition of water, replaces alkoxide groups (OR) with hydroxyl groups (OH). Subsequent condensation reactions, (b) and (c), involving the silanol groups (Si-OH) produce siloxane bonds (Si-O-Si) plus the by-products water or alcohol. Under most conditions, condensation commences before hydrolysis is complete. However, conditions such as, pH, H₂O/Si molar ratio (R), and catalyst can force completion of hydrolysis before condensation begins [97]. Additionally, because water and alkoxides are immiscible, a mutual solvent such as an alcohol is utilized. With the presence of this homogenizing agent, alcohol, hydrolysis is facilitated due to the miscibility of the alkoxide and water. As the number of siloxane bonds increases, the individual molecules are bridged and jointly aggregate in the sol. When the sol particles aggregate, or inter-knit into a network, a gel is formed. Upon drying, trapped volatiles (water, alcohol, etc.) are driven off and the network shrinks as further condensation can occur. It should be emphasized, however, that the addition of solvents and certain reaction conditions may promote esterification and depolymerization reactions according to the reverse of equations (a), (b), and (c). In the following sections, specific factors that influence the hydrolysis and condensation reactions, that is, nature and concentration of catalyst, and H₂O/Si molar ratio (R), of the sol-gel process will be discussed.

1-2-1 Hydrolysis

Nature and Concentration of Catalyst

Although hydrolysis can occur without addition of external catalysts, it is most rapid and complete when they are employed. Mineral acids (HCl) and ammonia are most generally used, however, other catalysts are acetic acid, KOH, amines, KF, and HF [98]. Additionally, it has been observed that the rate and extent of the hydrolysis reaction is most influenced by the strength and concentration of the acid- or base catalyst. Aelion et al. found that all strong acids behave similarly, whereas weaker acids require longer reaction times to achieve the same extent of reaction. From a plot of the logarithm of the hydrolysis rate constant versus acid concentration, a slope of one was obtained. They concluded that the reaction was first-order in acid concentration. Under basic conditions, the hydrolysis reaction was found to be first-order in base concentration. However, as the TEOS concentration was increased the reaction deviated from a simple first-order to a more complicated second-order reaction. With weaker bases such as ammonium hydroxide and pyridine, measurable speeds of reaction were produced only if large concentrations were present. Therefore, compared to acidic conditions, base hydrolysis kinetics is more strongly affected by the nature of the solvent [99].

Acid-Catalyzed Mechanism

Under acidic conditions, it is likely that an alkoxy group is protonated in a rapid first step. Electron density is withdrawn from the silicon atom, making it more electrophilic and thus more susceptible to attack from water. This results in the formation of a penta-coordinated transition state with significant SN₂-type character [98]. The transition state decays by displacement of an alcohol and inversion of the silicon tetrahedron, as seen in Figure 1-9.

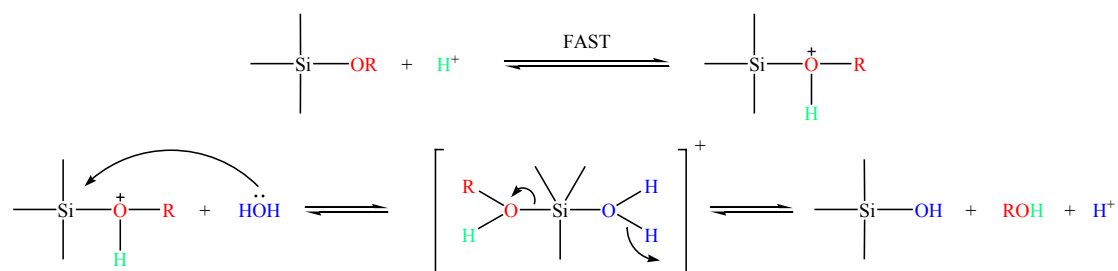


Figure 1-9: Acid-catalyzed hydrolysis.

Base-Catalyzed Mechanism

Base-catalyzed hydrolysis of silicon alkoxides proceeds much more slowly than acid-catalyzed hydrolysis at an equivalent catalyst concentration [99]. Basic alkoxide oxygens tend to repel the nucleophile, -OH . However, once an initial hydrolysis has occurred, following reactions proceed stepwise, with each subsequent alkoxide group being more easily removed from the monomer than the previous one [100]. Therefore, more highly hydrolyzed silicones are more prone to attack. Additionally, hydrolysis of the forming polymer is more sterically hindered than the hydrolysis of a monomer. Although hydrolysis in alkaline environments is slow, it still tends to be complete and irreversible [97]. Thus, under basic conditions, it is likely that water dissociates to produce hydroxyl anions in a rapid first step. The hydroxyl anion then attacks the silicon atom. Again, an $\text{S}_{\text{N}}2$ -type mechanism has been proposed in which the -OH displaces -OR with inversion of the silicon tetrahedron. This is seen in Figure 1-10.

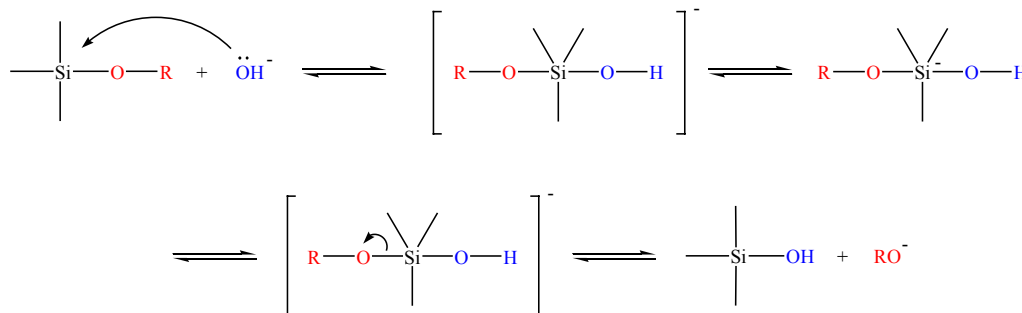


Figure 1-10: Base-catalyzed hydrolysis.

$\text{H}_2\text{O}/\text{Si}$ Molar Ratio (R)

As described before, the hydrolysis reaction has been performed with R values ranging from less than 1 to over 50, depending on the desired polysilicate product. From equation 2, an increased value of R is expected to promote the hydrolysis reaction. Aelion et al. found the acid-catalyzed hydrolysis of TEOS to be first-order in water concentration; however, they observed an apparent zero-order dependence of the water concentration under basic conditions [99]. This is probably due to the production of monomers by siloxane bond hydrolysis and redistribution reactions (i.e.,

reverse reactions (b) and (c)). Nonetheless, the most obvious effect of the increased value of R is the acceleration of the hydrolysis reaction. Additionally, higher values of R caused more complete hydrolysis of monomers before significant condensation occurs. Different extents of monomer hydrolysis should affect the relative rates of the alcohol- or water-producing condensation reactions. Generally, with under-stoichiometric additions of water ($R \ll 2$), the alcohol producing-condensation mechanism is favored, whereas, the water-forming condensation reaction is favored when $R > 2.28$. Although increased values of R generally promote hydrolysis, when R is increased while maintaining a constant solvent: silicate ratio, the silicate concentration is reduced. This in turn reduces the hydrolysis and condensation rates, resulting in longer gelation times. Finally, since water is the by-product of the condensation reaction (reaction (c)), large values of R promote siloxane bond hydrolysis (reverse (c)).

1-2-2 Condensation

Nature and Concentration of Catalyst

As with hydrolysis, condensation can proceed without catalyst, however, their use in organosiloxanes is highly helpful. Furthermore, the same type of catalysts are employed: generally those compounds that exhibit acidic or basic characteristics. It has been shown that condensation reactions are acid and base specific [101]. In addition, Iler has shown that under more basic conditions, gelation times are observed to increase [88]. Condensation reactions continue to proceed, however, gelation does not occur. Again, catalysts that dictate a specific pH value can and do drive the type of silica particle produced as seen in the previous discussion on pH.

Acid-Catalyzed Mechanism

It is generally believed that the acid-catalyzed condensation mechanism involves a protonated silanol species. Protonation of the silanol makes the silicon more electrophilic and thus susceptible to nucleophilic attack. The most basic silanol species (silanols contained in monomers or weakly branched oligomers) are the most

likely to be protonated. Therefore, condensation reactions may occur preferentially between neutral species and protonated silanols situated on monomers, end groups of chains, and so on [98].

Base-Catalyzed Mechanism

The most widely accepted mechanism for the base-catalyzed condensation reaction involves the attack of a nucleophilic deprotonated silanol on a neutral silicic acid [88], the mechanism is as shown in Figure 1-11.

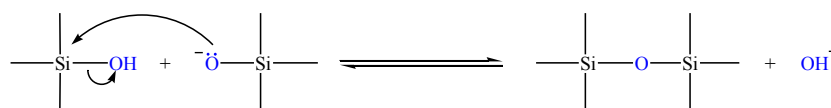


Figure 1-11: Nucleophilic attack to form siloxane bond.

Furthermore, it is generally believed that the base-catalyzed condensation mechanism involves penta- or hexa-coordinated silicon intermediates or transition states, similar to that of a SN2 type mechanism [98].

1-2-3 Summary

According to Iler, Sol-gel polymerization occurs in three stages:

1. Polymerization of monomers to form particles
2. Growth of particles
3. Linking of particles into chains, then networks that extend throughout the liquid medium, thickening into a gel.

Many factors affect the resulting silica network, such as, pH, temperature and time of reaction, reagent concentrations, catalyst nature and concentration, H₂O/Si molar ratio (R), aging temperature and time. However, it can generally be said that sol-gel derived silicon oxide networks, under acid-catalyzed conditions, yield primarily linear

or randomly branched polymers that entangle and form additional branches resulting in gelation. On the other hand, silicon oxide networks derived under base-catalyzed conditions yield more highly branched clusters that do not interpenetrate prior to gelation and thus behave as discrete clusters, as shown in [Figure 1-12](#).

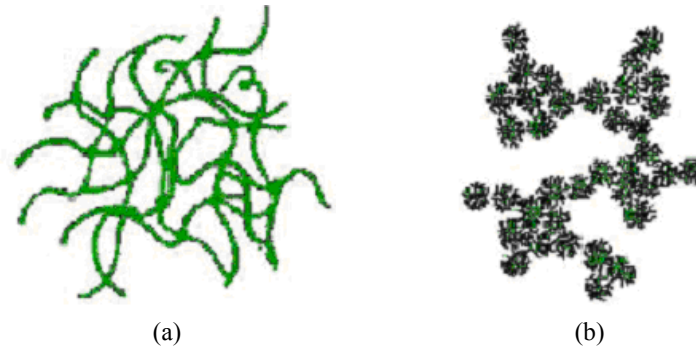


Figure 1-12: Different sol-gel conditions: (a) acid-catalyzed, and (b) base-catalyzed sol-gel polymer.

1-3 Tire Performance

Vehicle tires are the most prominent rubber articles regarding volume and importance. They are also the most important design and spring element of the vehicle. More than half of the Natural Rubber and Synthetic Rubbers produced in the world are consumed in the tire industry [\[102\]](#).

The Idea of a solid wheel has been around for over 5000 years but a Scotsman, Richard Thompson (1822-1873), first patented the concept of a pneumatic tire in 1845. His invention was for elastic bearing to be fitted around a carriage wheel so that it could be filled with spring, stuffed with horsehair or even inflated with air. The claim was for the carriage on which it was fitted to be drawn along using less power and to make it less noisy when in motion. The original idea was soon forgotten, but it was recollected and reinvented by another Scottish gentleman, John Boyd Dunlop in 1888. Dunlop invented and patented a system where air is constrained within a rubber and

fabric tube fitted to the edge of a wheel. The tires produced were found to roll well over cobbles, going further and more smoothly than the conventional solid tires, in which the most valuable material of all in the development history is therefore that free and abundant gas that is all around us, air [103-107].

In 1895, only 9 years after Daimler produced the first commercial automobile, the Michelin brothers applied pneumatic tire technology to four-wheeled vehicles as a commercial product. Since then tires and wheels have gone through a slow period of evolution with just an occasional discrete revolution such as the advent of the radial ply tire in 1948 or the early attempts at run-flat technology in the mid 1970s.

If one just thinks for a moment about what goes on when he or she drives a car. Each tire, and there are only four on cars; a few more on trucks, touches the ground on an area not much larger than the average person's footprint. First of all the tire must then transmit the driving, braking and cornering forces applied by the vehicle as it accelerates, brakes and goes around corners over a wide range of speeds in dry and wet conditions, even in atrocious storms, snow and ice. It must carry this out without generating excessive noise within the environment. Roads may be covered by potholes, ramps, sharp objects, debris and all other manner of obstacles. The tire must be capable of passing these obstacles without detracting from the ride comfort of the occupants or sustaining any damage that may cause it to fail.

There are several performance criteria the designer and compounder must consider; Out of these criteria, three main performance qualifications are of exceptional importance: traction, abrasion resistance and rolling resistance.

A tire must deliver high traction and cornering forces on wet and dry roads, also called wet and dry grip. The steering characteristics under all handling situations should be predictable. This high traction force between tread and road is necessary to create a good grip on the road surface, thereby avoiding slippage. Traction depends on three main tire features: the tire construction; the tire tread compound and tread profile design; the road conditions.

A tire must also show low wear and good durability and give a satisfactory driving comfort: the resistance to abrasion should be as high as possible to create a high mileage [108,109]. With regard to environment and driving costs, the rolling resistance should be as low as possible, leading to low fuel consumption. Rolling resistance, being one of the main performance criteria covered in this thesis, will be discussed in more detail in section 1-3-1.

Figure 1-13 shows these three basic performances considered in modern tire production. These three most important properties: traction, abrasion resistance and rolling resistance form the so called: “Magic Triangle” of tire properties. “Triangle” means that a balance must be found between these properties. “Magic” means these requirements are always conflicting, as it is impossible to improve all three characteristics at the same time. A compromise between these characteristics should always be achieved [110].

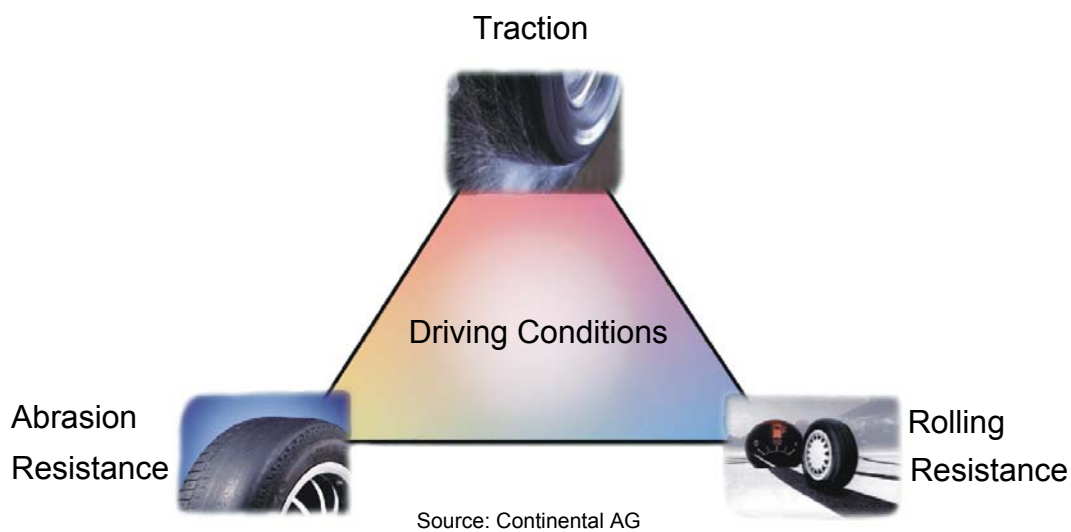


Figure 1-13: Tire performance.

1-3-1 Rolling Resistance

The last three decades, tire producers have put much emphasis on reduction of the tire rolling resistance, while simultaneously improving other aspects of tire performance

[111]. A tire consumes energy as it is constantly changing its shape as the sidewalls deflect and the tread flattens into the contact patch. This consumes a small but definite amount of energy by virtue of hysteresis and consequently fuel [109]. A tread with high hysteresis losses will have a higher rolling resistance and a better road grabbing than a tread made out of resilient rubber. By use of proper tread compounds, the hysteresis characteristics can be controlled, thereby providing lower rolling resistance without affecting wet grip and wear resistance. Rolling resistance plays a surprisingly large role in fuel consumption: for passenger cars and light trucks, a decrease in rolling resistance with minimum of 10% can yield fuel consumption improvements ranging from 0.5 to 1.5%, and for heavy trucks, an improvement of 10% can yield fuel savings of 1.5 to 3.0% [108]. That is to say, that for passenger cars and light trucks 5 to 15% of the fuel energy is consumed by rolling resistance and 15 to 30% for heavy trucks. Figure 1-14 schematically shows the basic mechanism how rolling force contributes to fuel consumption.

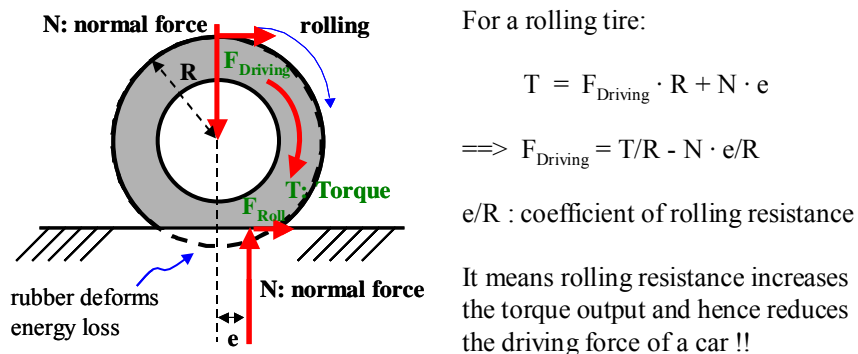


Figure 1-14: Mechanism of rolling resistance.

Tire rolling resistance is defined as the energy consumed per unit distance of travel as a tire rolls under load. The energy consumed by the tire is converted into heat. The proper unit of rolling resistance is J/m, which equals Newton, the unit of force. It should be kept in mind though, that there is a distinct qualitative difference between the two units. Rolling resistance is the energy loss per unit length and, hence, a scalar – not a vector as the unit Newton would imply. Thus, the rolling resistance, F_{Roll} , is given by the equation:

$$F_{\text{Roll}} = dH / dL \quad (1-2)$$

where dH denotes the energy converted by the tire into heat over the distance dL traveled. Or, since $dL = Vdt$, where V is the road speed of the tire, and dt is the time taken for a distance dL ,

$$F_{\text{Roll}} = \dot{H} / V \quad (1-3)$$

where the rate of heat development $\dot{H} (\equiv dH / dt)$ is often termed power loss, P_{Roll} :

$$\dot{H} \equiv P_{\text{Roll}} \quad (1-4)$$

Then,

$$F_{\text{Roll}} = P_{\text{Roll}} / V \quad (1-5)$$

Holt and Wormeley [112] considered the energy balance of the tire roadwheel system. They argued that part of the input power delivered by the motor is converted into heat by the tire, and the rest, the output power, is used to drive the car. Thus,

$$P_{\text{Roll}} = P_{\text{Input}} - P_{\text{Output}} \quad (1-6)$$

where P_{Input} is the tire input power provided by the motor, and P_{Output} is the tire output power supplied to traction of the car. The rest, P_{Roll} , is dissipated as heat by the tire through deformation and friction. Therefore,

$$F_{\text{Roll}} = \frac{P_{\text{Input}} - P_{\text{Output}}}{V} \quad (1-7)$$

This is the general definition of rolling resistance. It includes all losses within the tire structure, between tire and roadway, and within the roadway. Bearing losses are excluded however [108].

1-3-2 Relation Between Rolling Resistance and Dynamic Mechanical Properties

Rubber is a viscoelastic material: as it deforms, a fraction of the energy is stored elastically, and the remainder is dissipated as heat in a hysteretic manner. These hysteretic losses within a tire, as well as aerodynamic drag and friction in the contact patch and with the rim, are irrecoverable losses and contribute to the total drag force on a moving vehicle.

Viscoelastic behavior is most commonly characterized in a so-called oscillatory dynamic mechanical measurement. The application of an oscillatory shear strain γ of angular frequency ω ,

$$\gamma(t) = \gamma_0 \sin \omega t \quad (1-8)$$

results for a linear viscoelastic material in a sinusoidal stress σ , out of phase with the strain:

$$\sigma(t) = \sigma_0 \sin (\omega t + \delta) \quad (1-9)$$

The strain lags behind the stress by a phase angle δ .

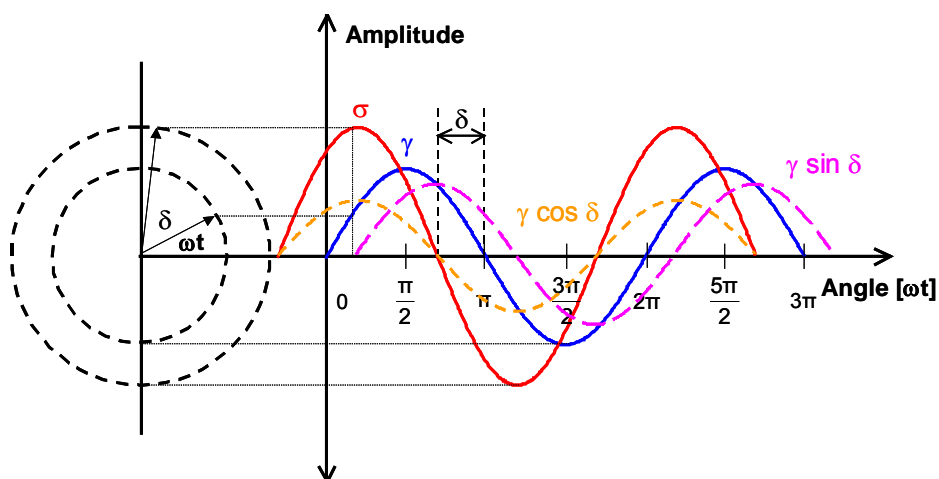


Figure 1-15: Vector illustration of an oscillating stress leading a strain by a phase angle δ .

A vector representation of the dependence of γ and σ on ωt is shown in [Figure 1-15](#). [Equation \(1-9\)](#) can be rewritten as follows:

$$\sigma(t) = (\sigma_0 \cos\delta) \sin \omega t + (\sigma_0 \sin\delta) \cos \omega t \quad (1-10)$$

This equation shows that the stress consists of two components: one in phase with the strain ($\sigma_0 \cos\delta$); the other 90° out of phase ($\sigma_0 \sin\delta$). Therefore, if we apply a shear stress upon a viscoelastic material the relationship between stress and strain in this dynamic experiment can be redefined by writing:

$$\sigma(t) = \gamma_0 (G' \sin \omega t + G'' \cos \omega t) \quad (1-11)$$

in which

$$G' = \frac{\sigma_0}{\gamma_0} \cos \delta \quad \text{and} \quad G'' = \frac{\sigma_0}{\gamma_0} \sin \delta \quad (1-12)$$

Thus the component of stress $G'\gamma_0$ is in phase with the oscillatory strain; the component $G''\gamma_0$ is 90° out of phase. G' is termed the shear storage modulus, and G'' the shear loss modulus. The tangent of the phase angle, also called loss tangent is:

$$\tan \delta = \frac{G''}{G'} \quad (1-13)$$

The effects of rubber materials on rolling loss are profound and complex. Rolling loss depends not only on the basic polymers, their blending ratios, the other compounding ingredients and the state of cure, but also on the stresses, strains, temperatures and frequencies these materials experience at different locations in the tire structure. Schuring [108] assumed that nearly all energy losses in a tire must be generated in the rubber. The general dissipative mechanism of viscoelastic materials such as rubber is reasonably well understood; but its mathematical formulation is rather complex, except in simple models. The model preferred for tires is the one-dimensional, sinusoidal deformation of linear viscoelastic materials in a geometrically simple specimen, as exemplified above. In reality, rubber deformations in a tire are neither

one-dimensional nor sinusoidal. Each volume element of a tire, as it goes through one tire revolution, is subjected to a three-dimensional, non-sinusoidal strain cycle, which hampers a mathematical analysis. The analysis is complicated further by nonlinearities of the material response, and by temperature and frequency effects. These are complexities, which forced tire researchers to resort to the much simpler linear, sinusoidal model: [Figure 1-15](#). The model is only a rough guide but, if handled judiciously, it is quite useful.

1-3-3 Rubber Polymer Influences on Tire Performance

The $\tan \delta$ level has a highly predictive value for the most important properties of a tire tread. The significance of the $\tan \delta$ curve for a number of important functions of a tread rubber is shown in [Figure 1-16](#) [112].

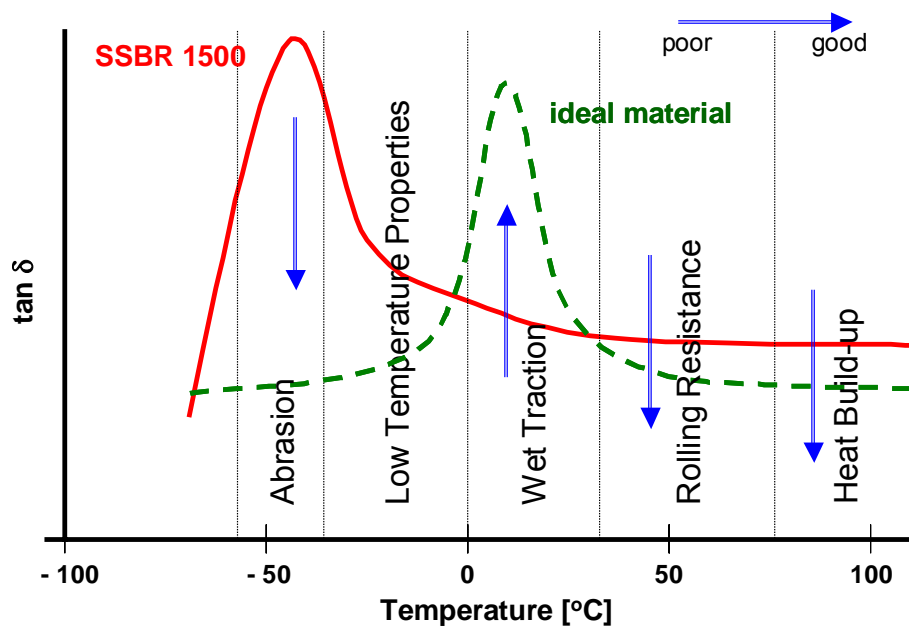


Figure 1-16: Tread rubber evaluation, $\tan \delta$ as a function of temperature.

A prediction of the suitability of the tire tread for winter use can be made with the help of the behavior in the low temperature range, where the beginning of the glass

state indicated by a strong upturn of the loss tangent marks the limit of elastic behavior. As an indication of skidding behavior (grip, traction) on wet, icy or dry roads, the level of the loss tangent around 0°C till approximately +30 °C can be taken. The range between +30 °C and approximately +70 °C comprises the running temperatures of a tire. Under these temperature conditions the loss factor essentially determines the degree of rolling resistance. At temperatures exceeding this limit the tire enters into a region of maximum stress and reaches the limit of safe operation with the risk of destruction. The values of $\tan \delta$ in this range indicate the heat build-up behavior and allow an estimate of incipient thermal decomposition and the limit of good tire performance [112].

Since the peak in $\tan \delta$ correlates with the glass transition temperature T_g of the polymer, this value became a tool for the selection of a suitable tire rubber. Nordsiek reported the dependence of $\tan \delta$ on temperature with several rubber polymers [112]. The summary of the experimental results supported the concept of the relation between rubber molecular mobility and viscoelastic behavior. The choice of the rubber polymer with the optimum glass transition temperature T_g therefore plays a key role in achieving a compromise between many tire requirements [112,113]. The influence of different rubber polymers is not further investigated in this thesis. In all cases the same combinations of Solution-SBR and BR are employed.

1-4 Payne Effect

One of the consequences of incorporation of filler into a polymer is a considerable change in dynamic mechanical properties of the rubber, both modulus and hysteresis. This phenomenon has been investigated in depth especially in relation to rubber products. It has been recognized that for a given polymer and cure system, the filler parameters influence dynamic properties in different ways, i.e., multiple mechanisms may be involved. Among others, filler networking, both its architecture and strength

seems to be the main (though not the only) parameter to govern the dynamic behavior of the filled rubber.

Figure 1-17 shows the classification of filler structures. It is known that the filler aggregates in the polymer matrix have a tendency to associate to agglomerates, especially at high loading, leading to chain-like filler structures or clusters. These are generally termed secondary structure or, in some cases, filler network, even though the latter is not comparable to the continuous three-dimensional polymer network structure. The existence of the filler network and its impact on rubber properties, viscoelastic behavior in particular, has been reviewed in depth in several articles [114-116].

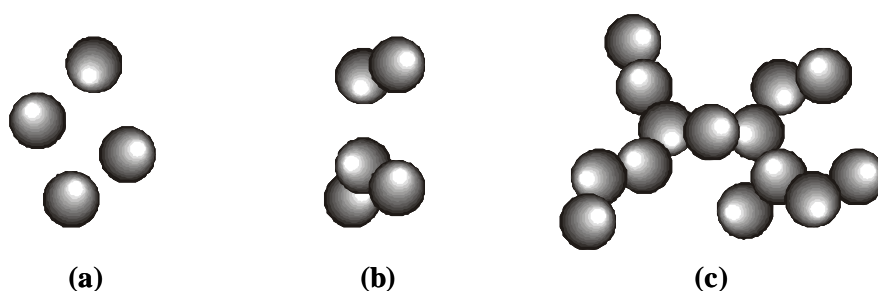


Figure 1-17: Filler and filler network classification: (a) primary particles (10-100 nm), (b) aggregates (30-300 nm) and (c) agglomerates ($\sim \mu\text{m}$).

The dependence of the complex modulus (G^*) on strain amplitude for a reinforced rubber vulcanizate is shown in **Figure 1-18**. The G^* modulus of a filled rubber vulcanizate is built up of: (a) a strain-independent contribution of the rubber network, which is the result of the proportionality of the G^* modulus to νRT , where ν is the number of moles of elastically effective network chains per unit volume, as a result of vulcanization. However, if the material is not a vulcanizate, a non-crosslinked rubber for example, the G^* modulus will depend on strain amplitude, just as a viscoelastic material having a linear viscoelastic region and non-linear viscoelastic region. (b) a strain-independent hydrodynamic effect of the filler, which was first derived by A. Einstein [117,118], and later exemplified for rubber in the Guth, Gold and Smallwood equation [119,120].

$$G = G_0 (1 + 2.5\phi + 14.1\phi^2) \quad (1-14)$$

where G and G_0 are the moduli of the filled and unfilled system, respectively, and ϕ is the volume fraction of the filler. (c) a strain-independent effect due to chemical/physical rubber to filler interaction and (d) a strain-dependent contribution of the filler, which is also known as the Payne effect [121].

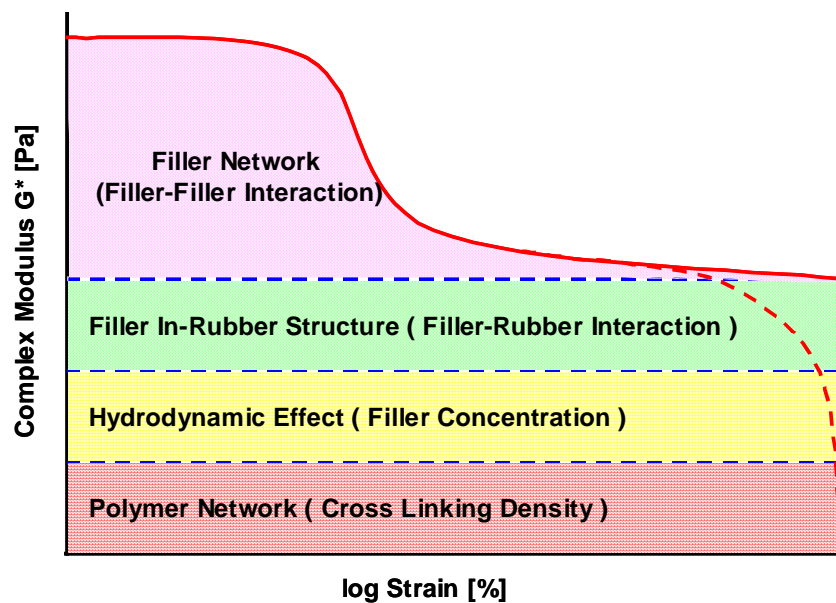


Figure 1-18: The G^* modulus as a function of strain for a reinforced rubber. (solid line for vulcanizates and dash line for uncrosslinked rubbers)

It has been proposed that the reinforcement mechanism of carbon black is essentially due to the formation of a co-continuous network. Upon applying a strain to a rubber sample, since the chemical polymer network is stronger than the physical filler one, the polymer network stores energy and the filler network is disrupted, which releases energy in the form of heat. Upon removal of the strain, the stored energy present in the polymeric matrix reforms the filler network. These exchanges of energy are possible because the filler network is mechanically “trapped” in the net of the polymer matrix, which is the deformation carrier. This mechanism has been proposed by several researchers [121-123] and is supported by the experiments of Gerspacher et al. [124,115]. The disruption of the silica network in rubber matrix generally takes place

at a higher strain than that of carbon black, which means that the energy loss for a rolling tire is therefore less for a silica reinforced compound when compared to a carbon black compound, resulting in a lower hysteresis and consequently a lower rolling resistance of the tire [126].

At low temperature or high frequency deformation, the polymer plays the main role. The effect of the polymer, which is still part of the filler polymer network, is complemented by the influences of filler subnetworks or clusters [127]. At moderate-high temperature / high frequency or at low temperature / low frequency deformations, the filler-filler interactions are mostly responsible for the reinforcement and hysteretic effects [128]. The filler particles are, considering their volume concentration, in the “percolation” state, i.e., the filler particles touch each other in a “filler-network” [122,129,130].

In order to explain the Payne effect in another way, Göritz supposed a Langmuir type polymer chain adsorption to the carbon black. The network density in the neighborhood of a filler particle increases due to the adsorption of network chains to the filler particle. A distribution of differently strong links between filler particles and segments of elastomer chains exists. During mixing, the first macromolecules that come in contact with the filler “see” the whole free surface. When a first link is formed, neighboring segments have a higher probability to attach to the next interaction position and so on. This process comes to an end when all neighboring sites on the filler surface are occupied. Chains, which arrive at the surface at a later moment, find the area widely covered and their possibilities of stabilization are reduced. The last chains attached to the sites have very weak links to the particle. The storage modulus of a filled rubber sample, caused by entropy elasticity is directly proportional to the network density and the temperature. In the adsorption mechanism the network density is composed of three different parts: (a) the chemical network density; (b) the density of network chains attached by stable bonds to the filler surface; and (c) the density of unstable bonds between chains and filler. Upon increasing desorption of chains with increasing deformation, these weakly bonded chains are torn off the filler surface and the density of unstable bonds between chains and filler decreases. By means of the theory of entropy elasticity it is then possible to describe

the strain dependent modulus using a derivation similar to the theory of Langmuir concerning adsorption of gases to a planar metal surface [131].

Freund and Niedermeier first studied the applicability of both filler networking and polymer adsorption theories [132]. Carbon black, graphitized carbon black, silica and hydrophobized silica were used to vary filler agglomeration and polymer adsorption strength both in non-polar NR and polar NBR. Payne type testing of all compounds, including a relaxation study, led to the conclusion that the filler networking is the dominant Payne mechanism in the case of silica, whereas polymer adsorption dominates in the case of carbon black.

As discussed above, the Payne effect has a closer relationship with the interaction between polymer matrix and filler. Nevertheless, in tire industry application of the Payne effect will surely affect the tire performance described before; that is, the stronger the Payne effect is the more rolling resistance a tire tread compound will possess. Nowadays even though there is no exact mechanism that explains the contribution to the rolling resistance, people believe that the filler agglomeration – deagglomeration mechanism is to be blamed for the high rolling resistance since the agglomeration – deagglomeration process causes heat dissipation and therefore increases the rolling resistance [133,134]. However, how can one come to a compromise between filler reinforcement and the Payne effect, which means on one hand how to reduce the tendency of filler to form agglomerates but on the other hand such an action will not suppress the filler reinforcement? The answer would be how to control the filler-filler and polymer-filler interactions.

1-5 Polymer-Filler Interaction

The use of fillers in polymers has been going on for years. In the early history of filled polymers, fillers were added to the polymers rather empirically. Wood flour was one

of the first fillers used to in thermosetting phenol-formaldehyde resins because the combination was found to be valuable in enhancing certain properties whereas the addition of some other finely divided material to such resin conferred no benefit at all and hence was never done. The presence of the wood flour increased strength and prevented cracking of the resin by reducing the exotherm in the curing reaction. Similarly the use of carbon black as a reinforcing agent in rubber has been going on since early in the last century, as it was a major factor in the development of durable automobile tires. Glass fiber in nylon and asbestos in polypropylene confer useful properties but, if the filler and polymer are switched, i.e. asbestos is put into nylon and glass into polypropylene the results are not nearly so good unless the fillers are treated with appropriate coupling agents. Polypropylene is also often filled with calcium carbonate and talc with constructive results. Little thought was given in the early days towards the reasons for the observed behavior. Nowadays, however, the marriage of filler to polymer is done on a scientific basis and the reason for the addition of the specific filler can be elucidated on the desired property it imparts [135]. Some typical examples of filled polymer systems using a thermoset, elastomer and thermoplastic are given in [Table 1-1](#).

Table 1-1: Some typical examples of filled polymer systems

Polymer	Filler
Thermoset: Phenol-formaldehyde resin	Wood flour / Cotton flock
Elastomer: Styrene butadiene rubber	Carbon black
Thermoplastic: Polypropylene	Calcium carbonate / Talc

The escalating cost of engineering thermoplastics over the last couple of decades and the awareness of dwindling supply of petrochemicals has created renewed incentives to restrict the quantities of resins used through the addition of fillers to the polymer matrix. Besides savings in cost, certain fillers provide the added advantage of modifying specific mechanical, thermal and electrical properties of thermoplastic products as can be seen from [Table 1-2](#) [136].

Table 1-2: Reasons for the use of fillers in thermoplastics

1.	To increase stiffness, strength and dimensional stability
2.	To increase toughness or impact strength
3.	To increase heat deflection temperature
4.	To increase mechanical damping
5.	To reduce permeability to gases and liquids
6.	To modify electrical properties
7.	To reduce the cost of the product

The improvements in mechanical properties through the use of fillers acting as reinforcing agents have been discussed in detail by Nielsen and Landel [137]. Such filled systems wherein the fillers provide reinforcements are often referred to as reinforced polymer systems or reinforced plastics. One or more of the physical, mechanical and thermal properties of polymers can be effectively modified by the use of different types of fillers. For example, in the tire industry, the addition of the carbon black in vulcanized rubber enhances properties, such as elastic modulus, tear strength and abrasion resistance [138-140] and it also influences extrusion characteristics like extrudate distortion, extensional viscosity and die swell behavior [141-147]. Thus, carbon black functions as a reinforcing agent and a processing aid in the rubber industry. Different types of fillers serve different types of purposes. For instance, titanium trihydroxide acts as an economic flame retardant and smoke suppressing agent. In most applications, the proper balance of properties is no less important than an improvement in one property can in all likely lead to deterioration of others and consequently, it is the overall performance of the filler in a given formulation that determines its choice. The predominant function of some typical fillers is given in Table 1-3 [136].

Table 1-3: Predominant function of some typical fillers

Function	Typical Fillers
Cost Saving	Woodflour, saw dust, cotton flock
Reinforcement	Glass fiber, cellulosic fibers, synthetic fibers, asbestos fibers
Hardness	Metallic powders, mineral powders, silica, graphite
Thermal Insulation	Asbestos, ceramic oxides, silica
Chemical Resistance	Glass fibers, synthetic fibers, metallic oxides, graphite

Let us go back to the question, why glass fiber in nylon and asbestos in polypropylene confer useful properties but, if the filler and polymer are switched, i.e. asbestos is put into nylon and glass into polypropylene the results are not nearly so good unless the fillers are treated with appropriate coupling agents? The answer to it is obvious: the polymer-filler interaction plays an extremely important role.

When a filler is added to a polymer with the specific idea of reinforcement, it is expected that the reinforcing filler component that is strong and stiff should bear most of the load or stress applied to the system while the polymer which is of low strength, fairly tough and extensible should effectively transmit the load to the filler. Maximum reinforcement benefits would be achieved from fillers when conditions occur in accordance with this concept [148]. In order that the load transfer takes place effectively, the matrix must have sufficiently high cohesive and interfacial shear strength. Thus, apart from the filler and the polymer, it is the inevitable region between them, namely, the interphase that plays a vital role in the fabrication and subsequent behavior of the filled polymer systems in service. The interface is that region separating the filler from the polymer and comprises the area in the vicinity of the interface. It would be synonymous with the word “interfacial region” but different from the term “interface”, which would be the contacting surface where two materials under consideration meet. Thus, for some filled polymer systems, there could exist more than one interface as in the case of coated fiber-filler polymer. In such case, the fiber-coating interface and the coating-polymer interface would have characteristics of their own. However, normally a less atomistic view is taken and the characteristics of the “interface region”, as a whole, are generally investigated.

Good mechanical strength can be achieved only if there is uniform and efficient stress transfer through a strong interfacial bond between the filler and the polymer. It is important that the bond is uniform on a fine scale rather than unevenly strong in local regions as areas of the polymer-filler interface that are not in contact begin to act as cracks under an applied stress. In the absence of a good interfacial bond, fibrous fillers will pull out of the polymer and result in an annulment of the reinforcing effect [149]. Controlled debonding at the weak polymer-filler interface, on the other hand, results in increased toughness of the system, but at the cost of concurrent decrease in

the transverse strength on fatigue resistance [150]. The toughness of a filled polymer material can be adjudged by the behavior of the polymer-filler interface during fracture. Toughness is about to be enhanced when the state of stress ahead of a crack tip is blunted during interfacial failure due to weak interfacial bonding.

Such a phenomenon of polymer-filler delamination has been observed [151] at stress less than half of the ultimate tensile strength in the case of glass fiber reinforced resin. Thus one can see why it is difficult to achieve a simultaneous increase in mechanical strength and toughness. Attempts have been made to solve the tensile strength/toughness dilemma [152,153] through the use of duplex fibers or coupled rubber fillers or duplex systems of metal coated carbon fibers, but with only limited success. In any case, it is the behavior of interface during service that finally decides the performance of the filled polymer product. It is, therefore, prudent to understand the interface through a careful study of the polymer.

Three possible types of filler-polymer interactions can be visualized as follows:

Type 1

The filler is only physically present in a nonpolar polymer with no interaction at all. The filler then merely acts as a diluent and is expected to weaken the material by its presence.

Type 2

The filler is physically present in the polymer and its surface is wetted by the polymer either because of the inherent polymer affinity for the filler or because the filler is appropriately surface treated to provide this affinity. A physical bond is developed causing an increase in the frictional resistance to the movement of the filler and thereby resulting in an increase in the tensile strength and a decrease in the elongation at break. The extent of the increase in the mechanical properties is dependent on the strength of the mechanical bonding between the filler and the polymer.

Type 3

The filler establishes a true chemical bond with the polymer. This results in an exceptional strengthening effect. This type of interaction may be present in carbon

black reinforced rubber and glass fiber reinforced plastics, though in both cases it might be debatable whether an actual chemical bond or a strong physical adhesion as in Type 2 is present. In order to illustrate the interaction of Type 2 and Type 3, **Figure 1-19** shows the function groups on carbon black and silica surface [154-158].

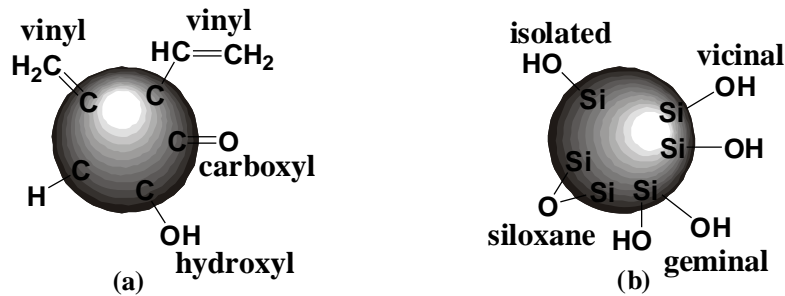


Figure 1-19: Various groups on (a) carbon black and (b) silica surface.

For carbon black filled rubbers, the nature of the interaction has been studied [159,160] and though it is generally agreed that van der Waals forces are sufficient to give reinforcing effects, there is evidence of chemical grafting between carbon-black and rubber [161]. The process by which polymer molecules are grafted to carbon black surface is by free radical mechanism, as carbon black is an efficient free radical acceptor. The high degree of adhesion produced by such chemical grafting probably contributes to the extraordinary reinforcing properties of these materials. However, excessive grafting can also lead to difficulties in dispersing the filler, formation of an undesirable large gel fraction before vulcanization and other deleterious effects that might affect product properties. Several possible polymer-filler interactions of carbon black and silica filled polymer systems are schematically shown in **Figure 1-20**.

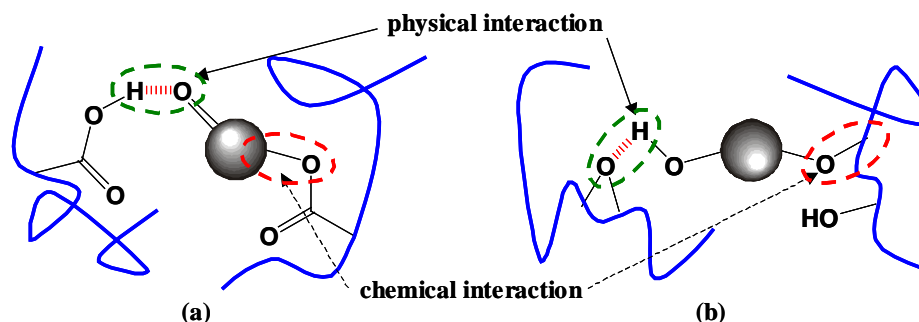


Figure 1-20: Interaction (a) between carbon black and carboxylated nitrile rubber (b) between silica and epoxidized rubber.

Fillers of Type 1 are called “inactive fillers”, whereas fillers of Type 2 and 3 are named “active fillers”. Some illustrative examples are as shown in [Figure 1-21](#) and [Figure 1-22](#) [162].

Example : **Tensile properties**

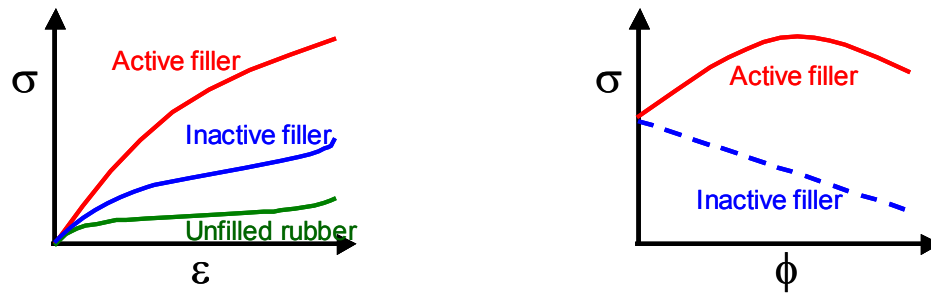


Figure 1-21: Different reinforcing behavior of fillers. (σ : stress, ε : strain, Φ : filler volume fraction)

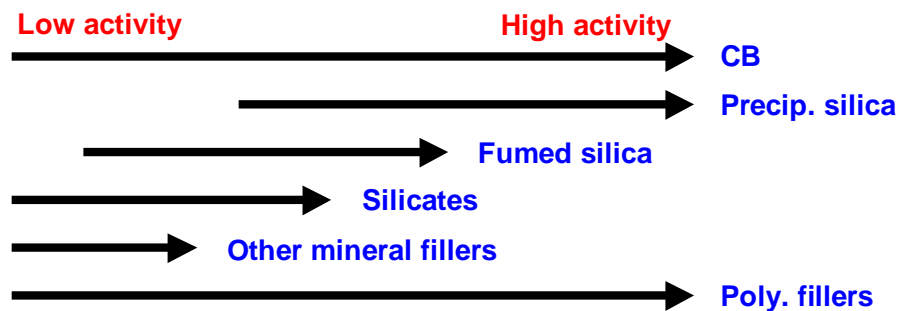


Figure 1-22: Comparison of filler activity.

In the following there are short descriptions of some of factors affecting polymer-filler interaction.

1-5-1 Filler Geometry (shape, size and porosity)

The filler-polymer interaction can be adjudged from the effect of filler addition on the stiffening and strengthening characteristics of the polymers. At a given volume concentration of the filler, the degree of stiffening is directly proportional to the filler surface area. It has been shown [163] that high mechanical strength is achieved

through strong interfacial bonds when interfacial areas are extremely high, e.g. through the use of 1 mm^3 of a 50% by volume fiber composite with a fiber diameter of $7.5 \text{ }\mu\text{m}$ giving an approximate interfacial area of 6500 mm^2 . However, large interfacial area would lead to physicochemical instability resulting in spheroidization and agglomeration of the filler due to high interfacial energy. The presence of undispersed or agglomerated zones of fillers is generally detrimental to the properties of the filled polymer systems. Surface area depends upon the particle size, particle shape and porosity of the filler. It has been shown [164] that there is a linear relationship between the increase in stiffness and particle size for fillers below 0.2 mm in average particle diameter. The same cannot be said about larger particle sizes. For carbon black filled elastomers, it has been shown [159] that for significant reinforcement, the mean particle diameter between $0.02 \text{ }\mu\text{m}$ and $0.05 \text{ }\mu\text{m}$ is most effective. Small particle size is, therefore, a prerequisite for reinforcement. Particle consideration, such as inability to attain satisfactory dispersion and interference with vulcanization reactions due to high adsorptive capacity, place a lower limit on the particle size, which in the case of carbon blacks is around 150 \AA . Porosity too, has a direct influence on polymer-filler interaction as in the case of non-crystalline fibers that have room inside their amorphous structures for other materials like water causing a detrimental effect on adhesion and reinforcing properties.

1-5-2 Volume Fraction

Concentrations of fillers are preferably measured by volume than by weight due to the wide variations in the densities of available fillers. A number of the filled polymer system properties like tensile strength, abrasion resistance, viscosity of the melts, etc. have been found to show change at some critical volume fraction. A reduction in tensile strength, for example, is observed when the pigment content in paints is above “the critical pigment volume concentration” (CPVC). Anomalies in the behavior at high levels of extender pigment in the coating area have led to the development of the concept of CPVC, which is the pigment volume content at which enough binder is present to fill all the voids between the pigment particles. The CPVC is directly

related to the surface area of the pigment particles and hence affects the polymer-filler interaction. It can be calculated by the method described in Bierwagen [165]. Figure 1-23 shows one of the models elucidating the effect of filler amount. As can be seen, an increase in the filler content decreases the average particle distance. When a relative small number of particles are present (a), particles influence the surrounding matrix but there is enough available bulk that is not subject to interactions with the filler surface (line shaded areas are particles of filler, black areas correspond to the tightly bound resin, gray areas to loosely bound resin). There is only one glass transition. This indicates that the mobility of the polymer next to the immobilized layer is not significantly affected. The magnitude of the first glass transition does increase indicating that some polymer is involved in the formation of tightly bound layers. When the concentration of particles becomes close to a critical value, the mobility of all chains in the composite becomes affected (b). At this point, the second glass transition temperature can be detected, signifying formation of a substantial amount of loosely bound polymer. As more filler particles are incorporated (c) more of the polymer becomes tightly bound pretty much in amount proportional to the increase in filler concentration. The second glass transition temperature becomes less easy to detect. At high concentration of filler (d), most of the polymer is immobilized [166].

The conclusions from this model are:

- (c) Tightly and loosely bound polymer are two distinct and different physical materials
- (b) Filler-matrix interaction affects chain mobility
- (c) Chain mobility is controlled by the concentration of filler

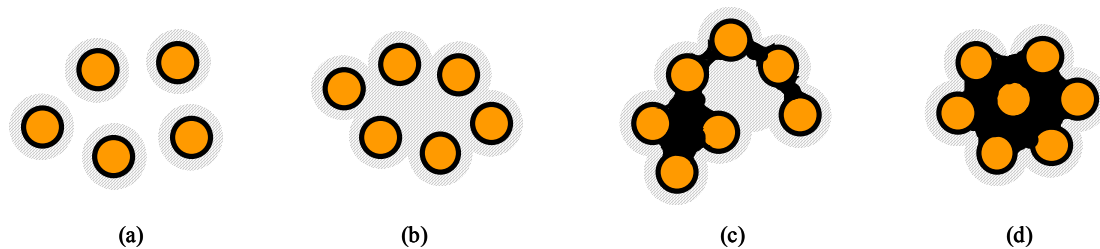


Figure 1-23: Schematic model of morphological transformations in filled polymers: (a) silica content less than 10 wt%, (b) silica content ~ 10 wt%, (c) silica content ~ 20 wt%, (d) silica content over 50 wt%.

The second model shows how chains can get attached to the surface of carbon black, as shown in [Figure 1-24](#). The chain can be attached at a single point (a), at more than one point (b), or the chain can bridge two or more filler particles (c). This model does not indicate if a chemical reaction is involved but it can be anticipated that, since reactive functional groups can be positioned in the middle of a chain or at its ends, the reactions may involve chain segment or terminal group. It might be thought that both models complement each other by showing that the probability of particles bridging increases with filler concentration. In a rubber matrix, one can expect that a gel is formed but only when configuration (c) occurs (two or more particles are connected) in the systems.

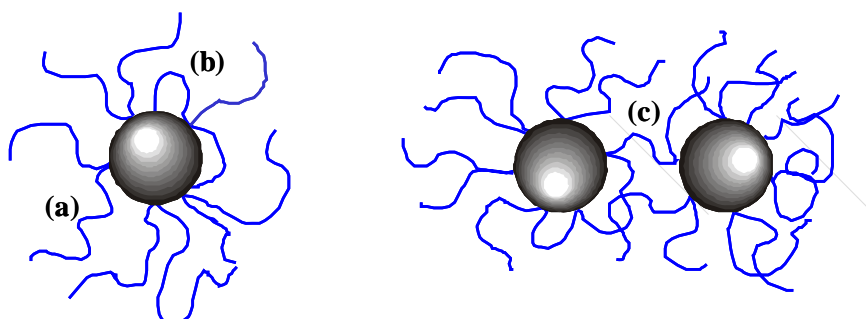


Figure 1-24: The concept of segmental interaction with a carbon black surface.

Hydrodynamic effect, due to the addition of fillers into polymer systems, could also contribute to additional polymer-filler interaction. The mathematical expression of hydrodynamic effect was first derived by A. Einstein, and later exemplified for rubber in Guth, Gold and Smallwood equation (see [Equation \(1-4\)](#), Section 1-4).

1-5-3 Filler Surface

Apart from surface area and volume fraction of the filler, it is the microconfiguration and frictional properties of the filler surface that plays an important role in the polymer-filler interaction [\[167\]](#). Friction implies the presence of a compressive force normal to the interface; however, studies show that friction itself is a mere local

welding between the filler and the polymer and is dependent to a great extent on the filler surface. Smooth filler surfaces offer less opportunity for keying adhesion of the polymer chain but they are more easily wetted than those with less regular surfaces. Of course, smooth fillers would have on their surfaces uneven and undeclared adsorbed layers of water and contaminants that can seriously affect adhesion. In any case, perfect wetting i.e. complete exclusion of voids on the filler surface is generally an ideal situation that is never achievable. Thus, two fillers with different surface properties will surely affect their reinforcing ability and they contribute to different physical reinforcements to a polymer.

1-5-4 Wettability

It has been shown [168,169] that a prerequisite for a good bond is an intimate contact between the filler and the polymer brought together by good wetting. The wetting of a solid by a liquid is dependent upon the relative interfacial energies among the solid, liquid and vapor phase above them as shown in **Figure 1-25**.

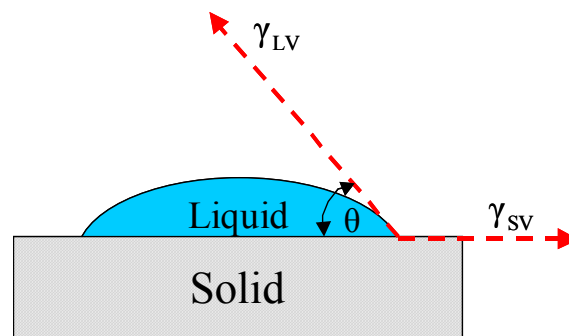


Figure 1-25: Schematic diagram showing the contact angle when a liquid drop has contact with a flat solid surface.

The contact angle θ of the liquid drop on the flat solid is given as:

$$\cos \theta = \frac{\gamma_{SV} - \gamma_{LS}}{\gamma_{LV}} \quad (1-15)$$

where γ is the interfacial energy and subscripts S, L, V refer to solid, liquid and vapor phases, respectively. When the liquid drop on the solid surface exhibits a finite contact angle with the solid, the surface is not completely wetted and only particle bonding is possible. If, however, a liquid drop collapses on the solid surface spontaneously by spreading and wets the surface uniformly, the contact angle is zero. It thus seems logical to aim for situations where the critical surface tension, γ_c values on the filler surface are considerably less than those of the polymer. The foregoing condition for good wetting is based on the presence of the solid, liquid and vapor phases to be in chemical equilibrium, though in reality, this is not truly the case. There are normally adsorbed gases on the solid surface leading to an increase in the contact angle. Also the solid surface is not smooth leading to a decrease in the contact angle. The liquid itself contains contaminants that prevent chemical equilibrium. All these factors greatly affect the wetting behavior. In filled polymer systems, if a polymer does not wet the filler then there is entrapment of air bubbles, which act as stress risers and represent areas of zero load transfer, thereby weakening the filled polymer product. The strength realized in many reinforced systems is limited by the presence of voids or air inclusion in the system [170]. There are other aspects of wetting that significantly affect the filled polymer properties. For example, the rate at which a polymer wets particular filler and the final degree of wetting determines the strength of the system. Wettability also affects the ease of dispersion of the filler in the polymer that in turn is a factor in the property effectiveness. It has been shown that in the case of carbon black reinforced rubber, wettability of the pigments not only ensures easy dispersion of the filler in the rubber but also implies a favorable relation between carbon black-elastomer adhesion and elastomer cohesion which ensures that the effectiveness of the filler would hold even up to high ultimate elongations of several 100% and survive strains that would befall during normal service conditions.

1-5-5 Filler Surface Modification

Fillers that are generally used as reinforcement are fibers with diameters of the order of 10 μm corresponding to a surface area of the order of 10^3 - 10^5 cm^2/g . The surface

chemistry and physics of the polymer-filler interface show considerable variations affecting the wetting and bonding characteristics which are determining factors in the ultimate bond strength of the polymer to the filler. The best way of determining whether a satisfactory strong bond has been established is by correlating the final physical properties of the filled system based upon maximum fiber density. In practice, as pointed out earlier, it is difficult to form a strong bond between the filler and the matrix due to poor wettability of the filler especially in non-polar, high melt viscosity polymeric systems, and due to the presence of contaminants or multi-molecular layers of water on the mostly hydrophilic surfaces of fillers, which prevents physical or chemical adsorption of the polymer molecules. The interfacial bond can be enhanced and the mechanical performance of the composites improved by suitable surface modification. These days, most of the fillers are pretreated before they are used as secondary phases in composite materials. A surface modification helps in a number of ways:

- (a) helps to protect surface cracks, surface steps, notches and other imperfections from damage during processing and thereby preserve the strength of the materials;
- (b) helps to eliminate the influence of surface flaws and abrasion during processing of the filled systems;
- (c) helps to keep out excessive damp and protects the filler from water attack which weakens the composite;
- (d) helps to develop a stronger interfacial bond and hence improves the strength of the composite.

The most common pretreatments involve surface cleaning and the use of surface modifiers in the form of sizes, finishes and coupling agents. The type of pretreatment to be given depends on the type of the filler. For example, in the case of carbonaceous or graphite fibers which are useful for ablative and structural purposes, it has been found [171] that the fibers are difficult to wet with conventional thermosetting resins, are contaminated with pyrolysis products and alkali salts, and contain moisture - all of which are detrimental for interfacial bonding. The surface of graphite fibers is essentially chemically neutral and possesses low and variable surface area. Hence, a surface cleaning is first done by way of controlled oxidation through a 24-hour boiling process in 60% nitric acid that increases the chemical functionality and surface area of

the fiber. The surface cleaned fibers are then protected by means of a polymeric coating of polyvinyl alcohol, polyvinyl acetate, polyacrylonitrile or polyurethane. Surface cleaning of graphite fibers and protecting the altered surface by polymeric coating is very important [172]. Oxidized graphite fibers are known to give three times as high composite shear strength as non-oxidized fibers and the reason for this is attributed more to higher chemical activity than increased surface area. This is understandable because the pores induced during oxidation would be too small to be occupied by the large polymer molecules of the matrix. Other means of physically interlocking graphite fibers with the polymer matrix have been recently contemplated through the growth of whiskers like those of silicon carbide, for example, with successful results in achieving higher inter-laminar strengths. In the case of glass fibers which are by far the most widely used inorganic fillers as reinforcing agents in unsaturated polyesters and epoxy resins, the surface treatment is done through the use of surface modifiers which may be in the form of finishes, sizes or coupling agents. Coatings improve the strength of the fiber. Furthermore, the fracture of a composite containing coated fibers is known to occur without fiber pull out, unlike the case of uncoated fibers. The coatings, which are generally applied to “as drawn” glass fibers, improve wetting and adhesion and help to provide sufficient protection to withstand the rigors of mechanical abrasions and chemical attacks, and also exclude moisture from the interface in filled polymer systems. A good example for this is the proprietary HTS epoxy finish that is applied to some glass fibers as they are drawn. In the case of fused silica fibers, another way of achieving the same benefits as those through finishes and sizes is achieved by the deposition of carbon on freshly drawn fibers. Finishes, which are commonly used for coating fibers, include vinyltrichlorosilane, styrene, ethylene oxide, epichlorohydrin, phenylsilane and vinyl dimethylethoxysilane. These, when applied to the fibers, help to eliminate or reduce polymer crazing or strains adjacent to the fiber apart from improving the interfacial bonding. Amine and silane finishes provide strong interfacial bonding with oxide-type fibers but they are worthless for accomplishing the same function with carbonaceous or graphite fibers for which surface cleaning, as discussed earlier, is necessary for providing interfacial bonding. **Table 1-4** summarizes modification methods and reasons why such modification methods are used with the common fillers [136].

Table 1-4: Filler modification and its reasons

Modification	Reason	Typical fillers
Physical treatment methods thermal (800-1500°C) thermal oxygen plasma surface oxidation (various) microwave plasma acetylene gas, plasma	improved dispersion interaction with CSPE reinforcement interfacial adhesion water resistance reinforcement	talc silica carbon fibers carbon fibers aramid fibers CaCO ₃ , carbon fibers
Acid treatment hydrochloric stearic stearic stearic fatty metal soaps maleic derivatives	rubber crosslinking reinforcement surface hydrophobization dispersion dispersion interaction with H(CH ₂) _n H	ZnO CaCO ₃ clay, CaCO ₃ Al(OH) ₃ , Mg(OH) ₂ Al(OH) ₃ , Mg(OH) ₂ CaCO ₃
Isocyanates isocyanate isocyanate polyethylene glycol, isocyanate	reinforcement colloidal behavior resistance to solvents	hydroxyapatite kaolin kaolin
Other low- molecular dimeric aluminates oxyethylenes with N and S hexadecanol dicarboxylic acid anhydride doping and coating	reinforcement surface hydrophobization interaction with matrix sedimentation weather resistance	CaCO ₃ silica silica Al(OH) ₃ TiO ₂
Grafting and resin coating radical trapping polymerization various polymers acrylamide acrylamide maleic anhydride PP functionalized polymers polybutadiene coating polyether	grafting initiation improved dispersion colloidal dispersion toughening, reinforcement wettability, hydrophilic coupling dispersion, adhesion chromatographic media dispersability	carbon black carbon black carbon black, silica CaCO ₃ BaSO ₄ mica, talc Al(OH) ₃ , Mg(OH) ₂ Al ₂ O ₃ carbon whisker
Silane treatment silanes silanes silanes silanes silanes silanes silanes silanes silanes silanes silanes silanes silanes silanes silanes silanes silanes	coupling controlled coating thickness increase/decrease adhesion understanding surface fire retardant improvement reinforcement adhesion to matrix whisker orientation coupling and adhesion coupling coupling ion exchange reinforcement nanoparticle synthesis Dense covering Matrix-mineral adhesion reinforcement	clay silica silica fumed silica Mg(OH) ₂ wollastonite basalt, sludge A1B whisker kaoline, talc, mica Al(OH) ₃ , Mg(OH) ₂ GF, silica, quartz hydroxyapatite natural fibers ceramic, metal silica silica, steel, plastic wollastonite

Table 1-4: Filler modification and its reasons (continued)

polymeric silane titanates titanates	nanoparticles dispersion, coupling coupling, reinforcement	silica Al(OH) ₃ , Mg(OH) ₂ kaolin, silicate, CaCO ₃
--	--	--

1-5-6 Carbon Black versus Silica

Among all the fillers studied, carbon black and silica are the most popular reinforcing agents and have been appealing to much attention in a rubber compound [173-181]. As shown in **Figure 1-19**, Carbon black and silica have very different surface chemistry from each other. A variety of functional groups such as hydroxyl, carbonyl, lactone, pyrone, ketone, quinine and phenol exist on the carbon black surface, however, the amount is limited and the functionality depends on the way it is produced [174]. Silica has a number of hydroxyl groups on the surface, which results in strong filler-filler interactions and adsorption of polar materials by hydrogen bonds [178, 182]. Since the hydrogen bonds in between the individual particles are strong, silica particles can aggregate tightly [179,183]. Its property causes a poor dispersion of silica resulting in a delay of the scorch time and reduction of the delta torque of silica-filled rubber compounds, and hence these compounds have different cure characteristics from those of carbon black-filled ones [184-191]. However, carbon black and silica have one thing in common: the particles themselves are prone to form strong inter-particle aggregates and networks, and the tendency thereof depends on the surface characteristics. Therefore, taking these two most-popular fillers into account, it is worth to compare them with each other.

Application of carbon black results in an increase in strength properties, wear resistance and fatigue resistance. In addition, due to its color it is an excellent absorber of light. It therefore absorbs most of the ultraviolet components of sunlight, which can otherwise initiate oxidative degradation of the rubber. The effects of the presence of carbon black on the dynamic mechanical properties of various types of filled rubbers has been studied by many authors [192-195] and was reviewed by Medalia [196]. The general conclusion from this early work was that the incorporation

of carbon black in different types of rubber gives in most of the cases an increase in the storage and loss moduli, G' and G'' , and an increase in hysteresis, $\tan \delta$. Increases in strain amplitude give decreases in storage modulus G' and increases in G'' simultaneously: the so-called Payne effect, which was discussed in Section 1-4.

Especially after the introduction of the Energy[®] tire by Michelin, silica has become more important as reinforcing filler for the rubber industry. The main reason is the greater reinforcing power of silica when compared to carbon black. The additional effect of temperature dependence of $\tan \delta$ for reinforced rubber compounds is the result of the characteristics of reinforcing fillers to form a filler network. Comparing the $\tan \delta$ values at different temperatures for silica and carbon black filled rubbers, as shown in **Figure 1-26**, a considerably higher $\tan \delta$ is found for the silica filled one at lower temperatures ($\sim 0^\circ\text{C}$), which means that silica provides a better traction for a rubber compound in tire tread application. In the rubbery state (at temperatures beyond 20°C) the value of $\tan \delta$ and hysteresis of a carbon black filled rubber is still higher than that of a silica filled one, meaning that silica provides a better (less) rolling resistance for tire application (A).

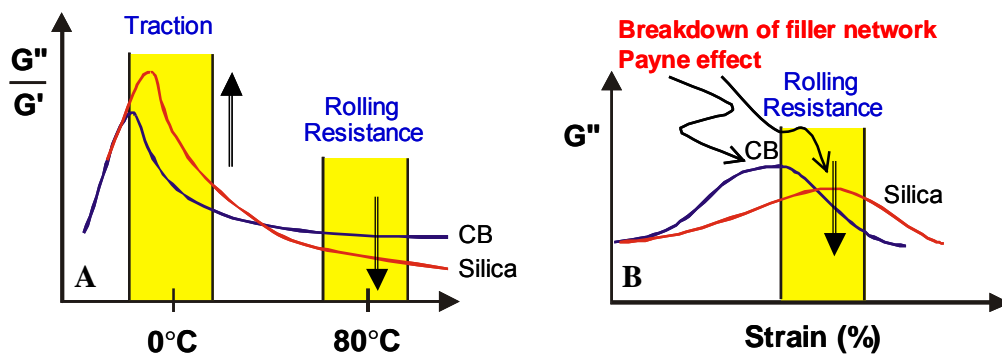


Figure 1-26: Comparison of $\tan \delta$, hysteresis property and rolling resistance between a carbon black and a silica filled rubber for tire application. (A: temperature dependence of $\tan \delta$, B: strain dependence of G'' , the Payne effect)

The difference of carbon black and silica reinforcement can also be seen in a strain-dependent dynamic analysis. Note that G'' for a carbon black filled rubber reaches its maximum at a lower strain and besides, its peak value is still higher than that for a silica filled one. From the knowledge in Section 1-4 (the maximum of G'' upon

straining at a low strain represents the breakdown of the filler network), it is now clear that for the silica filled rubber it involves less rolling resistance for tire application (B).

Replacement of carbon black by silica therefore results in a decrease of $\tan \delta$ at higher temperatures, and thereby in a reduction in the rolling resistance. In addition the use of silica leads to a comparable $\tan \delta$ at lower temperatures, providing a comparable ice- and wet grip of a tire [197]. The higher hysteresis of carbon black at higher temperatures is mainly due to the energy dissipation upon repeated destruction and reconstruction of the filler network, which leads to a rapid decrease of $\tan \delta$ with increasing temperature primarily due to a reduction of filler-filler interaction as well as filler-polymer interaction. Conversely the hysteresis of the silica-filled rubber increases with increasing temperature. Again, this may be anticipated from strongly and highly constructed filler clusters. As the temperature increases, weakening of the filler-filler interaction would result in an increase in the portion of filler network, which can be broken down and reformed during cyclic deformation at low strain amplitudes [198]. The advantages and weaknesses of silica and carbon black in tire properties and their production are given in Table 1-5 [199].

Table 1-5: Comparison between carbon black and silica

Carbon Black	Silica
<i>Advantages</i>	
Excellent cost/performance ratio	Excellent rolling resistance
Wide variety of products	Excellent wet traction
Easy processing	Excellent winter properties
Excellent abrasion resistance	
Excellent dry traction	
<i>Weaknesses</i>	
High rolling resistance	High products and processing cost
Poor wet traction	Poor abrasion resistance
Color	Limited products diversity

Moreover, since silica particles form stronger networks via hydrogen bonding interaction than carbon black, upon straining the equilibrium between agglomeration state and deagglomeration state is “more” in favor of the agglomeration state than

carbon black despite the fact that a strain force pushes the equilibrium towards deagglomeration. The simplified mechanism explaining this difference between carbon black and silica is shown in **Figure 1-27**.

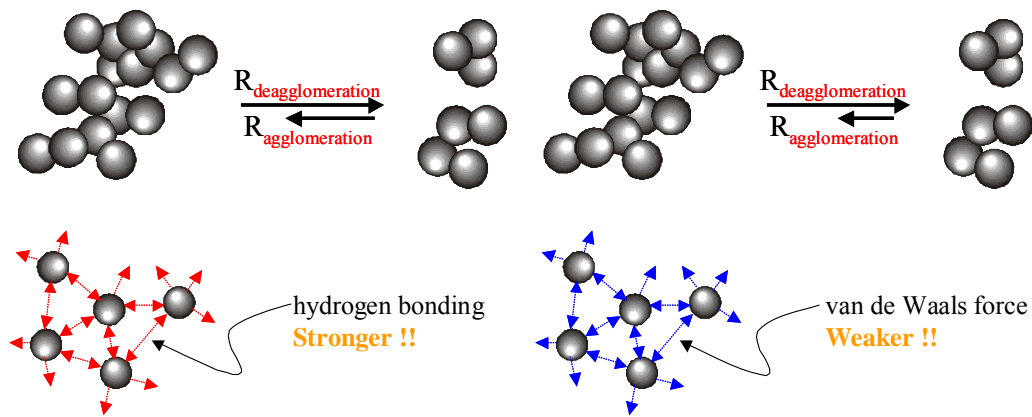


Figure 1-27: Schematic illustration of the agglomeration - deagglomeration mechanism between silica particles and carbon black particles. (the length of the arrow denotes the tendency thereto)

Compounding with silica enables tire technicians to reduce the filler content due to the greater reinforcing power of silica. A decrease in filler content corresponds to a higher amount of elastic rubber in proportion to the damping filler phase in the compound and is an effective way to reduce rolling resistance. The curve of $\tan \delta$ is shifted downwards in temperature towards the unfilled rubber [200].

1-6 Objectives of the Work

Nowadays more than half of the natural rubber and synthetic rubbers produced in the world are consumed in tire industry. As it is, vehicle tires are the most prominent rubber articles in terms of production volume and importance, and on the other hand they are also the most important damping elements of a vehicle.

A tire is not just a simple black and round rubber article as it looks. Actually a tire means much more: geometrically it is a torus and mechanically a flexible-membrane pressure container; it is structurally a high-performance composite and chemically it consists of materials made from long chain macromolecules and all other reinforcing ingredients. Since the invention of the world's first pneumatic tires in 1845 by a Scotsman, Richard Thompson, continual investigations in finding better materials for better tire performance have exploded thereafter. The tire engineers and, of course the customers, know exactly what a good tire should act like. First, a good tire is expected to offer the highest possible traction force between its surface and the road of all kinds of weather conditions. Second, the steering characteristics of a good tire are supposed to be precise and predictable under normal driving conditions. Third, the most demanded feature for you and me is that economically it should have the lowest possible fuel consumption (low rolling resistance) and highest possible mileage (high wear resistance). Unfortunately, up to now tire designers are still not able to discover an “invincible” or a “super” material which perfectly meets all the requirements for a good tire. Nevertheless, the continuous development in novel reinforcing agents offers tire designers new opportunities to understand the reinforcing mechanism better and to design new materials for better tire performance.

In tire history, the introduction of carbon black as a reinforcing agent in 1904 was admittedly a breakthrough. Carbon black brings about a strong increase in wear traction and the other physical properties. However due to the surface nature of carbon black and its specific reinforcing mechanism, the high rolling resistance and hence the high fuel consumption of carbon black reinforced tires has always been a critical issue.

Since the promotion of “Energy Tire” by Michelin, silica has been intensively investigated in tire compounding. According to their studies, the use of silica can result in a reduction in rolling resistance of 20 % and more relative to carbon black, which in turn saves a fuel consumption of 5 %. However due to the strong interparticle hydrogen bonding interaction, many studies reported that silica gives poor processibility in tire production. Moreover, it is also found to offer less wear resistance.

To accommodate the overwhelming demand in looking for better rubber materials, our work mainly focuses on the synthesis and characterization of new elastomer nanocomposites for tire applications. The basic idea of this work is to get benefits from hydrogen bonding interaction between reinforcing agents and the rubber matrix. On one hand it is expected that the filler agglomeration is reduced, and on the other hand this specific interaction further enhances the mechanical properties of these nanocomposites. In order to attach hydrogen bonding interacting moieties, the rubbers used in this study are chemically modified via several pathways. Instead of carbon black and conventional silica particles, the reinforcing agents used here are polymeric fillers and silica nanoparticles whose effectiveness in reducing the Payne effect are also examined.

The thesis is constructed according to the following manner:

In Chapter 1, a thorough introduction to the chemical modification of rubber, sol-gel synthesis is given, followed by practical introductions to tire performance (especially the rolling resistance) and the theories involved (Payne effect and filler-rubber interaction).

In Chapter 2, a simple pathway towards quantitative modification of rubber is described. The modification technique employed in this section gives a novel thermoreversible crosslinking rubber comprising supramolecular hydrogen bonding networks. This chapter has been published on *Macromolecules*. All work described in this chapter was done independently by myself.

In Chapter 3, the detail synthesis and characterization of silica nanoparticles is given. The silica nanoparticles are synthesized via the original Stöber method and the corresponding modified pathway. Silica nanoparticles with well-defined size and different surface functionalities are used as fillers for investigating filler-rubber hydrogen bonding interaction in the subsequent chapter. Besides, we also explore the possibility of using *in-situ* DLS technique to monitor the growth of silica nanoparticle. The in-situ study has been submitted to *Journal of Colloid & Polymer Science*. In this chapter, the synthesis part of silica nanoparticles was done by myself. However, the

characterizations were done with the help of Markus Burkhardt (DLS measurement), Astrid Göpfert and Markus Drechsler (TEM micrographs).

In Chapter 4, we characterize the nanocomposites consisting of modified rubbers described in Chapter 2 and the silica particles synthesized in Chapter 3. The influences of the surface functionality and silica loading, the degree of rubber modification and the temperature on the mechanical properties are discussed in detail. This Chapter has been published on *Polymers for Advanced Technologies*. Except for that the characterization parts were done with the help of Astrid Göpfert and Markus Drechsler (TEM micrographs), all the other work was performed alone by myself.

In Supplement, the collaboration project with Deutsches Institut für Kautschuktechnologie e.V. (DIK) involving the use of polymeric fillers of different surface functionalities and the trials of rubber modification is given. In this chapter dynamic mechanical analysis, both Rubber Process Analyzer (RPA) and Advanced Rheometric Expansion System (ARES), is used as the main measure to compare the reinforcing ability of different polymeric microgels and their specific interactions with rubber matrix.

References

- [1] J. Le Bras, A. Delande, “*Lea derives Chemigues du Cautchouc Natural*”, Dunod, Paris, 1950.
- [2] G.F. Bloomfield, E. H. Farmer, *J. Soc. Chem. Inc.*, **53**, 43 (1934).
- [3] H.I. Fisher, *Ind. Eng. Chem.*, **19**, 1325 (1927).
- [4] M. L. Kaplan, P. G. Bebbington and R. L. Hartless, *J. Polym. Sci. Polym. Lett. Ed.*, **11**, 357 (1973).
- [5] C. Pinnazzi, R. Pautrat and R. Charitat, *Makromol. Chem.*, **70**, 260 (1964).
- [6] C. S. L. Baker, D. Barnard, *Polymer Preprints*, ACS, Division of Polymer Chemistry, **26(2)**, 29 (1985).
- [7] H. M. R. Hoffmann, *Angew. Chem. Int. Ed.*, **8(8)**, 556 (1969).
- [8] G. T. Knight, B. Pepper, *Tetrahedron*, **27**, 6201 (1971).
- [9] F. Ferrero, M. Panetti and G. B. Saracco, *La Chimica e L’Industria*, **66**, 3 (1984).
- [10] D. Derouet, P. Phinyocheep, J. C. Brosse and G. Boccaccio, *Eur. Polym. J.*, **26(12)**, 1301 (1990).
- [11] K. Chino, M. Ashiura, *Macromolecules*, **34**, 9201 (2001).
- [12] M. E. Cain, G. T. Knight, P. M. Lewis and B. Saville, *Rubber J.*, **150(11)**, 10 (1968).
- [13] M. E. Cain, G. T. Knight, K. F. Gazeley and P. M. Lewis, *Ger. Offen.*, 2 058 544, June 16th, 1971.
- [14] C. S. L. Baker, D. Barnard and M. Porter, *Rubber Chem. Technol.*, **43**, 501 (1970).
- [15] N. Rabjohn, *J. Am. Chem. Soc.*, **70**, 1181 (1948).
- [16] P. J. Flory, N. Rabjohn and M. C. Shaffer, *J. Polym. Sci.*, **4**, 225 (1949).
- [17] D. Barnard, K. Dawes and P. G. Mente, *Proc. Int. Rubber Conf.*, Kuala Lumpur, **4**, 215 (1976).
- [18] J. Sauer, B. Schröder, *Chem. Ber.*, **100**, 678 (1967).
- [19] W. H. Pirkle, J.C. Stickler, *Chem. Comm. (London)*, **15**, 760 (1967).
- [20] R. Stadler, J. Burgert, *Makromol. Chem.*, **187**, 1681 (1986).
- [21] R. Stadler, L. Freitas, *Coll. & Polym. Sci.*, **264**, 773 (1986).
- [22] L. Freitas, R. Stadler, *Macromolecules*, **20**, 2478 (1987).
- [23] L. Freitas, R. Stadler, *Coll. & Polym. Sci.*, **266**, 1095 (1988).
- [24] R. Stadler, L. Freitas, *Coll. & Polym. Sci.*, **266**, 1102 (1988).
- [25] R. Stadler, L. Freitas, *Macromolecules*, **22**, 714 (1989).
- [26] R. Stadler, L. Freitas, *Makromol. Chem. Macromol. Symp.*, **26**, 451 (1989).
- [27] C. Hilger, R. Stadler, *Makromol. Chem.*, **191**, 1347 (1990).
- [28] C. Hilger, R. Stadler, *Macromolecules*, **23**, 2097 (1990).
- [29] U. Seidel, J. Hellman, D. Schollmeyer, C. Hilger and R. Stadler, *Supramolecular Sci.*, **2**, 45 (1995).
- [30] C. Hilger, R. Stadler, *Makromol. Chem.*, **192**, 805 (1991).
- [31] R. Pummer, P. A. Burkhard, *Über Kautschuk Ber.*, **55**, 3458 (1922).
- [32] A. Rosowsky, in “*Heterocyclic Compounds with Three and Four Membered Rings*”, Interscience, New York, 1964.
- [33] D. Swern, in “*Organic Peroxides*”, Wiley Interscience, New York, Vol. 2, 1971.
- [34] L. P. Witnauer, D. Swern, *J. Am. Chem. Soc.*, **72**, 3364 (1950).

- [35] N. A. Koshel, B. S. Turov, V. V. Papov, B. F. Ustavshchikov, T. P. Nikitina and Y. Y. Musabekov, *Chem. Abstr.*, **86**, 172762 (1977).
- [36] J. A. Mairs, J. Todd, *J. Chem. Soc.*, **38C** (1932).
- [37] A. Saffer, B. L. Johnson, *Ind. Eng. Chem.*, **40**, 538 (1948).
- [38] C. Roux, R. Pautrat, R. Cheritat, F. Ledran and J. C. Danjard, *J. Polym. Sci. Part C*, **16**, 4687 (1969).
- [39] P. Dreyfuss, J. P. Kennedy, *J. Appl. Polym. Sci., Appl. Polym. Symp.*, **30**, 165 (1977).
- [40] P. Dreyfuss, J. P. Kennedy, *Anal. Chem.*, **47**, 771 (1975).
- [41] I. R. Gelling, J. F. Smith, Proc. Int. Rubber Conf., Milan, Italy, 140, 1979.
- [42] Nippon Zeon Co. Ltd., Japanese Patent 8040 604, 1980.
- [43] D. R. Burfield, K. L. Lim and K. S. Law, *J. Appl. Polym. Sci.*, **29**, 1661 (1984).
- [44] S. Nonagaki, H. Moroshita, Japanese Patent 74769 983, 1974.
- [45] R. W. Terry, A. F. Jacobs, British Patent 2008 125, 1979.
- [46] B. M. Badran, E. M. Abdel-Bary, *Chem. Ind.*, 314 (1997).
- [47] F. P. Greenspan, "Chemical Reactions of Polymers", Vol. 19, Interscience, New York, 1964.
- [48] I. R. Gelling, British Patent No. 2113 692, 1984.
- [49] M. S. Ryabova, S. N. Sautin, Y. M. Volin, S. Y. Lazarev and V. A. Shibaev, *Zh. Prikl. Khim.*, **56**, 1116 (1983).
- [50] D. Zuchowska, *Polymer*, **21**, 514 (1980).
- [51] Nippon Zeon Co. Ltd., Japanese Patent 8118 605, 1981.
- [52] C. S. L. Baker, I. R. Gelling, *Rubber India*, **37**, 9 (1985).
- [53] X. Jian, A. S. Hay, *J. Polym. Sci. Polym. Lett.*, **28**, 285 (1990).
- [54] X. Jian, A. S. Hay, *J. Polym. Sci. Part A. Polym. Chem.*, **29**, 1183 (1991).
- [55] K. Griesbaum, *Angew. Chem. Int. Ed. Engl.*, **9**, 273 (1970).
- [56] I. A. Tutorskii, S. V. Novikov and B. A. Dogadkin, *Vysokomolek. Soedin.*, **6**, 1844 (1964).
- [57] G. E. Serniuk, F.W. Banes, M.W. Swaney, *J. Am. Chem. Soc.*, **70**, 1804 (1948).
- [58] E. Ceausescu, S. Bittman, V. Fieroiu, E. G. Badea, E. Gruber, A. Ciupitoiu, and V. Apostol, *J. Macromol. Sci. Chem.*, **A22**, 525 (1985).
- [59] O. Ajiboye, G. Scott, *Polym. Degrad. Stab.*, **4**, 397 (1982).
- [60] K. W. S. Kularatne, G. Scott, *Eur. Polym. J.*, **15**, 827 (1979).
- [61] J. I. Cunneen, F. W. Shipley, *J. Polym. Sci.*, **36**, 77 (1959).
- [62] G. Boutevin, B. Ameduri, B. Boutevin, and J. P. Joubert, *J. Appl. Polym. Sci.*, **75**, 1655 (2000).
- [63] B. Boutevin, Y. Hervaud, and G. Mouledous, *Polym. Bull.*, **41**, 145 (1998).
- [64] F. Schapman, J. P. Couvercelle, and C. Bunel, *Polymer*, **39**, 4955 (1998).
- [65] F. Romani, E. Passaglia, M. Aglietto, and G. Ruggeri, *Macromol. Chem. Phys.*, **200**, 524 (1999).
- [66] F. Ciardelli, M. Aglietto, E. Passaglia, and F. Picchioni, "Polymers for Advanced Technologies", **11**, 371, 2000.
- [67] N. Kharasch, Z. S. Ariyan, *Intra-Sci. Chem. Repts.*, **1**, 337 (1967).
- [68] E. Kühle, *Synthesis*, **11**, 561 (1970).
- [69] A. Brydon, Ph.D. thesis, University of Aberdeen, 1972.
- [70] H. Holdschmidt, G. Pampus, N. Schön and J. Witte, *Makromol. Chem.*, **101**, 271 (1967).
- [71] I. J. Gardner, G. E. Serniuk, F. P. Baldwin and T. A. Manuel, *Ger. Offen.*, 1 906 521, September 25th, 1969.
- [72] J. T. Davis, E. K. Rideal, in "Interfacial Phenomena", Academic Press, New

- York, 1963.
- [73] P. J. Flory, “*Principles of Polymer Chemistry*”, Cornell University Press, Ithaca, New York, 1953.
- [74] M. Ebelmen, *Ann. Chimie Phys.*, **16**, 129 (1846).
- [75] M. Ebelmen, *C. R. Acad. Sci.*, **25**, 854 (1847).
- [76] T. Graham, *J. Chem. Soc.*, **17**, 318 (1864).
- [77] R. E. Liesegang, *Photogr. Archiv.*, 221 (1896).
- [78] H. K. Heinrich, “*Crystal Growth in Gel*”, Pennsylvania State University Press, PA, 1970.
- [79] W. Z. Ostwald, *Phys. Chem.*, **27**, 365 (1897).
- [80] L. Rayleigh, *Philos. Mag.*, **38**, 738 (1919).
- [81] D. J. Lloyd, p767 in “*Colloid Chemistry*”, Chemical Catalog Co., New York, 1926.
- [82] H. N. Holmes, p796 in “*Colloid Chemistry*”, Chemical Catalog Co., New York, 1926.
- [83] K. H. Stern, “*Bibliography of Liesegang Ring*”, National Bureau of Standards Miscellaneous Publication No. 191, 1967.
- [84] D. M. Roy, R. Roy, *Am. Mineral*, **39**, 957 (1954).
- [85] R. J. Roy, *J. Am. Ceram. Soc.*, **39**, 145 (1956).
- [86] R. J. Roy, *J. Am. Ceram. Soc.*, **52**, 344 (1969).
- [87] G. J. McCarthy, R. Roy, J. M. McKay, *J. Am. Ceram. Soc.*, **54**, 637 (1971).
- [88] R. K. Iler, “*The Chemistry of Silica*”, Wiley, New York, 1955.
- [89] W. Stöber, A. Fink, E. Bohn, *J. Colloid Interface Sci.*, **26**, 62 (1968).
- [90] C. G. Tan, B. D. Bowen, N. Epstein, *J. Colloid Interface Sci.*, **118**, 290 (1987).
- [91] J. D. Mackenzie, *J. Non-Cryst. Solids*, **41**, 1 (1982).
- [92] L. L. Hench, S. H. Wang, J. L. Noguez, p76 in “*Multifunctional Materials*”, SPIE, Bellingham, WA, 1988.
- [93] L. L. Hench, “*Ultrastructure Processing of Ceramics, Glasses and Composites*”, Wiley, New York, 1984.
- [94] C. J. Brinker, *J. Non-Cryst. Solids*, **100**, 31 (1988).
- [95] S. Sakka, K. J. Kamiya, *J. Non-Cryst. Solids*, **48**, 31 (1982).
- [96] S. Sakka, p91 in “*Better Ceramics Through Chemistry*”, Elsevier-North Holland, New York, 1984.
- [97] K. D. Keefer, p227 in “*Silicon Based Polymer Science: A Comprehensive Resource*”, ACS Advances in Chemistry, Washington DC, 1990.
- [98] C. J. Brinker, G. W. Scherer, “*Sol-Gel Science: The Physics and Chemistry of Sol-Gel Processing*”, Academic Press, New York, 1990.
- [99] R. Aelion, A. Loebel, F. Eirich, *J. Am. Chem. Soc.*, **72**, 5705 (1950).
- [100] L. W. Kelts, N. J. Effinger and S. M. Melpolder, *J. Non-Cryst. Solids*, **83**, 353 (1986).
- [101] E. R. Pohl and F. D. Osterholtz, p.157 in “*Molecular Characterization of Composite Interface*”, H. Ishida and G. Kumar Ed., Plenum, New York, 1985.
- [102] W. Hofman, “*Rubber Technology Handbook*”, Hanser/Gardner, Munich, 1996.
- [103] Internet page, www.firestone.co.za/passenger/tips/consumer_history.htm
- [104] Internet page, intagecars.about.com/library/weekly/aa082298.htm?once=true&
- [105] C. M. Blow and C. Hepburn, “*Rubber Technology and Manufacture*”, Plastics and Rubber Institute, London, 1982.
- [106] J. L. White, “*Rubber Processing: technology, material and principle*”, Hanser, Munich, 1995.
- [107] M. S. Evan, “*Tyre Compounding for Improved Performance*”, Rapra

- Technology Ltd., UK, 2002.
- [108] D. J. Schuring, *Rubber Chem. Technol.*, **53**, 600 (1980).
- [109] Indian Rubber Institute, “*Rubber Engineering*”, McGraw-Hill, New York, 1999.
- [110] R. Engehausen, A. Rawlinson and J. Trimbach, *Tire Technol. Int. Ann. Review*, **2001**, 36 (2001).
- [111] D. E. Hall and J. C. Moreland, paper No. 29 presented at a meeting of ACS, Rubber Division, Dallas, Texas, April 4-6.
- [112] W. L. Holt and P. L. Wormeley, *Technol. Papers of Bur. Stand.*, **19**, 213 (1925).
- [113] K. H. Nordsiek, *Kautsch. Gummi Kunstst.*, **38**, 178 (1985).
- [114] A. R. Payne, Ch. 3. in “*Reinforcement of Elastomers*”, G. Kraus Ed., Interscience Publishers, New York, 1965.
- [115] A. R. Payne, R. E. Whittaker, *Rubber Chem. Technol.*, **44**, 440 (1971).
- [116] A. I. Medalia, *Rubber Chem. Technol.*, **51**, 437 (1978).
- [117] A. Einstein, *Ann. Der Physik*, **19**, 289 (1906).
- [118] A. Einstein, *Ann. Der Physik*, **34**, 591 (1911).
- [119] E. Guth and O. Gold, *Phys. Rev.*, **53**, 322 (1938).
- [120] H. M. Smallwood, *J. Appl. Phys.*, **15**, 758 (1944).
- [121] A. R. Payne, *Rubber Chem. Technol.*, **39**, 365 (1966).
- [122] E. M. Dannenberg, *Rubber Chem. Technol.*, **48**, 410 (1975).
- [123] G. Kraus, *Rubber Chem. Technol.*, **37**, 6 (1964).
- [124] M. Gerspacher, C. P. O’Farrell and H. H. Yang, *Kautsch. Gummi Kunstst.*, **47**, 349 (1994).
- [125] M. Gerspacher, C. P. O’Farrell, H. H. Yang and W. A. Wampler, Paper No. C presented at a meeting of ACS, Rubber Division, Montreal, Quebec, Canada, 5-8th May, 1996.
- [126] J. B. Donnet, *Kautsch. Gummi Kunstst.*, **47**, 628 (1994).
- [127] M. Gerspacher, C. P. O’Farrell, L. Nikiel and H. H. Yang, *Rubber Chem. Technol.*, **69**, 569 (1996).
- [128] M. Klüppel, R. H. Schuster and G. Heinrich, *Rubber Chem. Technol.*, **70**, 243 (1997).
- [129] M. Gerspacher, *Rubber Chem. Technol.*, **64**, 118 (1991).
- [130] A. Voet, *Rubber Chem. Technol.*, **41**, 1208 (1968).
- [131] P. G. Maier, D. Göritz, *Kautsch. Gummi Kunstst.*, **49**, 18 (1996).
- [132] B. Freund, W. Niedermeier, *Kautsch. Gummi Kunstst.*, **51**, 444 (1998).
- [133] G. Kraus, *J. Appl. Polym. Sic. - Appl. Polym. Symp.*, **39**, 75 (1984).
- [134] G. Heinrich, M. Klüppel, *Adv. Polym. Sci.*, **160**, 1 (2002).
- [135] H. S. Katz, J. V. Milewski (eds), “*Handbook of Fillers and Reinforcements*”, Van Nostrand Reinhold, New York, 1978.
- [136] G. Wypych, “*Handbook of Fillers 2nd ed.*”, ChemTec Publishing, Toronto, 2000.
- [137] L. E. Nielsen, R. F. Landel, “*Mechanical Properties of Polymers and Composites*”, Marcel Dekker, New York, 1994.
- [138] L. Mullins, “*The Chemistry and Physics of Rubberlike Substances*”, MacLaren, London, 1963.
- [139] J. W. Snyder, M. H. Leonard, “*Introduction to Rubber Technology*”, Van Nostrand Reinhold, Princeton, New Jersey, 1965.
- [140] M. L. Stuebarker, “*Reinforcement of Elastomer*”, Wiley, New York, 1965.
- [141] C. C. McCabe, N. Mueller, *Trans. Soc. Rheol.*, **5**, 329 (1961).
- [142] N. V. Zakharenko, F. S. Tolstukhina and G. M. Bartenev, *Rubber Chem.*

- Technol.*, **35**, 326 (1961).
- [143] J. R. Hopper, *Rubber Chem. Technol.*, **40**, 463 (1967).
- [144] G. R. Cotton, *Rubber Age*, **100**, 51 (1968).
- [145] A. I. Medalia, *J. Colloid Interf. Sci.*, **32**, 115 (1970).
- [146] G. V. Vinogradov, A. Ya. Malkin, E. P. Plotnikova, O. Yu. Sabsai and N. E. Nikolayeva, *Int. J. Polym. Mater.*, **2**, 1 (1972).
- [147] J. L. White, J. W. Crowder, *J. Appl. Polym. Sci.*, **18**, 1013 (1974).
- [148] F. W. Maine, B. E. Riseborough and J. E. Theberge, Polymer structures and properties, *SPE RETEC*, Toronto, 1976.
- [149] L. C. Cessna, J. B. Thomson and R. D. Hanna, *SPE J.*, **25**, 35 (1969).
- [150] J. Cook, J. Gordon, *Procc. Roy. Soc.*, **4282**, 508 (1964).
- [151] L. J. Broutman, *Polym. Eng. Sci.*, **6**, 263 (1966).
- [152] J. G. Morley, *Chem. Brit.*, **10**, 478 (1974).
- [153] J. G. Morley, R. S. Millman, *J. Mat. Sci.*, **9**, 1171 (1974).
- [154] L. G. Tang, J. L. Kardos, *Polym. Composites*, **18**, 100 (1997).
- [155] J. T. Byers, Paper B presented at a meeting of ACS, Rubber Division, Cleveland, 1995.
- [156] S. Bandyopadhyay, P. P. De, D. K. Tripathy and S. K. De, *Polymer*, **37**, 353 (1996).
- [157] S. Wolff, *Rubber Chem. Technol.*, **69**, 325 (1996).
- [158] L. R. Evans, Paper D presented at a meeting of ACS, Rubber Division, Montreal, 5-8th May, 1996.
- [159] G. Kraus, Interaction between elastomers and reinforcing fillers, in "Reinforcement of Elastomers", Wiley, New York, 1965.
- [160] J. H. Bachmann, J. W. Sellers, M. P. Wagnes and R. F. Wolf, *Rubber Chem. Technol.*, **32**, 1286 (1959).
- [161] W. F. Waston, Chemical interactions of fillers and rubbers during cold milling, in "Reinforcement of Elastomers", Wiley, New York, 1965.
- [162] R. Schuster, "Filler Reinforcement", Educational Symposia, IRC '03, Nürnberg, Germany, 2003.
- [163] C. C. Channis, Interfaces in Polymer Matrix Composites, in "Composite Materials", 6, Academic Press, 1974.
- [164] H. Alter, *J. Appl. Polym. Sci.*, **9**, 1525 (1965).
- [165] G. P. Bierwagen, *J. Paint Tech.*, **44**, 46 (1972).
- [166] G. Tsagaropoulos, A. Eisenberg, *Macromolecules*, **28**, 6067 (1995).
- [167] J. H. Davis, *Plastics and Polymer*, **39**, 137 (1971).
- [168] W. A. Zisman, *Ind. Eng. Chem.*, **35**, 18 (1963).
- [169] W. A. Zisman, *Ind. Eng. Chem. Prod. Res. Dev.*, **8**, 98 (1969).
- [170] R. T. Schwartz, H. S. Schwartz, "Fundamental Aspects of Fiber-reinforced Materials", Wiley, New York, 1968.
- [171] A. Laskaris, J. Herrick, R. Lurie, L. McAllister and P. Roy, Carbon fibers in reinforced plastics, in "Advances in Structural Composites", 12, Western Periodicals, North Hollywood, California, 1967.
- [172] J. Herrick, A. Travers, paper presented at Annual Reinforced Plast. Tech. Manag. Conf., Washington D. C., 1968.
- [173] G. R. Cotton, *Rubber Chem. Technol.*, **57**, 118 (1984).
- [174] S. Wolff and U. Görl, *Kautsch. GummiKunstst.*, **44**, 941 (1991).
- [175] T. C. Gruber and C. R. Herd, *Rubber Chem. Technol.*, **70**, 727 (1997).
- [176] A. K. Ghosh and B. Adhikari, *Kautsch. GummiKunstst.*, **52**, 681 (1999).
- [177] H. Raab, J. Fröhlich and D. Göritz, *Kautsch. GummiKunstst.*, **53**, 137 (2000).

- [178] J. T. Byers, *Rubber World*, **218**, 38 (1998).
- [179] S. Wolff and M. J. Wang, *Rubber Chem. Technol.*, **65**, 329 (1992).
- [180] B. B. Boonstra, H. Cochrane and E. M. Dannenberg, *Rubber Chem. Technol.*, **48**, 558 (1975).
- [181] A. Voet, J. C. Morawski and J. B. Donnet, *Rubber Chem. Technol.*, **50**, 342 (1977).
- [182] Y. C. Ou, Z. Z. Yu, A. Vidal and J. B. Donnet, *Rubber Chem. Technol.*, **67**, 693 (1994).
- [183] Y. Li, M. J. Wang, T. Zhang, F. Zhang and X. Fu, *Rubber Chem. Technol.*, **67**, 693 (1994).
- [184] G. R. Cotton, *Rubber Chem. Technol.*, **45**, 129 (1972).
- [185] C. H. Chen, J. L. König, J. R. Shelton and E. A. Collins, *Rubber Chem. Technol.*, **55**, 103 (1982).
- [186] E. F. Devlin, *Rubber Chem. Technol.*, **59**, 666 (1986).
- [187] S. S. Choi, *Elastomer*, **36**, 37 (2001).
- [188] S. S. Choi, *Kor. Polym. J.*, **8**, 285 (2000).
- [189] W. A. Wanpler, M. Gerspacher and H. H. Yang, Paper 26 presented at a meeting of ACS, Rubber Division, Washington DC, 1993.
- [190] U. Görl and A. Hunsche, Paper 38 presented at a meeting of ACS, Rubber Division, Washington DC, 1997.
- [191] A. S. Hashim, B. Azahari, Y. Ikeda and S. Kohjiya, *Rubber Chem. Technol.*, **71**, 289 (1998).
- [192] H. Roelig, *Rubber Chem. Technol.*, **12**, 384 (1939).
- [193] W. S. J. Naunton and J. R. S. Waring, *Trans. Inst. Rubber Ind.*, **14**, 340 (1939).
- [194] S. D. Gehman, D. E. Woodford and R. B. Stambaugh, *Ind. Eng. Chem.*, **33**, 1032 (1941).
- [195] R. B. Stambaugh, *Ind. Eng. Chem.*, **34**, 1358 (1942).
- [196] A. I. Medalia, *Rubber Chem. Technol.*, **51**, 437 (1978).
- [197] P. Cochet, L. Barriquand, Y. Bomal and S. Touzet, Paper 74 presented at a meeting of ACS, Rubber Division, Cleveland, 1995.
- [198] M. J. Wang, *Rubber Chem. Technol.*, **71**, 520 (1998).
- [199] R. Stober, Kautschuk-Herbst-Kolloquium 2002, Hannover, Germany, 2002.
- [200] L. Gatti, *Tire Technol. Int. Ann. Review*, **39**, 2001 (2001).

Chapter 2

A Simple Pathway toward Quantitative
Modification of Polybutadiene - A New
Approach to Thermoreversible Crosslinking
Rubber Comprising Supramolecular
Hydrogen Bonding Networks

A Simple Pathway toward Quantitative Modification of Polybutadiene - A New Approach to Thermoreversible Crosslinking Rubber Comprising Supramolecular Hydrogen Bonding Networks

*Chih-Cheng Peng*¹, *Volker Abetz*²

¹Makromolekulare Chemie II, Universität Bayreuth, Universitätsstrasse 30, 95447 Bayreuth, Germany

²Institut für Chemie, GKSS-Forschungszentrum Geesthacht GmbH, Max-Planck-Strasse 1, 21502 Geesthacht, Germany

(published on *Macromolecules*)

2-1 Abstract

A commercial polybutadiene (PB) was modified by a simple three-step polymer analogous reaction (epoxidation, oxirane ring-opening and sulfonyl isocyanate addition) and the degree of modification is quantitatively controlled by the epoxidation reaction. Due to the introduction of sulfonyl urethane groups (-O-CO-NH-SO₂-) which are prone to self-complementary thermoreversible supramolecular hydrogen bonding (HB) networks, the PB was modified from a rubbery material to a thermoplastic elastomer. The modified rubbers were characterized by using ¹H-NMR, FTIR, DSC and dynamic mechanical analysis. FTIR spectra showed a shift of S=O stretching to lower frequency with increasing degree of modification as a result of the formation of HB complexes. DSC analysis showed that the crystalline melting was suppressed and the glass transition was elevated to higher temperatures. From the dynamic mechanical analysis it revealed much clearer the crystallization suppression and the glass transition shifts. The changes in thermal and mechanical properties were attributed to the formation of HB supramolecular networks in the modified polybutadienes.

2-2 Introduction

Chemical modifications of rubber-like material, especially natural rubber (NR), have been a useful pathway to new polymeric materials for many years. The first

commercially available modified NR was produced 50 years ago (hydrochlorinated, chlorinated and cyclized rubbers). Due to the high reactivity of double bonds, an organic compound carrying functional groups can be easily grafted onto an olefin by reactions such as electrophilic, nucleophilic and radical addition reactions. The reactivity, however, is often less in a polymer compared with a simple olefin, which is not surprising since a double bond in a macromolecule is less accessible than a structurally similar double bond in a small olefin. The steric barriers to reactions on polymers may become quite marked when attempts are made to carry a reaction to completion, which on the other hand could mean the reactions are not quantitatively satisfactory [1-3].

Among all the well-known chemical modifications of polydiene materials, epoxidation reaction has been the most promising and advantageous method [4-8] since the epoxidized polydienes can be prepared with performic acid at moderate temperature in solution, which makes mass industrial production possible. Moreover, the oxirane ring on the epoxidized polydiene backbone is of great interest because numbers of chemical reactions can be employed for further modifications: for instance, carboxylic acids [9-12], amines [13-16], phosphoric acid derivatives [17,18] and alcohols [19,20] were respectively investigated for synthesis of drug release, vulcanized, antioxidant, photocrosslinkable and flame-resistant materials. However, due to the low degree of secondary modification, the mentioned reactions should be conducted at higher temperatures and are always not satisfactory in terms of conversion.

Alternatives to functionalize polydienes are via thermal ene-reaction of 4-phenyl-1,2,4-triazoline-3,5-dione derivatives [21-23] and sulfenyl halide [24,25] addition onto the double bonds. Though these two reactions are straightforward (one step modification) and quantitative at the laboratory scale, the applicability for mass industrial production is limited. There are mainly two reasons for that: First, the chemicals needed for the modification are not available commercially. Second, the synthesis routes for the modifying chemicals are tedious and, moreover, it requires highly toxic reagents such as phosgene [24] or nitrogen dioxide [21].

Despite the fact that hydrogen bonding has been extensively studied in supramolecular systems as a mean of polymer formation or modification between small molecules or oligomers via a self-complementary process [26-29], very few studies of polymer modification systems using hydrogen bonding between (i) the side groups of polymers [30-34] or (ii) the side group of a polymer and a small molecule were investigated. Meijer reported that supramolecular interaction between (i) the styrene-maleimide alternating copolymer and melamine or (ii) the copolymer of styrene and 2,4-diamino-6-vinyl-1,3,5-triazine is capable of enhancing compatibility between each other [35]. Nevertheless, the chemistry employed in the above work on supramolecular systems was not applicable to industrial applications. Recently, D. Chino et al. applied the ene-reaction of maleic anhydride to modifying natural rubber in order to synthesize thermoreversible crosslinking rubber using a hydrogen bonding network [36]. The main drawback of this ene-reaction between maleic anhydride and rubber is that the grafting efficiency depends strongly on several factors, for instance reaction time and temperature, molecular weight and microstructure of the rubber [37]. Therefore, such procedure is not always a satisfactory way to modifying rubber. Here we present a new, economical and simple three-step polymer analogous reaction based on epoxidation reaction (Figure 2-1) to quantitatively modify polydiene polymers. This results in a thermoreversible crosslinked supramolecular network which is formed in the rubber matrix. Moreover, simply by controlling the degree of modification one is able to design rubber materials which meet special requirements for different sorts of rubbery products.

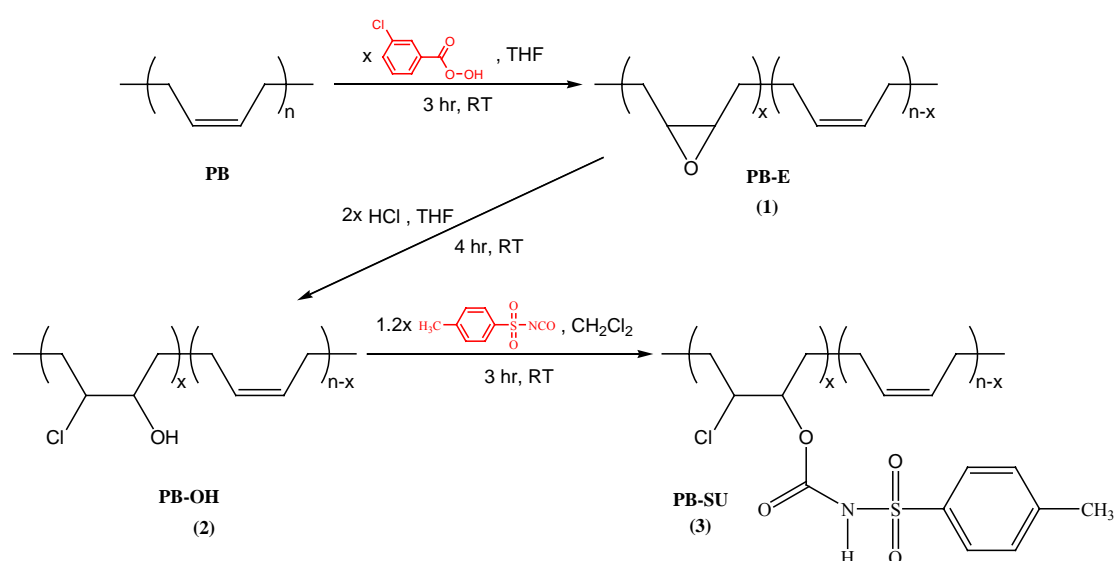


Figure 2-1: Three-step pathway toward quantitative modification of polybutadiene.

2-3 Experimental Section

2-3-1 Materials

Technical grade polybutadiene, Bayer Buna[®] CB 10, with 96% *cis*-1,4 units and Mooney viscosity = 47 (ML1+4 at 100 °C) (GPC data with PS standard: $M_w=576,000$ g/mol, $DPI=2.6$) was received from Deutsches Institut für Kautschuktechnologie e.V. (DIK, Germany). According to the supplier, this material has a fairly wide molecular weight distribution and a medium degree of long-chain branching. *m*-chloroperbenzoic acid (MCPBA, 70%, Fluka), hydrochloric acid (32 wt% HCl, Merck) and *p*-toluenesulfonyl isocyanate (PTSI, 96%, Aldrich) were used as received. Tetrahydrofuran (THF), dichloromethane (analytical grade) were purchased from Merck and were used without any further purification.

2-3-2 Synthesis of PB-E (1) (Epoxidation)

The epoxidation reaction was performed and modified according to literature procedure [38,39], and here PB with 5 mol% degree of modification is highlighted as a typical example. In a 1 L one-neck round bottom flask equipped with magnetic stirrer, 16.2 g CB 10 (0.3 mol C=C) was first dissolved in 600 mL THF (typical concentration for various degrees of modification). A solution of 3.69 g of MCPBA (0.015 mol) in 50 mL THF was then added drop-wise at room temperature into the polymer solution at such a rate that the MCPBA solution was added completely after 1 hour. The reaction mixture was then further stirred for another 2 hours and 2 mL reaction solution was taken out for ¹H-NMR before the ring-opening reaction. The degree of modification was calculated using ¹H-NMR technique as described in literature [40].

2-3-3 Synthesis of Hydrochlorinated PB, PB-OH (2) (Ring-opening)

A solution of 3.42 g hydrochloric acid (0.03 mol HCl) in 50 mL THF was first prepared and transferred into a 100 mL dropping funnel, it was then added drop-wise at room temperature into the epoxidized PB solution prepared previously. After the addition of HCl solution, the reaction mixture was further stirred for another 3 hours in order to complete the ring-opening reaction. Afterwards the polymer was isolated by precipitation into 400 mL methanol and then dried at 50 °C under vacuum for two days. The yield of the hydrochlorinated PB was 99% and the extent of oxirane ring-opening was verified using ¹H-NMR.

2-3-4 Synthesis of PB-SU (3) (Sulfonyl isocyanate addition)

In a 200 mL one-neck round bottom flask, equipped with magnetic stirrer, 5.0 g of 5 mol% hydrochlorinated PB, (2), (4.42×10^{-3} mol -OH) was first dissolved in 100 mL CH₂Cl₂. 1.09 g PTSI (5.30×10^{-3} mol) was then added at one dose into the solution and the system was stirred at room temperature for 3 hours. After the reaction, the final product was isolated by precipitation into 100 mL methanol and then dried at 50 °C under vacuum for two days. The yield of the isolated product was 98%, and the extent of reaction was verified by using ¹H-NMR. PBs of other degrees of modification were also prepared according to the above recipe and the details are summarized in [Table 2-1](#) and [Table 2-2](#).

Table 2-1: PBs of various degrees of hydrochlorination.

Sample ID	Degree of Hydroxylation (based on C=C unit)	MCPBA (g)	HCl (g)	Yield (%) ^a
PB-OH-1	1 mol%	0.74	0.68	99
PB-OH-2	2 mol%	1.48	1.37	99
PB-OH-5	5 mol%	3.69	3.42	99
PB-OH-10	10 mol%	7.39	6.84	98
PB-OH-20	20 mol%	14.78	13.68	95

^a yield is calculated for 16.2 g of PB by $\frac{w/[54 + x(35.5 + 17)]}{16.2/54} \times 100\%$, where w is product weight in gram and x is the degree of modification in mol %.

Table 2-2: PBs of various degrees of modification.

Sample ID	Degree of Modification (based on [OH]/[C=C] ₀)	PTSI (g) ^a	Yield (%) ^b
PB-SU-1	1 mol%	0.23	98
PB-SU-2	2 mol%	0.44	98
PB-SU-5	5 mol%	1.09	98
PB-SU-10	10 mol%	1.66	95
PB-SU-20	20 mol%	3.82	90

^a the amount of PTSI required is calculated based on mole of -OH in 5.0 g of PB-OH. $-\text{OH mol} = \frac{5.0x}{54 + x(17 + 35.5)}$, where x is the degree of modification in mol%.

^b yield is calculated by $\frac{w/[54 + x(17 + 35.5 + 197)]}{5.0/[54 + x(17 + 35.5)]} \times 100\%$, where w is product weight in gram and x is the degree of modification in mol%.

2-3-5 Characterizations

¹H-NMR spectra were recorded on a Bruker 250 MHz spectrometer using CDCl₃ as solvent, the signals were normalized by unifying the methylene protons at 2.08 ppm. FTIR spectra were recorded at room temperature using a Bruker FTIR EQUINOX 55/S spectrometer at a resolution of 4 cm⁻¹. The samples for FTIR analysis were first dissolved in CH₂Cl₂ (10 mg PB in 1 mL CH₂Cl₂) and prepared by solution casting onto a KBr plate and the absorption signals were normalized by unifying the asymmetric methylene stretching absorption at 2941 cm⁻¹. DSC experiments were run on a Perkin-Elmer Pyris 1, with a scanning rate of 40 °C/min between -120 and 60 °C and the transition temperatures were taken from the second heating curves. The crystalline melting (T_m) and crystallization (T_c) temperatures were taken at the peak values (local extrema), the glass transition (T_g) temperatures were taken at the midpoint (1/2 Δ C_p) of the curves. All transition temperatures were taken without extrapolating to zero scanning rate. Dynamic mechanical measurements were performed using an Advances Rheometrics Expansion System (ARES) from TA Instrument, dynamic shear moduli were recorded employing the “dynamic temperature ramp test” program (scanning from 80 to -100 °C at a rate of -2 °C/min) with 8 mm parallel-plate geometry. Sample films of 8 mm diameter were prepared by compression molding (a 25 mg sample was first heated and molded under pressure at 80 °C for 10 minutes in an 8 mm diameter mold and the button-like specimen was

taken out after the mold was cooled to room temperature). All tests were performed at an oscillating frequency of 1 Hz and dynamic strain-sweep tests were done before the temperature ramp tests to ensure that all the measurements were made within the linear viscoelastic regime.

2-4 Results and Discussion

2-4-1 Chemical modification of PB

The epoxidation reaction of polybutadiene by using *m*-chloroperbenzoic acid showed excellent efficiency and was in agreement with literature data [20], i.e. the reaction was quantitative. The extents of the subsequent reactions were verified by using $^1\text{H-NMR}$, by monitoring the proton signals on the oxirane ring and the one adjacent to the hydroxyl group. As shown in Figure 2-2, from the vicissitudes of proton signals the oxirane ring was successfully cleaved and PTSI was added with excellent efficiency. However, as a result of the increasing hydrophilicity, which is in favor of the solubility of modified PBs in methanol, the yields of the isolated products were decreased with increasing sulfonyl urethane content (Table 2-2). $^1\text{H-NMR}$ spectra of other different degree of modification are also given in Figure 2-3 (1, 2, 10 and 20 mol%).

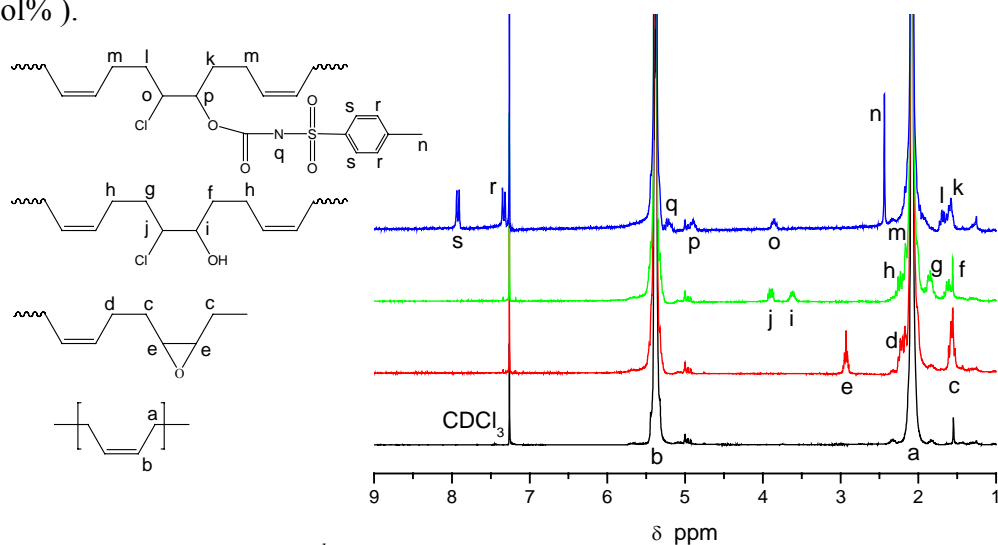


Figure 2-2: $^1\text{H-NMR}$ spectra of PB with 5 mole% modification.

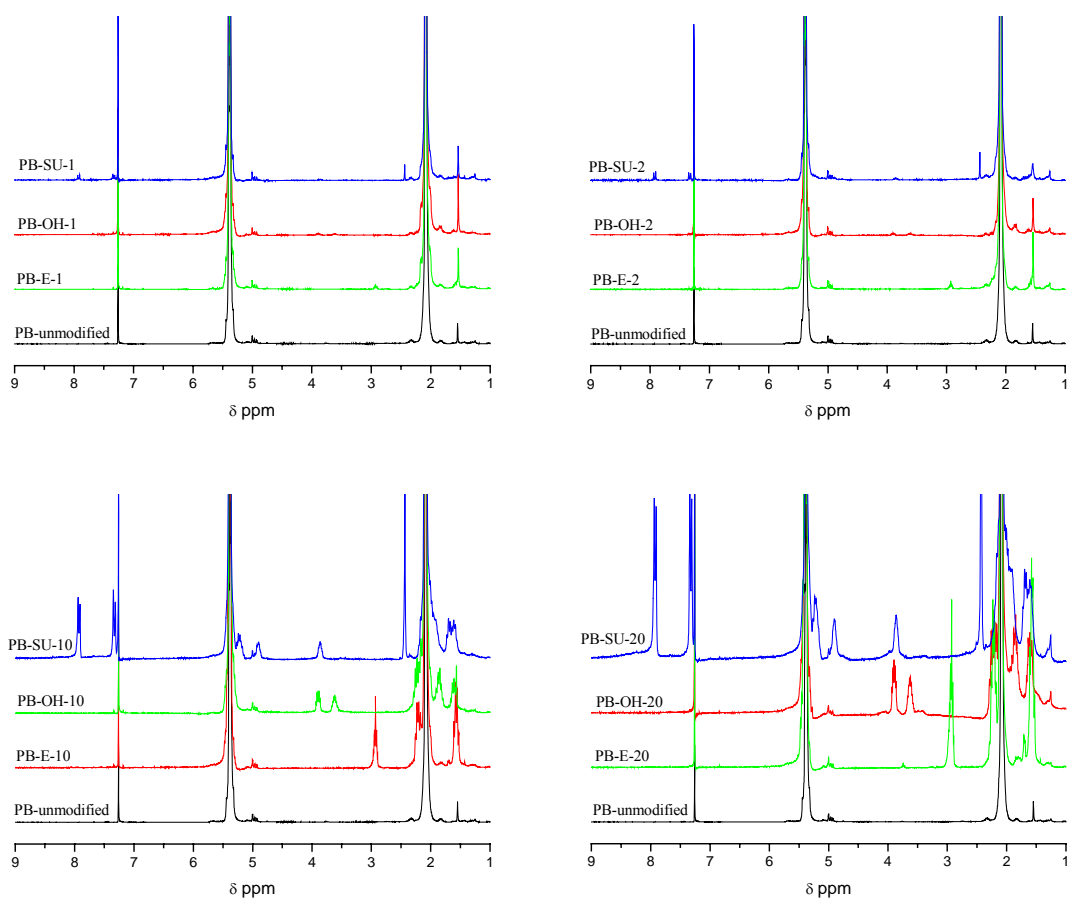


Figure 2-3: $^1\text{H-NMR}$ spectra of different degree of modification. (the degree is indicated as a number)

2-4-2 FTIR Analysis

FTIR spectra of modified PBs are shown in **Figure 2-4**. First, typical N-H, C=O and S=O stretching vibrations from the sulfonyl urethane group ($-\text{O}-\text{CO}-\text{NH}-\text{SO}_2-$) were observed at 3245 cm^{-1} , 1751 cm^{-1} , 1362 cm^{-1} (asymmetric) and 1163 cm^{-1} (symmetric). Their intensities were significantly increased with increasing degree of modification. Second, since the sulfonyl urethane groups present in the polymer matrix are capable of forming a supramolecular hydrogen bonding network, it is possible to verify the hydrogen bonding formation by keeping eyes on the variation of specific absorption bands, such as the C=O and S=O stretching modes, for example. It was found that the C=O vibration band was split into two peaks: one (stronger, free C=O) was at 1751

cm^{-1} and the other (weaker, HB-bonded $\text{C}=\text{O}$) showed up as a shoulder at 1718 cm^{-1} . Nevertheless, since the $\text{C}=\text{O}$ absorption was too strong, it is difficult to tell if the formation of HB network was enhanced with increasing sulfonyl urethane content alone by the relative intensity of these two peaks. On the contrary, note that the asymmetric $\text{S}=\text{O}$ stretching band of sulfonyl urethane did tell the story about how the HB network was effected by increasing the degree of modification: with increasing sulfonyl urethane content, the asymmetric stretching band vanished at 1362 cm^{-1} and was shifted to 1349 cm^{-1} . This observation, as it was, did not contradict the known fact that the hydrogen bonding strength of $\text{C}=\text{O}\cdots\text{H}-\text{N}$ is higher than that of $\text{S}=\text{O}\cdots\text{H}-\text{N}$.

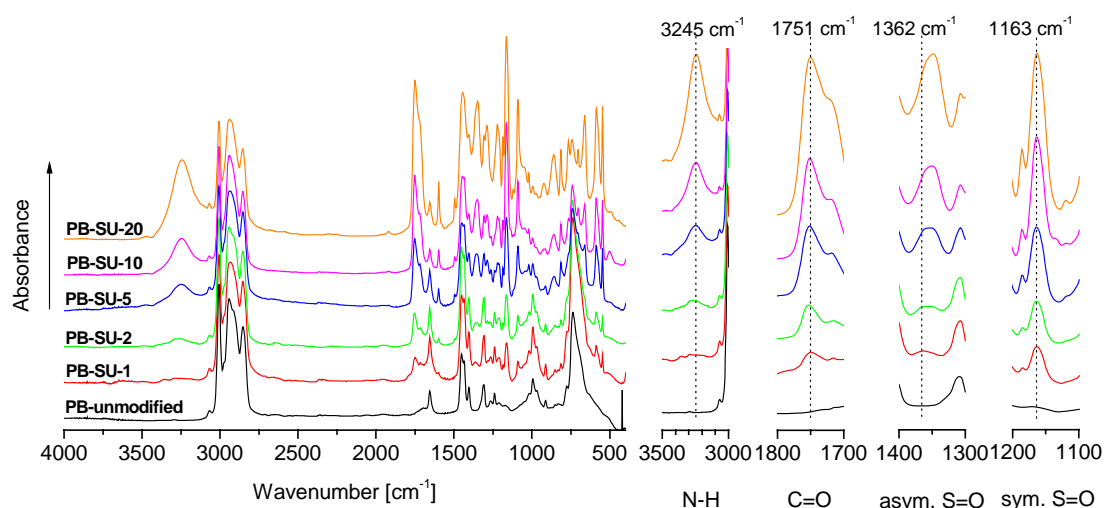


Figure 2-4: FTIR spectra of PBs with various degrees of modification.

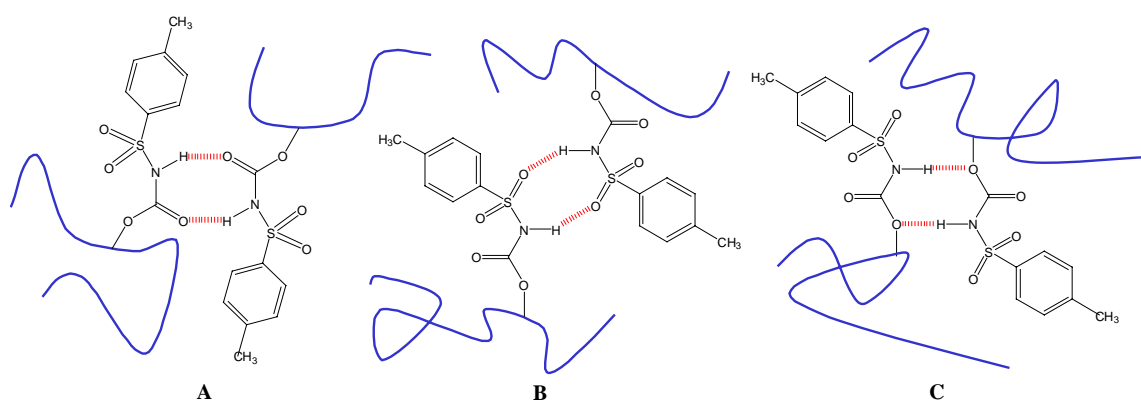


Figure 2-5: Schematic representation of three possible hydrogen bonding complexes between two sulfonyl urethane groups.

A possible reason could be that the IR molar absorptivity of C=O and asymmetric S=O stretching of a sulfonyl urethane are much higher than that of symmetric S=O stretching, thus the relative absorption bands vicissitudes of the formers were less significant. Taking into account the high flexibility of the PB matrix together with the FTIR analysis, we propose that there could be three different kinds of HB complexes, A, B and C as shown in Figure 2-5, formed in PB matrix.

2-4-3 DSC Analysis

Several interesting behaviors were observed in the DSC analysis of both the unmodified and the modified PBs. First, since the commercial polybutadiene investigated in this study contains basically high *cis*-1,4 units, as shown in Figure 2-6, it turned out that the unmodified CB 10 had a glass transition at $-103.4\text{ }^{\circ}\text{C}$ and a crystalline melting temperature at $-9.6\text{ }^{\circ}\text{C}$.

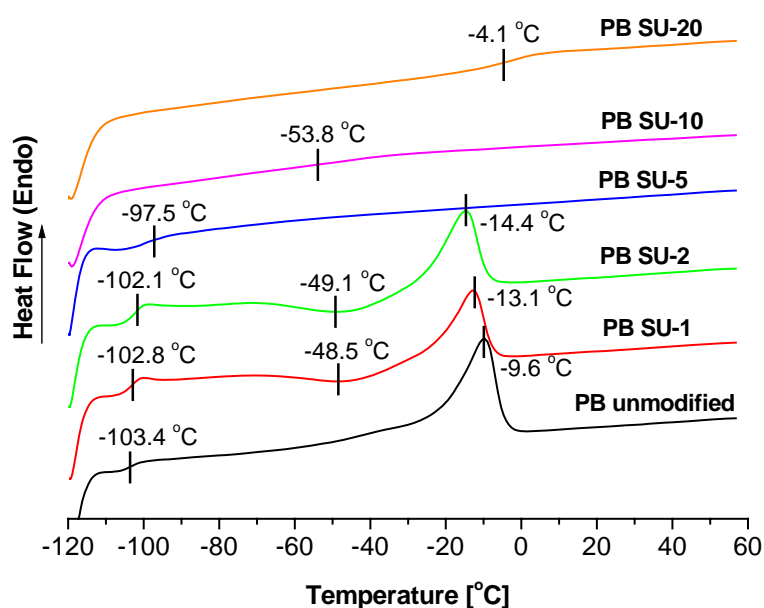


Figure 2-6: DSC traces of PBs with various degrees of modification. (second heating; heating rate $40\text{ }^{\circ}\text{C}/\text{min}$; normalized data)

Second, for the PBs with lower degrees of modification, T_m was slightly shifted to lower temperatures and it was totally suppressed upon a 5 mol% modification. A

possible explanation is that the introduction of few side chains disturbed the well-ordered *cis*-1,4 crystalline structure, therefore the smaller crystals melted at a lower temperature. Third, the glass transition temperatures of the modified PBs were first shifted moderately to higher temperatures up to 5 mol% modification, similar to results described in literature [32], which was attributed to a phase separation between the polar groups and the non-polar polybutadiene. On the other hand, due to the formation of strong hydrogen bonding network, the glass transition was greatly shifted to higher temperatures with higher degree of modifications (Figure 2-6). It is important to note that the glass transition temperature was elevated from $-103\text{ }^{\circ}\text{C}$ to $-4.1\text{ }^{\circ}\text{C}$ upon a 20 mol% modification. Finally, the most interesting observation was that with increasing degree of modification up to 2 mol%, crystal formation (T_c) at $-49\text{ }^{\circ}\text{C}$ can be observed in the DSC traces. To our knowledge it has never been reported before and the induced crystallization could result from the nucleating effect of the low sulfonyl urethane group concentration that acted as a heterogeneity in the semi-crystalline PB matrix.

2-4-4 Dynamic Mechanical Analysis

Because of the difference in sensitivity to thermal transitions, dynamic mechanical analysis was used as an independent method to probe the thermal behavior of the modified PBs. As shown in Figure 2-7, for the unmodified polybutadiene the region where the storage shear modulus (G') fell steeply and the loss shear modulus (G'') soared corresponds to the crystalline melting temperature. However, since CB 10 has a high molecular weight, a fairly wide molecular weight distribution and a medium degree of long-chain branching, the storage modulus was still high enough to sustain a rubbery material even if the surrounding temperature was above T_m (G' still higher than G'' , due to the effective constrained entanglements from the long chain branching [41,42]). First, for the modified PBs with lower degree of modification up to 5 mol%, T_m was shifted to lower temperatures and the values of G' below T_m were reduced. This observation was mainly attributed to the suppression of PB crystallization caused by modification (DSC traces showed that crystalline melting was no longer detectable

upon a 5 mol% modification). Second, despite the fact that modification influenced the PB crystallinity, the thermoreversible hydrogen bonding network served as a mechanically effective crosslinking, G' increased with higher degree of modification. Finally, the shift of the maximum in $\tan \delta$ (T_g) to higher temperature again gives a clear evidence that the introduction of this self-complementary hydrogen bonding moiety is capable of forming an effective “pseudo” crosslinking network. The G' of modified PBs at temperatures above 0 °C shows an interesting behavior. The data show that G' was increased only slightly with higher degree of modification, which is indeed strange at the first glance. However, this behavior could be due to the long chain branching nature of CB 10, which implies that the branched chains were “long enough” to form “effective entanglements”, and the introduction of hydrogen bonding networks lead only to a small increase of the entanglements.

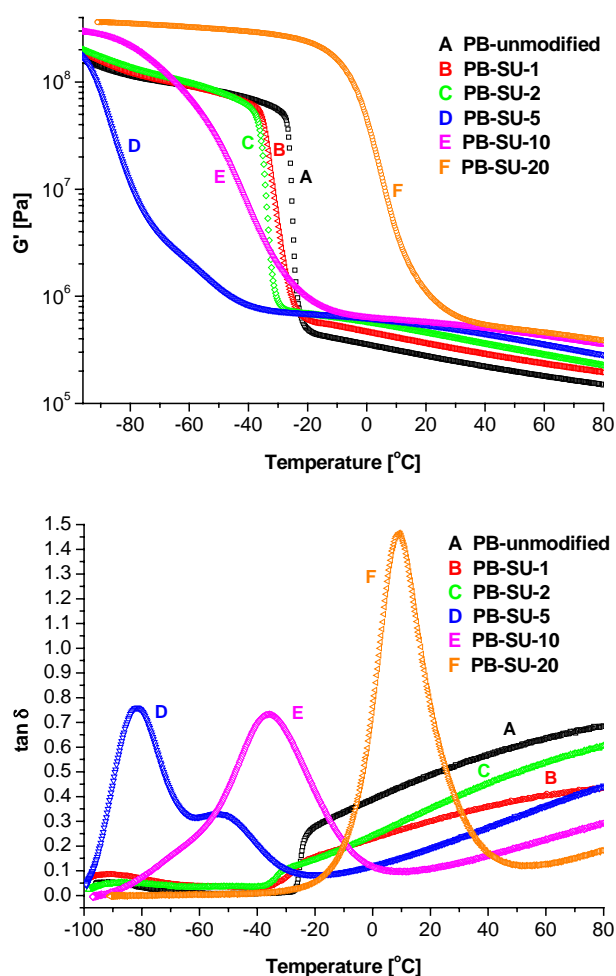


Figure 2-7: Dynamic mechanical spectra of modified PBs. (data obtained at $f = 1$ Hz)

Figure 2-8 shows the master curve of unmodified CB 10, in which data was collected from the frequency sweeps (100 rad/s to 0.1 rad/s) at three different temperatures (100 °C, 50 °C and 0 °C, reference T = 50 °C) in the linear viscoelastic regime.

The detailed explanation of the above remark is given here. It turns out that even at a temperature as high as 100 °C (T_m of CB 10 is at -9.6 °C), G' is still higher than G'' and they do not cross each other. From the reptation theory for polymer melts, the relaxation time is measured experimentally as the reciprocal of the frequency at the crossover point, that is:

$$\tau_r = 2\pi / \omega_{cr} \quad (2-1)$$

where τ_r is the (longest) terminal relaxation time and ω_{cr} is the crossover frequency. In the case of CB 10 there is no crossover point before the terminal flow region, which implies that the time for the chains to escape from their “tubes” (reptation time) is too long to be observed. This behavior also reflects that the entanglements of the chains are too strong and too complicated to disentangle, so that the chains’ motion is strictly hindered. It is also very interesting to see that the complex viscosity is monotonically increased with decreasing frequency, which again gives another clear evidence that

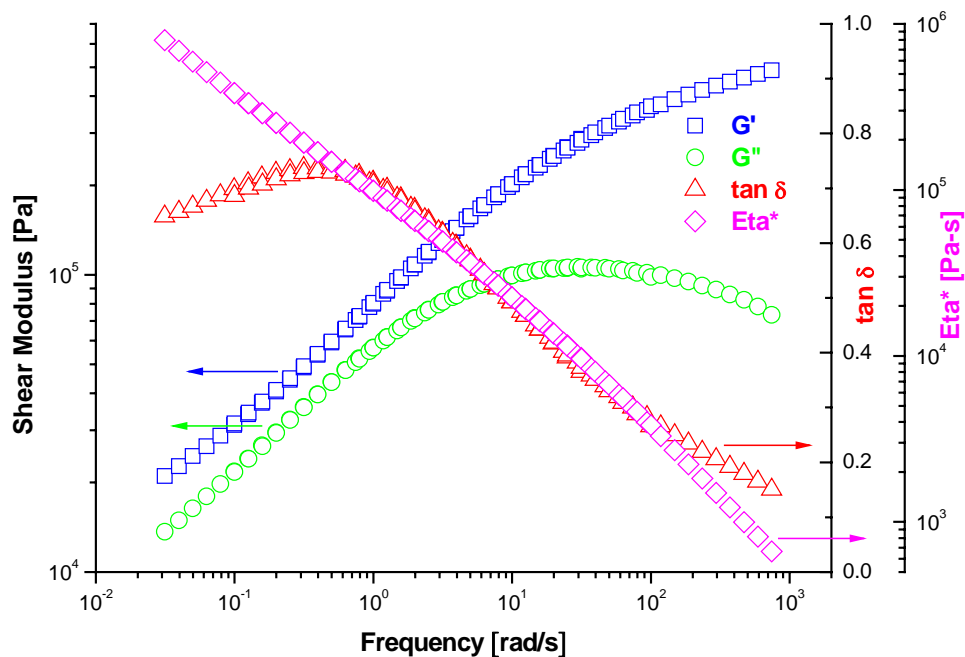


Figure 2-8: Master curve of unmodified CB 10.

even at very low shear frequency the entangled chains are not relaxed at all. As it is, the rheological behavior of CB 10 is more or less like a lightly crosslinked rubber or a filled rubber. However, since the CB 10 is freely dissolved in THF, toluene or other non-polar organic solvents and it contains no fillers, it is concluded that the rheological behavior is attributed to the “effective and constrained” entanglements.

2-5 Conclusion

In this study a commercial polybutadiene rubber, CB 10, was quantitatively modified from 1 to 20 mol% by a three-step polymer analogous reaction, by which the modified PBs were capable of forming supramolecular hydrogen bonding networks. The reactions were monitored by using $^1\text{H-NMR}$ and the formation of hydrogen bonding complexes was verified by FTIR analysis. DSC analysis showed that crystallinity of the investigated PB was suppressed with a degree of modification > 2 mol% and the glass transition was shifted from -103 °C to -4.1 °C upon a sample with 20 mol% modification. Dynamic mechanical analysis showed that upon a 5 mol% modification, the crystallization was totally restrained and with higher degrees of modification the glass transition was further elevated to higher temperatures. These observations indicate that the introduction of this type of hydrogen bonding complexes lead to the formation of effective supramolecular networks. The proposed modification pathway is a simple, economical and highly effective route for rubber and tire industries to design products of new generation.

2-6 Acknowledgement

The experimental part of this work was carried out at the University of Bayreuth. The authors thank Prof. Axel Mueller and the other members of Makromolekulare Chemie

II for their hospitality and instrumental help. Financial support was given by the German Federal Ministry of Education and Research (NMT/03N8645B).

References

- [1] P. W. Allen, G. F. Bloomfield, in “*The Chemistry and Physics of Rubber-Like Substances*”, Maclaren & Sons, Ltd., London, 1963.
- [2] M. A. Golub, S. A. Fuqua, N. S. Bhacca, *J. Am. Chem. Soc.*, **84**, 4981 (1962).
- [3] J. C. Brosse, I. Campistron, D. Derouet, A. E. Hamdaoui, S. Houdayer, D. Reyx, S. Ritoit-Gillier, *J. Appl. Polym. Sci.*, **78**, 1461 (2000).
- [4] S. C. Ng, L. H. Gan, *Eur. Polym. J.*, **17**, 1073 (1981).
- [5] I. R. Gelling, *Rubber Chem. Technol.*, **58**, 86 (1985).
- [6] I. R. Gelling, J. F. Smith, in Proc. Int. Rubber Conf., Milan, Italy, 1979.
- [7] J. S. Park, E. Ruckenstein, *Polymer*, **31**, 175 (1990).
- [8] I. R. Gelling, *J. Nat. Rubber Res.*, **6**, 184 (1991).
- [9] J. C. Brosse, J. C. Soutif, C. P. Pinazzi, *Makromol. Chem.*, **180**, 2109 (1979).
- [10] J. C. Soutif, J. C. Brosse, *Makromol. Chem.*, **185**, 839 (1984).
- [11] D. Derouet, J. C. Brosse, L. M. K. Tillekerantne, *J. Nat. Rubber Res.*, **5**, 296 (1990).
- [12] L. C. Teik, in Proc. Int. Rubber Conf., Kualalampur, Malaysia, 1985.
- [13] S. Jayawardena, D. Reyx, D. Durand, C. P. Pinazzi, *Makromol. Chem.*, **185**, 2089 (1984).
- [14] V. P. Kirpichev, A. I. Yakubchik, G. N. Maglysh, *Rubber Chem. Technol.*, **43**, 1225 (1970).
- [15] M. C. S. Perera, *J. Appl. Polym. Sci.*, **39**, 749 (1990).
- [16] A. S. Hashim, S. J. Kohjiya, *J. Appl. Polym. Sci.*, **32**, 1149 (1994).
- [17] D. Derouet, N. Radhakrishnan, J. C. Brosse, G. Boccaccio, *J. Appl. Polym. Sci.*, **52**, 1309 (1994).
- [18] D. Derouet, F. Morvan, J. C. Brosse, *J. Nat. Rubber Res.*, **11**, 9 (1995).
- [19] D. Derouet, J. C. Brosse, A. Challioui, *Eur. Polym. J.*, **37**, 1315 (2001).
- [20] D. Derouet, J. C. Brosse, A. Challioui, *Eur. Polym. J.*, **37**, 1327 (2001).
- [21] R. Stadler, J. Burgert, *Makromol. Chem.*, **187**, 1681 (1986).
- [22] R. Stadler, L. Freitas, *Coll. & Polym. Sci.*, **264**, 773 (1986).
- [23] L. L. Freitas, M. M. Jacobi, G. Goncalves, R. Stadler, *Macromolecules*, **31**, 3379 (1998).
- [24] A. Brydon, Ph.D thesis, University Aberdeen, 1972.
- [25] H. Holdschmidt, G. Pampus, N. Schön, J. Witte, *Makromol. Chem.*, **101**, 271 (1967).
- [26] G. M. Whitesides, J. P. Mathias, C. T. Seto, *Science*, **254**, 1312 (1991).
- [27] R. P. Sijbesma, F. H. Beijer, L. Brunsveld, B. J. Folmer, J. H. Hirschberg, R. F. Lange, J. K. Lowe, E. W. Meijer, *Science*, **278**, 1601 (1997).
- [28] M. Muller, A. Dardin, U. Seidel, V. Balsamo, B. Ivan, H. W. Spiess, R. Stadler, *Macromolecules*, **29**, 2577 (1996).
- [29] J. H. K. K. Hirschberg, F. H. Beijer, H. A. van Aert, P. C. M. M. Magusin, R. P. Sijbesma, E. W. Meijer, *Macromolecules*, **32**, 2696 (1999).
- [30] C. Hilger, R. Stadler, *Macromolecules*, **25**, 6670 (1992).
- [31] R. Stadler, *Kautschuk, Gummi, Kunststoffe*, **46**, 619 (1993).
- [32] J. Hellmann, C. Hilger, R. Stadler, *Polym. Adv. Technol.*, **5**, 763 (1994).
- [33] S. Schadebrodt, S. Ludwig, V. Abetz, R. Stadler, *Kautschuk, Gummi, Kunststoffe*, **52**, 555 (1999).
- [34] O. Colombani, C. Barioz, L. Bouteiller, C. Chaneac, L. Fomperie, F. Lortie, H.

- Montes, *Macromolecules*, **38**, 1752 (2005).
- [35] R. F. M. Lange, E. W. Meijer, *Macromolecules*, **28**, 782 (1995).
- [36] K. Chino, M. Ashiura, *Macromolecules*, **34**, 9201 (2001).
- [37] F. Ferrero, M. Panetti, G. B. Saracco, *La Chimica e L'Industria*, **66**, 3 (1984).
- [38] J. M. Stellmann, A. E. Woodward, *J. Polym. Sci.*, **A2**, 52 (1971).
- [39] J. Malhotra, D. Zuchowska, P. Hruszka and J. Jurga, *Polymer*, **30**, 467 (1989).
- [40] D. Zuchowska, *Polymer*, **21**, 514 (1980).
- [41] J. D. Ferry, “*Viscoelastic Properties of Polymers*” 3rd ed., John Wiley & Sons, Inc., 1980.
- [42] F. A. Morrison, “*Understanding Rheology*”, Oxford University Press, 2001.

Chapter 3

Synthesis and Characterization of Silica Nanoparticles

Synthesis and Characterization of Silica Nanoparticles

Chih-Cheng Peng¹, Markus Burkhardt¹, Astrid Göpefrt¹, Markus Drechsler¹, Volker Abetz²

¹Makromolekulare Chemie II, Universität Bayreuth, Universitätsstrasse 30, 95447 Bayreuth, Germany

²Institut für Polymerforschung, GKSS-Forschungszentrum Geesthacht GmbH, Max-Planck-Strasse 1, 21502 Geesthacht, Germany

(in-situ DLS part was submitted)

3-1 Abstract

In this chapter we present two different hydrolytic sol-gel routes of synthesizing silica nanoparticles. The first method is in the light of the modified Stöber process in which silica nanoparticles are prepared directly from organotrialkoxysilane precursors. The second method is based on Stöber synthesis of silica nanoparticles combined with particle surface modification. Both methods are effective in silica particle synthesis and its surface modification without using an expensive surfactant, however the particle size and its distribution thereof are different. Based on the second method, silica nanoparticles of smaller size (down to 20 nm in diameter) could be prepared simply by changing the reaction media and the reaction time.

It is well known that the size of silica nanoparticle prepared from the Stöber method can be controlled by changing the reaction temperature, the reaction media (usually alcohols), the reaction time and concentrations of various reagents. But the question is, could one “exactly” synthesize silica nanoparticle of a certain size without losing much time in searching for a proper reaction system? Thus at the end of this chapter, we explored the possibility of monitoring the growth of silica nanoparticles by *in-situ* dynamic light scattering (DLS). This method is based on the robust DLS in determining particle sizes for colloids and it turns out that this *in-situ* strategy was accurate for nanoparticles of sizes smaller than 100 nm under certain reaction conditions. To our knowledge this strategy has never been reported before and it not only offers a means to understanding the mechanism of particle growth but also can be used in a very small scale to tailor the particle size and its distribution before the scaled-up production of silica nanoparticle of demanding sizes in a short time.

3-2 Introduction

Over the past few years, the synthesis of organic-inorganic hybrids has become the subject of extensive investigations because of the exceptional opportunities to tailor the properties of these materials for use in a range of applications, including their use as polymer additives [1-6]. The sol-gel process has been used extensively to provide a versatile method for production of organic-inorganic hybrid material. Although a range hybrids, such as organically-modified silicas (ormosils) [7-9], has been prepared in the form of monolithic products, the use of this process as a route to hybrid nanocomposite particles has been overlooked until quite recently. Such particles have real potential as speciality nanofillers, where the organic group can be tailored for compatibility with the matrix.

The well-established hydrolytic sol-gel approach, which enables the preparation of nanoparticles by base-catalyzed hydrolysis and condensation reactions of monomeric precursors in an aqueous solvent system, has begun to receive considerable attention. In recent years, a range of organically-modified silica particles has been synthesized successfully by a modified Stöber method [10-16]. This hydrolytic sol-gel approach was developed originally for the preparation of unmodified silica nanoparticles from tetraalkoxysilane precursors, such as tetraethoxysilane (TEOS) [17], and has been extended to the formation of silsequioxane particles (with empirical formula $[R_2Si_2O_3]_n$) from mixtures of TEOS and organotrialkoxysilane precursors $(RSi(OR')_3)$, with R = methyl, phenyl, octyl, aminopropyl, etc., and R' = methyl or ethyl [10-12] or directly from organically-modified precursors [13-16]. However, this type of synthesis usually limits the preparation of ormosil particles with diameters larger than 500 nm [18].

Applications involving silica nanoparticles are of interest not only in the academic field of physical chemistry, dealing with stability and interactions in dispersions, but also in numerous industrial fields including ceramics, catalysis, chromatography, pigments, and pharmaceuticals. Over the years several techniques have been developed for the synthesis of powders with uniform size, shape and composition.

The most convenient method for the preparation of the so-called monodisperse particles is the control of chemical reaction in homogenous solutions. With the method developed by Stöber et al. [17] it is possible to synthesize extraordinary spherical particles that were used by many research groups as model system for further studies of rheology [19], electrorheology [20], light scattering [21], sintering [22] or sedimentation [23]. Modifications of the hydrophilic surface have been realized by polymer adsorption [24], graft polymerization [25], esterification [26], and silylation with silane coupling agents [27] in order to adjust the properties and to improve dispersibility in organic media.

The first route of silica nanoparticle synthesis used here is following the procedures reported by Buining et al. [28], Arkhireeva et al. [29,30], who showed that sodium silica solution can be used as a seed for further growth of unmodified silica particles, the sol prepared from an aqueous sodium silicate solution was used as the seed for silsesquioxane nanoparticle formation from organotrialkoxysilane. The synthesis was performed at ambient temperature for 1 hour.

The second route is based on the Stöber method but the detailed synthesis way is by modifying the procedure reported by Gellermann et al. [31] and Vacassy et al. [32], in which we first synthesized silica nanoparticle and further modified its surface polarity. The concentrations of catalyst, TEOS, H₂O, and the reaction time utilized here were devised to prepare silica nanoparticles of a diameter of 100 nm. The nanoparticles produced were further verified by TEM and FTIR.

Researchers have put much emphasis upon the mechanism of the growth of silica nanoparticles (both on hydrolysis and condensation reactions), however, no work has been reported on solving a basic problem – how could one design an optimal reaction system for synthesizing silica nanoparticles of certain sizes before spending too much time? Despite the well-known fact that the size of silica nanoparticles prepared from the hydrolytic route (Stöber synthesis) can be controlled by changing the reaction temperature, the reaction media (usually alcohols), the reaction time and concentrations of various reagents [17, 33-45], either there is no universal recipe for people who are interested only in synthesizing silica nanoparticles on their own.

For practical purpose, of course, the control the silica particle size and its distribution is extremely important. In order to determine the final sizes and the size distribution of silica nanoparticles, several techniques, such as transmission and scanning electron microscopy (TEM, SEM) and light scattering, have been utilized. Dynamic light scattering (DLS) is a technique to investigate the scattering intensity fluctuation and get the size information of molecules. Since DLS is less sensitive to stationary impurities than other techniques and it provides rapid, accurate determinations of particle size (especially for monodisperse hard sphere the autocorrelation function is reduced to a single exponential equation), we came up with the idea to use the DLS technique *in-situ* during the particle synthesis.

In order to justify our idea, one should check the basic theory behind DLS before going any further. As mentioned before, for monodisperse hard spheres, the field autocorrelation function, $g(\tau)$, can be reduced to a single exponential equation [46]:

$$g(\tau) = \exp(-Dq^2\tau) \quad (3-1)$$

where D is the translational diffusion coefficient, τ is the instant time and q is called the length of the scattering vector expressed as:

$$q = \frac{4\pi n}{\lambda_0} \sin\left(\frac{\theta}{2}\right) \quad (3-2)$$

where λ_0 is wavelength of the laser source, n is the refractive index of the solution and θ is the scattering angle. Thus, with the data collected from the scattered light, the hydrodynamic radius, R_h , can be calculated by Stokes-Einstein equation [47]:

$$R_h = \frac{kT}{6\pi\eta_s D} \quad (3-3)$$

where k is Boltzmann constant, T is the absolute temperature and η_s is the viscosity of the solvent. It is assumed here that due to the low concentrations of reagents (TEOS, NH_3 and H_2O) in EtOH, the refractive index does not change in the course of particle growth and that the hydrodynamic interactions between particles are negligible.

Additionally, because the silica particles produced are hard spheres, we further assume that the particle radius is equivalent to the hydrodynamic radius acquired from the DLS measurement.

3-3 Experimental

3-3-1 Materials

Sodium metasilicate (grain Na_2SiO_3), tetraethoxysilane (TEOS) (98%, $d = 0.934$, Aldrich), phenyl trimethoxysilane (PTMS) (94+%, $d = 1.049$, Aldrich) were used as received. Ammonia aqueous solution (25 wt% NH_3), methanol (analytical grade) and absolute ethanol were purchased from Merck and were used without further purification. Fresh-made deionized water was used here as a co-solvent and a hydrolysis catalyst.

3-3-2 Synthesis of Modified Silica Nanoparticles via Modified Stöber Method

The effect of the reaction parameters, such as the rate of addition of organotrimethoxysilane, reaction time, water, ammonia, seed solution, and organotrimethoxysilane concentrations, on the size of the ormosil particles have been studied by Arkhireeva et al. [29,30]. In order to synthesize silica nanoparticles of a diameter of 100 nm, the molar ratio of $\text{H}_2\text{O}/\text{NH}_3/\text{PTMS}/\text{EtOH}/\text{Na}_2\text{SiO}_3$ of 300/75/2/160/0.044 was taken in the light of literature data [29].

Sodium silicate solution was first prepared by dissolving 0.27 g Na_2SiO_3 (2.2 mmol) in 36 ml deionized H_2O (2 mol). Under vigorous stirring this solution was rapidly mixed with 184 g absolute EtOH (4 mol) to obtain a dilute, virtually transparent sol. This suspension was then added to a solution containing 42.75 g deionized H_2O

(2.375 mol), 184 g absolute EtOH (4 mol) and 255 g 25 wt% ammonia aqueous solution (3.75 mol NH₃, 10.625 mol H₂O) and the mixture was further stirred for 2 minutes before the addition of PTMS. Finally 21.1 g PTMS was added quickly at one dose into the above solution and the system was stirred at room temperature. After 1 hour, a large excess of deionized water (3 parts of water per 1 part of the solution) was added to the reaction mixture and the product was dried in air for approximately 3 days and it was further dried under vacuum at 80 °C for another 24 hours to yield fine white powders. The particle size and its surface functionality were determined by TEM and FTIR.

3-3-3 Synthesis of Unmodified Silica Nanoparticles via Stöber Method

In order to synthesize silica nanoparticles of a diameter of 100 nm via the Stöber method, the molar ratio of H₂O/NH₃/TEOS/EtOH of 11.3/4/1/78 was optimized from the *in-situ* DLS experiments, so that the ratio of H₂O/Si was kept in the range between 7 and 25.

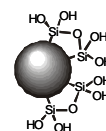
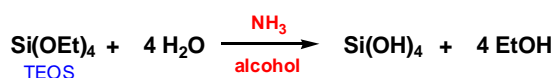
To a solution containing 359 g absolute EtOH (7.80 mol) and 27.2 g 25 wt% ammonia aqueous solution (0.40 mol NH₃, 1.13 mol H₂O), 21.3 g TEOS (0.10 mol) was added quickly at one dose under stirring and the resulting solution was kept stirred for 5 minutes to ensure homogeneity, finally the reaction mixture was kept at room temperature without stirring for 24 hours (there is no precipitation could be seen at the bottom of the reaction flask). The purification procedure was as follows: The suspension was first centrifuged at a rotational speed of 4000 rpm at 15 °C for 60 minutes to give a precipitated gel separated from the solvent and the residual reactants. After removing the non-gel parts, the as-precipitated SiO₂ particles were again redispersed in EtOH after an ultrasonic treatment. In order to have well-defined and non-aggregated silica nanoparticles, it is important to note that the purification procedure must be repeated for at least 4 times before drying. After purification the particles (hereafter **Si-OH**) were dried under vacuum at 80 °C for 48 hours before characterization. The particle size and its surface functionality were determined by

TEM and FTIR, the specific surface area was measured by BET method (**B**runauer, **E**mmett and **T**eller who invented the method). Based on similar procedure, silica nanoparticles of size of 20 nm (diameter) could be synthesized by changing the reaction media (from EtOH to MeOH) and the reaction time (1 hour instead of 24 hour), and the details will be discussed later in this chapter.

3-3-4 Synthesis of Modified Silica Nanoparticles via Stöber Method

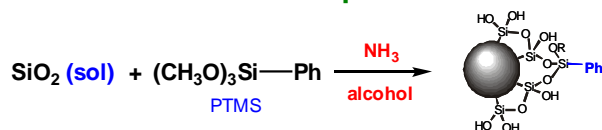
The surface modified silica nanoparticles (hereafter **Si-Ph**) were prepared by following the procedure described in 3-3-3. Here in order to attach PTMS onto the silica surface, instead of purifying the reaction suspension that had been kept for 24 hours, under stirring a portion of 10 mol% PTMS based on the amount of TEOS was added into this solution and the solution was stirred at least for 5 minutes. Again, the suspension should be kept at room temperature without stirring for another 24 hours and during the course of reaction no precipitation could be seen at the bottom of the flask. The purification procedure was the same as proposed in 3-3-3. The particle size and its surface modification of the final product were determined by TEM and FTIR, the specific surface area was measured by BET method. Comparison of synthesis methods discussed in Section 3-3-3 and 3-3-4, and the particle surface functionalities are summarized as follows:

a. unmodified silica particle

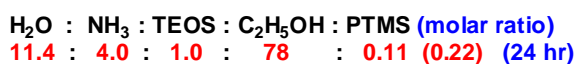


polar surface

b. surface modified silica particle



less polar surface



3-3-5 *In-situ* Dynamic Light Scattering in Monitoring Silica Particle Growth

DLS experiments were performed on an ALV DLS/SLS-SP 5022F compact goniometer system with an ALV 5000/E correlator and a He-Ne laser ($\lambda_0 = 632.8$ nm). The *in-situ* investigation was performed according to the principle of the Stöber process, and here one trial (**SP-2**) with a final particle size of 100 nm in diameter is highlighted as a typical example. Before the preparation of the reaction solution, a dried cuvette was mounted in the isothermal bath (25 °C) of the DLS equipment and the laser detector (the photomultiplier) was fixed at an angle of 90 degree referring to the incident light. 1.2 g of 25 wt% ammonia aqueous solution (18 mmol NH₃ and 50 mmol H₂O) and 20 mL of absolute EtOH (34 mmol) were first mixed in a 40 mL thoroughly cleaned and dried cylindrical glass vial. To the above fresh-prepared solution 1.0 mL of TEOS (4 mmol) was then added and the whole mixture was vigorously shaken for 10 seconds. Starting by using a 10 mL plastic syringe, 8 mL of the solution was drawn in and the it was soon mounted with a Millipore filter of a pore size of 200 nm (housing: polypropylene, membrane: polytetrafluoroethylene). Immediately after the first step, the solution was injected into the cuvette drop by drop. It is important to note here the first few drops of the solution were discarded and used as a washing solution for the filter before injecting any solution into the cuvette. Upon an injection of around 2 mL, the cuvette was capped and the experiment was allowed to start. In this study each measurement was kept running at least for 10 hours and the scattered light was detected at a fixed angle of 90 degree. The experiment was also programmed so that each measurement was run for 1 minute in every 5 minutes. Note that the time span starting from the preparation of the reaction solution to the onset of the measurement should be kept within 1 minute. Different trials using different reagent concentrations (the ratios of H₂O/Si were always kept between 7 and 25) were also performed following the same procedure described above and the detailed profiles are listed in **Table 3-1**. By using the ALV 5000/E-WIN program the information of particle size and its distribution can be obtained by CONTIN analysis. It is also important to note that the intensity regulator of the laser source and the detector were subject to changes once the particle concentration is too high and/or the intensity of scattered light was too large.

Table 3-1: Detailed concentration profiles of reagents for in-situ DLS

ID	TEOS (mL)	EtOH (mL)	25 wt% NH _{3(aq)} (g)	H ₂ O (g) ^a	H ₂ O/Si ^b
SP-1	1.0	20	2.0	-	19.0
SP-2	1.0	20	1.2	-	11.4
SP-3	1.0	20	0.6	0.45	11.4
SP-4	0.5	20	1.2	-	22.8
SP-5	0.5	20	0.6	0.45	22.8
SP-6	0.5	20	0.6	-	11.4

^athe additional amount of deionized water added^bthe molar ratio of total amount of water to TEOS

3-3-6 Characterizations

TEM micrographs were obtained using a Zeiss LEO 922 transmission electron microscope. The suspensions for TEM were prepared by dissolving 10 mg dried silica nanoparticles in a 250 mL round bottom flask filled with 100 ml acetone, the systems were then ultrasonified for 5 minutes to give clear suspensions. Clean plastic micropipettes were used to transfer a droplet of the silica particle suspension that was then dipped onto copper carrier grids (200 mesh) covered with a carbon film.

FTIR spectra were recorded at room temperature using a Bruker FTIR EQUINOX 55/S spectrometer at a resolution of 4 cm⁻¹. The samples for FTIR analysis were prepared by grinding 10 mg dried silica nanoparticles with 1.0 g dried KBr grain until very fine powders were obtained. Afterwards about 100 mg of the fine powder were transferred into a circular mold and pressed using a hydraulic presser to give thin circular pellets. In order to prove the effectiveness of silica surface modification, the FTIR signals were normalized by unifying Si-O-Si stretching absorption at around 1150 cm⁻¹ to prove the effectiveness of silica surface modification.

Surface data were obtained from nitrogen adsorption measurements at -196 °C using a Quantachrome Autosorb-1 instrument. Samples were outgassed for 12 hours at 150 °C prior to the analysis. Specific surface area data were calculated using the BET method, which were generated automatically by the program associated with the instrument.

3-4 Results and Discussion

3-4-1 Modified Silica Nanoparticles via Modified Stöber Method

TEM micrographs of the silica nanoparticles synthesized via the modified Stöber method are shown in [Figure 3-1](#). Instead of results claimed in literatures [\[29\]](#), we found that the size and its distribution of the silica particles prepared in this way were not satisfactory; the majority of the particles were of sizes larger than 200 nm and they were not “relatively” monodisperse.

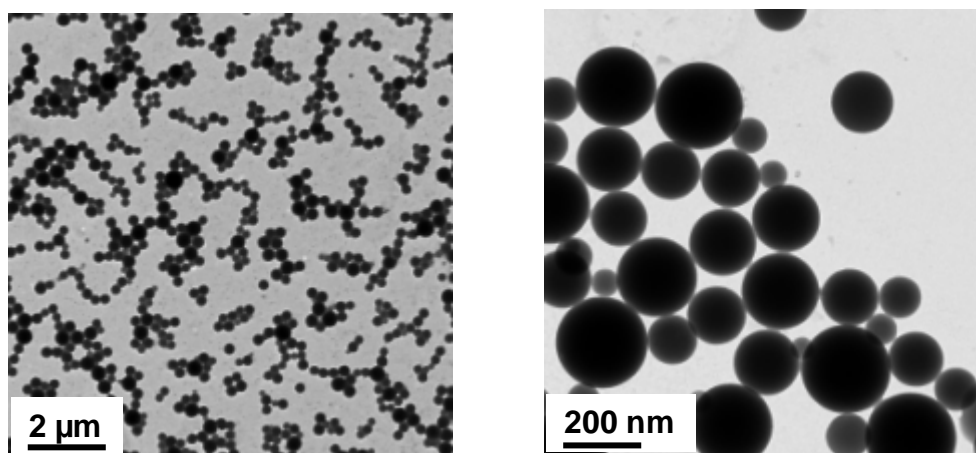


Figure 3-1: TEM micrographs of silica particles synthesized via the modified Stöber method.

FTIR spectrum of the particle prepared is shown in [Figure 3-2](#) and it confirms that the formation of Si-O-Si bonds and the retention of Si-C linkages during the hydrolysis and condensation reactions [\[48\]](#). It can be seen that the silsesquioxanes exhibit well-defined absorptions between 1410 cm^{-1} and 1430 cm^{-1} , characteristic of symmetric deformations in Si-C groups. C-H and Si-C stretching vibrations are observed at about 2900 cm^{-1} to 3070 cm^{-1} and 700 cm^{-1} to 780 cm^{-1} , respectively. The presence of Si-O-Si linkages is supported by sharp, intense absorptions at 1150 cm^{-1} (stretching) and 1030 cm^{-1} (flexing), and distinct vibrations at about 430 cm^{-1} to 500 cm^{-1} (bending). It also shows a well-defined benzene ring absorption at 1590 cm^{-1} and weak absorptions characteristic of -OH groups are observed between 3100 cm^{-1} and 3600 cm^{-1} .

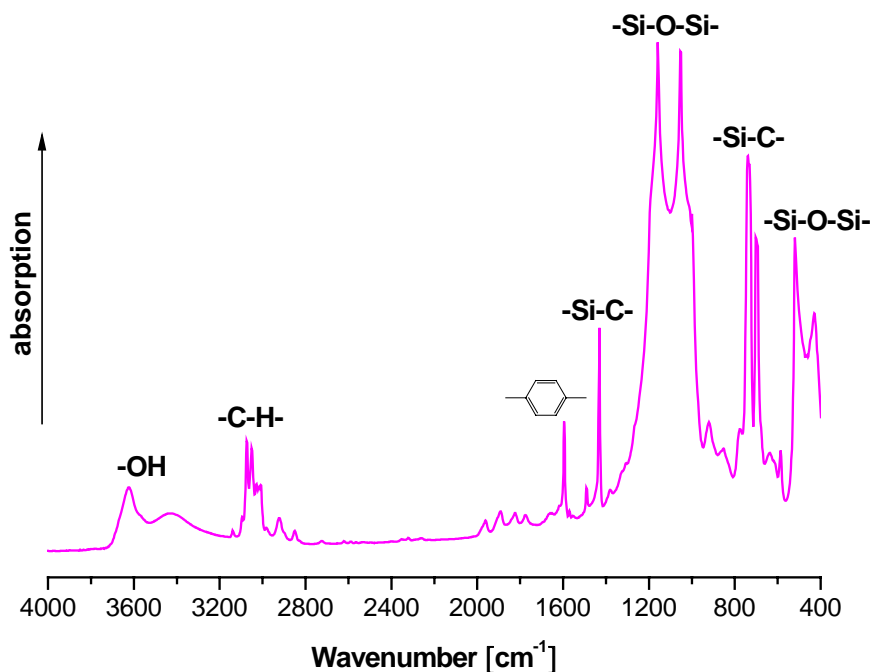


Figure 3-2: FTIR spectrum of silica particles synthesized via the modified Stober method.

For our purpose of investigating the influence of non-covalent interaction on the properties of nano-filler filled materials, the defects of this synthesis method in particle size as well as its distribution will bring about many other unnecessary parameters to the materials. Thus, the second synthesis method for silica particles is counted on to fulfill our objective.

3-4-2 Surface Unmodified and Modified Silica Nanoparticles via Stober Method

TEM micrographs of **Si-OH** and **Si-Ph** silica nanoparticles synthesized via the Stober method are shown in [Figure 3-3](#) and [Figure 3-4](#). As can be seen here this synthesis method gives spherical and monodisperse particles of a size of 100 nm for both particles, meaning the surface modification did not significantly change the particles size of original **Si-OH** used as surface modification precursor.

The BET measurement showed that the specific surface area these silica particles were 63 and 47 m²/g for **Si-OH** and **Si-Ph**, respectively. It means that the surface modification does not significantly change the effective surface area of the original **Si-OH** used for surface modification silica particles. Together with the observation from TEM micrographs, we conclude that these two different particles can be further used in investigating the influence of non-covalent interaction exclusively on the properties of nano-filler filled materials since they have similar particle size and specific surface area.

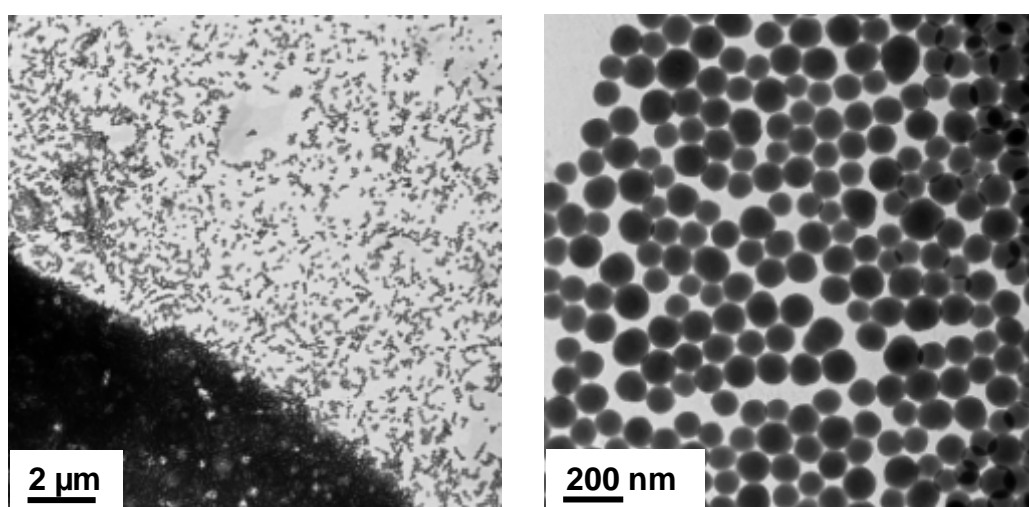


Figure 3-3: TEM micrographs of surface unmodified silica particles synthesized via the Stöber method.

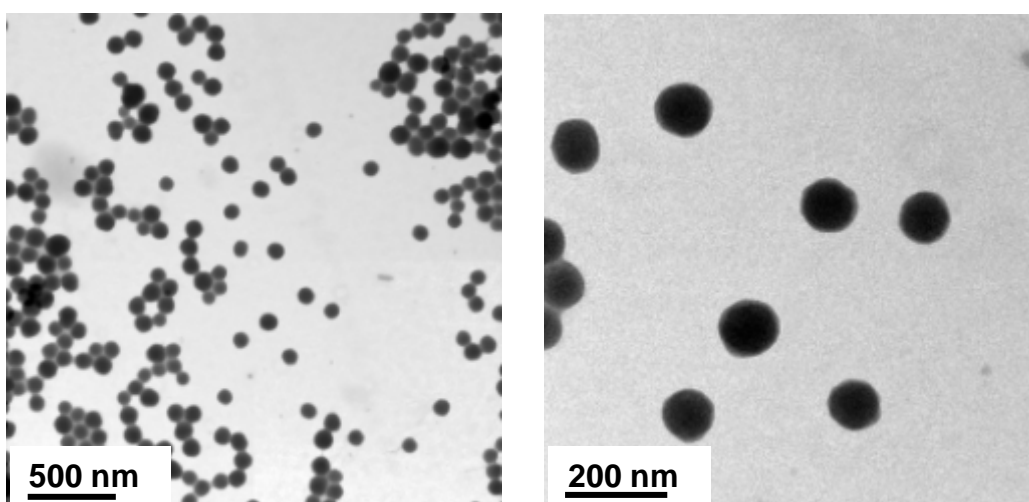


Figure 3-4: TEM micrographs of surface unmodified silica particles synthesized via the Stöber method.

FTIR spectra of the particles prepared are shown in Figure 3-5. For the surface unmodified silica particle, the presence of Si-O-Si linkages is supported by sharp, intense adsorptions at 1150 cm^{-1} (stretching), and distinct vibrations at about 430 cm^{-1} to 450 cm^{-1} (bending) [49], however, strong characteristic of OH groups are observed between 2900 cm^{-1} and 3600 cm^{-1} .

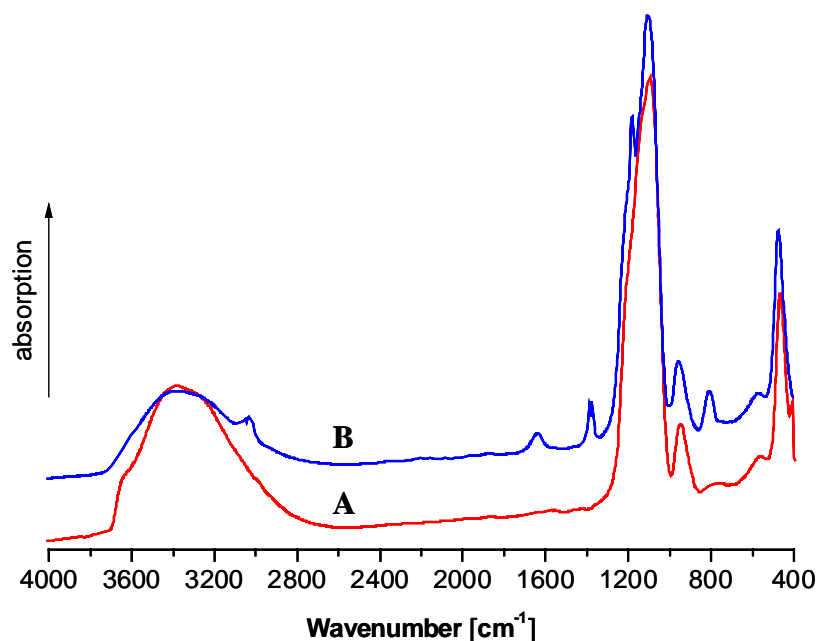


Figure 3-5: FTIR spectra of silica particles synthesized via the Stöber method. (A: **Si-OH**, B: **Si-Ph**)

Compared with **Si-OH**, for **Si-Ph** silica particle there are a weak benzene ring adsorption at 1610 cm^{-1} and 1400 cm^{-1} , and much weaker adsorptions characteristic of OH groups observed between 2900 cm^{-1} and 3600 cm^{-1} . These results show that the surface modification via addition of PTMS onto **Si-OH** surface successfully reduce the OH groups present on **Si-OH** surface and these two particles with different surface polarity can be used in investigating rubber-filler interaction.

Here comes a question, based on similar method if one can synthesize silica particles of smaller sizes simply by changing certain reaction parameters? According the arguments made by previous researchers, it is generally believed that the final silica particle size synthesized via the Stöber method (hydrolytic route) is controlled by the

reaction rate of hydrolysis of tetraalkoxysilane and the rate of condensation of hydrolyzed intermediate, e.g. $\text{Si}(\text{OH})_4$ [17, 33-45]. It means that one may synthesize silica particles of different sizes by changing the reagents' (NH_3 , H_2O , alcohol and tetraalkoxysilane) concentrations, cosolvents (alcoholic), the alkoxy groups on tetraalkoxysilane and the reaction time.

Figure 3-6 shows the TEM images of the resulting silica particles which were synthesized by replacing EtOH by MeOH (method A), and reducing the reaction time from 24 hours to 2 hours (method B). The former method gives silica particles of a size of 15 nm and the latter gives ones of 18 nm. Interestingly, although one is able to see the individual primary particles from the micrographs, the particle morphologies are distinct from each other.

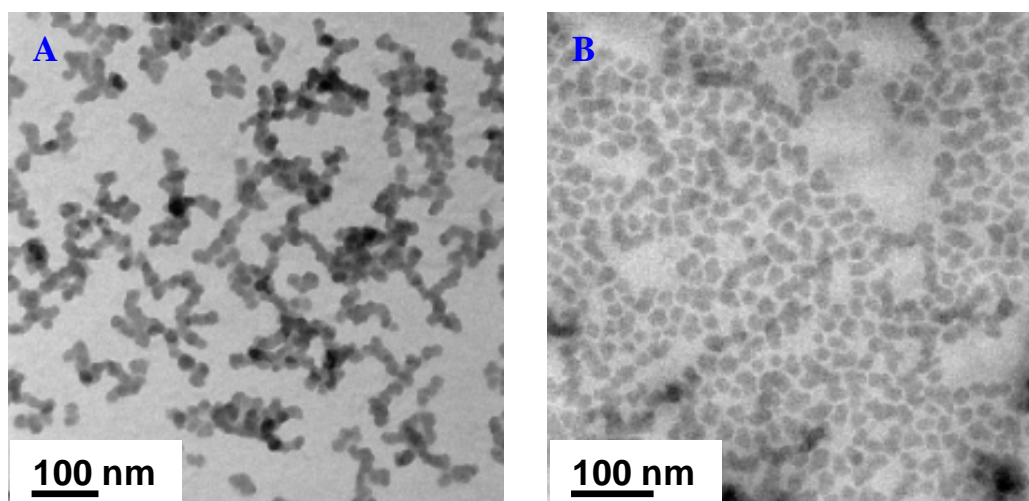


Figure 3-6: TEM micrographs of silica particles synthesized via the Stöber method with different reaction parameters. (A: replacing EtOH by MeOH, B: reducing reaction time from 24 hours to 2 hours)

Method A gives an “Iler view of aging” type silica particle, which was first described by Iler [50]. This morphology is attributed to that the higher solubility of surfaces with positive curvatures causes dissolution near the particle surface and reprecipitation on interparticle contacts that have negative curvatures and lower solubilities. This coarsening process, as sketched in Figure 3-7, which is driven by a

reduction in the solid-liquid interfacial energy, builds necks between particles that significantly strengthen the gel network. One possible reason of forming such a structure is due to the fact that the replace of EtOH by MeOH accelerates both hydrolysis and condensation reaction [51]. Contrary to particles prepared by method A, method B gives non-coarsening type porous particles.

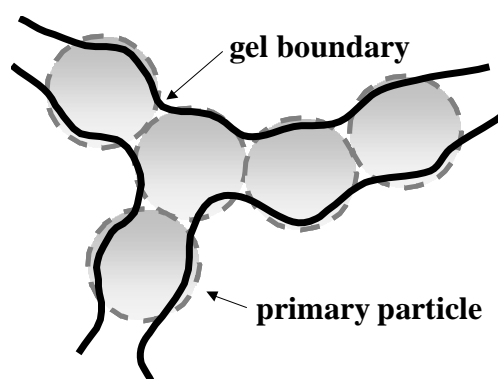


Figure 3-7: Coarsened structure that results from aging a network of particles under conditions in which there is partial solubility of the condensed phase.

3-4-3 *In-situ* Dynamic Light Scattering

The results of real time monitoring of silica particle growth by DLS are shown in **Figure 3-8**. As can be seen, the particles grew very fast in the first 100 minutes and thereafter the rates of particle growth decreased. These time-resolved curves imply that the size of the silica nanoparticles was controlled by the initial reaction rate since the reactive species were at higher concentrations at the first reaction stage. As the reaction proceeded, possibly due to the equilibrium between all species, the particles did not grow significantly and they were stabilized in the suspensions. It is interesting to note that the higher the initial rate is, the larger the final particle resulted. Besides, it is found that the initial concentrations of reagents did contribute differently to the final particle sizes. In summary, higher concentration of NH_3 (**SP-2** vs. **SP-3** and **SP-4** vs. **SP-5**) and H_2O (**SP-5** vs. **SP-6**) resulted in larger particles, whereas higher concentration of TEOS resulted in smaller particles.

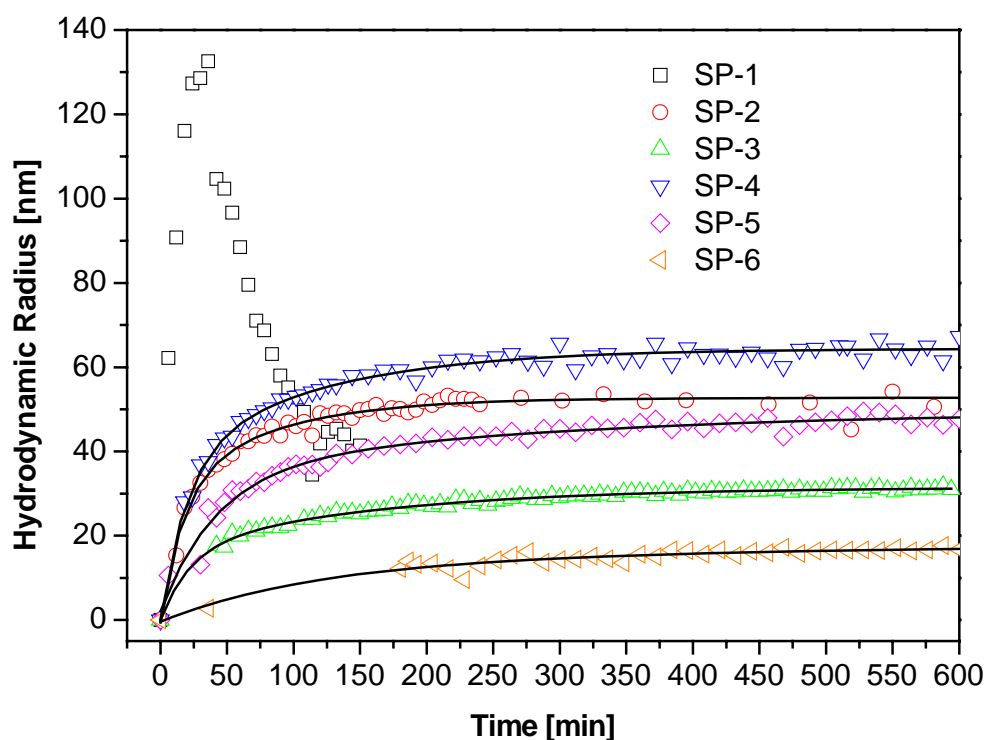


Figure 3-8: Time-resolved silica particle growth via in-situ DLS measurement. (solid lines were drawn using an exponential fitting).

Unfortunately, for **SP-1**, the curve did not behave the same way as the others. The curve soared most quickly in the first period, but soon after it started and continued to drop instead of reaching a constant value. It does not make any sense if one just regards the drop of the curve as a size reduction resulting from particles decomposition before all the reactions (hydrolysis and condensation) reached equilibrium. One possible explanation is that the reaction condition for **SP-1** was prone to form larger silica particles that continued to precipitate after the first stage of growth, and the plunge of the scattered data were collected from the residual smaller particles that were still suspended in the solution. This speculation was further justified since there was appreciable amount of solid precipitation at the bottom of cuvette after the *in-situ* run of **SP-1**.

To verify the *in-situ* DLS, TEM micrographs of **SP-2** and **SP-6**, as shown in [Figure 3-9](#) and [Figure 3-10](#), were used as an example. It can be seen that the resulting hydrodynamic radius acquired from DLS are in good agreement with the radius

measured by TEM, meaning that for the chosen experiments the *in-situ* DLS technique holds good in monitoring the growth of silica nanoparticles.

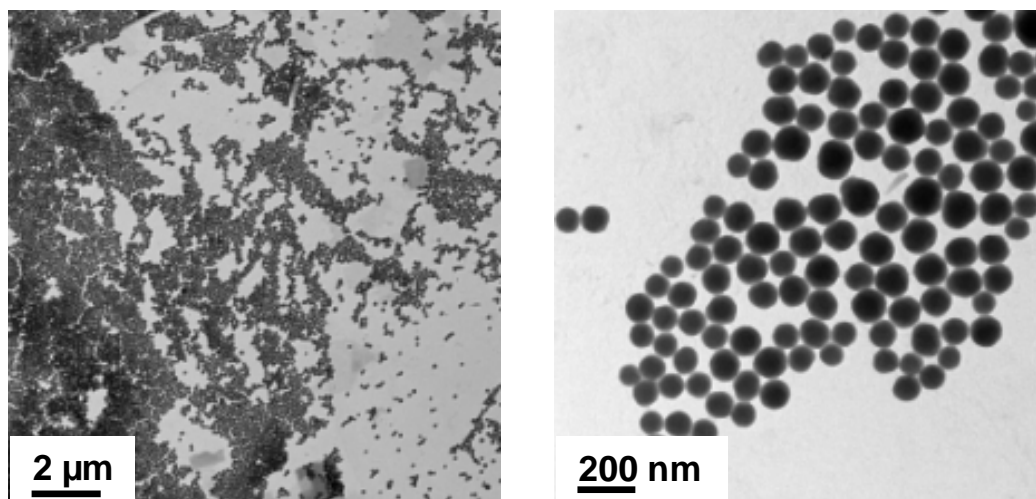


Figure 3-9: TEM micrographs of silica particles from SP-2.

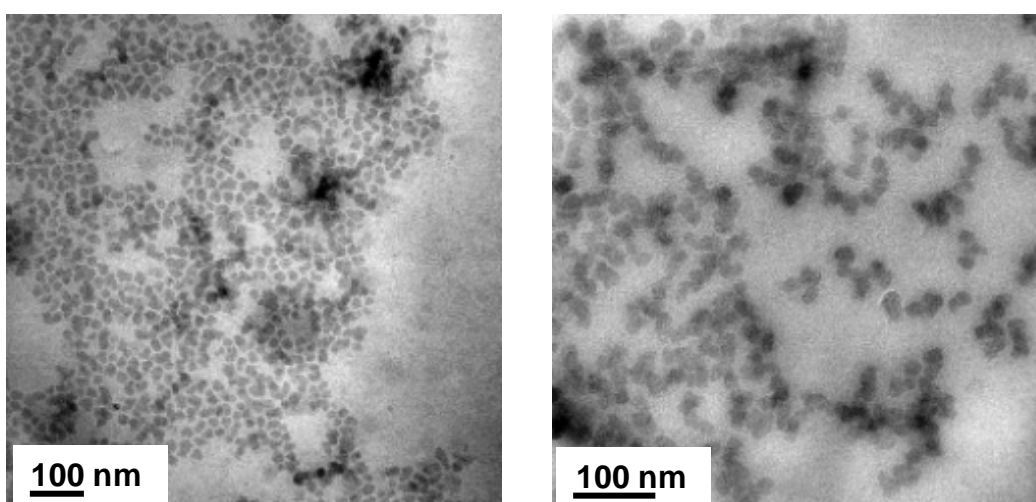


Figure 3-10: TEM micrographs of silica particles from SP-6.

Figure 3-11 shows the radius distribution of different samples acquired at the end of each measurement. These curves reveal that the *in-situ* DLS gives radius information similar to that from the TEM analysis, again meaning that our previous assumptions do apply to this *in-situ* study on the growth of silica nanoparticles under certain conditions. Additionally, for **SP-1** it is believed that the shoulder appearing at a higher radius right next to the main peak is corresponding to the larger silica particles that were prone to coagulation and precipitation under its reaction condition.

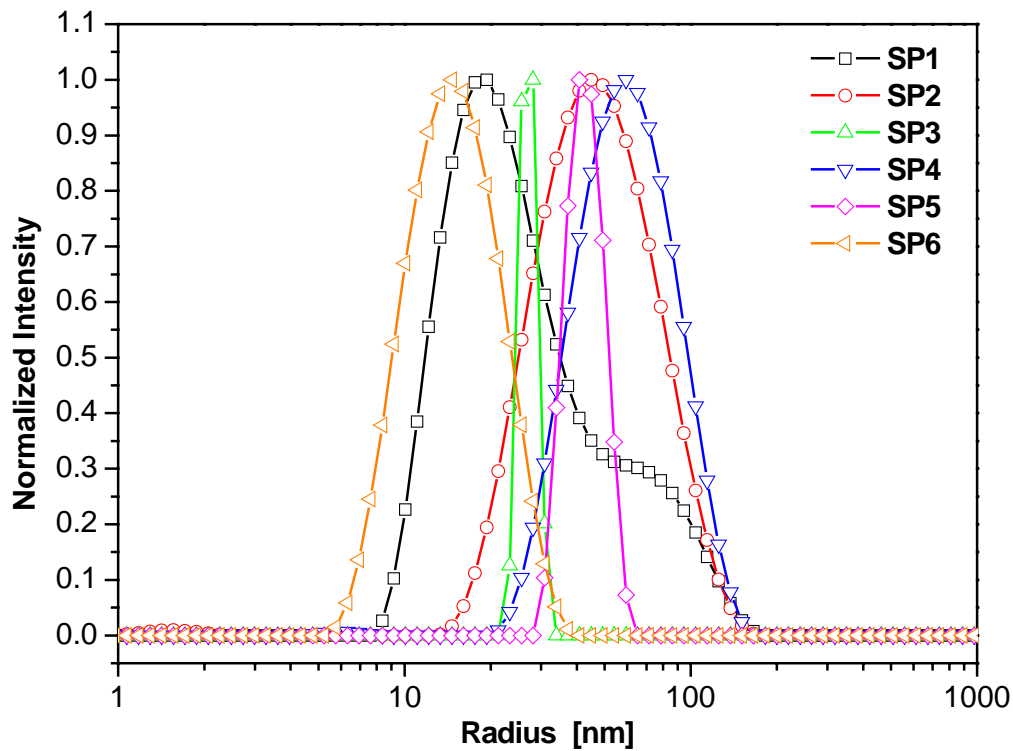


Figure 3-11: Radius distribution plots of in-situ DLS measurements.

4-5 Conclusion

In this study we synthesize silica nanoparticles without surfactants via two different methods: the modified Stöber method and the original Stöber method. The former method unfortunately gives silica particle with unsatisfactory particle size and its distribution, which does not meet our requirement since it brings about unnecessary parameters in investigating filler-rubber interaction. On the contrary, the latter method gives monodisperse, surface unmodified silica particles of a size of 100 nm. Moreover, the modification of such silica particles also gives monodisperse particles with less surface polarity. As well as specific surface area, both particles have similar size and its distribution, which will be used and discussed in the following investigation of filler-rubber interaction in virtue of hydrogen bonding interaction.

We also explored the possibility of real-time monitoring the growth of silica nanoparticles by *in-situ* DLS. This method is based on the robust DLS in determining particle sizes for colloids and it turns out that this *in-situ* strategy was proved to be accurate for nanoparticles of sizes smaller than 100 nm. To our knowledge this strategy has never been reported before and it not only offers a means to understanding the mechanism of particle growth but also can be used in a very small scale to tailor the particle size and its distribution before the scaled-up production of silica nanoparticle of desired sizes in a short time.

3-6 Acknowledgement

The authors thank the members of Makromolekulare Chemie II for their hospitality and instrumental help. We are also grateful to Dr. Dmitry Pergushov (Dept. of Polymer Science, Moscow State University) and Yu Mei (Physikalische Chemie I, Universität Bayreuth) for their fruitful discussion on dynamic light scattering. Financial support was given by the Bundes Ministerium für Bildung und Forschung (BMBF-project NMT/03N8645B), Bayreuth Institut für Makromolekülforschung (BIMF) and Verband der Chemischen Industrie (VCI).

References

- [1] H. Schmidt, *J. Non-Cryst. Solids*, **73**, 681 (1985).
- [2] G. L. Wilkes, B. Orlor and H. Huang, *Polym. Prepr.*, **26**, 300 (1985).
- [3] K. R. Finnie, R. Haasch and R. G. Nuzzo, *Langmuir*, **16**, 6968 (2000).
- [4] J. Zheng, Z. Zhu, H. Chen and Z. Liu, *Langmuir*, **16**, 4409 (2000).
- [5] A. Ulman, *Chem. Rev.*, **96**, 1533 (1996).
- [6] J. Y. Wen and G. L. Wilkes, *Chem. Mater.*, **8**, 1667 (1996).
- [7] T. Iwamoto and J. D. Mackenzie, *J. Sol-Gel Sci. Tech.*, **4**, 141 (1995).
- [8] D. L. Ou and A. B. Seddon, *J. Non-Cryst. Solids*, **210**, 187 (1997).
- [9] J. N. Hay, D. Porter and H. M. Raval, *J. Mater. Chem.*, **10**, 1811 (2000).
- [10] F. Hatakeyama and S. Kanzaki, *J. Am. Ceram. Soc.*, **73**, 2107 (1990).
- [11] A. van Blaaderen and A. Vrij, *J. Colloid. Interface Sci.*, **156**, 1 (1993).
- [12] C. R. Silva and C. Airoidi, *J. Colloid. Interface Sci.*, **195**, 381 (1997).
- [13] R. Yin and R. M. Ottenbrite, *polym. Prepr.*, **36**, 265 (1996).
- [14] J. Y. Choi, C. H. Kim and D. K. Kim, *J. Am. Ceram. Soc.*, **81**, 1184 (1998).
- [15] K. Katagiri, K. Hasegawa, A. Matsuda, M. Tatsumisago and T. Miami. *J. Am. Ceram. Soc.*, **81**, 2501 (1998).
- [16] A. Matsuda, T. Sasaki, T. Tanaka, M. Tatsumisago and T. Minami, *J. Sol-Gel Sci. Tech.*, **23**, 247 (2002).
- [17] W. Stöber, A. Fink and E. Bohn, *J. Colloid. Interface Sci.*, **26**, 62 (1968).
- [18] R. M. Ottenbrite, J. S. Wall and J. A. Siddiqui, *J. Am. Ceram. Soc.*, **83**, 3214 (2000).
- [19] D. A. R. Jones, B. Leary and D. V. Boger, *J. Colloid. Interface Sci.*, **147**, 479 (1991).
- [20] Y. Otsubo, M. Sekine and S. Katayama, *J. Rheol.*, **36**, 479 (1992).
- [21] A. P. Philipse and A. Vrij, *J. Chem. Phys.*, **87**, 5634 (1987).
- [22] H. Giesche and K. K. Unger, in *Proceedings of Ceramic Powder Processing Science, 2nd International Conference*, Berchtesgaden, 1988, edited by H. Hausner, G. L. Messing and S. Hirano (Deutsche Keramische Gesellschaft, Köln, 1989).
- [23] A. P. Philipse, *J. Mater. Sci. Lett.*, **8**, 1371 (1989).
- [24] C. Thies, *J. Colloid. Interface Sci.*, **54**, 13 (1976).
- [25] K. Bridger, D. Faihurst and B. Vincent, *J. Colloid. Interface Sci.*, **68**, 190 (1979).
- [26] A. K. van Helden, J. W. Jansen and A. J. Vrij, *J. Colloid. Interface Sci.*, **81**, 354 (1981).
- [27] R. B. Badley, W. T. Ford, F. J. McEnroe and R. A. Assink, *Langmuir*, **6**, 792 (1990).
- [28] P. A. Buining, L. M. Liz-Marzán and A. P. Philipse, *J. Colloid. Interface Sci.*, **179**, 318 (1996).
- [29] A. Arkhireeva and J. N. Hay, *J. Mater. Chem.*, **13**, 3122 (2003).
- [30] A. Arkhireeva and J. N. Hay, *Polymer and Polymer Composites*, **12**, 101 (2004).
- [31] C. Gellermann, W. Storch and H. Wolter, *J. Sol-Gel Sci. Tech.*, **8**, 173 (1997).
- [32] R. Vacassy, R. J. Flatt, H. Hofmann, K. S. Choi and K. Singh, *J. Colloid. Interface Sci.*, **227**, 302 (2000).
- [33] G. Kolber, Dissertation, Jena, 1956.
- [34] G. H. Bogush, M. A. Tracy and C. F. Zukoski, *J. Non-Cryst. Solids*, **104**, 95 (1988).

- [35] C. H. Byers, M. T. Harris and D. F. Williams, *Ind. Eng. Chem. Res.*, **26**, 1923 (1987).
- [36] M. T. Harris, R. R. Brunson and C. H. Byers, *J. Non-Cryst. Solids*, **121**, 397 (1990).
- [37] T. Matsoukas and E. Gulari, *J. Colloid. Interface Sci.*, **124**, 252 (1988).
- [38] T. Matsoukas and E. Gulari, *J. Colloid. Interface Sci.*, **132**, 13 (1989).
- [39] T. Matsoukas and E. Gulari, *J. Colloid. Interface Sci.*, **145**, 557 (1991).
- [40] G. H. Bogush and C. F. Zukoski, “*The Colloid Chemistry of Graving Silica Spheres*”, Plenum, New York, 1987.
- [41] S. Kim and C. F. Zukoski, *J. Colloid. Interface Sci.*, **139**, 198 (1990).
- [42] G. H. Bogush and C. F. Zukoski, *J. Colloid. Interface Sci.*, **142**, 1 (1991).
- [43] G. H. Bogush and C. F. Zukoski, *J. Colloid. Interface Sci.*, **142**, 17 (1991).
- [44] J. K. Bailey and M. L. J. Mecartney, in “*Better Ceramics Through Chemistry III*”, Mat. Res. Soc., Pittsburgh, 1988.
- [45] J. K. Bailey and M. L. J. Mecartney, *Colloid Surf.*, **63**, 151 (1992).
- [46] K. S. Schmitz, “*An Introduction to Dynamic Light Scattering by Macromolecules*” Academic Press, San Diego, 1990.
- [47] W. R. Burchard, *Progr. Colloid & Polymer Sci.*, **80**, 151 (1989).
- [48] D. R. Anderson, in “*Analysis of Silicones*”, ed. A. L. Smith, Wiley-Interscience, New York, 1974.
- [49] A. van Blaaderen and A. Vrij, “*Synthesis and Characterization of Colloid model Particles Made from (Organo)-Alkoxysilane*”, paper presented at R. K. Iler Memorial Symposium, Washington, DC, 1990.
- [50] R. K. Iler, *The Chemistry of Silica*, Wiley, New York, 1978.
- [51] A. van Blaaderen, J. van Geest and A. Vrij, *J. Colloid. Interface Sci.*, **154**, 481 (1992).

Chapter 4

“Smart” Silica-Rubber Nanocomposites in virtue of Hydrogen Bonding Interaction

“Smart” Silica-Rubber Nanocomposites in virtue of Hydrogen Bonding Interaction

Chih-Cheng Peng¹, Astrid Göpfert¹, Markus Drechsler¹, Volker Abetz²

¹Makromolekulare Chemie II, Universität Bayreuth, Universitätsstrasse 30, 95447 Bayreuth, Germany

²Institut für Polymerforschung, GKSS-Forschungszentrum Geesthacht GmbH, Max-Planck-Strasse 1, 21502 Geesthacht, Germany

(published on *Polymers for Advanced Technologies*)

4-1 Abstract

In this paper we present a kind of “smart” nanocomposites comprising Stöber silica nanoparticles of two different surface polarities and a novel thermoreversible crosslinking rubber carrying self-complementary hydrogen bonding (HB) moiety. This strategy is based on the idea that the introduction of HB between silica and the modified rubber improves both the filler-rubber interaction and the mechanical properties. The resulting nanocomposites were mainly characterized using transmission electron microscopy (TEM) and dynamic mechanical analysis. Interestingly it is found that the competition and symbiosis between the filler-filler, filler-rubber and rubber-rubber HB interaction, as well as the dynamic mechanical properties were controllable simply by changing the silica loading, the degree of rubber modification and the temperature. Besides, TEM micrographs showed that both the modifications of silica nanoparticles and rubber promoted better silica dispersion in the rubber matrix. By this strategy it is evident that the Payne effect was reduced and it is possible to modify the mechanical properties of such silica filled composites in a controlled way, which could, as an example, meet the requirements for tire applications.

4-2 Introduction

Filler reinforced elastomers are used in a wide range of applications, particularly in automotive tires, under several conditions of temperature, frequency and deformation. For a filled rubber material the phenomenon of strain-dependent modulus upon dynamic straining was first investigated by Payne 40 years ago [1]. A widely held view is that filler agglomeration and its network formation are responsible for the high degree of reinforcement and that the deagglomeration and network breakdown of fillers, on the other hand, are responsible for the non-linearity between stress and strain [2,3]. A general schematic representation of reinforcement in filled vulcanites and non-vulcanites is given in Figure 4-1 [4]. The modulus of a filled rubber is composed of the following parts (from bottom to top): the pure rubber network, the hydrodynamic effect, specific filler-rubber interaction, and in addition, a strain-dependent part caused by filler network. Based on the agglomeration-deagglomeration mechanism, it is generally believed that the strong filler-filler interaction is responsible for the intensity of the Payne effect and a better filler-rubber interaction on the contrary reduces its magnitude [5].

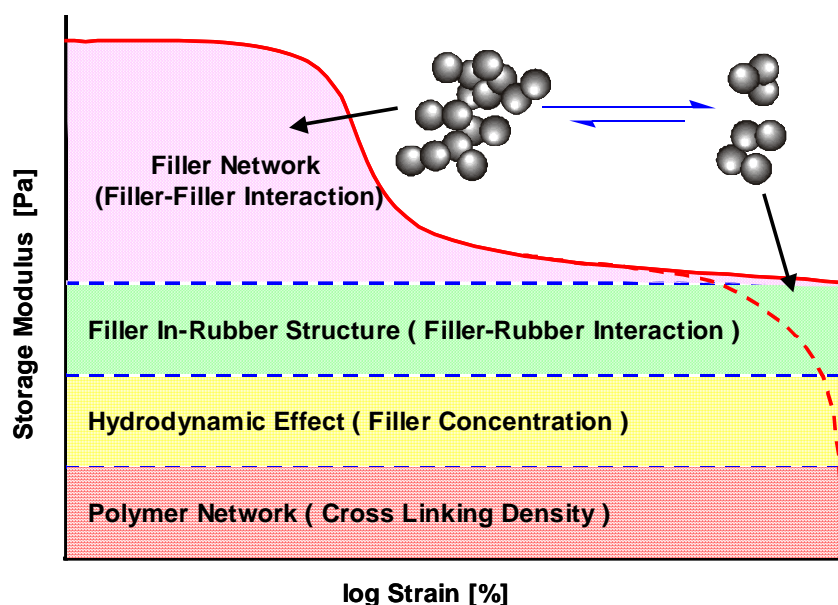


Figure 4-1: Modulus contributions in filled rubber materials. (solid line for vulcanites and dash line for non-vulcanites)

Silica particles have become more important in tire applications since the introduction of the Green Tire[®] by Michelin. As a filler, silica has greater reinforcing power, such

as improving tear strength, abrasion resistance, age resistance and adhesion properties than carbon black [6-8]. However, due to the strong inter-particle hydrogen bonds between hydroxyl groups, the agglomeration nature of silica is generally believed to be responsible for the significant Payne effect which brings about considerable rolling resistance for tire applications. In order to reduce the filler-filler interaction and/or to enhance the mechanical properties of silica filled composites, researchers have been working for many years on different strategies to improve silica-rubber interaction and, in turn, to reduce the rolling resistance. Among these strategies, chemical modifications of rubbers by attaching functional groups interacting with silica [9-22] and surface treatments of silica by reducing surface polarity with different silane coupling agents [22-36] are the most popular techniques.

However, these techniques admittedly have quite a few drawbacks. For the former technique, the chemical modification reaction of rubber was usually not applicable to commercial production and its degree of modification was usually very low [9,11,14,18,22]. Additionally, the chemical modification was limited to rubber chain ends [12,17,20], meaning that the final silica composite was unsatisfactory in terms of reducing silica agglomeration. For the latter, the used coupling agents are expensive and it could possibly lower the crosslinking density by reacting with the chemical ingredients for vulcanization. This technique would lead to lower overall cure rates [34,35], and at the same time it degraded the mechanical performance of such silica filled material for tire applications. In summary, due to these flaws none of the methods mentioned above could simultaneously ensure both the ability in reducing the silica agglomeration and improving the material performance.

In order to improve the filler-rubber interaction without compromising with similar defects, as well as to investigate the influence of hydrogen bonding (HB) interaction on the dynamic mechanical properties, as illustrated in **Figure 4-2**, we devise a kind of “smart” nanocomposites containing surface unmodified and modified silica nanoparticles from Stöber synthesis, and a thermoreversible crosslinking rubber with quantitative functionality. This strategy enables the incorporation of HB interacting moieties not only between silica particles themselves but also between silica particles and rubber. First, from the dynamic strain-sweep analysis the resulting composites

were able to reduce the intensity of the Payne effect without using expensive silane coupling agents. Second, it is also found that simply by changing the silica loading, the degree of rubber modification and the testing temperature, the temperature dependent mechanical properties were tunable. These specific characteristics were mainly attributed to the competition and symbiosis of HB interactions between filler and rubber.

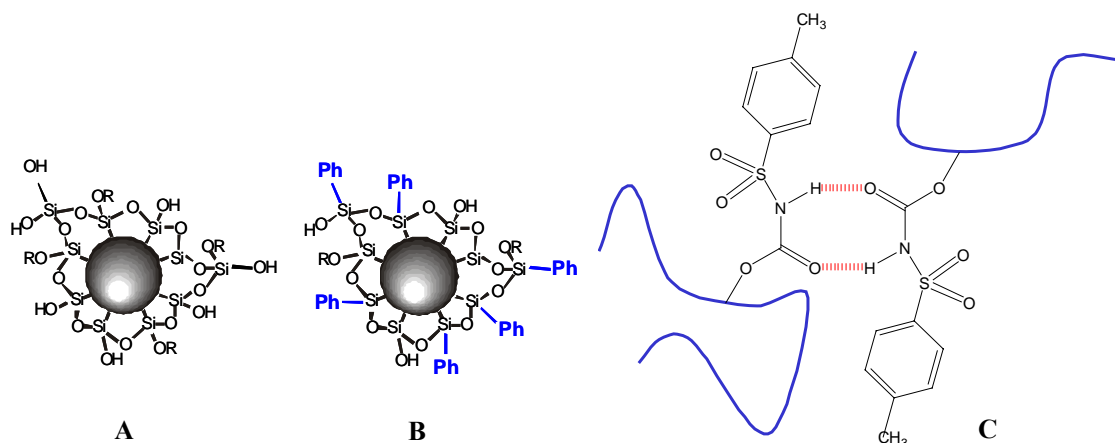


Figure 4-2: Components for the smart silica-rubber nanocomposites. (A: surface unmodified silica; B: surface modified silica; C: thermoreversible crosslinking rubber)

4-3 Experimental Section

4-3-1 Materials

Tetraethoxysilane (TEOS) (98%, $d = 0.934$, Aldrich), phenyl trimethoxysilane (PTMS) (94+%, $d = 1.049$, Aldrich), ammonia aqueous solution (25 wt% NH_3 , Merck), and absolute ethanol (Merck) were used without any further purification. Fresh-prepared deionized water was used as a co-solvent and as a hydrolysis catalyst for silica particle synthesis. The chemical modification reaction of rubber comprising self-complementary hydrogen bonding moiety was done by modifying a technical grade polybutadiene PB (Bayer Buna CB 10, with 96% *cis*-1,4 units, received from the

Deutsches Institut für Kautschuktechnologie e. V., Hannover) [37]. In order to reduce the number of samples, as well as to save unnecessary experimental trials, not at a cost of a systematic study, here we chose 0, 2, 5 and 10 mol% modified PBs as the interacting rubber matrices for the investigation on the HB interaction with silica nanoparticles.

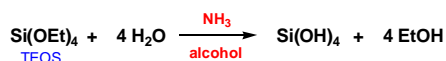
4-3-2 Synthesis of Surface Unmodified (Si-OH) and Modified (Si-Ph) Silica Nanoparticles

In order to synthesize silica nanoparticles of a diameter of 100 nm via the Stöber method, the molar ratio of H₂O/NH₃/TEOS/EtOH of 11.3/4/1/78 was optimized from the former experimental data [38] so as to keep the ratio of H₂O/Si in the range between 7 and 25. To a solution containing 359 g of absolute EtOH (7.80 mol) and 27.2 g of 25 wt% ammonia aqueous solution (0.40 mol NH₃, 1.13 mol H₂O), 21.3 g TEOS (0.10 mol) was added quickly at one dose under stirring. The resulting reaction mixture was stirred for 5 minutes to ensure homogeneity, and finally the suspension was kept at room temperature without stirring for 24 hours (no precipitation could be observed at the bottom of the reaction flask during the reaction course). The purification procedure was as follows: The suspension was first centrifuged at a rotational speed of 4000 rpm at 15 °C for 60 minutes to give precipitated silica particles separated from the solvent and the residual reactants. After removing the non-gel parts, the as-precipitated silica particles were again redispersed in EtOH using an ultrasonic treatment for 5 minutes. In order to have well-defined and non-aggregated silica nanoparticles, it is important to note that the purification procedure must be repeated for at least 4 times before drying. After purification the particles were dried under vacuum at 80 °C for 48 hours before characterization.

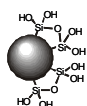
The surface modified silica nanoparticles were prepared using the surface unmodified silica described above as precursor. However, in order to attach PTMS onto the silica surface, instead of purifying the reaction suspension which had been kept for 24 hours, under stirring a portion of 10 mol% PTMS based on the amount of TEOS was added to this solution and stirred for 5 minutes. Again, the resulting suspension should be

kept at room temperature without stirring for another 24 hours and during the course of reaction no precipitation could be seen at the bottom of the flask. The purification procedure was the same as described for the unmodified nanoparticles. The particles size and their surface functionalities were verified by TEM and FTIR, respectively, and the specific surface areas were measured by BET method (**B**runauer, **E**mmett and **T**eller). The synthesis methods are summarized and depicted as follows:

a. Surface unmodified silica particle

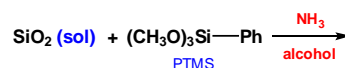


$\text{H}_2\text{O} : \text{NH}_3 : \text{TEOS} : \text{C}_2\text{H}_5\text{OH}$ (molar ratio)
11.4 : 4.0 : 1.0 : 78 (24 hr)

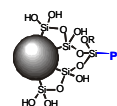


polar surface

b. Surface modified silica particle



$\text{H}_2\text{O} : \text{NH}_3 : \text{TEOS} : \text{C}_2\text{H}_5\text{OH} : \text{PTMS}$ (molar ratio)
11.4 : 4.0 : 1.0 : 78 : 0.11 (0.22) (24 hr)



less polar surface

4-3-3 Preparation of Silica-Rubber Nanocomposites

The silica loadings for the preparation of nanocomposites were chosen to be 0, 10, 20, 40, 80 and 120 phr (parts by weight per hundred parts rubber). Here a composite consisting of 5 mol% modified PB with 80 phr surface unmodified silica (named as **PB-5/Si-OH-80**) is highlighted as a typical example [39]. In a 40 mL cylindrical glass vial 0.16 g of **Si-OH** was added in 30 mL dioxane, and the solution was ultrasonified for 10 minutes in order to get a good suspension. 0.2 g of 5 mol% modified PB was then dissolved in the suspension, and this suspension mixture was subjected to ultrasonic treatment for 5 minutes if flocculation was found after dissolution. The resulting mixture was then quickly frozen by liquid nitrogen and freeze dried under vacuum to give a solid composite. It is important to note that we did not crosslink the rubber matrix in a future step in order to avoid complications resulting from the influence of chemical crosslinked network on the dynamic mechanical behavior and to avoid the influence of silica nano-fillers in alternating the nature of the chemical crosslinking [40].

4-3-4 Characterizations

TEM micrographs were obtained from a Zeiss LEO 922 transmission electron microscope. The suspensions for TEM were prepared by dissolving 10 mg dried silica nanoparticles in a 250 mL round bottom flask filled with 100 ml acetone, the systems were then ultrasonified for 5 minutes to give clear suspensions. Clean plastic micropipettes were used to transfer a droplet of the silica particle suspension onto copper carrier grids (200 mesh) covered with a carbon film. The nanocomposite samples for TEM were prepared by the following procedure: sample films of 8 mm diameter were prepared from compression molding (a 25 mg sample was first heated and molded under pressure at 80 °C for 10 minutes in an 8 mm diameter mold, and the button-like specimen was taken out after the mold was cooled down to room temperature), and the resulting films were ultra-thin cut using a Reichert-Jung Ultracut E equipped with a diamond knife. The cut sections (approximately 60 nm thick) were transferred onto the same copper carrier grid used for silica nanoparticles.

FTIR spectra were recorded at room temperature using a Bruker FTIR EQUINOX 55/S spectrometer at a resolution of 4 cm⁻¹. The samples for FTIR analysis were prepared by grinding 10 mg dried silica nanoparticles with 1.0 g dried KBr grain until very fine powders were obtained. About 100 mg of the fine powder were transferred into a circular mold of 1 cm diameter and pressed using a hydraulic press to give thin circular pellets. FTIR signals were normalized using Si-O-Si stretching absorption at 1150 cm⁻¹ as a reference to prove the effective reduction of hydroxyl groups on silica surface by PTMS modification.

Surface data of silica particles were obtained from nitrogen adsorption measurements at -196 °C using a Quantachrome Autosorb-1 apparatus. Samples were outgassed for 12 hours at 150 °C prior to the analysis. Specific surface area data were calculated using the BET method, which were generated automatically by the operating program developed for the apparatus.

Dynamic mechanical measurements were performed using an Advances Rheometrics Expansion System (ARES) from TA Instruments mounted with an 8 mm parallel-

plate geometry. The dynamic shear moduli were recorded employing the “dynamic strain sweep” program for the Payne effect analysis (running from 0.08 to 100 % shear strain at 50°C and at a frequency of 1 Hz). Furthermore, the “dynamic temperature ramp test” program (scanning from 80 to –90 °C at a rate of –2 °C/min and a frequency of 1 Hz) and the “dynamic frequency sweep” program (scanning from 100 to 0.1 rad/s at 0 and 50 °C) were used to study the temperature and frequency dependent properties. Sample films of 8 mm diameter were prepared by the same procedure used for TEM analysis of nanocomposites. Dynamic strain sweep tests were performed before the temperature and frequency sweeps to ensure that all these measurements were made within the limits that silica agglomerates were not perturbed.

4-4 Results and Discussion

4-4-1 Surface Unmodified (Si-OH) and Modified (Si-Ph) Silica Nanoparticles

TEM micrographs of **Si-OH** and **Si-Ph** nanoparticles synthesized via the Stöber method are shown in **Figure 4-3**. As can be seen this synthesis method gives spherical

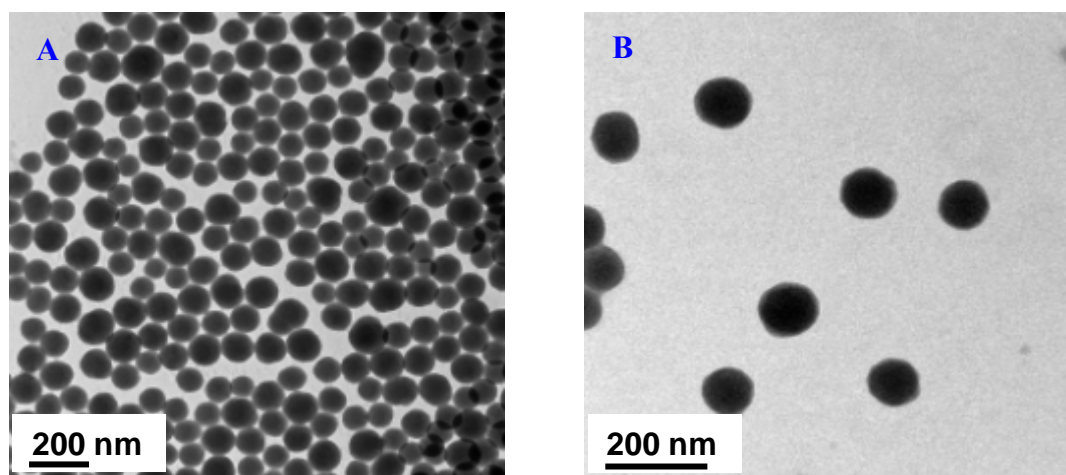


Figure 4-3: TEM micrographs of silica nanoparticles synthesized via the Stöber method. (A: Si-OH, B: Si-Ph)

and monodisperse particles of a size of 100 nm for both **Si-OH** and **Si-Ph** particles, meaning the surface modification did not significantly change the particles size of original **Si-OH** particles used as precursors for surface modification.

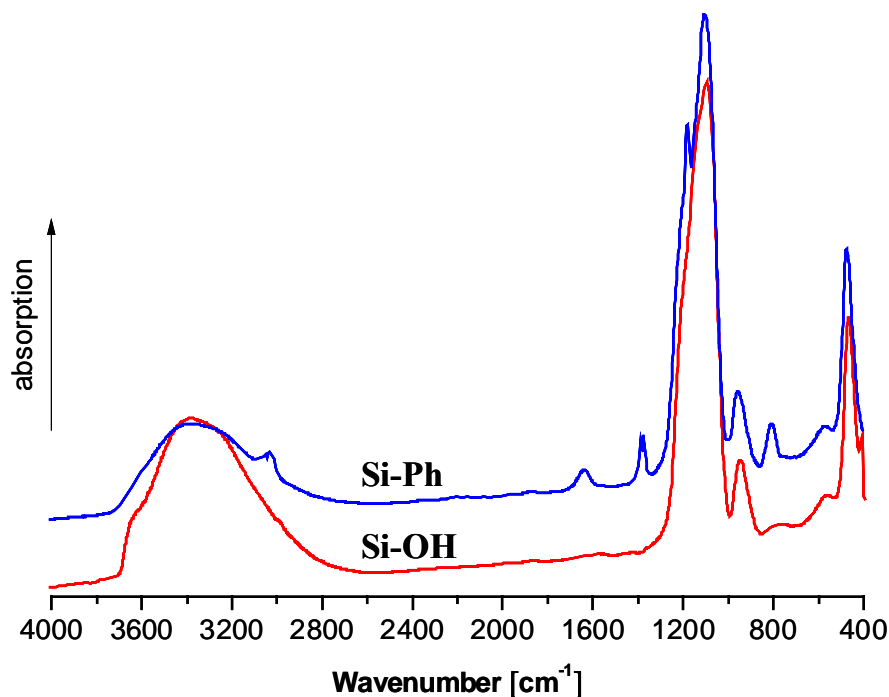


Figure 4-4: FTIR spectra of silica particles synthesized via the Stöber method.

FTIR spectra of the **Si-OH** and **Si-Ph** particles are shown in Figure 4-4. For both particles, the presence of Si-O-Si linkages was supported by an intense absorption at 1150 cm^{-1} (stretching) and a distinct vibration band at about 430 cm^{-1} to 450 cm^{-1} (bending) [41], and a characteristic absorption of OH was also observed between 2900 cm^{-1} and 3600 cm^{-1} . Moreover, for **Si-Ph** there were weak benzene ring absorptions at 1610 cm^{-1} and 1400 cm^{-1} and a much weaker absorption of OH observed between 2900 cm^{-1} and 3600 cm^{-1} . These results showed that the surface modification via addition of PTMS successfully reduced the surface OH groups on **Si-OH** surface.

The BET measurement showed that the specific surface areas of these silica particles were 63 and $47\text{ m}^2/\text{g}$ for **Si-OH** and **Si-Ph** particles, respectively. It means that the surface modification did not significantly change the effective surface area of the original **Si-OH** used for surface modification. Together with the observation from

TEM and FTIR analysis, we conclude that these two particles with different surface polarities are satisfactory for the investigation of the influence of hydrogen bonding interaction on the mechanical properties of nanoparticle filled rubber since the influence of particle size and specific surface area could be excluded in this case.

4-4-2 Dynamic Strain Sweep (Payne Effect Analysis)

The dynamic strain sweep analysis (Payne effect analysis) for the **PB-0** nanocomposites is shown in **Figure 4-5**. The storage shear modulus (G') of **Si-OH** and **Si-Ph** filled composites below 40 phr was similar, meaning that no filler agglomerates existed because obviously the hydrodynamic effect (the mere addition of hard dispersed particles into a soft polymer matrix) dominated the modulus over any other reinforcing contributions below that level of loading [42,43]. Not surprisingly, since the unmodified PB is highly hydrophobic and the highly hydrophilic **Si-OH** particles formed more and stronger agglomerates, at same silica loadings the G' of **Si-OH** filled composites was always higher than that of **Si-Ph** filled ones at lower strains.

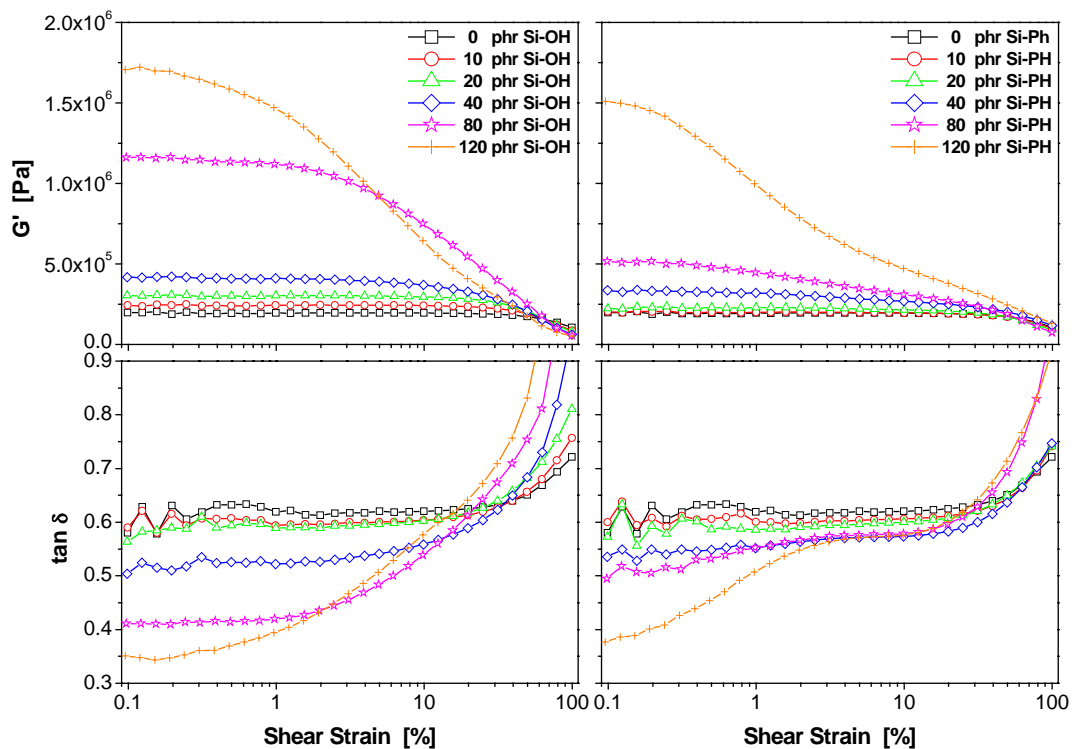


Figure 4-5: Dynamic strain sweep plots for **PB-0** nanocomposites.

Additionally, the critical filler loading for the agglomeration (percolation threshold, recognized as a sudden soar in modulus) for **Si-OH** was lower than that for **Si-Ph**. (80 phr versus 120 phr)

In the Payne effect analysis, at a certain strain amplitude where the storage shear modulus drops substantially and simultaneously a corresponding peak of $\tan \delta$ arises is regarded as the criterion of the deagglomeration of fillers [44]. However, for the silica nanocomposites studied here, the value of $\tan \delta$ connected to the deagglomeration process is not remarkable. One possible explanation could be that we used uncrosslinked PBs for the composites and for this reason the mechanical strength as such is much weaker than in a crosslinked PB, and the breakdown of filler agglomerates and rubber structure could happen simultaneously. In this case the curves of $\tan \delta$ for both processes would overlap with each other and this overlapping mechanism is illustrated in **Figure 4-6**.

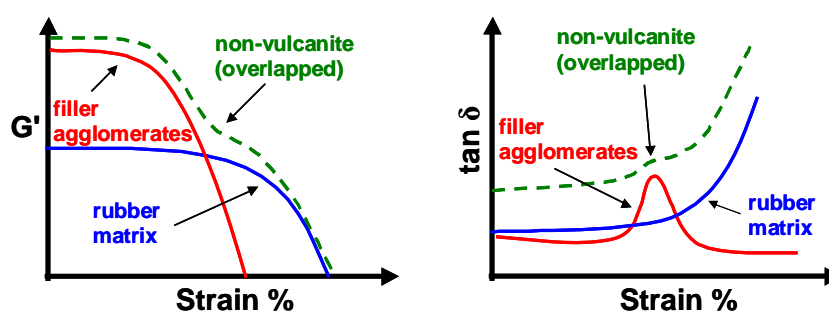


Figure 4-6: Curves overlapping mechanism for uncrosslinked PB filled with silica.

In addition to the observations mentioned above, it is also found that the deagglomeration process arose at a higher strain (15 % versus 4 %) and the value of corresponding $\tan \delta$ was higher for **Si-OH** filled PBs (0.6 versus 0.55) than for **Si-Ph** filled PBs. This result was attributed to the fact that thermodynamically the equilibrium between the agglomeration and the deagglomeration for **Si-OH** particles was relatively in favor of the former and kinetically the shear stress needed to disrupt **Si-OH** agglomerates was also higher in the unmodified hydrophobic PB.

Besides the similar observations for **PB-0** nanocomposites, for **PB-2** nanocomposites, as shown in **Figure 4-7**, it is found that G' was higher and the peak value of $\tan \delta$ corresponding to the deagglomeration was less significant at same silica loadings.

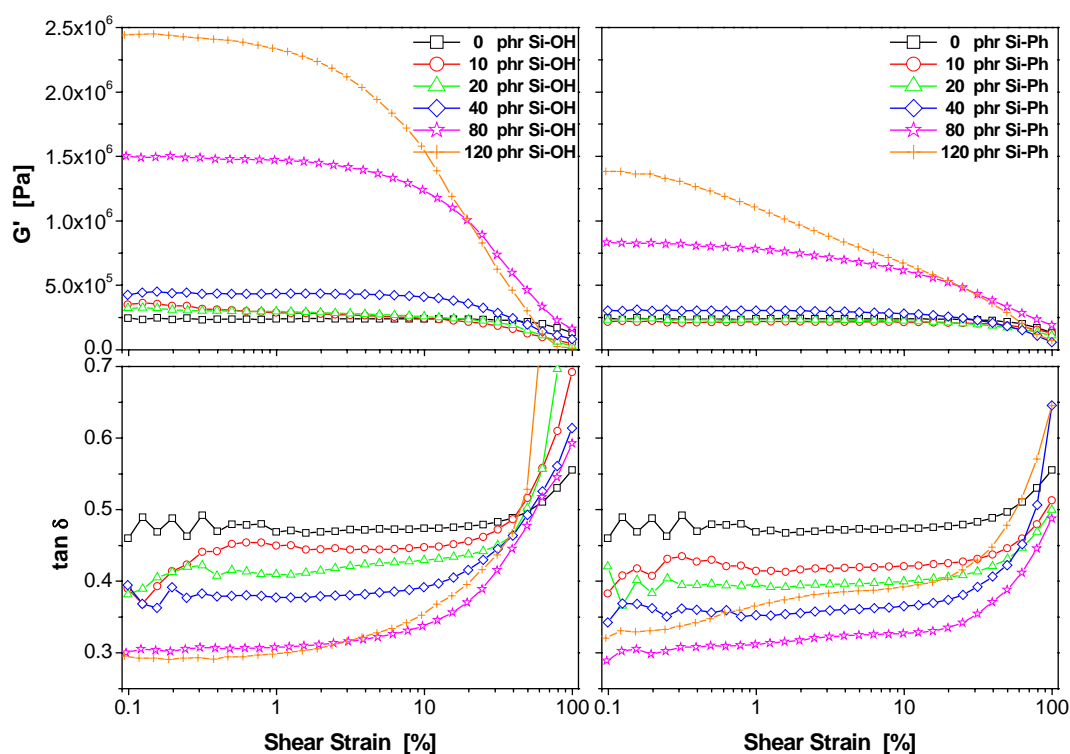


Figure 4-7: Dynamic strain sweep plots for **PB-2** nanocomposites.

In this case, the deagglomeration process occurred at a lower strain than in the unmodified PB composites. These interesting findings were ascribed to the increasing filler-rubber interaction and the decreasing filler-filler interaction resulted from the introduction of HB interaction between the silica nanoparticles and the modified PB. It also means that the introduction of additional HB interaction triggered the competition of HB interaction between the filler-filler, filler-rubber and rubber-rubber.

Comparison of the G' between **Si-OH** and **Si-Ph** particles filled **PB-5** nanocomposites, dramatic changes in the dynamic strain sweep analysis were found. As shown in **Figure 4-8**, at 10 and 20 phr the G' for both silica nanoparticles filled composites were similar, meaning that the hydrodynamic effect dominated at these silica loadings. However, as the silica loading increased from 40 to 120 phr, the relative values of G'

were varied following the order: **PB-5/Si-OH-40** > **PB-5/Si-Ph-40**, **PB-5/Si-OH-80** \approx **PB-5/Si-Ph-80** and **PB-5/Si-OH-120** < **PB-5/Si-Ph-120**. These results revealed that the competition and symbiosis between HB interactions took place in **PB-5** nanocomposites. First, with increasing silica loading from 20 to 40 phr, a small amount of silica agglomerates formed. Taking into account the amount of OH groups on the silica surface relative to the amount of HB interacting sites on the modified PB, at 40 phr the filler-filler interaction surpassed the filler-rubber interaction in terms of total amount of HB interaction. It follows that the filler-filler HB interaction from **Si-OH** particles themselves dominated G' over the filler-rubber HB interaction at lower strains. In other words silica agglomerates overwhelmed the contribution of filler-rubber HB interaction.

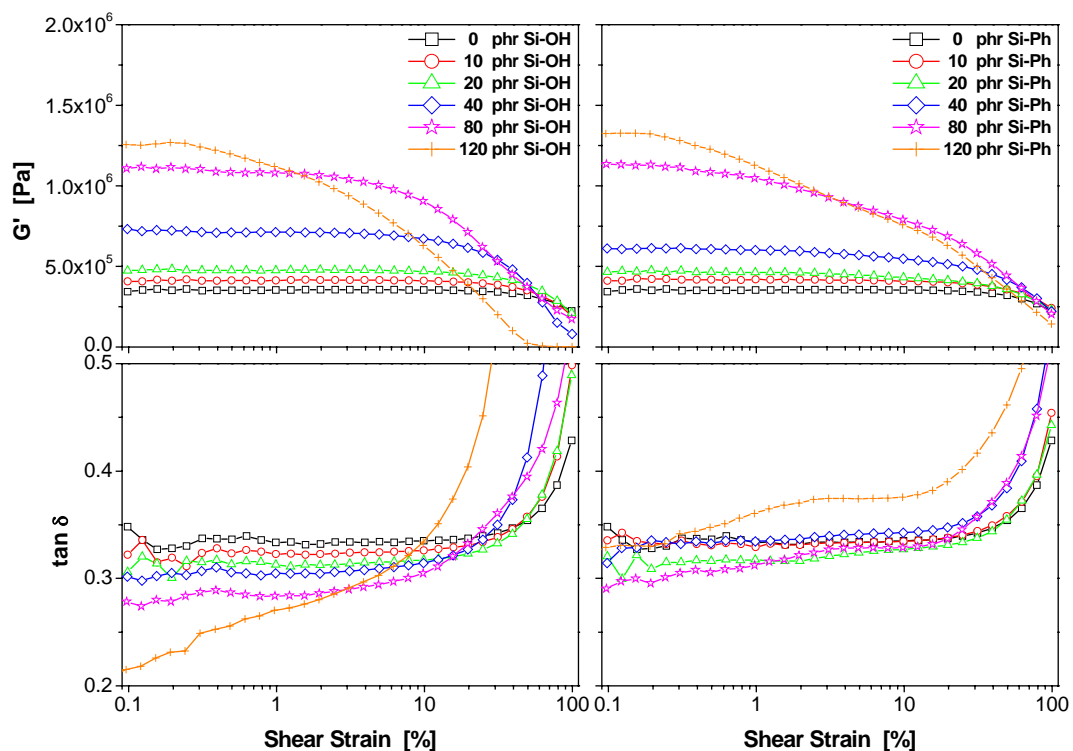


Figure 4-8: Dynamic strain sweep plots for **PB-5** nanocomposites.

Second, the amount of both the filler-rubber and the filler-filler HB interaction increased but the amount of the rubber-rubber interaction decreased faster at 80 phr silica loading. However, since the relative growing amount of the filler-rubber HB interaction in **PB-5/Si-OH-80** surpassed that in **PB-5/Si-Ph-80**, the amount of silica

agglomerates increased for **PB-5/Si-Ph-80** was higher than that **PB-5/Si-OH-80**. This resulted in a similar modulus for **PB-5** at 80 phr silica loading. With rising silica loading at upmost 120 phr, admittedly there were up-growing filler-filler and filler-rubber HB interaction. But in this case, in **PB-5/Si-OH-120** there existed much less silica agglomerates than in **PB-5/Si-Ph-120** since **Si-OH** particles have more OH groups on the surface and they were more accessible to the HB interacting sites on the modified PB. Consequently, the modulus of **PB-5/Si-Ph-120** was higher than that of **PB-5/Si-OH-120** at lower strains.

Up to this point, one should examine the effectiveness of the modified PBs on reducing the Payne effect. As can be seen in [Figure 4-5](#), [4-7](#) and [4-8](#), for **PB-0**, **PB-2** and **PB-5** composites the G' at 10, 20 and 40 phr silica loading was similar and almost independent of strain. By comparing the G' between **PB-X** composites at higher silica loadings we could not observe a systematic reduction of G' with increasing degree of PB modification. Although it has been shown that the HB interacting sites on the modified PB did reduce the amount of silica agglomerates (this will be shown in the following TEM analysis), we believe this dilemma was attributed to the fact that the chemical modification did not contribute “much” to G' even though there were self-complementary HB networks in the PB matrix [\[37\]](#). In other words, the modification of PB did enhance the HB interaction between silica and PB, but the loading of silica particles on the contrary reduced the strength of rubber networks.

Taking into consideration the degree of PB modification, the amount of HB complexes and their relative strength as shown in [Figure 4-9](#) [\[45,46\]](#), the conclusions on the competition and symbiosis between the HB interactions can be qualitatively illustrated as shown in [Figure 4-10](#).

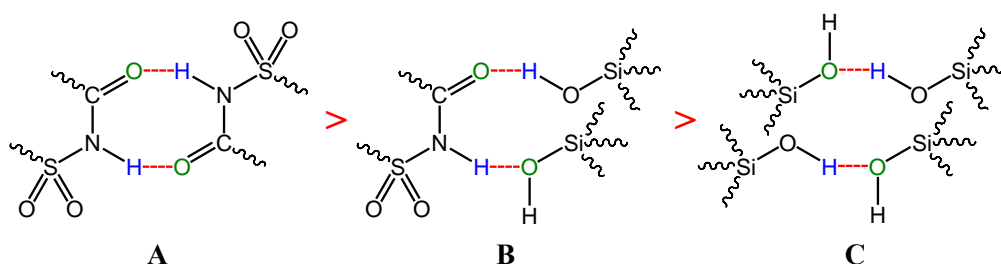


Figure 4-9: Relative hydrogen bonding strength between rubber-rubber (A), filler-rubber (B) and filler-filler (C).

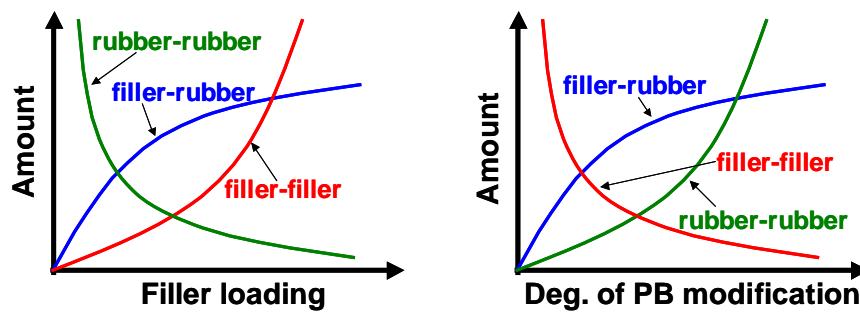


Figure 4-10: Qualitative representation of the amount of hydrogen bonding complexes as a function of filler loading and degree of PB modification.

Figure 4-11 shows the dynamic strain sweeps for **PB-10** composites. From the conclusions made before and as illustrated in Figure 4-10, it is understandable that the competition between the HB interactions is in favor of the filler-rubber HB interaction with increasing degree of PB modification. This is evident following the observation that **Si-Ph** filled **PB-10** showed higher G' than **Si-OH** filled one. It implies that **Si-Ph**

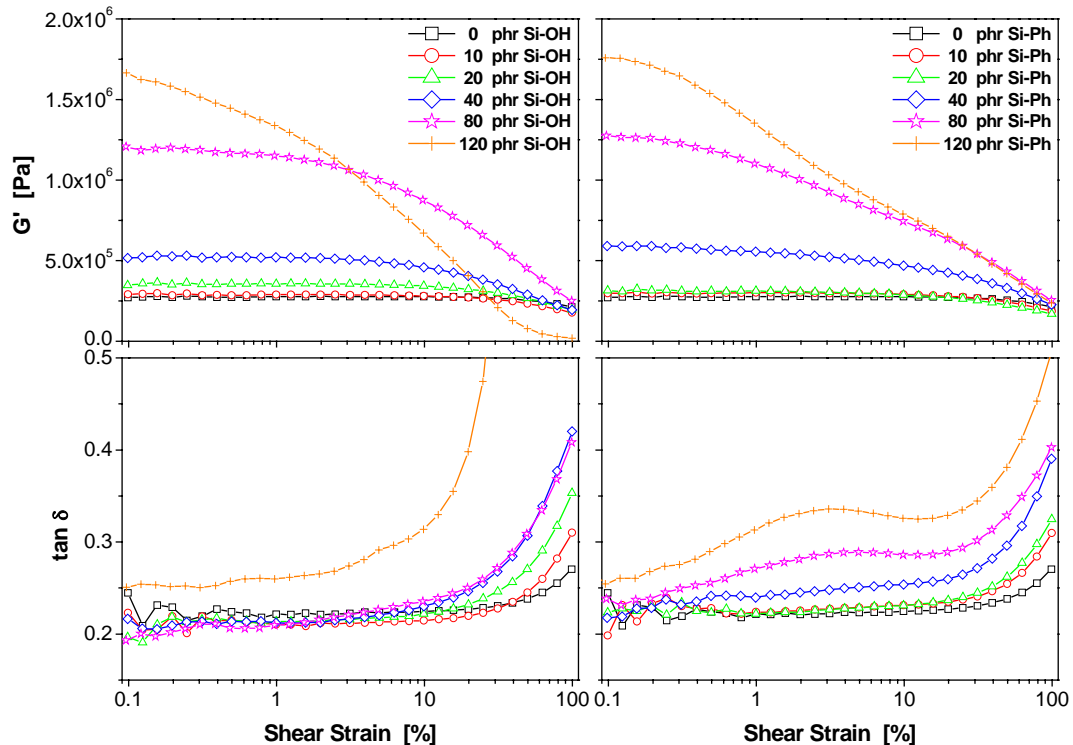


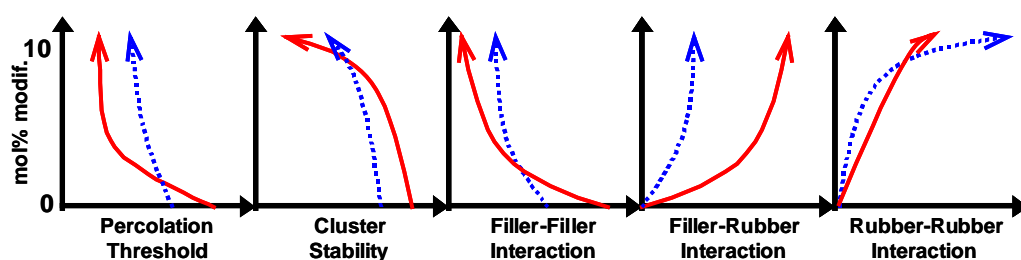
Figure 4-11: Dynamic strain sweep plots for **PB-10** nanocomposites.

particles formed relative higher amount of agglomerates than **Si-OH** in **PB-10** due to the surpassing increasing amount of the filler-rubber HB interaction between **Si-OH** particles and the modified PB.

Additionally, ascribing to the falling amount of the filler-filler HB interaction with increasing degree of PB modification, first it is found that the silica agglomerates were less stable and the deagglomeration process for **PB-10** occurred at a lower strain than those for the other composites. Second, the difference between the foot and tan δ maximum of **PB-10** was also lower. It goes without saying that these observations again justified the better filler-rubber HB interaction resulting from a higher degree of PB modification, which in turn reduced the relative amount of the filler-filler HB interaction.

From the dynamic strain sweeps performed on the silica-rubber nanocomposites studied here, as qualitatively illustrated in **Figure 4-12**, one is able to conclude how the degree of PB modification, the filler loading and silica surface polarity impact the filler-filler, filler-rubber and rubber-rubber HB interactions, as well as the other properties.

A. The influence of PB modification:



B. The influence of filler loading:

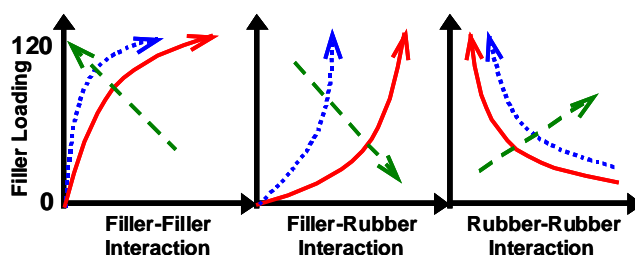


*Figure 4-12: Qualitative illustration of how silica surface polarity and the silica loading impact the HB interactions and the other composites' properties. (solid line: **Si-OH**; short dash line: **Si-Ph**; long dash line: degree of PB modification)*

4-4-3 Dynamic Temperature Sweep

The corresponding dynamic temperature sweeps of the composites are shown in [Figure 4-13](#). First, similar to the observations on several types of nano-fillers reported by many researchers [35,36,47-52], for these composites it is found that the melting and glass transition temperatures did not show significant change with silica loading despite their surface polarities (see the former work [37] for the detailed interpretations of T_m and T_g for the modified PBs). This behavior does not contradict the knowledge that fillers or filler agglomerates hinder the molecular motion of the rubber chains. Possible explanations are that the length scale of molecular motion is not comparable to that of the specific interaction between the silica and the PBs [53] or that the sensitivity of dynamic mechanical measurements are not able to detect changes in molecular motions of PB chains at the vicinity of a silica surface [52]. Nevertheless, the values of $\tan \delta$ maximum (T_g) were suppressed with increasing silica loading, meaning that the loading of silica did bring reinforcement in reducing the hysteresis properties of the unfilled PBs. Second, interestingly it is also found that the silica particles (whose bulk G' is about 30 times higher than that of the glassy PBs) had little effect on G' at lower temperatures despite their surface polarities. This result suggests that the silica agglomerates were hard but brittle so that their G' was slightly higher than that of the PBs in the glassy state. It also implies that the filler-filler interaction had little effect on the mechanical strength of the rubber in the glassy state.

The most interesting temperature dependent features of the composites are discussed here. If one keeps an eye on the G' in the temperature span between -10 and 80 °C, it is clear that its values of **Si-OH** particles filled **PB-0** and **PB-2** were always higher than those of **Si-Ph** filled ones. In other words, the corresponding G' did not cross each other in this temperature range, which indicates that the filler-filler HB interaction dominated over the temperature span and that temperature did not contribute much to the competition between the HB interactions. However, it is possible to observe the influence from the temperature and the degree of modification upon the relative value of the G' in **PB-5** and **PB-10**. First, below 40 phr silica loading the values of the G' of **Si-OH** and **Si-Ph** particles filled **PB-5** were similar, suggesting that up to this loading the hydrodynamic effect dominated. Second, upon 40 phr the

curves of the G' cross each other at 1 °C: below 1 °C the G' of **PB-5/Si-OH-40** was lower than that of **PB-5/Si-Ph-40**, but at temperatures higher than -1 °C their relative magnitude turned exactly the reverse.

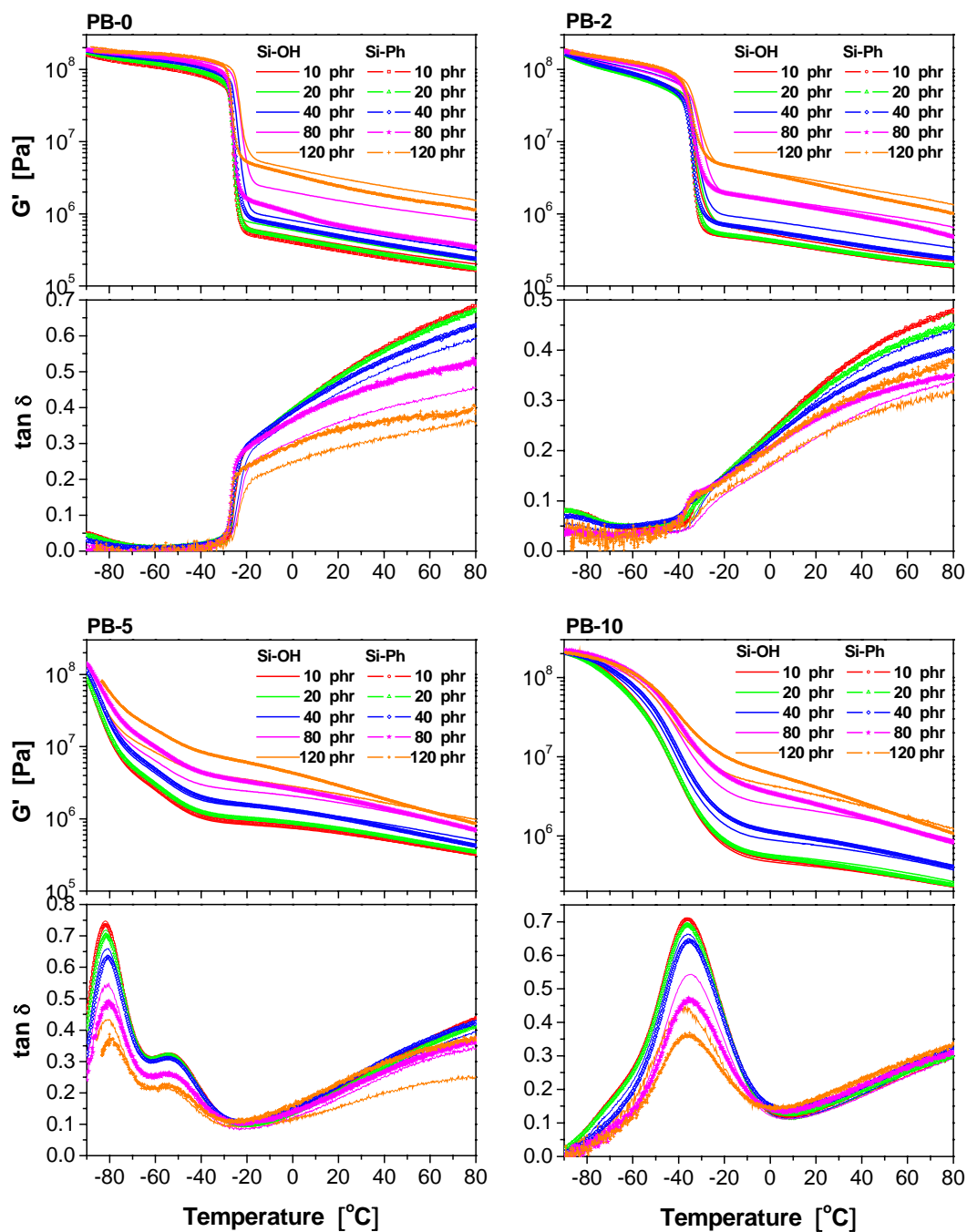


Figure 4-13: Dynamic temperature sweeps for **PB-X** nanocomposites.

Before giving any explanations to this extraordinary behavior of **PB-5**, one should consider the temperature dependence of the HB interactions between filler-filler,

filler-rubber and rubber-rubber involved in this study. Taking into account the thermodynamic equilibrium between HB association and dissociation and the corresponding enthalpy of HB dissociation (ΔH_d), we have:



where X is the HB accepting functionality. By referring to Equation 4-1, it follows that the equilibrium constant, K, between association and dissociation can be expressed as:

$$K = \frac{[R-X][H-R']}{[R-X \cdots H-R']} \quad (4-2)$$

By incorporating the van't Hoff equation [54]:

$$\ln\left(\frac{K_2}{K_1}\right) = \frac{-\Delta H_d}{R} \left(\frac{1}{T_2} - \frac{1}{T_1}\right) \quad (4-3)$$

where R is the universal gas constant and K_1 , K_2 are the equilibrium constants at absolute temperatures T_1 and T_2 , respectively.

Here one should again refer to the relative strength of the filler-filler, filler-rubber and rubber-rubber HB interactions shown in Figure 4-9 and the corresponding equilibrium between their association and dissociation. Since the relative HB strength is of the order: rubber-rubber > filler-rubber > filler-filler, it is clear that the relative value of ΔH_d of these HB is of the order: rubber-rubber > filler-rubber > filler-filler. Furthermore, it follows that the order of the sensitivity of these HB interactions to temperature is: rubber-rubber > filler-rubber > filler-filler. In sum, it suggests that the stronger the HB interaction, the higher the dissociation enthalpy and the sensitivity of it to temperature are. It follows that the temperature-dependent stability of these HB complexes can be qualitatively sketched as shown in Figure 4-14.

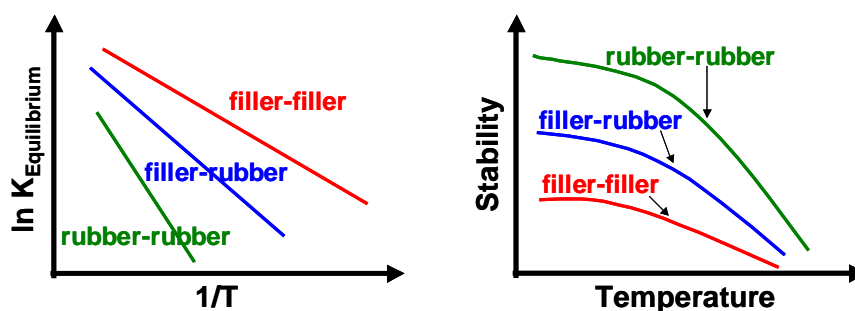


Figure 4-14: Qualitative illustration of the temperature-dependent equilibrium constants and stability of the HB complexes.

These findings can be summarized as follows:

1. silica agglomerates formed at lower loadings and the number of the filler-filler HB interaction increased largely with filler loading in spite of the fact that the amount of filler-rubber HB interaction was still larger (Figure 4-10).
2. at the same filler loading there was higher filler-rubber HB interaction in **Si-OH** particles filled **PB-5** than in **Si-Ph** particles filled **PB-5** (Figure 4-12).
3. the filler-rubber HB interaction was more sensitive to temperature than the filler-filler HB interaction, meaning the relative HB stability of the former was enhanced more than the latter as the temperature dropped (Figure 4-14).
4. in this case **Si-Ph** particles formed more agglomerates than **Si-OH** at lower temperatures since the **Si-OH** particles had more filler-rubber HB interaction with **PB-5**.
5. thus the G' of **PB-5/Si-Ph-40** was higher than that of **PB-5/Si-OH-40** at temperatures lower than 1 °C. However, at higher temperatures their relative values turned exactly the reverse.

More interesting features can be seen if one again keeps an eye on the G' curves at 80 and 120 phr silica loadings for **PB-5** and **PB-10**. First, there were two crossover temperatures both for **PB-5** and **PB-10** above 1 °C. Second, for the same composite the higher the silica loading, the lower the crossover temperature was located. Third, at the same filler loading the higher the degree of PB modification, the lower was the crossover temperature (crossover data are summarized in Table 4-1).

Table 4-1: Crossover data for PB-5 and PB-10

Composite	40 phr	80 phr	120 phr
PB-5	1 °C	67 °C	59 °C
PB-10	-	55 °C	53 °C

These interesting observations can be explained by performing the same analysis as discussed before. In the first place we will discuss why the crossover temperature shifted from 1 to 67 °C for **PB-5**. With larger amount of silica particles, of course, both the filler-filler and the filler-rubber HB interaction increased. However, for a PB with higher degree of modification the amount of the latter was higher for **Si-OH** particles than that for **Si-Ph** particles, resulting in that **Si-Ph** particles formed more agglomerates and the G' of **Si-Ph** particles filled composite was higher at lower to ambient temperatures (Figure 4-10). Nevertheless, due to the fact that **Si-OH** particles had more OH groups on the surface than **Si-Ph** particles and that the filler-filler HB interaction was less sensitive to temperature than the filler-rubber one (Figure 4-14), the amount of **Si-OH** agglomerates was relatively higher than that of **Si-Ph** at higher temperatures in spite of the falling amount of agglomerates from both silica. This resulted in the shift of crossover temperature from 1 to 67 °C as the silica loading increased from 40 to 80 phr for **PB-5**.

As the silica loading was increased from 80 to 120 phr, the filler-filler HB interaction between **Si-OH** particles soared more rapidly than those between **Si-Ph** particles, implying that the former could surpass the latter at lower temperatures. This change resulted in a lower crossover temperature as the silica loading increased.

Referring again to Figure 4-10, it is clear that the filler-rubber HB interaction soared more rapidly than the filler-filler one with increasing degree of PB modification. However, the former was more sensitive to temperature so that it decayed more at moderate temperatures, meaning that the latter could surpass the former in the total amount of HB interactions at lower temperatures for **PB-10** composites at higher silica loadings.

4-4-4 Dynamic Frequency Sweep

Possibly due to the formation of hydrogen bonding complexes between the filler particles themselves, the composites did not show a thermo-rheologically simple behavior, i.e. the temperature dependence of the activation energies associated with the different relaxations was different. As an example for this observation, the resulting time-temperature shift curves of **PB-0/Si-OH-10** and **PB-0/Si-Ph-10** are shown in [Figure 4-15](#).

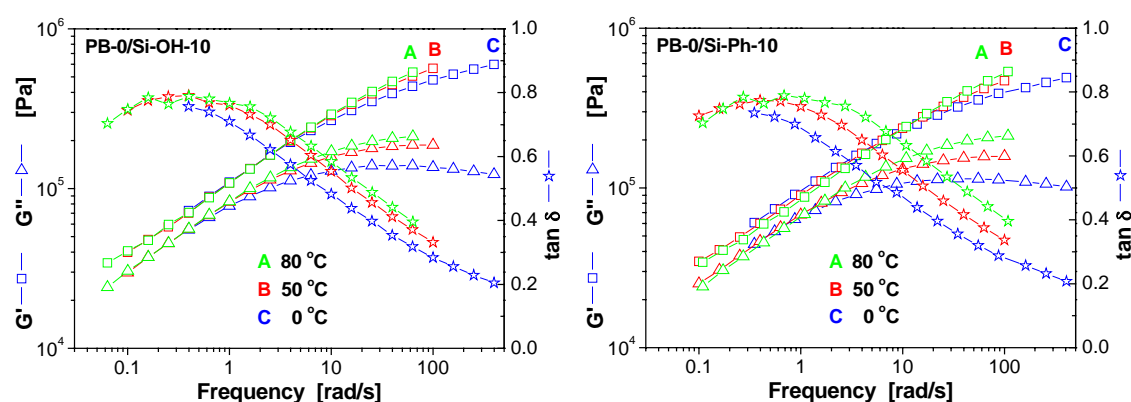


Figure 4-15: The resulting master curves for **PB-0/Si-OH-10** and **PB-0/Si-Ph-10** nanocomposites. (frequency sweeps at 0, 50 and 80 °C, $T_{ref} = 50$ °C)

4-4-5 TEM Analysis

TEM analysis offered further evidence for the improved filler-rubber interaction and better silica particle dispersion in the rubber matrix. [Figure 4-16](#) shows the silica-rubber nanocomposites at 80 phr **Si-OH** and **Si-Ph** loadings. It is clear that for composites consisting of rubbers with lower degrees of modification (**PB-0** and **PB-2**), the silica particles were prone to agglomeration in the non-polar rubber matrix. A significant transition from agglomeration to a good dispersion of silica nanoparticles was found in composites of rubbers with higher degrees of modification. This transition was attributed to the increasing amount of the filler-rubber HB interaction. Note that for **PB-5** and **PB-10** composites, it is found that the silica particles were

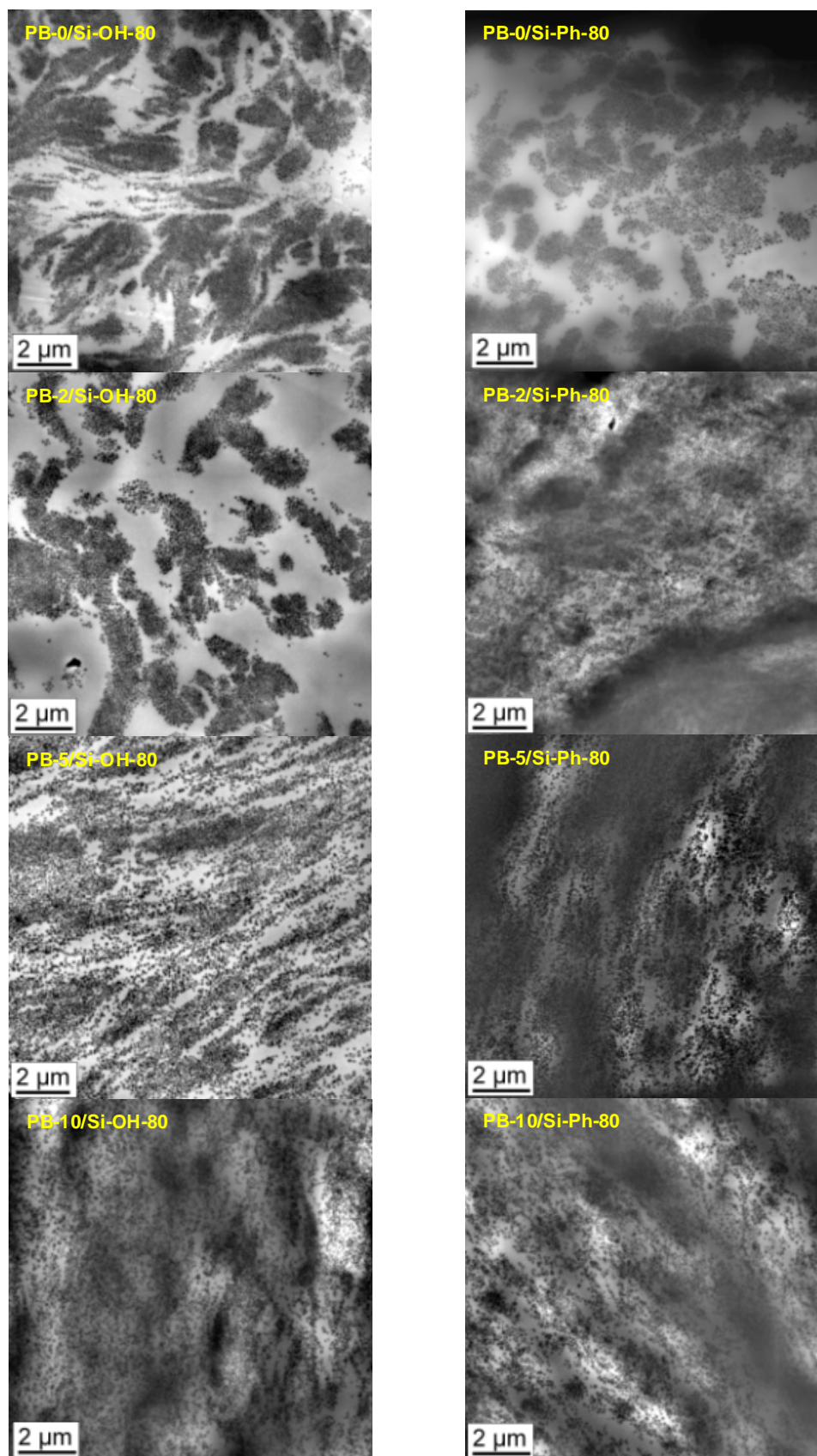


Figure 4-16: TEM micrographs for silica-rubber nanocomposites at 80 phr silica loadings.

well dispersed and larger silica agglomerates could hardly be observed in the rubber matrix. Besides it is also found that **Si-OH** particles formed larger agglomerates than **Si-Ph** particles in **PB-0** and **PB-2** composites, and that **Si-Ph** particles formed less and smaller silica agglomerates than **Si-OH** particles in **PB-10** composite although this effect is not very distinct. These observations are in good agreement with the conclusions made from the Payne effect analysis and dynamic temperature sweeps. In short, simply from TEM analysis it follows that the rubber modification reduced the tendency of silica nanoparticles toward agglomeration and improved the particle dispersion. Moreover, the surface modification of silica nanoparticles contributed to better silica dispersion in less polar rubber matrices as well.

4-5 Conclusion

Here we presented a kind of “smart” silica nanocomposites containing surface unmodified and modified silica nanoparticles from Stöber synthesis, and a thermoreversible crosslinking rubber. The influence of hydrogen bonding interaction between silica and rubber on the Payne effect, and the temperature dependent dynamic mechanical properties were systematically investigated. The dynamic mechanical analysis showed that the competition and symbiosis between the filler-filler, filler-rubber and rubber-rubber HB interaction were controllable simply by changing the silica functionality, the silica loading, the degree of rubber modification and the temperature. TEM micrographs showed that both the modifications of silica nanoparticles and rubber promoted better silica dispersion in the rubber matrix. By this strategy it is clear that the Payne effect was reduced and it is possible to modify the mechanical properties of such silica filled composites in order to meet the requirements for tire applications.

4-6 Acknowledgement

The authors thank the members of Makromolekulare Chemie II for their hospitality and instrumental help. We are also grateful to Ms. Katrin Sattler (Anorganische Chemie I, Universität Bayreuth) for her sincere help with BET measurements. Financial support was given by the Bundes Ministerium für Bildung und Forschung (BMBF-project NMT/03N8645B), Bayreuth Institut für Makromolekülforschung (BIMF) and Verband der Chemischen Industrie (VCI).

References

- [1] A. R. Payne, *J. Appl. Polym. Sci.*, **6**, 57 (1962).
- [2] G. J. Kraus, *J. Appl. Polym. Sci. Appl. Poly. Symp.*, **39**, 75 (1984).
- [3] G. Heinrich and M. Klüppel, *Adv. Polym. Sci.*, **160**, 1 (2002).
- [4] J. B. Donnet, R. C. Bansal and M. J. Wang, "Carbon Black", Marcel Dekker, New York, 1993.
- [5] A. Voet, *J. Polym. Sci.*, **15**, 327 (1980).
- [6] P. Cochet, L. Barriquand, Y. Bomal and S. Touzet, paper presented at a meeting of ACS, Rubber Division, Cleveland, Ohio, 1995.
- [7] Y. C. Ou, Z. Z. Yu and A. Vidal, J. B. Donnet, *J. Appl. Polym. Sci.*, **59**, 1321 (1996).
- [8] L. Gatti, *Tire Technol. Int. Ann. Review*, **39**, 2001 (2001).
- [9] J. H. Bachman, J. W. Sellers, M. P. Wagner and R. F. Wolf, *ibid.*, **32**, 1286 (1959).
- [10] G. J. Briggs, D. C. Edwards and E. B. Storey, *Rubber Chem. Technol.*, **36**, 621 (1963).
- [11] R. S. Chahal and L. E. St. Pierre, *Macromolecules*, **1**, 20 (1968).
- [12] D. C. Edwards, *Rubber Chem. Technol.*, **49**, 703 (1975).
- [13] D. C. Edwards and K. Sato, *ibid.*, **52**, 84 (1979).
- [14] D. C. Edwards and K. Sato, *ibid.*, **53**, 66 (1980).
- [15] N. Nagata, T. Kobatake, H. Watanabe, A. Ueda and A. Yoshioka, *Rubber Chem. Technol.*, **60**, 703 (1987).
- [16] H. Hozoji, O. Horie, M. Ogata, S. Numata and N. Kinjo, *Kobunshi Ronbunshu*, **47**, 483 (1990).
- [17] A. Saito, H. Yamada, T. Matsuda, N. Kubo and N. Ishimura, paper presented at Rubber Expo 2001, Fall Technical Program, 160th, Cleveland, 2001.
- [18] D. M. Roggeman, D. F. Graves, W. J. Kern and Y. Horikawa, US Patent 6,313,232, 2001.
- [19] S. S. Choi, *J. Appl. Polym. Sci.*, **79**, 1127 (2001).
- [20] J. L. de la Fuente, M. Fernández-García and M. L. Cerrada, *J. Appl. Polym. Sci.*, **88**, 1705 (2003).
- [21] S. Sudip and A. K. Bhowmick, *Polym. Eng. Sci.*, **44**, 163 (2004).
- [22] S. Mücke, M. Grün and W. Nentwig, paper presented at Int. Rubber Conf. 2003, Nuremberg, 2003.
- [23] P. K. Pal and S. K. De, *Rubber Chem. Technol.*, **56**, 737 (1983).
- [24] R. N. Datta, P. K. Das, S. K. Manda and K. Basu, *Kautsch Gummi Kunstst.*, **41**, 157 (1988).
- [25] M. J. Wang, *Rubber Chem. Technol.*, **71**, 520 (1998).
- [26] H. D. Luginsland, *Kautsch Gummi Kunstst.*, **53**, 10 (2000).
- [27] J. Fröhlich and H. D. Luginsland, *Rubber World*, **4**, 28 (2001).
- [28] A. Hasse, O. Klockmann, A. Wehmeier, H. D. Luginsland, *Kautsch Gummi Kunstst.*, **55**, 236 (2002).
- [29] L. A. E. M. Reuvekamp, J. W. ten Brinke, P. J. van Swaaij and J. W. M. Noordermeer, *Kautsch Gummi Kunstst.*, **55**, 41 (2002).
- [30] J. W. ten Brinke, P. J. van Swaaij, L. A. E. M. Reuvekamp and J. W. M. Noordermeer, *Rubber Chem. Technol.*, **76**, 12 (2003).
- [31] A. Guillet, *Macromol. Symp.*, **194**, 63 (2003).

- [32] V. Tertykh, V. Yanishpolskii and Y. Bol'bukh, *Macromol. Symp.*, **194**, 141 (2003).
- [33] L. Ladouce-Stelandre, Y. Bomal, L. Flandin and D. Labarre, *Rubber Chem. Technol.*, **76**, 145 (2003).
- [34] L. Bokobza and O. Rapoport, *Macromol. Symp.*, **194**, 125 (2003).
- [35] V. Arrighi, I. J. McEwen, H. Qian and M. B. Serrano Prieto, *Polymer*, **44**, 6259 (2003).
- [36] C. Gauthier, E. Reynaud, R. Vassoille and L. Ladouce-Stelandre, *Polymer*, **45**, 1761 (2004).
- [37] C. C. Peng and V. Abetz, *Macromolecules*, **38**, 5575 (2005).
- [38] The optimized molar ratio of reagents was verified by *in-situ* DLS measurement. Also see C. C. Peng, Ph.D. thesis, Universität Bayreuth, 2006.
- [39] Hereinafter, all nanocomposites are named according the following rules. For example, PB-5/Si-OH-80 stands for the composite containing 5 mol% modified PB loaded with 80 phr Si-OH. And PB-10 means all the composites made of 10 mol% modified PB.
- [40] K. Yurekli, R. Krishnamoorti, M. F. Tsa, K. O. Mcelrath, A. H. Tsou and H. C. Wang, *J. Polym. Sci. Polym. Phys.*, **39**, 256 (2001).
- [41] D. R. Anderson, in “*Analysis of Silicones*”, ed. A. L. Smith, Wiley-Interscience, New York, 1974.
- [42] E. Guth and O. Gold, *Phys. Rev.*, **53**, 322 (1938).
- [43] H. M. Smallwood, *J. Appl. Phys.*, **15**, 758 (1944).
- [44] A. R. Payne, R. E. Whittaker and J. F. Smith, *J. Appl. Polym. Sci.*, **16**, 1191 (1972).
- [45] S. Scheiner, “*Hydrogen Bonding – A Theoretical Perspective*”, Oxford University Press, New York, 1997.
- [46] G. A. Jeffrey, “*An Introduction to Hydrogen Bonding*”, Oxford University Press, New York, 1997.
- [47] Z. Ren, R. A. Shanks and T. J. Rook, *J. Appl. Polym. Sci.*, **79**, 1942 (2001).
- [48] M. A. Kaeder, A. K. Bhowmick, *J. Appl. Polym. Sci.*, **90**, 278 (2003).
- [49] C. Wu and S. Akiyama, *Polym. Int.*, **52**, 1249 (2003).
- [50] E. Chabert, M. Bornert, E. B. Lami, J. Y. Cavaillé, R. Dendievel, C. Gauthier, J. L. Putaux and A. Zaoui, *Mater. Sci. Eng.*, **381**, 320 (2004).
- [51] H. Yan, G. Tian, K. Sun, Y. Zhang and Y. Zhang, *J. Polym. Sci. Polym. Phys.*, **43**, 573 (2005).
- [52] P. Mélé, C. D. Silva, S. Marceau, D. Brown, Y. D. Puydt and N. D. Albérola, *Macromol. Symp.*, **194**, 185 (2003).
- [53] S. Vieweg, R. Unger, G. Heinrich and E. Donth, *J. Appl. Polym. Sci.*, **73**, 495 (1999).
- [54] P. Atkins and J. de Paula, “*Atkins’ Physical Chemistry*”, 7th Ed., Oxford University Press, Oxford, 2002.

Supplement

Synthesis and Characterization of Polymeric Microgels Filled Elastomer

S-1 Introduction

For many applications of rubbery materials it is desirable to control their mechanical properties. Here rubber composites, which are composed of uncrosslinked rubbers filled with crosslinked microgels are presented. The components interact via thermoreversible links, especially hydrogen bonds. In order to investigate the effect of non-covalent interaction on filled rubber systems, the composites were designed in such a way, that hydrogen bonding acceptor and donor functionalities are attached onto different components (namely, rubber chain or filler), thus leading to an attractive interaction in between as shown in **Figure S-1**.

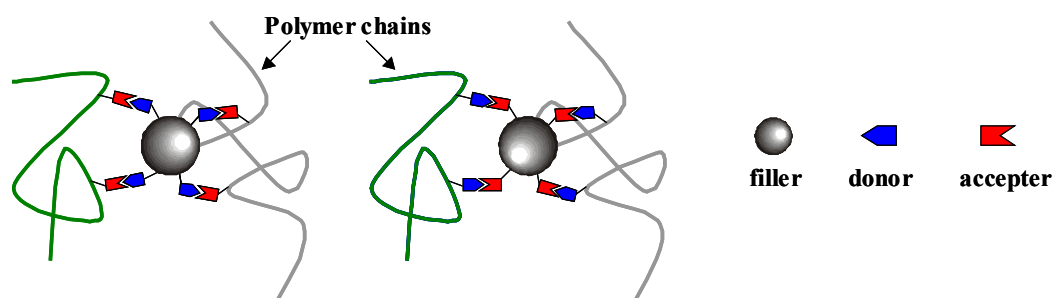


Figure S-1: Rubber-filler interaction through hydrogen bonds.

The way to realize the objective is to chemically modify rubber and polymeric fillers in the light of polymer analogous reaction, so that both of them could carry hydrogen bonding donating or accepting functionalities. Due to the enhanced interaction between rubber and filler, theoretically it is expected that the filler agglomeration could be significantly hindered and hence it results in better dispersion of filler in the rubber matrix. From the Payne effect point of view, the suppressed filler network will bring about less energy loss attributed to the breakdown of the filler network. For practical purposes, this idea also offers an alternative of exploring the applicability of such systems for tire industry. In order to have a straightforward insight into the rubber-filler interaction, the characterization was done exclusively by dynamic mechanical analysis.

The work reported here was done in collaboration with DIK (Deutsches Institut für Kautschuktechnologie e.V.) in Hannover.

As shown in **Figure S-2**, several examples of primary polymer analogous reactions can be carried out with polybutadiene (thereinafter PB) [1,2].

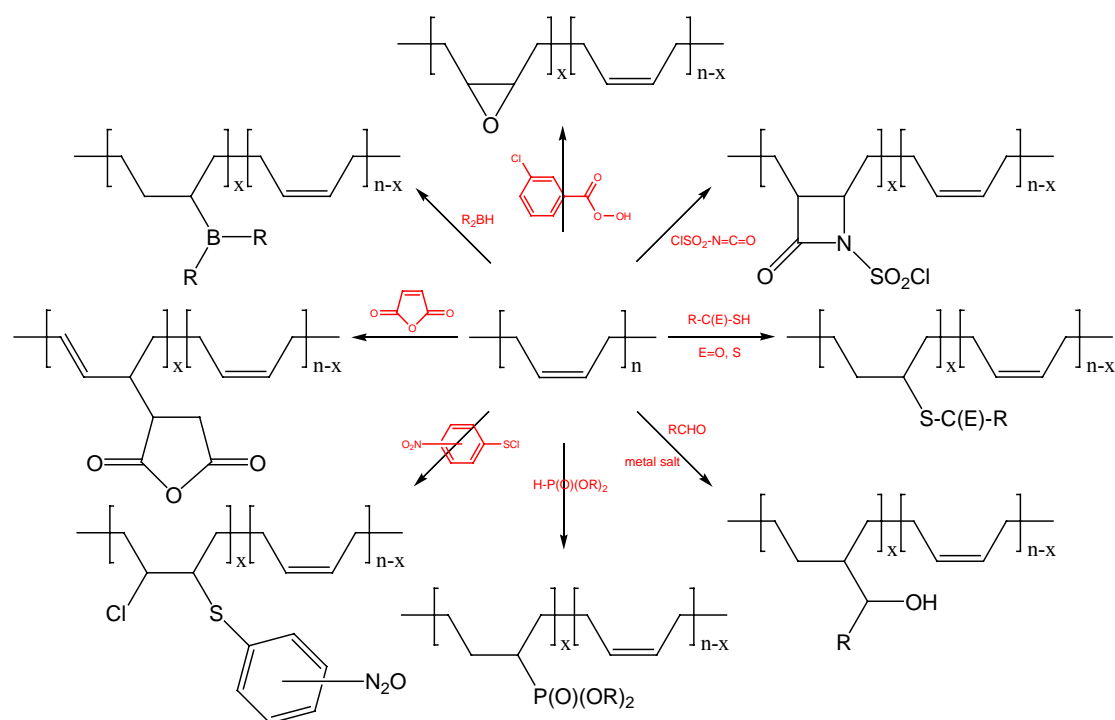


Figure S-2: Primary polymer analogous reaction for polybutadiene.

However, due to the low reactivity of maleic anhydride the trials of thermal ene reaction of maleic anhydride with PB were not satisfactory despite a number of literatures claimed the reaction to be rather efficient [3-5]. From our own experience the reaction needs a temperature higher than 200 °C and reaction time longer than 6 hours, which is not in favor for PB with a high molecular weight (it is prone to thermal crosslinking reaction). To avoid the use of metal-based catalysts and prolonged high temperature for the reaction, epoxidation with *m*-chloroperbenzoic acid (thereinafter MCPBA) [6] and the addition reaction of aromatic sulfenyl derivatives [7] best meet the requirements. In addition to the advantage of using MCPBA described in chapter 1 as shown in **Figure S-3** one could further modify the

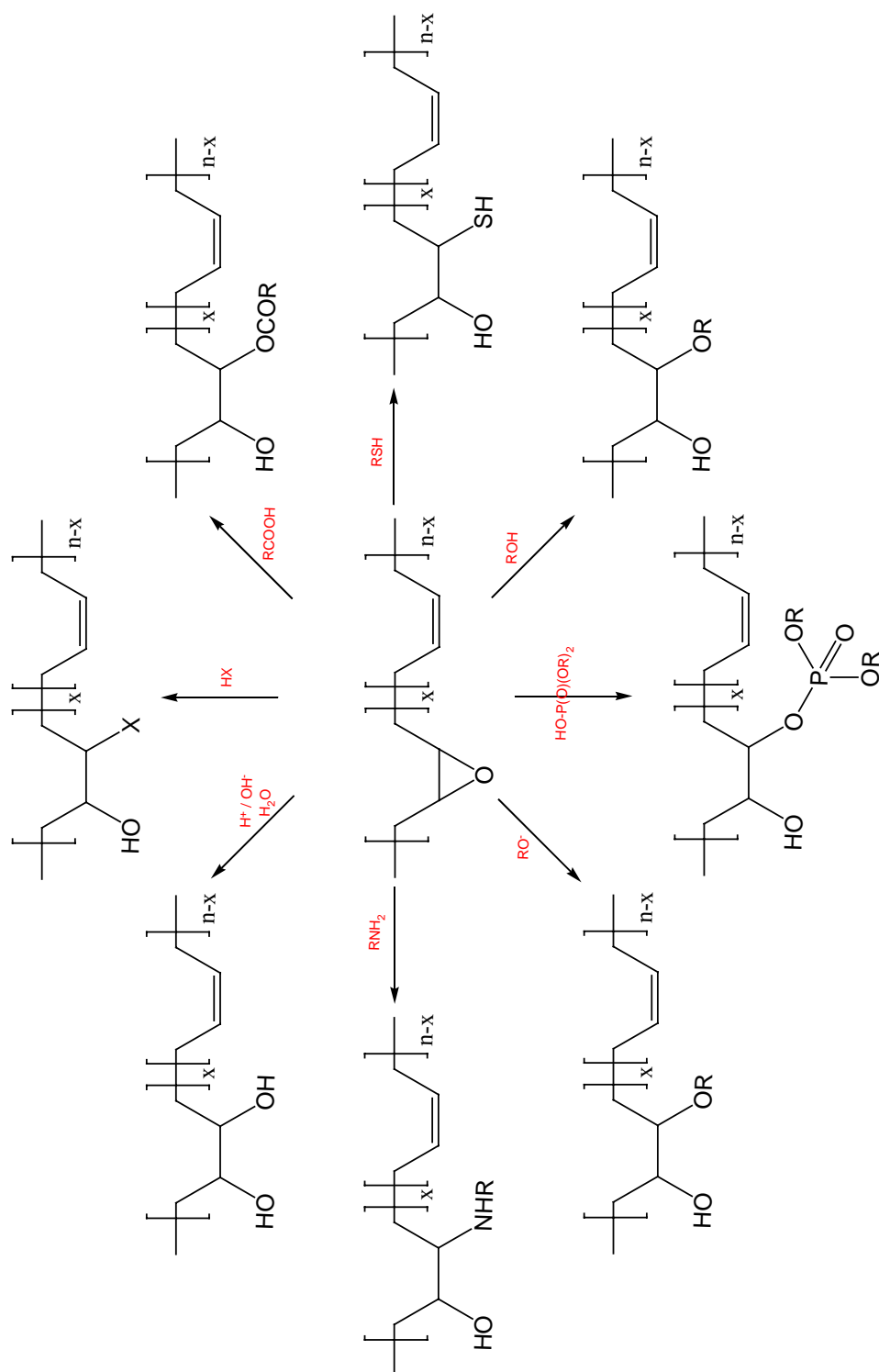


Figure S-3: Secondary modification of epoxidized polybutadiene.

reactive oxirane, ring with nucleophilic and/or electrophilic reagents which carry hydrogen bonding donating or accepting group [1].

Since the objective is to have a quantitative chemical modification of PB, the ring-opening of oxirane was done by adding hydrochloric acid. The reaction system has two advantages: extremely high reaction efficiency (the degree of ring-opening is always higher than 99%) and simple work-up of the final product. Nevertheless, it is necessary to further modify the ring-opened PB since hydroxyl group is good enough of forming hydrogen bonds with each other, especially at very low bulk concentration in rubber matrix (lower degree of modification). As shown in **Figure S-4** and **Figure S-5**, we proposed the following modification routes, as in order to have stronger hydrogen bonding donating and accepting groups on PB chain.

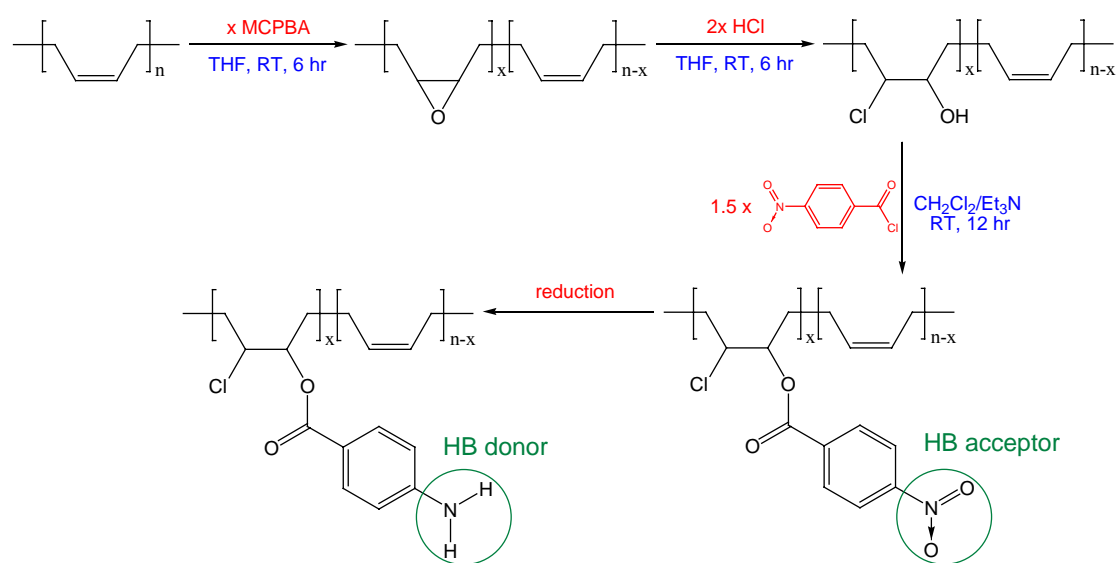


Figure S-4: Proposed modification route for PB. (based on epoxidation reaction)

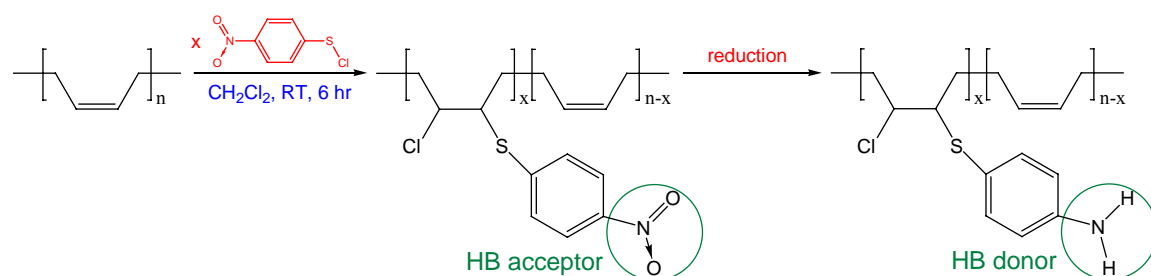


Figure S-5: Proposed modification route for PB. (addition of sulfenyl chloride)

S-2 Experimental

S-2-1 Materials

The unmodified PB used in this study was prepared by Dr. Mabel Graf, MCII, using standard anionic polymerization techniques, with 92% *cis*-1,4 microstructure, $M_n=250,000$ g/mol (PS standard) and $M_w/M_n= 1.04$. *m*-chloroperbenzoic acid (MCPBA, 70%, Fluka), hydrochloric acid (32 wt% HCl, Merck), *p*-nitrobenzoyl chloride (PNBC, 98%, Merck), *p*-nitrobenzenesulfonyl chloride (PNBSC, 95%, Aldrich), lithium aluminium hydride (97% powder, Merck), sodium-*bis*-(2-methoxyethoxy)-aluminumhydride (Red-Al[®], 65 wt% in toluene, Aldrich), hydrazine hydrate (> 99% N₂H₅OH, Merck), formic acid (98%, Fluka) and Pd/C (10 wt% palladium on active carbon, Merck) were used without further purification. All solvents used in each modification step were first distilled under normal pressure and stored with 3 Å molecular sieve before use.

S-2-2 Epoxidation of PB

The epoxidation reaction was performed and modified according to literature procedure [8,9], and here PB with 2 mol% degree of modification is highlighted as a typical example. In a 1 L one-neck round bottom flask equipped with magnetic stirrer, 16.2 g of PB (0.3 mol C=C) was first dissolved in 600 mL dry THF (typical concentration for various degrees of modification). A solution of 1.48 g of MCPBA (6.00 x 10⁻³ mol) in 50 mL dry THF was then added drop-wise at room temperature into the polymer solution at such a rate that the MCPBA solution should be completely dripped out in 1 hour. After the addition of MCPBA, the reaction mixture was further stirred for another 5 hours and 2 mL reaction solution was sampled for ¹H-NMR before the ring-opening reaction. The degree of modification was calculated using ¹H-NMR technique as described in literature [10].

S-2-3 Ring-opening of Epoxidized PB (Hydrochlorination)

A solution of 1.37 g hydrochloric acid (1.20×10^{-2} mol HCl) in 50 mL THF was first prepared and transferred into a 100 mL dropping funnel, it was then added drop-wise at room temperature into the epoxidized PB solution prepared previously. After the addition of HCl solution, the reaction mixture was further stirred for another 6 hours in order to complete the ring-opening reaction. Afterwards the polymer was isolated by precipitation into 400 mL methanol and then dried at 50 °C under vacuum for two days. The yield of the hydrochlorinated PB was 99%, and the extent of oxirane ring-opening reaction was verified using $^1\text{H-NMR}$.

S-2-4 Esterification of hydrochlorinated PB

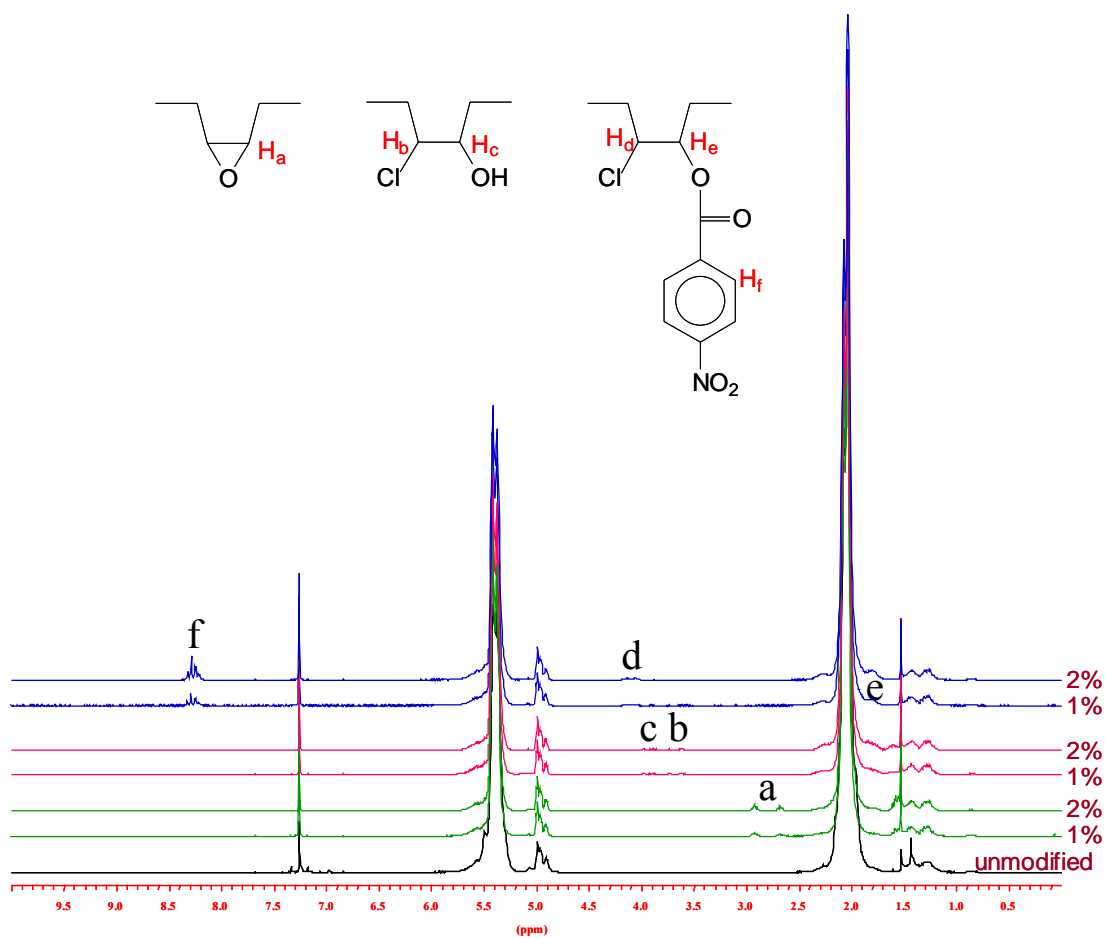


Figure S-6: $^1\text{H-NMR}$ spectra of 1 and 2 mol% modified PBs.

In a 200 mL one-neck round bottom flask, equipped with magnetic stirrer, 5.0 g of 2 mol% hydrochlorinated PB, (1.82×10^{-3} mol -OH) was first dissolved in a mixture of 100 mL dry CH_2Cl_2 and 5 mL dry Et_3N . 0.51 g PNBC (2.72×10^{-3} mol) was then added at one dose into the ice-bathed solution and the system was stirred at 0 °C for 12 hours. After the reaction, the final product was isolated by precipitation into 100 mL methanol and then dried at 50 °C under vacuum for two days. The yield of the isolated product was 98%, and the extent of reaction was verified by using $^1\text{H-NMR}$. $^1\text{H-NMR}$ spectra are given in **Figure S-6** and they show the reaction conversion is > 99%. PB with 1 mol% degree of modification was also prepared according to the above recipe and the details are summarized in **Table S-1** and **Table S-2**.

Table S-1: PBs of 1 and 2 mol% hydrochlorination

Sample ID	Degree of Hydroxylation (based on C=C unit)	PB used (g)	MCPBA (g)	HCl (g)	Yield (%) ^a
PB-OH-1	1 mol%	16.2	0.74	0.68	99
PB-OH-2	2 mol%	16.2	1.48	1.37	99

^ayield is calculated by $\frac{w/[54 + x(35.5 + 17)]}{16.2/54} \times 100\%$, where w is the weight of the product in gram and x is the degree of modification in %.

Table S-2: PBs of 1 and 2 mol% modification

Sample ID	Degree of Modification (based on [OH]/[C=C] ₀)	PB-OH used (g)	PNBC (g) ^a	Yield (%) ^b
PB-SC-1	1 mol%	5.0	0.26	98
PB-SC-2	2 mol%	5.0	0.51	98

^athe amount of PNBSC required is calculated based on mole of -OH. $-\text{OH mol} = \frac{5.0x}{54 + x(35.5 + 17)} \times 100\%$, where x is the degree of modification in %.

^byield is calculated by $\frac{w/[54 + x(35.5 + 16 + 150)]}{5.0/[54 + x(35.5 + 17)]} \times 100\%$, where w is the weight of the product in gram and x is the degree of modification in %.

S-2-5 Sulfenyl Chloride Addition onto PB

The addition reaction of PNBSC was performed and modified according to literature

procedure [11]. In a 1000 mL one-neck round bottom flask equipped with magnetic stirrer, 16.2 g PB (0.3 mol C=C) was first dissolved in 600 mL dry CH₂Cl₂ (a typical concentration for various degrees of modifications). A solution of 2.40 g of PNBSC (6.00 x 10⁻³ mol) in 50 mL dry CH₂Cl₂ was then added drop-wise at room temperature into the polymer solution at such a rate that the PNBSC solution should be completely dripped out in 1 hour. After the addition of PNBSC, the reaction mixture was further stirred for another 5 hours. Afterwards the polymer was isolated by precipitation into 400 mL methanol and then dried at 50 °C under vacuum for two days. The yield of the modified PB was 99%. The degree of modification was calculated using ¹H-NMR technique as described in literature [11]. ¹H-NMR spectra of are given in Figure S-7 and the reaction efficiency is greater than 99%.

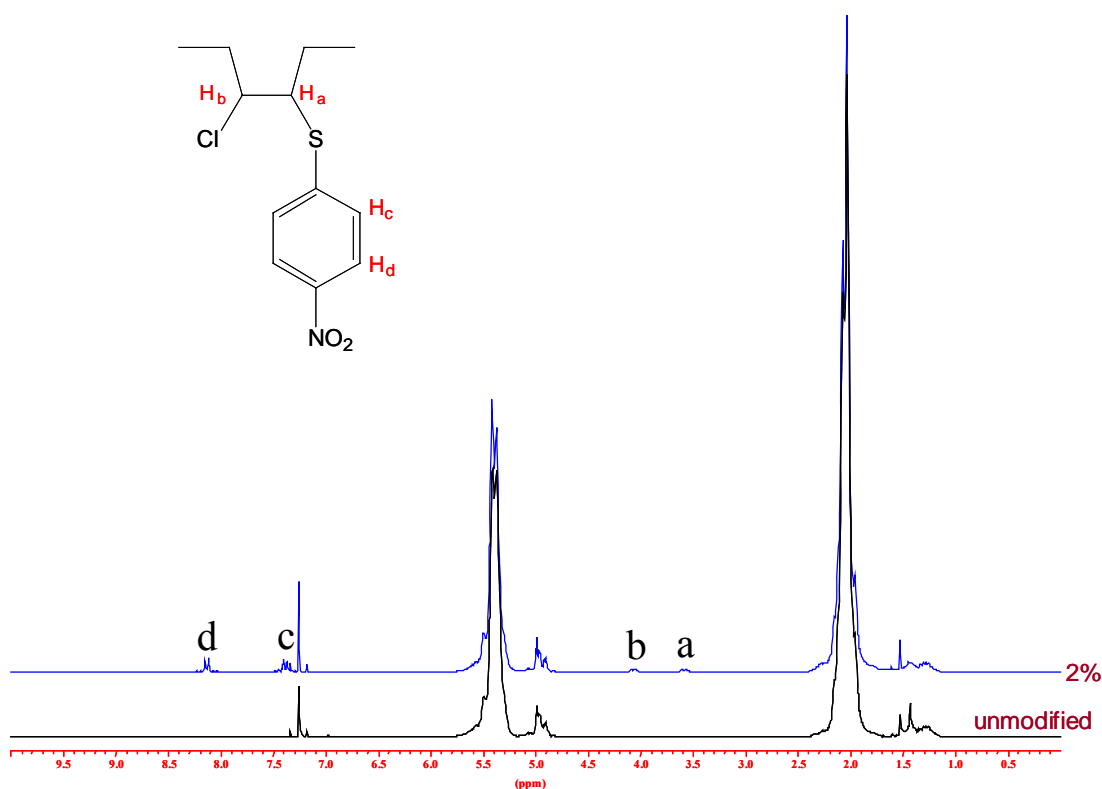


Figure S-7: ¹H-NMR spectra of 2 mol% PNBSC modified PBs.

S-2-6 Reduction of Nitro Compounds

In order to selectively reduce $-\text{NO}_2$ into $-\text{NH}_2$ (HB acceptor and donor, respectively) without disturbing the other functionalities [12,13], reactions were done using diverse reducing agents, as summarized in Table S-3. Besides, model compounds having the same functional groups were also synthesized to examine the validity of the reactions.

Table S-3: Conditions for nitro reduction reactions

A:

B:

C:

D:

Reagent ^a	Catalyst	Solvent	Temp. (°C)	A	B	C	D
LiAlH ₄		THF	25	phenyl azo	phenyl azo	crosslink	crosslink
Red-Al		THF	25	phenyl azo	phenyl azo	crosslink	crosslink
H ₂ ^b	Pd/C	THF/MeOH ^c	40	phenyl azo	thioether cleavage	crosslink	thioether cleavage
N ₂ H ₄	Pd/C	THF/MeOH ^c	25	reduction	thioether cleavage	inert	thioether cleavage
Cyclohexene	Pd/C	THF	25, 70	reduction	reduction	inert	inert
Fe/HCl		THF/MeOH ^c	25	reduction	reduction	crosslink	crosslink
HCOOH	Pd/C	THF/MeOH ^c	40	reduction	reduction	inert	inert
HCOOH	Pd/C	MeOH	25	reduction	inert	N/A	N/A

^areagent/ $-\text{NO}_2$ = 5 eq. ^bP = 4 bar, 50 hr ^c THF/MeOH = 10 Vol.

On one hand, the nitro group on the two model compounds can be easily reduced by several reducing agents and the ester and thiol ether were still intact. On the other hand, surprisingly and interestingly the same reducing reagents did not reduce the nitro group on PB at all. There could be several reasons for the different behaviors of nitro group on PB and model compounds. First, the total concentration of nitro group on PB chain is low (2 mol%), which means, from a kinetic point of view, the reaction is extremely slow. Second, if one compares the model compounds with polymer samples, the possibility of direct contact of catalysts and/or reducing agents with the nitro group is much less for polymer samples since the nitro group is more or less “encaged” in the PB chains. Third, solvent does affect the efficiency. It is well known that methanol has a higher dielectric constant than THF [12], which means methanol stabilizes the species for electron transfer and hence it facilitate the electron-involved

reduction reaction. Unfortunately, PB and its modified samples presented here are not soluble in methanol and the reduction turned out to be unsatisfactory. We also found crosslinked products under certain reaction conditions, which are attributed to the formation of azo intermediate in the course of nitro group reduction. It is also important to note that with some of the reducing agents used here, the ester and thioether functionalities were still intact even if the nitro group was successfully reduced in the model compounds.

S-2-7 Polymeric Microgel

Polymeric microgels with different organic functionalities were synthesized by and received from DIK [14]. Here butadiene rubber microgel (BR gel), acrylonitrile-butadiene rubber microgel (NBR gel), nitrated polystyrene microgel (NPS gel) and -CN reduced acrylonitrile-butadiene rubber microgel (RNBR gel) were used as polymeric fillers. They were synthesized by crosslinking reaction of the corresponding polymer latex with dicumyl peroxide (DCP). The surface functionalization for PS gel was done using nitric acid and the synthesis of NBR gel was done by reducing NBR gel using lithium aluminium hydride and also *p*-toluenesulfonyl hydrazide (Figure S-8).

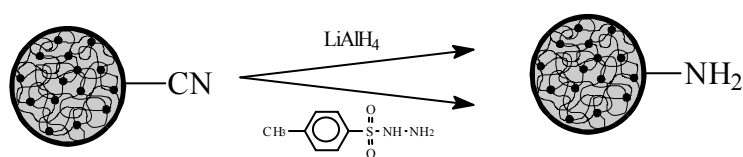


Figure S-8: Reduction of NBR gel to RNBR gel.

SEM images of microgels in Figure S-9 showed that the size of microgel particles are similar (about 100 nm), but their morphologies are quite diverse. FTIR spectra of the NPS gel, NBR gel and RNBR gel are all shown in Figure S-10.

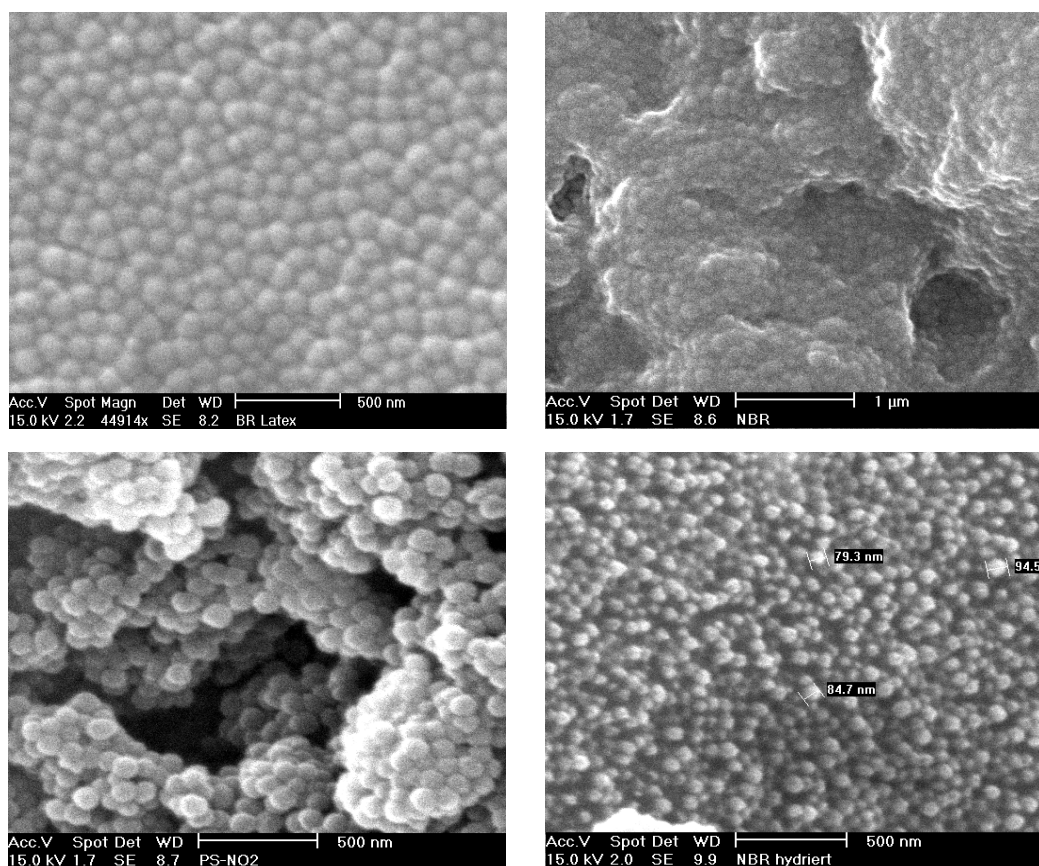


Figure S-9: SEM images of BR, NBR, NPS and RNBR microgels. (names are as given in the images)

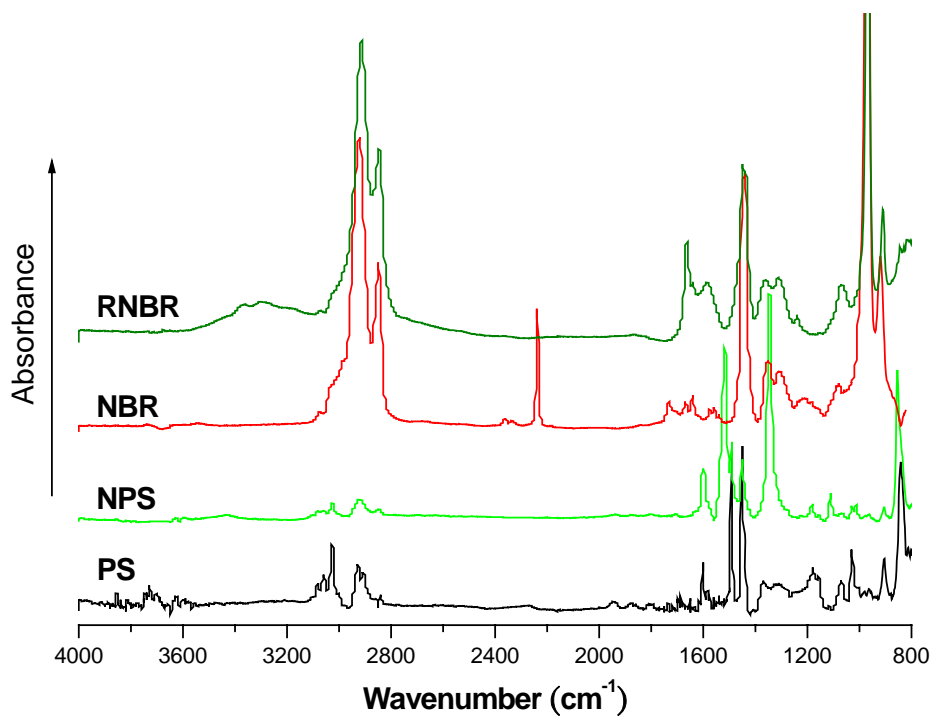


Figure S-10: FTIR spectra of PS, NPS, NBR and RNBR gel.

S-2-8 Dynamic Mechanical Analysis (RPA and ARES)

Since the reduction of -NO₂ for modified PB was not satisfactory and in order to simplify the synthetic route, the composites for dynamic mechanical analysis were chosen to be: 2 mol% PNBSC modified PB together with BR, NBR, NPS and RNBR microgel. The microgel content based on polymer mass were 20, 40 and 80 phr (parts by weight per hundred parts rubber). We used the uncrosslinked PB to avoid complications resulting from the influence of the crosslinked network and to avoid the influence of fillers in altering the nature of the crosslinking (interfering with crosslinking reaction) [15]. In order to blend the microgels with PB, the blendings were done using a two-roller miller since it was difficult to re-disperse the microgels in solvents: at room temperature 5 grams of modified PB was first milled at a rotational speed of 20 rpm and the corresponding amount of microgel was added in several portions in such a way that the microgel can be thoroughly mixed with PB. Upon the complete addition of the microgel, the blends were further mixed for 10 minutes in order to achieve homogeneous systems. The program for RPA 2000 (**R**ubber **P**rocess **A**nalyzer, Alpha Technologies) analyses was using strain-sweep with a shear strain span from 0.28 to 400%, and the test frequency and temperature were 1 Hz and 60 °C respectively [16]. Dynamic temperature- and frequency-sweep were done using ARES, with plate-plate geometry (25 mm plate with groove). A strain-sweep was performed before each measurement to ensure the linear viscoelastic behavior. The frequency range for frequency-sweep was from 0.1 to 100 Hz and temperature range for temperature-sweep was taken from 80 to -100 °C at a frequency of 1 Hz.

S-3 Results and Discussion

S-3-1 Payne Effect Analysis (RPA Strain-sweep)

Payne effect analysis is one of the best methods to characterize the filler-rubber interaction, simply through a dynamic strain-sweep test (less filler-rubber interaction will result in pronounced Payne effect). However, in addition to the idea of hydrogen bonding interaction, there are several other factors affecting filler-rubber interaction and hence the rheological properties as discussed in Chapter 1. In our case, in order to simplify the reinforcing mechanism some ideal assumptions for the systems were made before interpreting the results:

A. For PNBSC modified PB,

the polymer matrix is able to sufficiently transmit the “external” load to the fillers, namely, the PB is enough rigid and there are significant entanglements to sustain small shear deformation [17].

B. For polymeric microgels,

the size, shape, porosity, surface roughness and rigidity are similar despite intrinsic properties of individual filler material, namely, different fillers can then be regarded as if they were made of same material but with different interacting functionality on their surface.

The RPA analyses of blends of PNBSC modified PB with different microgels are shown in **Figure S-11**, and different behaviors can be seen therefrom. First, if one compares the value of dynamic storage modulus (G') with that of dynamic loss modulus (G'') of the modified PB, note that G'' was greater than G' ($\tan \delta > 1$). It revealed that instead of elastic, the viscous behavior dominated the rheological response even at 80 phr loading (except for NBR micrgel filled blends). Second, both G' and G'' were increased with increasing filler loading. It showed that the PB was reinforced in rigidity (shear modulus) by adding fillers and the reinforcing extent was also increased with increasing filler loading. Third, the span of linear viscoelastic region was reduced with increasing filler loading in all the blends, which on the other hand means that the yield point of the stress-strain curve was shifted to lower strain (blends became rigid and brittle). The above observations are reasonable since the rheological behavior is well known for filled rubber blends. Besides, it is generally believed that with increasing filler loading, filler particles are prone to filler network

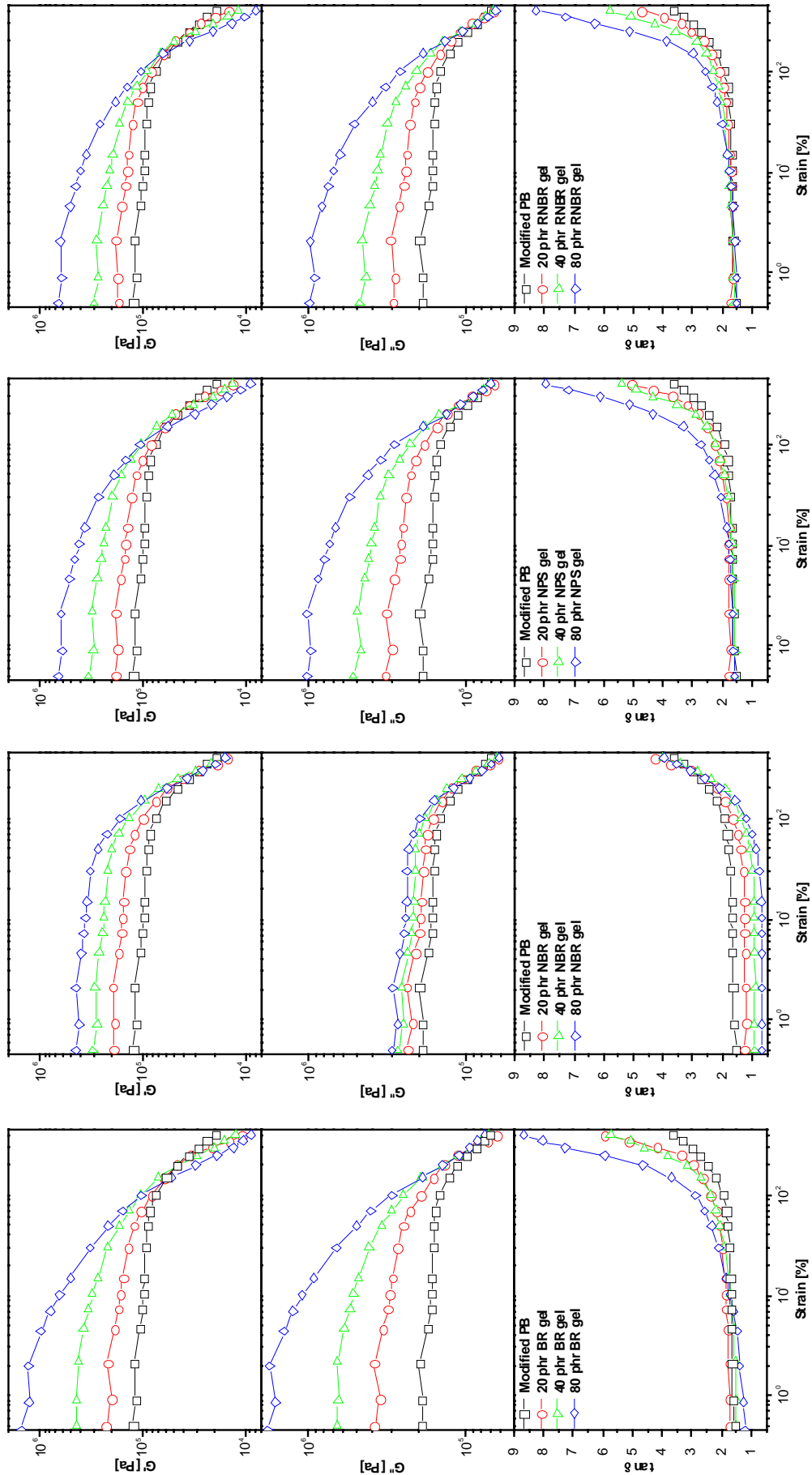


Figure S-11: RPA strain-sweep analysis of microgels filled systems. (plotted on same scale)

formation and that if there are more filler networks the linear viscoelasticity of rubber composite is more sensitive to external strain [18]. However, to our surprise, one is not able to have any insight into the effect of filler-rubber interaction on Payne effect because there were no local maxima of G'' showing up upon the beginning of the decline of G' , that is, no Payne effect was detectable in all the blends. If one thinks about the mechanism of filler network breakdown under strain (Payne effect), we mainly came up with three possible explanations for the non-pronounced filler network breakdown:

A. The PB matrix was not “rigid enough” to transmit external load to the filler at the testing temperature, which means most of the filler networks were still intact even as the PB chains were subjected to large strain. Under this circumstance, only if the applied strain and stress are large enough the filler network could be destroyed.

B. The filler aggregates were too large and too strong. It means that the filler-filler interaction was more significant than the interaction between filler and rubber. Hence the primary particles of the microgel strongly “stuck” together forming macroscopic clusters. The consequence thereof would result in worse filler dispersion in the rubber matrix and the reinforcement from filler in this case can be simply explained by hydrodynamic effects derived by Guth, Gold and Smallwood [19,20]:

$$G = G_0 (1 + 2.5 \varphi + 14.1 \varphi^2) \quad (\text{S-1})$$

where G and G_0 are the moduli of the filled and unfilled system, respectively, and φ is the volume fraction of the filler. However, due to the distinct density of each microgel the degree of modulus enhancement was thus different (same weight fraction but it resulted in various φ).

C. The surface properties of the microgel surface were not able to “effectively” adsorb the PB chains, which can be attributed to the micro-configuration and frictional properties which did not offer opportunity for keying adhesion of the rubber. In this case, of course, microgels with a smoother surface gave less friction force

against rubber chains but those with rougher surface did give more friction and exhibited complete exclusion of voids between primary particles [21].

The above postulations are considered to be reasonable as one keeps an eye on the increasing value of the loss factor ($\tan \delta$) with increasing filler loading, which suggested that there was a worse filler-to-rubber coupling and that the filler network was not completely broken down even at higher strains [22].

Interestingly the NBR microgel filled PB exhibited a totally different behavior from the other systems. First, it is obvious that the strain span of the linear viscoelastic region was similar regardless of filler loading. Second, the degree of modulus enhancement was much lower than in the other systems with the same filler loading. Third, note that at higher strains the $\tan \delta$ of different NBR microgel loadings were more or less identical, which could give us information about its specific microgel structure. However, up to this point we are not able to give any explanation for this unique behavior of the NBR microgel filled system until we have any further rheological analysis.

In addition, attributed to hydrogen bonding interaction between filler and modified PB it is expected that the RNBR filled systems would show the supreme depression of Payne effect and that there would exist the most remarkable filler-rubber interaction in its blends. Unfortunately, by comparing the G' of the four filled systems (Figure S-11), results revealed that at small strains the blends filled with BR microgel showed the most pronounced modulus enhancement among the other blends (order of modulus enhancement: BR > NPS > RNBR > NBR microgel) and that it did not give any straightforward evidence of further reinforcement and the influence on filler percolation threshold by this non-covalent interaction. On the other hand, at higher strains the value of $\tan \delta$ did uncover the aggregation nature of the microgel, and the order of extent of filler network breakdown is: NBR > NPS > RNBR > BR microgel (by relative value of $\tan \delta$). The unusual strain-dependent behaviors could be attributed to the non-well-defined properties of the polymeric microgels (ex. microgel particle size and its distribution, density, structures and the intrinsic mechanical properties). Nevertheless, with the help of RPA analysis we could have little

information about the strain-dependent behaviors of different microgel filled blends.

S-3-2 Frequency-dependent Properties Analysis (ARES Frequency-sweep)

Figure S-12 shows the master curves of microgel filled blends according to time-temperature superposition principle from two frequency-sweep analyses at 0 and 50 °C (reference temperature = 0 °C). First, same as in RPA analysis, it showed increased G' and G'' with increasing filler loading through out the frequency span. However, as one pays attention to the frequency dependence of the modulus on different microgels, the sensitivity of filler-rubber and filler-filler interaction at different frequencies differed. This observation will be discussed in depth later. Second, the rheological transition from elastic to viscous state for all filled blends was also visible since one could observe the so-called crossover point of G' with G'' (where $G' = G''$).

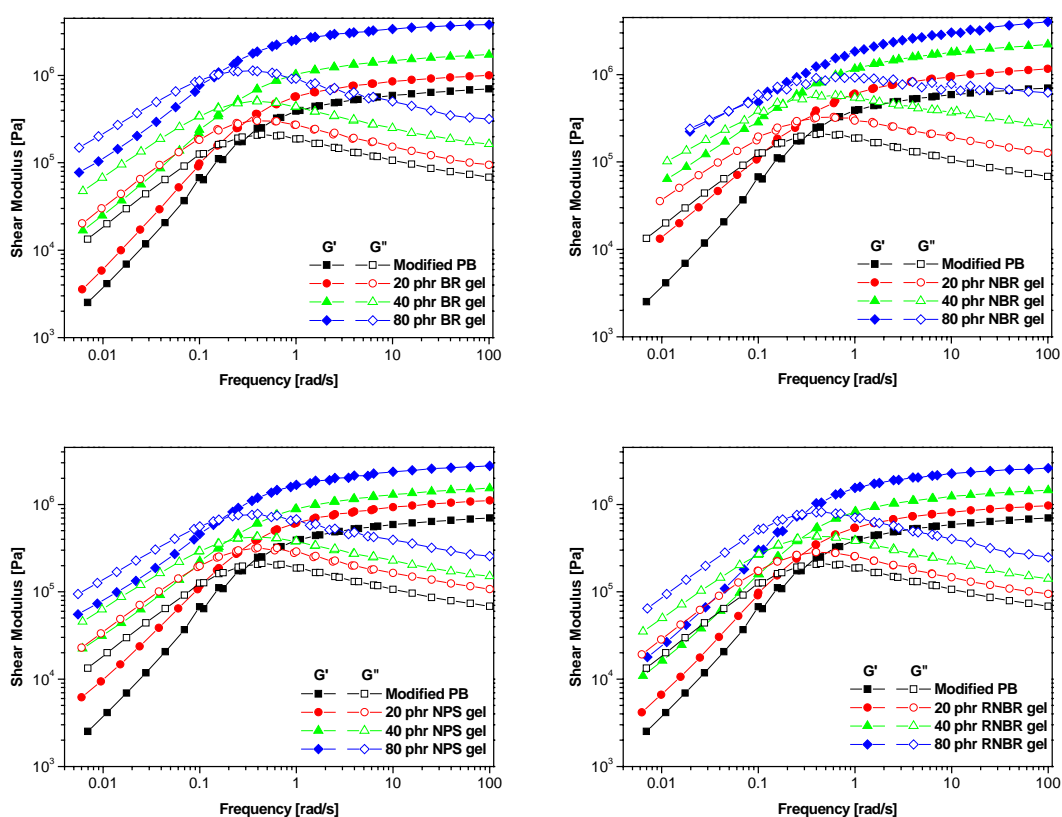


Figure S-12: Master curves of different microgels filled blends. (plotted on same scale)

The detailed frequency-dependent parameters at 50 °C of different microgel filled blends are listed in [Table S-4](#). It is interesting to keep an eye on the existence of a crossover point because the reciprocal of crossover frequency (ω_{cr}) reflects the (longest) terminal relaxation time (τ_r) of the polymer chains (the lifetime of transient network) [23]. The terminal relaxation time can be calculated by:

$$\tau_r = 2\pi / \omega_{cr} \quad (\text{S-2})$$

Obviously, the crossover points of all blends were shifted to lower frequencies and the crossover moduli (G_{cr}) as well were shifted to higher values with increasing filler loading. Since it is well known that the shift of the crossover point to a lower frequency can be referred to be a “hindered” or “lagged” chain relaxation process [23], we believe that with increasing filler loading there is an increasing amount of the PB chains “trapped” in the filler network and/or “adsorbed” on the filler surface and such fact would show a longer relaxation time [24-26]. It is also believed that with increasing filler loading the amount of the so-called “bound rubber” is as well increased (bound rubber is the fraction of rubber which is not extracted by a good solvent from a rubber-filler blend [27,28]).

Table S-4: Frequency-dependent transition data of filled blends ($T = 50$ °C)

Sample	f_{cr} (rad/s)	τ_r (sec.)	G_{cr} (MPa)	G_N (MPa) ^a	$ \eta^*_0 $ [MPa-s] ^a
Modified PB	4.81	1.31	0.22	0.63	0.14
20 phr BR gel	4.96	1.27	0.29	0.87	0.21
40 phr BR gel	3.70	1.70	0.47	1.53	0.47
80 phr BR gel	2.78	2.26	1.03	3.67	1.57
20 phr NBR gel	3.23	1.95	0.21	0.69	0.25
40 phr NBR gel	1.51	4.16	0.17	0.80	0.50
80 phr NBR gel	0.27	23.3	0.09	0.88	0.98
20 phr NPS gel	4.49	1.40	0.33	1.02	0.25
40 phr NPS gel	3.24	1.94	0.41	1.53	0.51
80 phr NPS gel	3.07	2.05	0.70	2.68	1.04
20 phr RNBR gel	4.67	1.35	0.29	0.86	0.20
40 phr RNBR gel	4.28	1.47	0.44	1.36	0.36
80 phr RNBR gel	4.14	1.52	0.78	2.33	0.64

^a G_N (plateau modulus) and η^*_0 (zero-shear complex viscosity) are calculated using RSI Orchestrator Ver. 6. 5. 8, Rheometric Sci.

From the crossover information listed in [Table S-4](#), the ability of microgel networks to retard the relaxation and/or to trap the PB chains at different filler loadings is shown in [Figure S-13](#), namely, a plot of relaxation time against filler loading.

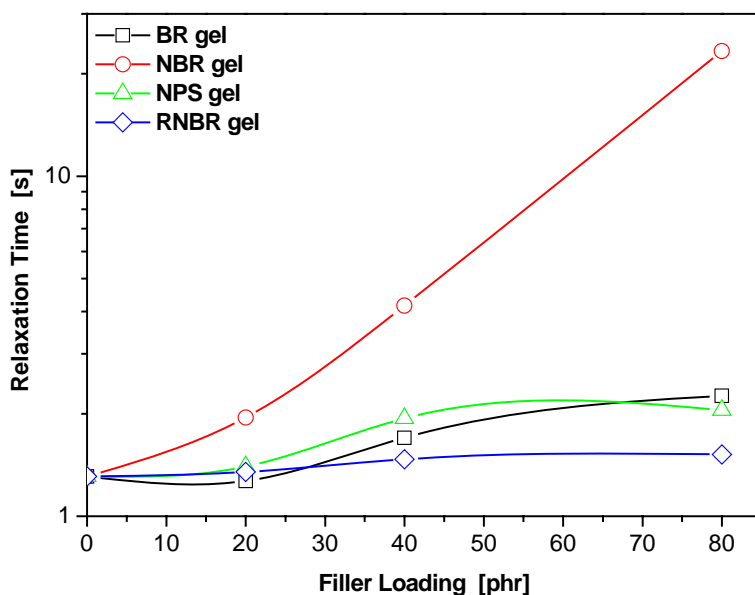


Figure S-13: The effect of filler loading on the PB relaxation time.

As mentioned before, the frequency-dependent behavior of filled rubber always changes with frequency. It is well known that the high frequency behavior for the filled rubber would only be affected by shorter length scale dispersion and interaction between rubber and filler, and on the contrary, the low frequency response would reflect the filler-filler interaction on a microscopic scale [15]. This specific frequency-dependent characteristic offers the best “mirror” for complex filled systems. Here, if the plateau modulus (G_N) was regarded as the high frequency modulus in the temperature of interest, it could act as an index of modulus enhancement and hence gives further information about the complex interacting systems. As tabulated in [Table S-4](#), it was found that the order of filler-rubber interaction between different microgel at high frequency are: NPS > BR > RNBR > NBR (filler loading ≤ 40 phr) and BR > NPS > RNBR > NBR (filler loading > 80 phr). The question now is, why these microgels acted contradictorily to the idea of increasing filler-rubber interaction via hydrogen bonding interaction?

As it is, this unusual behavior can be attributed to the rigidity and, at the same time, the size of microgel cluster (please note that the following remarks are based on the idea that the microgel network is still intact!). As shown in **Figure S-9**, it is clear that the size of primary particles for these four microgels is identical, but it could not impart any information about the rigidity of the individual particle. However, it has been reported that rigid particles, such as mineral fillers, and deformable droplets, such as rubber fillers, softeners and lubricants, have been two totally different kinds of fillers and they possessed divergent reinforcing ability. Besides, deformable particles are prone to the formation of larger clusters via mutual fusion [29-32]. Taking into account the mutual fusion nature of these microgels from the SEM images shown in **Figure S-9**, one could suppose that the order of microgel rigidity is: NPS > BR > RNBR > NBR, and it is clear that the order of microgel cluster size is: NBR > RNBR > BR > NPS, and hence the amount of interacting interface between individual particle and rubber chain is: NPS > BR > RNBR > NBR. This assumption also suggests that the order of “effective” volume fraction at the same loading (phr) is: NPS > BR > RNBR > NBR, which is in good agreement with the contribution of hydrodynamic effect to modulus enhancement developed by Guth, Gold and Smallwood [19,20].

Furthermore, on the basis of theoretical concepts (especially the hydrodynamic effect) of correlation between the parameters of viscous flow and the elasticity of solid, it is suggested that for non-interacting systems the viscosity of liquid containing filler and the shear modulus of a solid containing filler are related by [33]:

$$\eta / \eta_0 = G / G_0 \quad (\text{S-3})$$

where the subscript 0 denotes the characteristic properties of non-filled system. Here in order to correlate the steady shear viscosity (η) to complex viscosity (η^*), the Cox-Merz rule [34], as shown **Equation (S-4)**, is employed and it is further assumed that this relationship holds for the microgel filled systems.

$$\eta (\dot{\gamma}) = |\eta^* (\omega)| \quad (\text{S-4})$$

where $\dot{\gamma}$ is the steady shear rate and ω is the dynamic shear frequency. Besides, the

shear modulus (G) is replaced by the dynamic shear modulus at the rubber plateau (G_N). At this point, Equation (S-3) can now be rewritten as a frequency independent expression:

$$|\eta^*_{0}| / |\eta^*_{0,0}| = G_N / G_{N,0} \quad (\text{S-5})$$

where the second subscript 0 denotes the characteristic properties of the non-filled system.

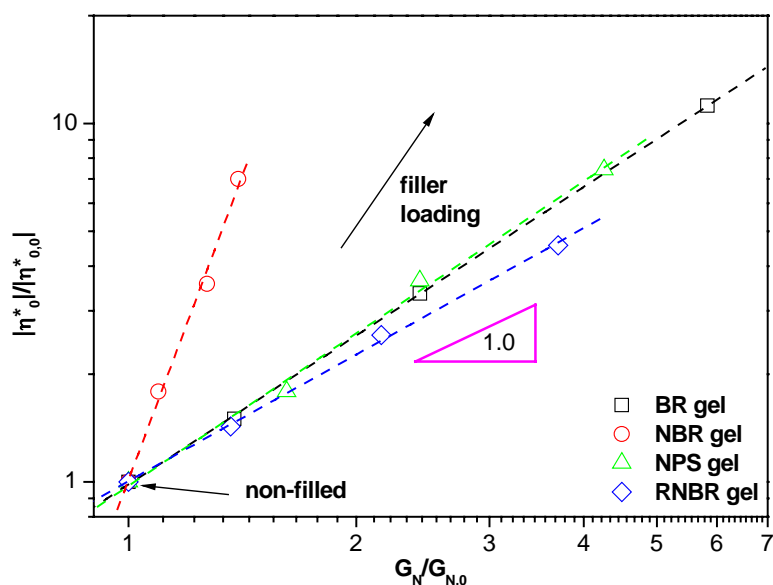


Figure S-14: Plot of complex viscosity against relative plateau modulus of filled and non-filled blends.

However, as shown in Figure S-14, instead of the relation shown in Equation (S-5) we found that there exists a power-law correlation for the microgel filled systems. The mathematical relation can be expressed as:

$$\log (|\eta^*_{0}| / |\eta^*_{0,0}|) = \log B + A \log (G_N / G_{N,0}) \quad (\text{S-6})$$

or

$$|\eta^*_{0}| / |\eta^*_{0,0}| = B (G_N / G_{N,0})^A \quad (\text{S-7})$$

where A and B are material parameters of the different microgel filled systems. Interestingly, from the linear regression analysis of different systems at various filler

loadings shown in [Figure S-14](#) (detailed data are listed in [Table S-5](#)) it is found that the values of B of each system are more or less equal to unity.

Table S-5: Linear regression data of the microgel filled systems (data collected from Figure S-14)

Parameter	BR gel	NBR gel	NPS gel	RNBR gel
A	1.38	5.64	1.41	1.17
B	0.98	1.01	0.98	1.00

It means that [Equation \(S-7\)](#) can be further simplified and rewritten to give a simple relationship between viscosity and shear modulus with an exponent A:

$$|\eta^*_{\omega}| / |\eta^*_{\omega,0}| = (G_N / G_{N,0})^A \quad (\text{S-8})$$

Similar to the terminal relaxation time analysis, note that the exponent A of the NBR microgel filled systems is extraordinarily higher than those of the other microgel filled ones. But, why NBR microgel filled systems exhibited a much higher terminal relaxation time and, at the same time, deviated from the theoretical background suggested from [Equation \(S-3\)](#)? Could we correlate this observation with the suggestions about the microgel natures made herein before? The reason is that NBR microgel is soft and rather flexible. To our surprise, instead of rigid particle behavior, NBR microgel shows characteristic rubber properties in the PB matrix. Thus, the surface on NBR microgel is slippery and it results in less bound PB. Besides, the NBR microgel filled system can also be regarded as an “immiscible”, two-phase blend of PB and NBR rubber, in which NBR microgel clusters exhibited a similar plateau modulus as the modified PB. It is clear that this unusual behavior explains why there was no significant hydrodynamic effect from the NBR microgel filled systems.

In addition to the analyses made above, K. Yurekli et al. [\[15\]](#) and Q. Zheng et al. [\[35,36\]](#) suggested two different ways to look into the filler reinforcement mechanism to the chain relaxation behavior and to verify the rigidity of filler from (dynamic) frequency-dependent measurements. The former reported that the Cole-Cole plot of G'' against G' and the latter of loss viscosity η'' ($= G''/\omega$, representing the elastic part)

against dynamic viscosity η' ($= G''/\omega$, representing the viscous part) would best reflect the change of relaxation behavior of polymer chains and filler network.

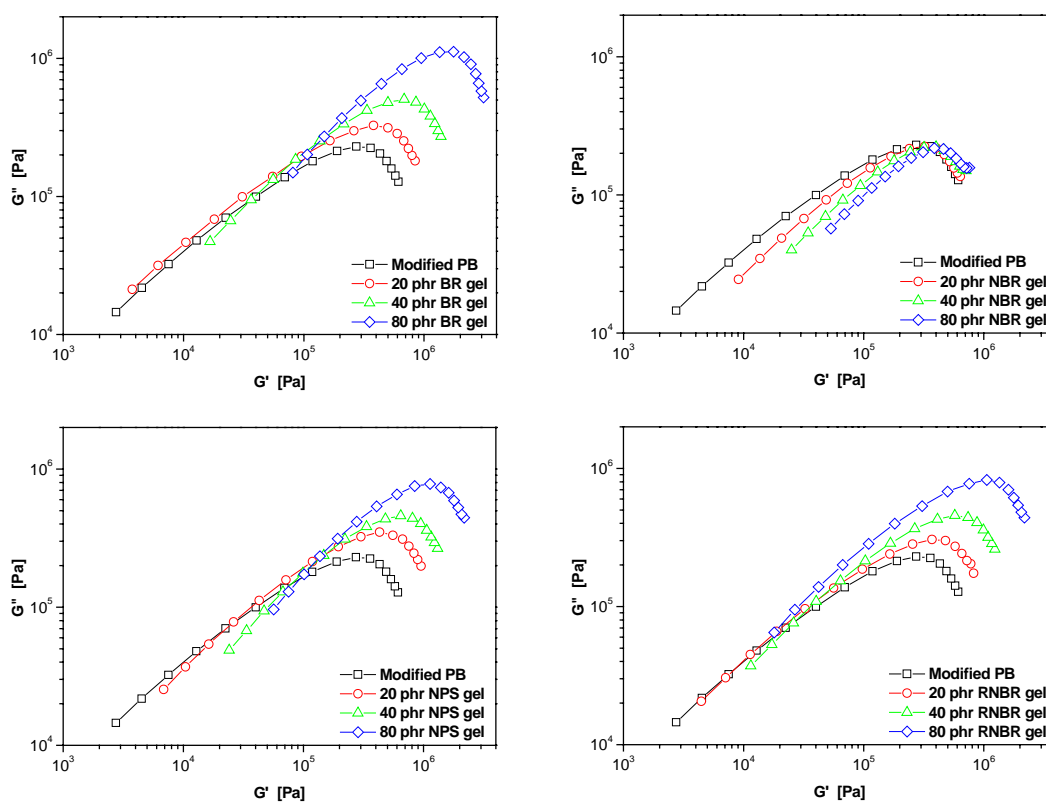


Figure S-15: Cole-Cole plot of G'' against G' . ($T = 50$ °C, plotted on same scale)

Figure S-15 shows the Cole-Cole plots of G'' against G' at 50 °C for different microgel filled systems. It is obvious that except for the NBR microgel filled systems all the other microgel filled systems showed monotonic increase in modulus with filler loading and the absence of any additional relaxation modes. One possible explanation is that the relaxations of the individual PB chains of these microgel filled system are slowed down, although the PB chains are not completely immobilized, as they are strongly adsorbed on the microgel surface [15]. This slowing down as a result of adsorption would lead to a bimodal distribution of relaxation times, corresponding to the slower relaxation of the adsorbed chains and the faster relaxation of the unaffected ones, respectively. However, the Cole-Cole plot of the NBR microgel filled systems showed similar shape and value. Interestingly upon an 80 phr NBR microgel loading, there exists a second increase of G'' at large G' . This increase, as

discussed before, is attributed to the relaxation of NBR microgel additional to that from the PB chains itself at higher frequencies. This analysis is in good agreement with the remark made before.

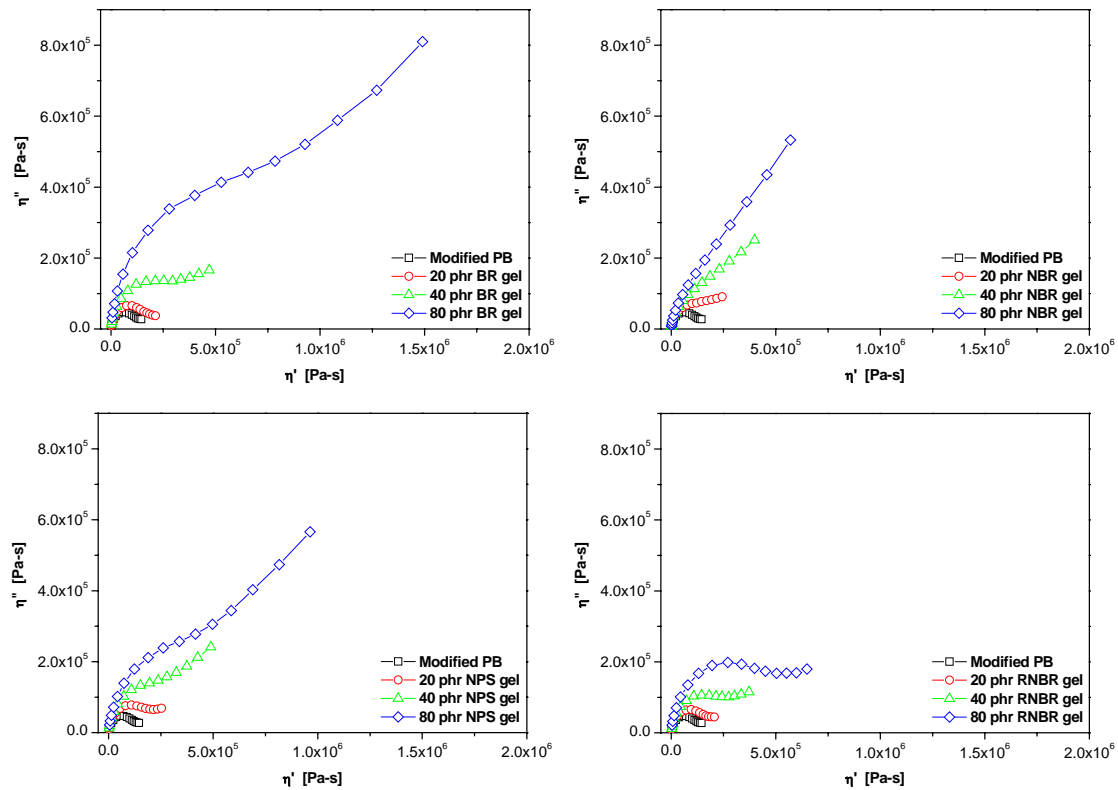


Figure S-16: Cole-Cole plot of η'' against η' . ($T = 50\text{ }^\circ\text{C}$, plotted on same scale)

Different from the analysis of the Cole-Cole plot at high frequency (high frequency \rightarrow high modulus), **Figure S-16** uncovers the nature of the different microgel filled systems at low frequency (low frequency \rightarrow high viscosity). It is worth noting that for NBR microgel filled systems, η'' in the region of long relaxation times (i.e., the low frequency region) dominantly increases as compared with η' , and the form of plot changes from arc to linear faster than for the other microgel filled systems. This phenomenon has been found in other multi-component polymer systems, too, in which there exists a phase separation or the network type structure formed by aggregation of filled particles [37]. Thus, together with the remark made in the crossover point analysis, we can conclude that NBR microgel forms the largest clusters and these clusters further exhibit the most rubber-like properties, and/or

actually they behave like a second elastic component, besides the PB. This change of curve from arc to linear also tells the story of mobility of polymer chains on filler surface. Only taking the BR, NPS and RNBR microgel filled systems into consideration, the plot of NPS filled systems shows faster changes of curve from arc to linear than BR microgel filled systems (except for 80 phr), whereas the plot of RNBR microgel filled systems shows less sensitivity to filler loading. This again strengthens the remark made on microgel rigidity and the amount of interacting interface between microgel and the PB chains. That is, the less sensitive is the plot to filler loading, the more mobile the PB chains are and the more interacting interface exists between microgel and the PB chains. (the amount of interacting surface: NPS > BR > RNBR)

Now, together with all the frequency-dependent observations and remarks, the ways of these microgels affecting the filler-rubber interaction become clear:

A. NBR microgel is rather soft and it is prone to form larger and deformable clusters. It implies that NBR microgel clusters can also be regarded as lightly crosslinked rubber and its shear modulus at rubber plateau is similar to that of the PB matrix. This remark exactly explains the lower plateau modulus (G_N) rather than the higher, “over-sheared” modulus expected from rigid particle filled systems. On the other hand, since the NBR microgel clusters are lightly crosslinked, compared to the other microgels filled systems the “extra-long” relaxation behavior was dominated by these large, high molecular weight NBR clusters (as it is, crossover point will be shifted to lower frequency with increasing molecular weight of a certain polymer without significantly affect the value of G_N). The Cole-Cole plot also implies that the addition of NBR microgel can be regarded as adding another “immiscible” component into the PB matrix. This conclusion is in good agreement with the SEM observation shown in [Figure S-10](#).

B. The cluster size, as well as its rigidity, in our case, dominates the relaxation process and filler-rubber interaction. Special attention should be paid to the relative value of the relaxation time and the plateau modulus. The relaxation time and the plateau modulus of NPS microgel filled blends were always higher than that of BR microgel

ones. However, upon 80 phr loading the later inversely surpassed the former in those properties. One explanation could be that BR microgel was coupled with a few of the PB chains due to the fact that BR as such is more compatible with PB (note that the degree of modification was 2 mol% only, and the unmodified PB unit was still much higher).

C. Due to the complex nature of different microgels, the idea of strengthening filler-rubber interaction via the introduction of hydrogen bonding interaction could not be realized. Only if there is a well-defined system (i.e., filler particle with similar rigidity, particle size, surface porosity and so on) one can find out the real competition mechanism of filler-filler and/or filler-rubber via hydrogen bonding interaction.

S-3-3 Temperature-dependent Properties Analysis (ARES Temperature-sweep)

In addition to the frequency-dependent analysis discussed in Section 2-3-2, the temperature-dependent analysis was also performed with microgel filled systems. The temperature profiles of these systems are shown in [Figure S-17](#). First, same as observed in the frequency analysis, both G' and G'' increase with increasing filler loading. It can be explained by similar reason as discussed herein before. However, the values of $\tan \delta$ in the temperature span between $-60\text{ }^{\circ}\text{C}$ to $20\text{ }^{\circ}\text{C}$ are similar for all the microgel filled systems and at various filler loadings. This could be understood by that the contribution of microgels to the enhancement of G' and G'' are similar, in other words, the introduction of microgels, in spite of their individual properties, into modified PB do not significantly change the hysteresis ($\tan \delta$) of the modified PB in the temperature span.

Second, if one keeps an eye on the variation of $\tan \delta$ at temperatures higher than $40\text{ }^{\circ}\text{C}$, it is obvious that with increasing filler loading its value decreases. This observation can be explained by the same arguments made in Section 2-3-2, due to the retardation of the terminal relaxation from microgels. This tendency toward decreasing the terminal relaxation is usually called “pseudo-solid-like” behavior [15]

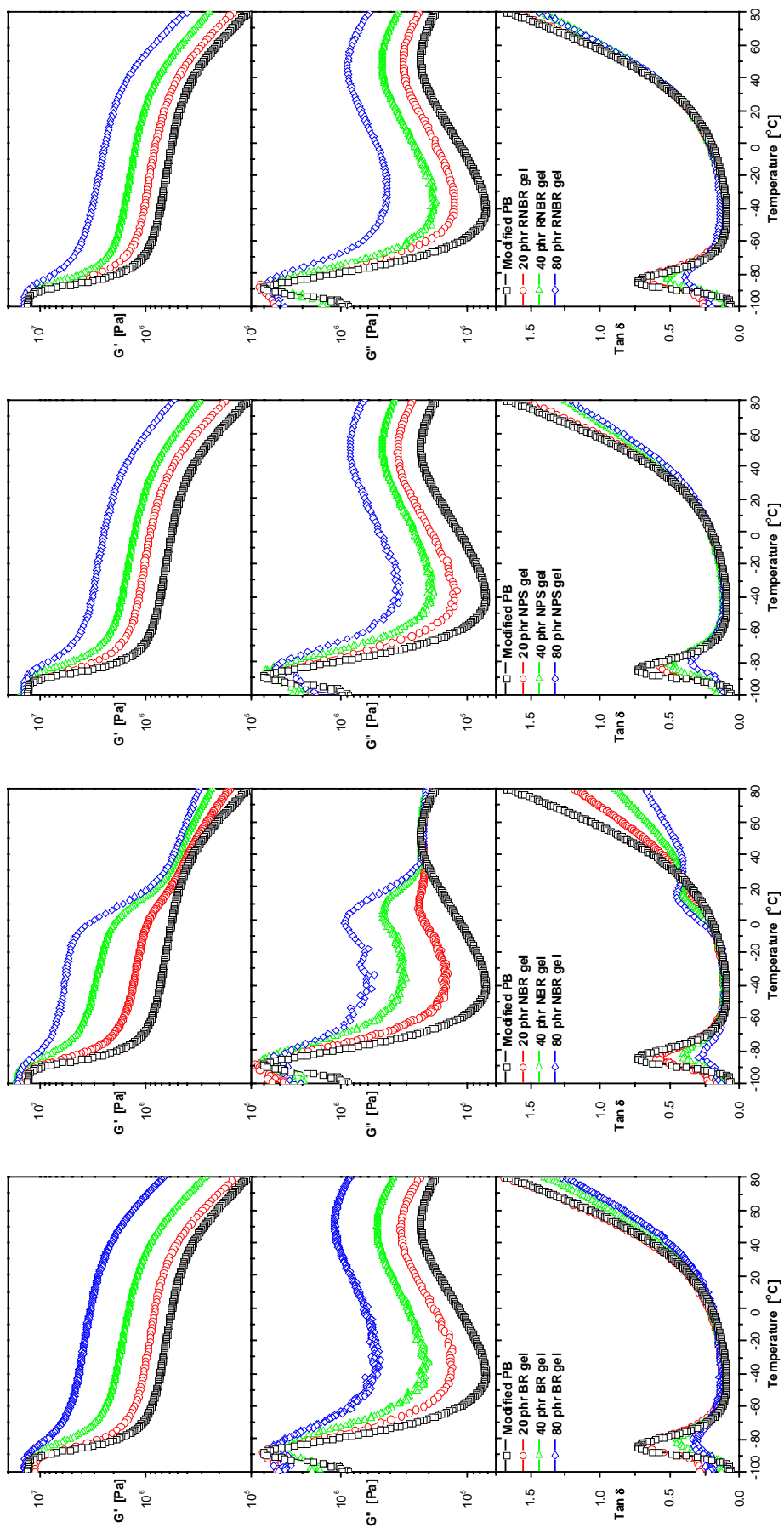


Figure S-17: ARES temperature-sweep analysis of microgels filled systems. (plotted on same scale)

and the ability of the retardation of the terminal relaxation from the microgels is the same as observed in the frequency-dependent analysis (the lower the value of $\tan \delta$, the higher is the ability). The order is: NBR > NPS > BR > RNBR.

Third, in the glassy state the value of G' is similar. This is due to the glassy shear modulus of the modified PB which is similar to that of microgels, in other words, fillers do not contribute to any modulus reinforcement in the glassy state.

Fourth, it is worth noting that for the NBR microgel filled systems, the curves show interesting behavior that is quite different from that of the other microgel filled systems. The curves of modulus against temperature show two drops in G' as well as two local maxima in G'' at two different temperatures. The curves of $\tan \delta$ simultaneously show two local maxima associated with the transition temperatures. Intuitively the curves look like typical polymer blends comprising two micro-phase separated rubbers since the first transition at the lower temperature indicates the glass transition of the PB matrix and the second transition correspond to the NBR glass transition. It has been mentioned in Section 2-3-2 that NBR microgel is rather soft and it is prone to form larger and deformable clusters. Furthermore, from the Cole-Cole plot, it also implies that the addition of NBR microgel can be regarded as adding another “immiscible” component into the PB matrix. Obviously at this point we can conclude that the “true nature” of the NBR microgel is, instead of a microgel at its glassy state (a rigid filler), actually a lightly crosslinked NBR rubber.

Before going into any details, it is also very interesting to mention the influence of the addition of microgel on the glass transition. It is known that the glass transition temperature is the temperature (range) where a polymer goes from the glassy state to the rubbery zone, at which it changes from a frozen state to an entangled state, or, if the chains are short enough, the polymer goes directly from the frozen state to the terminal flow region. Thus, the ability to affect the glass transition is also a criterion to evaluate the filler-rubber interaction. However, it is limited to the molecular motion with a mode length in the order of several nanometers [38]. It is also generally observed that the glass transition zone broadens and the peak height decreases (from the peak span of $\tan \delta$ associated with glass transition over a temperature range) with

increasing filler loadings [39]. The general behavior of the changes on T_g , not surprisingly, is dominated by the nature of the interfacial interaction between filler and rubber. Tsagaropoulos and Eisenberg [40,41] proposed a model drawn from filled rubber morphology, which envisages there are three regions around a filler particle, as shown in Figure S-18. The first region (layer A) nearest to the solid surface is an inner tightly bound layer in which the rubber chain is immobilized and its motion is severely restricted by interaction with the surface. In the middle region, there is an intermediate but more loosely bound layer (layer B), and finally the unrestricted bulk rubber. The thickness of individual layers is controlled by the size [42-44], the rigidity [45] and the surface properties (specific area, pore size, etc.) of the filler, the amount of filler loading [45], the nature of the rubber [46], and even the way of filled sample preparation [47].

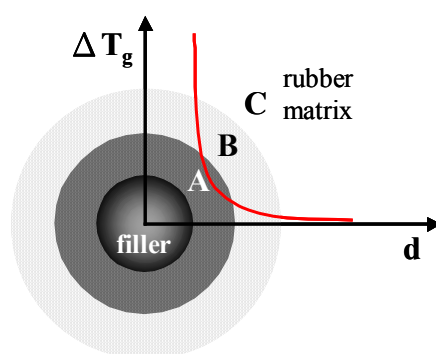


Figure S-18: Schematic representation of the three layers around a filler particle in a filled rubber matrix. (d : distance from the filler center)

Due to the difference in chain mobility, these three layers exhibit different T_g and it also explains the broadening of T_g and its decrease in peak height with increasing filler loading.

Fifth, with the help of the works reported by researchers, we can now examine the influence of these microgels upon T_g . Figure S-19 shows the relations between T_g and the height of $\tan \delta$ maximum. In general, T_g of the filled systems does not change significantly with increasing filler loading. However, the height of $\tan \delta$ maximum decreases with filler loading. Taking the filler-rubber interaction and the molecular mobility into account, the insignificant shift of T_g in all filled systems indicates that

the specific interactions between the two phases are not pronounced, however the introduction of microgels does decrease the rubber chain mobility simply by decreasing the amount of “unbound” rubber [48].

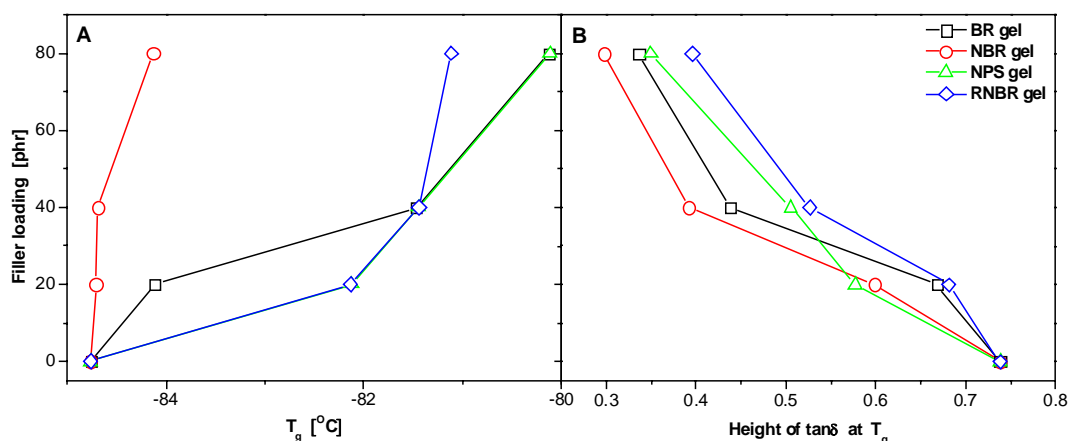


Figure S-19: The dependence of T_g and the height of $\tan \delta$ on filler loading. (A: $\tan \delta$ maximum; B: height of $\tan \delta$)

S-4 Conclusion

In this chapter, polymeric microgels of different surface functionalities and modified PB are applied to the investigation of filler-rubber interaction via non-covalent hydrogen bonding interaction. Dynamic mechanical analysis (RPA and ARES measurements) is used as the main tool to characterize these microgels filled PBs. Due to the poor-defined characteristics of these microgels (distinct rigidity as well as microgel cluster size), instead of the contribution of hydrogen bonding interaction the results show that the Payne effect and the mechanical properties are dominated mainly by microgel rigidity and cluster size. The results also reveal that in order to investigate and realize the concept of reinforcing filled rubber materials further by hydrogen bonding interaction, one needs well-defined fillers with well-defined characteristics, such as rigidity, size of primary particle and specific surface area.

References

- [1] J. C. Brosse et al., *J. Appl. Polym. Sci.*, **78**, 1461 (2000).
- [2] A. F. Halasa et al., “*Science and Technology of Rubber*”, 2nd Ed., Academic Press, 1994.
- [3] D. Derouet, P. Phinyocheep, J. C. Brosse and G. Boccaccio, *Eur. Polym. J.*, **26(12)**, 1301 (1990).
- [4] K. Chino, M. Ashiura, *Macromolecules*, **34**, 9201 (2001).
- [5] F. Ferrero, M. Panetti and G. B. Saracco, *La Chimica e L’Industria*, **66**, 3 (1984).
- [6] P. Dreyfuss, J. P. Kennedy, *Anal. Chem.*, **47**, 771 (1975).
- [7] A. Brydon, Ph.D. thesis, University of Aberdeen, 1972.
- [8] J. M. Stellmann, A. E. Woodward, *J. Polym. Sci.*, **A2**, 52 (1971).
- [9] J. Malhorta et al., *Polymer*, **30**, 467 (1989).
- [10] D. Zuchowska, *Polymer*, **21**, 514 (1980).
- [11] A. Brydon et al., *Makromol. Chem.*, **178**, 1739 (1977).
- [12] J. March, “*Advanced Organic Chemistry*”, 4th Ed., Wiley, 1992.
- [13] R. C. Larock, “*Comprehensive Organic Transformations*”, 2nd Ed., Wiley, 1999.
- [14] BMBF project “*Supramolekular strukturierte Elastomerkomposite mit adaptiver Energiedissipation*”, 2003.
- [15] K. Yurekli et al., *J. Polym. Sci. Part B. Polym. Phys.*, **39**, 256 (2000).
- [16] H. Pawlowski and J. Dick, *Rubber World*, **6**, 35 (1992).
- [17] F. W. Maine, B. E. Riseborough and J. E. Theberge, Polymer structures and properties, *SPE RETEC*, Toronto, 1976.
- [18] B. Freund, W. Niedermeier, *Kautsch. Gummi Kunstst.*, **51**, 444 (1998).
- [19] E. Guth and O. Gold, *Phys. Rev.*, **53**, 322 (1938).
- [20] H. M. Smallwood, *J. Appl. Phys.*, **15**, 758 (1944).
- [21] J. H. Davis, *Plastics and Polymer*, **39**, 137 (1971).
- [22] J. Fröhlich and H. D. Luginsland, *Rubber World*, **4**, 28 (2001).
- [23] J. D. Ferry, “*Viscoelastic Properties of Polymers*”, 3rd ed., Wiley, 1980.
- [24] G. M. Bartenev, “*Structure and Relaxation Properties of Elastomers*”, Khimiya, Moscow, 1979.
- [25] G. M. Bartenev, *Doklady Akad. Nauk USSR*, **300**, 1154 (1988).
- [26] G. M. Bartenev, *Vysokomol. Soed.*, **A25**, 1191 (1983).
- [27] D. F. Twiss, *J. Chem. Soc.*, **44**, 1067 (1925).
- [28] B. Meissner, *Rubber Chem. Technol.*, **68**, 297 (1995).
- [29] C. C. McCabe and N. Müller, *Trans. Soc. Rheol.*, **5**, 329 (1961).
- [30] J. L. White and J. W. Crowder, *J. Appl. Polym. Sci.*, **18**, 1013 (1974).
- [31] S. N. Maiti and P. K. Mahapatro, *Polym. Compos.*, **9**, 291 (1988).
- [32] G. I. Taylor, *Proc. Rheo. Soc. London Ser. A*, **146**, 501 (1934).
- [33] N. Mills, *J. Appl. Polym. Sci.*, **15**, 2791 (1975).
- [34] F. A. Morrison, “*Understanding Rheology*”, Oxford University Press, 2001.
- [35] Q. Zheng et al., *J. Appl. Polym. Sci.*, **86**, 3166 (2002).
- [36] D. Miao et al., *Nihon Reoroji Gakkaishi*, **31(5)**, 305 (2003).
- [37] Q. Zheng et al., *Polymer*, **42**, 5743 (2001).
- [38] S. Vieweg et al., *J. Appl. Polym. Sci.*, **73**, 495 (1999).
- [39] V. Arrighi, I. J. McEwen, H. Qian and M. B. S. Prieto, *Polymer*, **44**, 6259

(2003).

- [40] G. Tsagaropoulos and A. Eisenberg, *Macromolecules*, **28**, 396 (1995).
- [41] G. Tsagaropoulos and A. Eisenberg, *Macromolecules*, **28**, 6067 (1995).
- [42] S. Yano, T. Furukawa, M. Kodomari and K. Kurita, *Kobunshi Rondunshu*, **53**, 218 (1996).
- [43] Y. I. Tien and K. H. Wei, *J. Appl. Polym. Sci.*, **86**, 1741 (2002).
- [44] Z. S. Petrovic and W. Zhang, *Mater. Sci. Forum*, **352**, 171 (2000).
- [45] N. D. Alberola and P. Mele, *Polymer Composites*, **17**, 751 (1996).
- [46] A. Yim, R. S. Chahal and L. E. St. Pierre, *J. Colloid. Interface Sci.*, **43**, 583 (1973).
- [47] C. J. T. Landry, B. K. Coltrain, M. R. Landry, J. J. Fitzgerald and V. K. Long, *Macromolecules*, **26**, 3702 (1993).
- [48] M. Takayanagi, S. Uemura and S. Minami, *J. Polym. Sci.*, **C5**, 113 (1968).

Summary

This work mainly focuses on the synthesis and characterization of new elastomer nanocomposites by hydrogen bonding interaction between reinforcing agents and the rubber matrix. On one hand it was expected that the filler agglomeration is reduced, and on the other hand this specific interaction further enhances the mechanical properties of these nanocomposites. In order to attach hydrogen bonding interacting moieties, the rubbers used in this study were chemically modified via several pathways. Instead of carbon black and conventional silica particles, the reinforcing agents used here were polymeric fillers and silica nanoparticles whose effectiveness in reducing the Payne effect were also examined

In Chapter 2 a commercial polybutadiene rubber, CB 10, was quantitatively modified from 1 to 20 mol% by a three-step polymer analogous reaction. The resulting PBs are capable of forming supramolecular hydrogen bonding networks. The reactions were monitored using $^1\text{H-NMR}$ and the formation of hydrogen bonding complexes was verified by FTIR analysis. DSC analysis showed that crystallinity of the investigated PB was suppressed with a degree of modification > 2 mol% and the glass transition was shifted from -103 °C to -4.1 °C upon a sample with 20 mol% modification. Dynamic mechanical analysis showed that upon a 5 mol% modification, the crystallization was totally restrained and with higher degree of modification the glass transition was further elevated to higher temperatures. These observations indicate that the introduction of this type of hydrogen bonding complexes lead to the formation of effective supramolecular networks. The proposed modification pathway is a simple, economical and highly effective route for rubber and tire industries to design products of new generation.

In Chapter 3 silica nanoparticles were synthesized without surfactants via two different methods: the modified Stöber method and the original Stöber method. The former method unfortunately gave silica particle with unsatisfactory particle size and size distribution, which did not meet our requirement since it brought about unnecessary parameters in investigating filler-rubber interaction. On the contrary, the latter method gave monodisperse, surface unmodified silica particles of a size of 100

nm. Besides, the modification of such silica particles also gave monodisperse particles with less surface polarity. As well as the specific surface area, the resulting particles had similar size and size distribution, which ameliorated the defects of the polymeric microgels studied in Supplement. We also employed the *in-situ* DLS technique to monitor the growth of silica particles. The results show that this technique holds good for certain reaction conditions. *In-situ* DLS is simple, straightforward and economic in terms of time, and this method offers a template for size control in silica nanoparticle synthesis as well.

In Chapter 4 a kind of “smart” silica nanocomposites is presented containing surface unmodified and modified silica nanoparticles from Stöber synthesis, and a thermoreversible crosslinking rubber. Both the influence of hydrogen bonding interaction between silica and rubber on the Payne effect, and the temperature dependent dynamic mechanical properties were systematically investigated. The dynamic mechanical analysis showed that the competition and symbiosis between the filler-filler, filler-rubber and rubber-rubber HB interaction are controllable simply by changing the silica surface functionality, the silica loading, the degree of rubber modification and the temperature. TEM micrographs show that both the modifications of silica nanoparticles and rubber promote better silica dispersion in the rubber matrix. By this strategy it was shown that the Payne effect is reduced and it is possible to modify the mechanical properties of such silica filled composites in order to meet the requirements for different applications.

In Supplement, polymeric microgels of different surface functionalities and modified PB were synthesized to investigate the filler-rubber interaction via non-covalent hydrogen bonding. Dynamic mechanical analysis (both RPA and ARES measurements) was used as the main tool to characterize these microgels filled PBs. Due to the poor-defined characteristics of the microgels (distinct rigidity and cluster size), instead of the contribution of hydrogen bonding interaction the results showed that the Payne effect and the mechanical properties were dominated mainly by microgel rigidity and cluster size. The results also revealed that in order to realize the concept of reinforcing filled rubber materials further by hydrogen bonding interaction, one needs well-defined fillers with similar rigidity, size of primary particle and specific surface area, for instance.

Zusammenfassung

Die vorliegende Arbeit befasst sich hauptsächlich mit der Synthese und Charakterisierung von neuen Elastomer-Nanoverbundwerkstoffen. Diese neuen Nanokomposite besitzen Wasserstoffbrücken, die zwischen dem Füllstoff und der Matrix wirken können. Es wurde erwartet, dass durch diese spezifischen Wechselwirkungen die Agglomeration des Füllstoffes unterdrückt werden kann, wodurch die mechanischen Eigenschaften deutlich verbessert werden können. Zur Einführung der Wasserstoffbrückenbindungseinheiten an dem Matrixpolymer wurden verschiedene Wege mittels polymeranaloger Reaktionen gewählt. Im Gegensatz zur üblichen Verwendung von Ruß- oder konventionellen Silicapartikel kamen hier zur Verstärkung der Matrix polymere Füllstoffe und Silicananopartikel zum Einsatz. Von diesen wurde eine Verringerung des Payne-Effektes erwartet, was ebenfalls untersucht wurde.

In Kapitel 2 wurde ein kommerzielles Polybutadien, CB10, in einer einfachen dreistufigen polymeranalogen Reaktion in Ausmaßen von 1 – 20 mol% mit Wasserstoffbrückenbildnern modifiziert. Die resultierenden PB-Polymere besaßen die Fähigkeit zur Ausbildung supramolekularer Netzwerke über Wasserstoffbrückenbindungen. Die Reaktionen wurden mit $^1\text{H-NMR}$ verfolgt und die Ausbildung der Wasserstoffbrücken wurde durch FT-IR verifiziert. DMA und DSC Untersuchungen zeigten schließlich, dass die Kristallisation der untersuchten PB-Polymere ab einem Modifizierungsgrad größer 2% unterdrückt wurde und die Glasübergangstemperatur von -103°C bis auf -4.1°C (20% Modifizierung) anstieg. Diese Beobachtungen zeigen die erfolgreiche Ausbildung supramolekularer Netzwerke durch Einführung der Wasserstoffbrücken-bindungseinheiten. Der vorgeschlagene Modifizierungsweg könnte eine einfache, ökonomisch sinnvolle und hocheffektive Route für die Gummi- und Reifenindustrie darstellen, um neue Produkte zu entwickeln.

Kapitel 3 beschreibt die tensidfreie Synthese von Silicananopartikeln über zwei verschiedene Methoden: die modifizierte Stöbermethode und die ursprüngliche Stöbermethode. Die erste Methode ergab unglücklicherweise nur Silicapartikel mit

unzufriedenstellender Partikelgröße und Größenverteilung. Diese Partikel genügten somit nicht den hier gestellten Ansprüchen des Einsatzes wohldefinierter Partikel um die Füllstoff-Matrix Wechselwirkungen effektiv zu untersuchen. Mit dem zweiten Syntheseweg konnten dagegen monodisperse und oberflächen-unfunktionalisierte Partikel dargestellt werden. Die Modifizierung dieser Partikel ergab schließlich ebenfalls monodisperse Teilchen mit niedriger Oberflächenpolarität. Auf Grund der geeigneten spezifischen Oberfläche und der wohldefinierten Größe und Größenverteilung eigneten sich diese Partikel wesentlich besser als Füllstoffe, als die in Supplement vorgestellten Mikrogele. Es war ebenfalls möglich das Wachstum der Partikel mit in-situ DLS zu untersuchen. Diese Methode ist sehr einfach und zeitsparend und ermöglichte zudem eine Größenkontrolle und Größeneinstellung der Silicapartikel während der Synthese.

In Kapitel 4 wird eine Art „intelligenter“ Nanoverbundwerkstoff präsentiert. Dieser wurde unter Verwendung der modifizierten und unmodifizierten Nanopartikel der Stöbersynthese (Kapitel 3) und dem thermisch-reversibel vernetzten Polybutadien (Kapitel 2) hergestellt. Sowohl der Einfluss der Wasserstoffbrückenbindungen zwischen Silica and Polymer auf den Payne-Effekt, als auch die Veränderung der mechanischen Eigenschaften mit der Temperatur wurden systematisch untersucht. Die dynamisch-mechanischen Analysen zeigten, dass die Konkurrenz und die Symbiose der supramolekularen Wechselwirkungen zwischen Füllstoff-Füllstoff, Füllstoff-Polymer und Polymer-Polymer durch Variation der Oberflächenfunktionalisierung der Silicapartikel, des Füllstoffgehaltes, des Modifizierungsgrades des PB und der Temperatur einfach kontrollierbar sind. TEM Aufnahmen zeigten eine bessere Dispergierung der Nanopartikel, wenn sowohl die Partikel selbst, als auch das Polymer modifiziert waren. Mit dieser Strategie konnte der Payne-Effekt effektiv reduziert werden und es ist möglich die mechanischen Eigenschaften von solchen mit Silica verstärkten Verbundwerkstoffen zu variieren, um beispielsweise die Anforderungen der Reifenindustrie zu erfüllen.

Supplement beschreibt die Synthese von polymeren Mikrogele verschiedener Oberflächenfunktionalitäten, sowie die Modifizierung von Polybutadien selbst. Im Anschluss an die Einführung von Wasserstoffbrückenbindungseinheiten wurden die Veränderungen der dynamisch-mechanischen Eigenschaften (RPA & ARES) der

Mischungen untersucht. Es zeigte sich, dass auf Grund der schlecht definierten Eigenschaften der Mikrogele, (ausgeprägte Steifigkeit und Clustergröße) der Payne-Effekt und die mechanischen Eigenschaften hauptsächlich durch die Mikrogeleigenschaften selbst und nicht durch Wasserstoffbrücken bedingt sind. Die Ergebnisse verdeutlichen die Notwendigkeit des Einsatzes wohldefinierter Partikel (z.B. mit kontrollierter spez. Oberfläche) mit vergleichbarer Härte um zu einer Verstärkung von Nanoverbundwerkstoffen durch Wasserstoffbrückenbindungen zu gelangen.

Acknowledgement

Over a span of more than three years in Germany, I have realized that study abroad is not that easy, especially for a non-European student who took along the baggage and started the research life in a country far away from his own. Instead of feeling along during the stay in Bayreuth, I did receive a lot of kind help from people both in scientific work and in daily life. Were there no helps from the people around, no successful work would have been done.

In the first place I would like to thank Prof. Dr. Volker Abetz for offering me a position as a PhD student in Bayreuth, as well as a very interesting and practical research topic. I greatly appreciate his patient supervision, steady instruction and fruitful discussion.

Special thank goes to Prof. Dr. Axel H. E. Müller. I am grateful for his generous support of a fully “equipped” experimental environment during my PhD study in the University of Bayreuth. Besides I also benefited a lot from his adequate and instructive suggestions on my work.

For the suggestions on chemical modification of rubber and all the related chemistry, I would like to thank Prof. Dr. Karlheinz Seifert. His help is impressive and unforgettable since I always received very useful and wonderful suggestions from him in organic synthesis.

I thank Dr. Jonas Ziegler and Prof. Robert Schuster (DIK, Hannover) for the collaborative work and the possibility to use their Rubber Process Analyzer. They are so knowledgeable about everything in rubber composites that they always inspired me during each discussion.

Kerstin Matussek I thank for the detailed introduction to the ARES instrument, so that I became able to work on dynamic mechanical properties on my own. I thank Dr. Mabel Graf for the synthesis of some polybutadiene, and our invincible TEM team, Dr. Markus Drechsler and Astrid Göpfert, for their kind and patient helps with TEM micrographs. For the *in-situ* DLS experiments, I thank Dr. Dimitry Pergushov (Dept.

of Polymer Science, Moscow State University), Yu Mei (Physikalische Chemie I) and Markus Burkhardt for the fruitful discussion and suggestions. Markus Burkhardt also helped me a lot with the tedious experimental trials. Annette Krökel, the angel and the spirit of the laboratory, is deeply acknowledged for her patient and complete helps with everything I needed during the chemical experiment. Dr. Olivier Colombani and Dr. Alexander Terrenoir are also gratefully appreciated for their kind suggestions on chemical synthesis and physical measurements. I also thank Katrin Sattler (Anorganische Chemie I) for her help with BET measurements.

I appreciate the great help from Gaby Oliver. She explained all the German documentation that I did not understand and facilitated almost all the bureaucratic contacts with officials. Without her helps, lots of blocks would have handicapped my study in MCII. Also I would like to express my heartily gratefulness to all the colleagues in the group of Makromolekulare Chemie II for all their helps. Nemesio Martinez-Castro, Xavier Andre, Adriana Boschetti, Evis Penott, Gabi Cantea, Felix Plamper, Harald Becker, Youyong Xu, Jiayin Yuan, Manuela Fink, Sabine Wunder and Cornelia Lauble are always willing to give me supports at any time I need help. Special thanks goes to Andreas Walter for his great help with the wonderful translation of the summary of this thesis and for his on-and-go tutorial on interesting and popular German slang among young generation.

Without money, no work could be carried on. I thank Bundesministerium für Bildung und Forschung (BMBF) for the financial support during the first period of my PhD time.

I personally feel gratitude to my Chinese neighbors in Bürgerspital Studentenwohnheim. They have brought me a joyful non-scientific life and have tided me over whenever I felt frustrated and depressed.

I owe a great deal to my family. Their strong and continual spiritual supports encouraged my study in Germany. I also offer my heartfelt thank to my wife, Yanfei Liu, both for her useful scientific suggestions and the meticulous daily care during her postdoctoral stay in Bayreuth. Her every single support and love will be forever imprinted in my mind.

Erklärung

Die vorliegende Arbeit wurde von mir selbständig verfasst und ich habe dabei keine anderen als die angegebenen Hilfsmittel und Quellen benutzt.

Kapitel 2: Die Synthese von PB durch anionische Polymerisation wurde von Dr. Mabel Graf durchgeführt. Die Synthese und die Modifizierung von Mikrogelen wurden von Dr. Jonas Ziegler (DIK, Hannover) durchgeführt.

Kapitel 4 und Kapitel 5: Dr. Markus Drechsler und Astrid Göpfert machten die TEM-Aufnahmen. Die BET Messungen wurden von Frau Katrin Sattler durchgeführt.

Ferner habe ich nicht versucht, anderweitig mit oder ohne Erfolg eine Dissertation einzureichen oder mich der Doktorprüfung zu unterziehen.

Bayreuth, den 24.03.2006

Chih-Cheng Peng

Appendix

The Rubber Process Analyzer

A-1 Introduction

In the study described in this thesis dynamic mechanical measurements using the Rubber Process Analyzer (RPA) 2000 proved to be a valuable approach to understanding the reinforcement of filler by analysis of the strain dependency of modulus and loss factor. The RPA is a vulcameter that is able to measure the modulus of rubber compounds under shear deformation, with an advanced temperature control and fully automated operation modes, which allow a very reliable and detailed investigation of the dynamic mechanical behavior in a much easier and faster way than the common dynamic analysis, especially for vulcanites. The RPA is controlled through an external computer, which provides an easy way to handle and has numerous testing capabilities in terms of frequency, strain and temperature sweeps in wide ranges of strain amplitude and temperature. Compounds can be studied in the uncured (green compound), as well as in the cured state. Vulcanization can be performed with the same sample used for the green compound analysis, and therefore a good insight into several characteristics of the rubber compound can be obtained. Furthermore, it is also possible to measure samples repeatedly in a row to determine the stress softening and relaxation process.

A-2 Technical Information

Essentially the RPA consists of two main parts: the testing instrument itself and an outside computer for test monitoring, data recording and treatment. The testing part consists of a biconical sample chamber with grooved dies to avoid slippage, a problem often encountered with rubber testing. The advantage of this test geometry is that the strain rate is constant in the gap. The cavity is closed through the action of a ram operated with a pressure of 4 MPa and a slight excess of sample material is needed for reliable torque reading to be made. Two hard fluoroelastomer seals provide

the peripheral closure of the cavity. The excess material flows in a circular saw channel and further contributes to the sealing of the cavity. Tests are thus made under pressurized conditions, and therefore porosity does not develop in the sample when the instrument is operated as a curemeter. The lower die can be oscillated at controlled strain and frequency. The torque measuring system is attached to the upper die and calibrated with a torsion spring mounted between the two dies. The heart of the instrument is a special direct drive motor, which can move the lower die sinusoidally over a wide range of strains and frequencies. A harmonic torsion strain is exerted on the sample by the lower (oscillating) die and the transmitted torque is measured on the upper (fixed) wall. The sample periphery is neither free, nor spherical and its shape is imposed by the design of the seals.

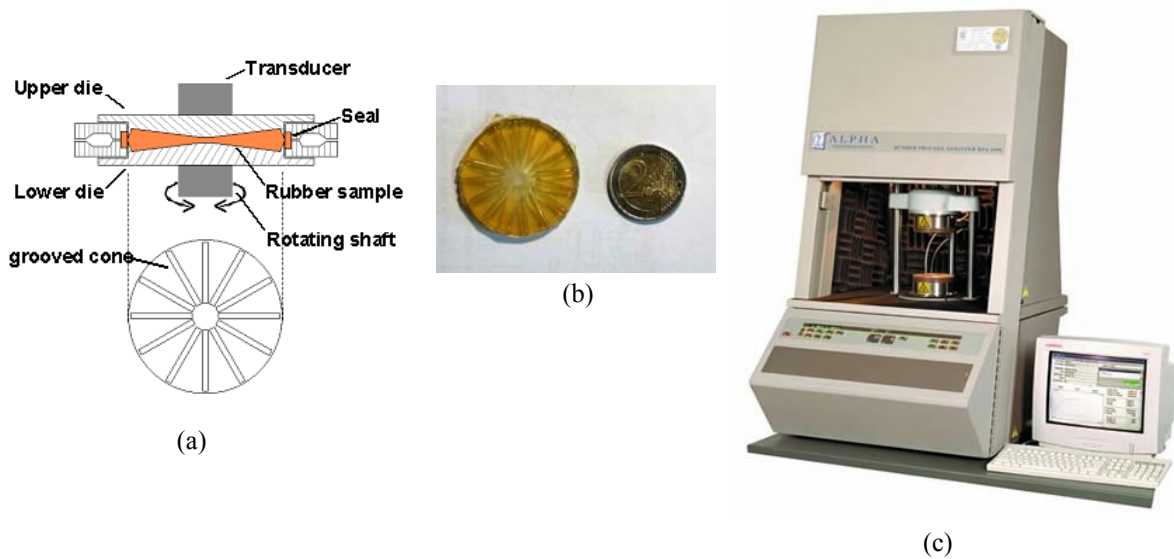


Figure A-1: A Set of Rubber Process Analyser 2000. (a) measuring principle (b) a rubber sample (c) instrument overview

The temperature control system of the RPA has a resolution of 0.1 °C, which, combining the thinness of the sample, allows isothermal tests to be performed in a temperature range of 50-200 °C. The desired temperature can be reached immediately and monitored by the controlling computer.

Once the sample is loaded and the chamber is closed, the lower die is oscillated at controlled frequency and strain. In dynamic testing, a sinusoidal strain is applied and, providing the tested viscoelastic material responds in a linear manner, the recorded

torque is also sinusoidal but out-of-phase by an angle δ , depending on the visco-elastic character of the tested material. In the RPA, the phase angle is actually not measured but the assumption is made that the sinusoidal strain produces a sinusoidal torque response. The complex torque signal S^* is first treated in such a manner that during one cycle several discrete values are read with respect to equal periods on the time scale. By applying a Fourier transform to the S^* signal, this is divided into an elastic component S' (in phase with the strain) and a viscous component S'' (90° out of phase with the strain). The phase angle δ can then be calculated. Using a shape factor for the considered test gap, the dynamic shear moduli can be obtained. Test data are automatically recorded and stored in the computer memory.

Whilst not all combinations are possible, the testing capabilities of the RPA are very broad:

- frequency range: 0.05 to 209.44 rad/s
- strain angle range: 0.01° to 90° (0.145 to 1256% strain)
- temperature range: 40 to 200 $^\circ\text{C}$

Owing to technical limitations of the strain gauge and the other transducers, the lower the frequency or the strain, the larger the experimental errors. The maximum strain is limited by the applied frequency, from 7% strain at $\omega = 200$ rad/s up to 1256% strain at 0.1 rad/s, for example.

There are several built-in testing modes, for instance: frequency and temperature sweeps, curing test, stress relaxation and dwell time that can be combined by the operator in various manners. For instance, one of the built-in tests can be easily repeated at different temperature by taking advantage of the RPA capability of fast temperature change within the die. Frequency sweep tests repeated at various higher temperatures provide all the data necessary to build master curves by applying the time-temperature superposition principle.

A-3 Test Programs

For illustrating the abilities of the RPA, the following examples elucidate how it is

possible to run experiments with the RPA in order to investigate filler-filler, filler-polymer interaction and the rolling resistance of a tire tread compound.

A-3-1 Strain Sweep

The difference in G' at low and intermediate strains, the so-called Payne effect is often used as a measure for the filler dispersion. To study the filler-filler interactions of the uncured compounds, the storage modulus G' was measured as a function of strain. During the strain sweep the temperature and frequency were kept constant at 100 °C and 0.500 Hz, respectively. G' was measured in a strain range of 0.56 – 100.04 % as well as a range of 0.56 – 900.05 %. The results of the latter strain range did not show additional information concerning filler dispersion and/or filler-filler interactions. Therefore most of the strain sweeps were restricted to the range of 0.56 – 100.04 %.

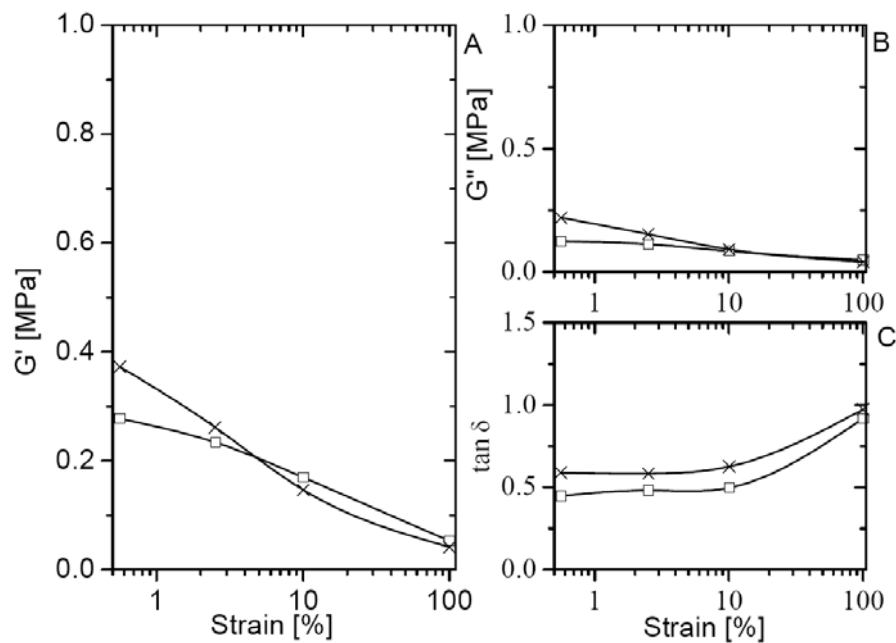


Figure A-2: G' as a function of strain for a rubber compound with different silica coupling agent. (\square) sulfur containing and (\times) sulfur free coupling agent (courtesy of DIK)

The compounds in **Figure A-2** show a different Payne effect. The sulfur containing compound has a marked lower G' -modulus at low strain. This lower G' -modulus at low strain is an indication of less filler-filler interactions, and consequently a better dispersion of the silica filler in the rubber matrix. The decrease in the G' -modulus at

higher strain levels is the result of break down of the filler network at higher strain.

A-3-2 Temperature Sweep

The effect of increasing temperature on the G' -modulus of the uncured compounds was used as an indication of scorch. Several sulfur containing coupling agents are known as scorch sensitive. During mixing, especially at high temperatures, the G' -modulus of the compound increases strongly for those with coupling agents. Therefore temperature sweep measurements were performed at 49.94 % strain and a frequency of 0.500 Hz in a temperature range 110 – 200 °C.

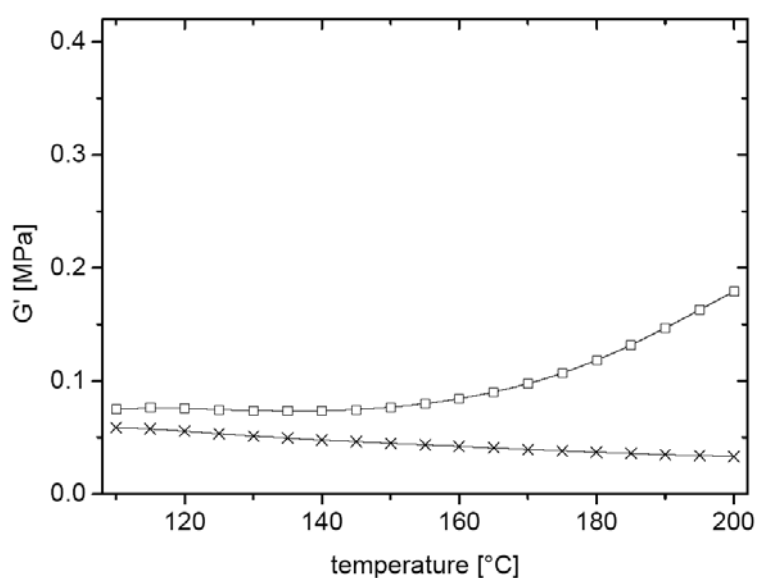


Figure A-3: G' as a function of temperature for a rubber compound with different silica coupling agent. (□) sulfur-containing and (×) sulfur-free coupling agent (courtesy of DIK)

As shown in [Figure A-3](#), the compound with the sulfur-containing coupling agent shows a strong increase in G' at 160 °C. This increase in G' is attributed to a reaction of the coupling agent with the rubber matrix, that is, a cross-linking reaction arises in heating. On the contrary, the compound with the sulfur-free coupling agent shows a typical temperature dependence of G' for a reinforced compound, since this coupling agent is not able to react with the rubber matrix. Therefore a temperature sweep is necessary if there would be unexpected side reactions would occur in the practical application, which enable the quality control for rubber industry.

A-3-3 Vulcanization Rheogram

Rheograms are typically made to study the vulcanization behavior of a compound after the addition of vulcanizing agents. By monitoring the change of shear torque during the vulcanization process, the degree of vulcanization increases with increasing time. As shown in **Figure A-4**, the soar in torque at 160 °C, 0.833 Hz and strain of 2.79 % was measured over a time period of 30 minutes. The optimal vulcanization time and scorch time of the compounds can be obtained from the rheogram, which is useful for rubber processing and manufacturing.

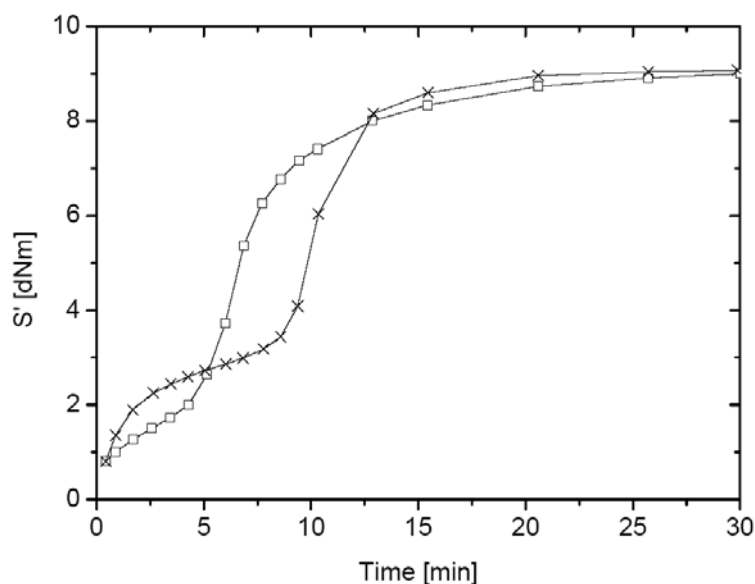


Figure A-4: Vulcanization behaviour of a rubber compound with different silica coupling agent. (□) sulfur containing and (×) sulfur free coupling agent (courtesy of DIK)

A-3-4 Frequency Sweep

Frequency sweeps are practically performed to measure $\tan \delta$ at 60 °C as an estimation of rolling resistance. For this measurement a freshly prepared, uncured sample is necessary in order to obtain a vulcanized sample corresponding to the optimal vulcanization time. After vulcanization the sample is cooled down to 60 °C and $\tan \delta$ is recorded at different frequency. The $\tan \delta$ at certain frequency is taken as a measure for the rolling resistance for different application.

Figure Index

Figure 1-1	General mechanism of ene reaction	3
Figure 1-2	Synthesis of addition of ATA to maleic polyisoprene	5
Figure 1-3	Speculated model of thermoreversible crosslinking structure. (six-point hydrogen bonding)	5
Figure 1-4	Addition of nitrosoarene to natural rubber by ene reaction	6
Figure 1-5	In-situ epoxidation reaction	9
Figure 1-6	Thiol addition at the double bonds of natural rubber	10
Figure 1-7	Sol-gel process in general	14
Figure 1-8	Reaction scheme of sol-gel process	15
Figure 1-9	Acid-catalyzed hydrolysis	17
Figure 1-10	Base-catalyzed hydrolysis	18
Figure 1-11	Nucleophilic attack to form siloxane bond	20
Figure 1-12	Different of sol-gel conditions: (a) acid catalyzed, and (b) base-catalyzed sol-gel polymer	21
Figure 1-13	Tire performance	23
Figure 1-14	Mechanism of rolling resistance	24
Figure 1-15	Vector illustration of an oscillating stress leading a strain by a phase angle δ	26
Figure 1-16	Tread rubber evaluation, $\tan \delta$ as a function of temperature	28
Figure 1-17	Filler and filler network classification: (a) primary particles (10-100 nm), (b) aggregates (30-300 nm) and (c) agglomerates ($\sim \mu\text{m}$)	30
Figure 1-18	The G^* modulus as a function of strain for a reinforced rubber. (solid line for vulcanizates and dash line for uncrosslinked rubbers)	31
Figure 1-19	Various groups on (a) carbon black and (b) silica surface	38
Figure 1-20	Interaction (a) between carbon black and carboxylated nitrile rubber (b) between silica and epoxidized rubber	38
Figure 1-21	1-21: Different reinforcing behavior of fillers. (σ : stress, ϵ : strain, Φ : filler volume fraction)	39
Figure 1-22	Comparison of filler activity	39
Figure 1-23	Schematic model of morphological transformations in filled polymers: (a) silica content less than 10 wt%, (b) silica content ~ 10 wt%, (c) silica content ~ 20 wt%, (d) silica content over 50 wt%	41
Figure 1-24	The concept of segmental interaction with a carbon black surface	42
Figure 1-25	Schematic diagram showing the contact angle when a liquid drop has contact with a flat solid surface	43
Figure 1-26	Comparison of $\tan \delta$, hysteresis property and rolling resistance between a carbon black and a silica filled rubber for tire application. (A: temperature dependence of $\tan \delta$, B: strain dependence of G'' , the Payne effect)	49
Figure 1-27	Schematic illustration of the agglomeration - deagglomeration mechanism between silica particles and carbon black particles. (the length of the arrow denotes the tendency thereto)	51
Figure 2-1	Three-step pathway toward quantitative modification of polybutadiene	64
Figure 2-2	$^1\text{H-NMR}$ spectra of PB with various mole degrees of modification	68
Figure 2-3	$^1\text{H-NMR}$ spectra of different degree of modification. (the degree is indicated as number)	69
Figure 2-4	FTIR spectra of PBs with various degrees of modification	70
Figure 2-5	Schematic representation of three possible hydrogen bonding complexes between two sulfonyl urethane groups	70
Figure 2-6	DSC traces of PBs with various degrees of modification. (second heating; heating rate $40\text{ }^\circ\text{C}/\text{min}$; normalized data)	71
Figure 2-7	Dynamic mechanical spectra of modified PBs. (data obtained at $f = 1\text{ Hz}$)	73
Figure 2-8	Master curve of unmodified CB 10	74
Figure 3-1	TEM micrographs of silica particles synthesized via the modified Stöber method	89
Figure 3-2	FTIR spectrum of silica particles synthesized via the modified Stöber method	90
Figure 3-3	TEM micrographs of surface unmodified silica particles synthesized via the Stöber method	91

Figure 3-4	TEM micrographs of surface unmodified silica particles synthesized via the Stöber method	91
Figure 3-5	FTIR spectra of silica particles synthesized via the Stöber method. (A: Si-OH , B: Si-Ph)	92
Figure 3-6	TEM micrographs of silica particles synthesized via the Stöber method with different reaction parameters. (A: replacing EtOH by MeOH, B: reducing reaction time from 24 hours to 2 hours)	93
Figure 3-7	Coarsened structure that results from aging a network of particles under conditions in which there is partial solubility of the condensed phase	94
Figure 3-8	Time-resolved silica particle growth via <i>in-situ</i> DLS measurement. (solid lines were drawn using an exponential fitting)	95
Figure 3-9	TEM micrographs of silica particles from ID SP-2	96
Figure 3-10	TEM micrographs of silica particles from ID SP-6	96
Figure 3-11	Radius distribution plots of in-situ DLS measurements	97
Figure 4-1	Modulus contributions in filled rubber materials. (solid line for vulcanites and dashed line for non-vulcanites)	103
Figure 4-2	Components for the silica-rubber nanocomposites. A: surface unmodified silica; B:surface modified silica; C: thermoreversible crosslinking rubber	105
Figure 4-3	TEM micrographs of silica particles synthesized via the Stöber method. (A: Si-OH , B: Si-Ph)	109
Figure 4-4	FTIR spectra of silica particles synthesized via the Stöber method	110
Figure 4-5	Dynamic strain sweep plots for PB-0 nanocomposites	111
Figure 4-6	Curves overlapping mechanism for uncrosslinked PB filled with silica	112
Figure 4-7	Dynamic strain sweep plots for PB-2 nanocomposites	113
Figure 4-8	Dynamic strain sweep plots for PB-5 nanocomposites	114
Figure 4-9	Relative hydrogen bonding strength between rubber-rubber (A), filler-rubber (B) and filler-filler (C)	115
Figure 4-10	Qualitative representation of the amount hydrogen bonding complexes as a function of filler loading and degree of PB modification	116
Figure 4-11	Dynamic strain sweep plots for PB-10 nanocomposites	116
Figure 4-12	Qualitative illustration of how silica surface polarity and the silica loading impact the HB interactions and the other composites' properties. (solid line: Si-OH ; short dash line: Si-Ph ; long dash line: degree of PB modification)	117
Figure 4-13	Dynamic temperature sweeps for PB-X nanocomposites	119
Figure 4-14	Qualitative illustration of the temperature-dependent equilibrium constants and stability of the HB complexes	121
Figure 4-15	The resulting master curves for PB-0/Si-OH-10 and PB-0/Si-Ph-10 nanocomposites. (frequency sweeps at 0, 50 and 80 °C, $T_{ref} = 50$ °C)	123
Figure 4-16	TEM micrographs for silica-rubber nanocomposites at 80 phr silica loadings	124
Figure S-1	Rubber-filler interaction through hydrogen bonds	130
Figure S-2	Primary polymer analogous reaction for polybutadiene	131
Figure S-3	Secondary modification of epoxidized polybutadiene	132
Figure S-4	Proposed modification route for PB. (based on epoxidation reaction)	133
Figure S-5	Proposed modification route for PB. (addition of sulfeyl chloride)	133
Figure S-6	¹ H-NMR spectra of 1 and 2 mol% modified PBs	135
Figure S-7	¹ H-NMR spectra of 2 mol% PBNSC modified PBs	137
Figure S-8	Reduction of NBR gel to RNBR gel	139
Figure S-9	SEM images of BR, NBR, NPS and RNBR microgels. (names are as given in the images)	140
Figure S-10	FTIR spectra of PS, NPS, NBR and RNBR gel	140
Figure S-11	RPA strain-sweep analysis of microgels filled systems. (plotted on same scale)	143
Figure S-12	Master curves of different microgels filled blends. (plotted on same scale)	146
Figure S-13	The effect of filler loading on the PB relaxation time	148
Figure S-14	Plot of complex viscosity against relative plateau modulus of filled and non-filled blends	150
Figure S-15	Cole-Cole plot of G'' against G'. (T = 50 °C, plotted on same scale)	152
Figure S-16	Cole-Cole plot of η'' against η'. (T = 50 °C, plotted on same scale)	153
Figure S-17	ARES temperature-sweep analysis of microgels filled systems. (plotted on same scale)	156
Figure S-18	Schematic representation of the three layers around a filler particle in a filled	158

rubber matrix. (d: distance from the filler center)
Figure S-19 The dependence of T_g and the height of $\tan \delta$ on filler loading. (A: $\tan \delta$ maximum; B: height of $\tan \delta$) 159

Table Index

Table 1-1	Some typical examples of filled polymer systems	34
Table 1-2	Reasons for the use of fillers in thermoplastics	35
Table 1-3	Predominant function of some typical fillers	35
Table 1-4	Filler modification and its reasons	47
Table 1-5	Comparison between carbon black and silica	50
Table 2-1	PBs of various degrees of hydrochlorination	66
Table 2-2	PBs of various degrees of modification	67
Table 3-1	Detailed concentration profiles of reagents for in-situ DLS	88
Table 4-1	Crossover data for PB-5 and PB-10	120
Table S-1	PBs of 1 and 2 mol% hydrochlorination	136
Table S-2	PBs of 1 and 2 mol% modification	136
Table S-3	Conditions for nitro reduction reactions	138
Table S-4	Frequency-dependent transition data of filled blends (T = 50 °C)	147
Table S-5	Linear regression data of the microgel filled systems (data collected from Figure S-14)	151